Научном већу Института за физику у Београду
Београд, 7. март 2022.

Предмет: Молба за покретање поступка за реизбор у звање научни сарадник

Молим Научно веће Института за физику у Београду да, у складу са Правилником о стицању истраживачких и научних звања прописаном од стране Министарства просвете, науке и технолошког развоја, покрене поступак за мој реизбор у звање научни сарадник.

У прилогу достављам:

1. Мишљење руководиоца лабораторије са предлогом чланова комисије
2. Стручну биографију
3. Преглед научне активности
4. Елементе за квалитативну оцену научног доприноса
5. Елементе за квантитативну оцену научног доприноса
6. Списак објављених радова и њихове копије
7. Податке о цитираности радова
8. Копију превода дипломе доктора наука и решења о нострификацији дипломе
9. Копију решења о претходном избору и реизбору у звање
10. Додатне прилоге за квалитативну оцену научног доприноса

С поштовањем,

Кузманоски

др Маја Кузманоски
научни сарадник
Институт за физику у Београду

Научном већу Института за физику у Београду
Београд, 7. март 2022.

Предмет: Мишљење руководиоца лабораторије о реизбору др Маје Кузманоски у звање научни сарадник

Др Маја Кузманоски је запослена у Лабораторији за физику животне средине Института за физику у Београду од фебруара 2011. године. Ради на темама из области опште и интердисциплинарне физике са посебним фокусом на анализи оптичких карактеристика атмосферских аеросола применом метода даљинске детекције и модела, као и испитивању утицаја природног аеросола на квалитет ваздуха.

С обзиром да кандидаткиња испуњава све услове предвиђене Правилником о стицању истраживачких и научних звања Министарства просвете, науке и технолошког развоја, сагласан сам са покретањем поступка за реизбор др Маје Кузманоски у звање научни сарадник.

За чланове комисије за реизбор др Маје Кузманоски у звање научни сарадник предлажем:

1. др Александра Нина, виши научни сарадник Института за физику у Београду
2. др Предраг Коларж, виши научни сарадник Института за физику у Београду
3. проф. др Владимир Ђурђевић, ванредни професор Физичког факултета Универзитета у Београду

Руководилац Лабораторије за физику животне средине

Зоран Мијић

др Зоран Мијић
виши научни сарадник
Институт за физику у Београду

2. СТРУЧНА БИОГРАФИЈА КАНДИДАТКИЊЕ

Маја Кузманоски је рођена 18. 5. 1973. године у Београду, где је завршила основну и средњу школу. Студије физике на Физичком факултету Универзитета у Београду уписала је 1992. године. Дипломирала је на смеру Теоријска и експериментална физика у децембру 1998. године, са просечном оценом 9,07. У мају 2000. године уписала је постдипломске студије на Физичком факултету Универзитета Нови Јужни Велс у Сиднеју, у Аустралији, у области атмосферске физике. У току докторских студија, у периоду од фебруара 2001. до јуна 2004. године, била је стипендиста Владе Аустралије (*International Postgraduate Research Scholarship*). Докторирала је у децембру 2005. године, под руководством проф. др Мајкла Бокса и др Гејл Бокс. Назив докторске дисертације је "Физичка и оптичка својства атмосферских аеросола у експерименталним кампањама" (*Physical and optical properties of aerosols from field campaigns*). Од маја 2005. до маја 2007. године, Маја Кузманоски је радила хонорарно за *Bay Area Environmental Research Institute* (*BAERI*) у Сан Франциску, у Калифорнији. У току тог периода је, у сарадњи са др Беатом Шмидом (*BAERI*) и др Филипом Раселом (*NASA Ames Research Center*) наставила рад у области оптичких карактеристика аеросола и њихове улоге у климатском систему. Упоредо са овим ангажовањем, радила је као наставник физике у Математичкој гимназији, од септембра 2005. до јуна 2011. године.

Од фебруара 2011. године, Маја Кузманоски је запослена у Институту за физику у Београду. Од 2011. до 2019. године је била ангажована на националном пројекту ИИИ 43007 "Истраживање климатских промена и њиховог утицаја на животну средину-праћење утицаја, адаптација и ублажавање", финансираном од стране Министарства просвете, науке и технолошког развоја Републике Србије. Била је учесник два међународна пројекта у оквиру *EU H2020* програма: *GEO-CRADLE* (*Coordinating and integRating state-of-the-art Earth Observation Activities in the regions of North Africa, Middle East, and Balkans and Developing Links with GEO related initiatives towards GEOSS*) у периоду 2016-2018. године и *ACTRIS-2* (*Aerosols, Clouds, and Trace gases Research InfraStructure Network) Integrated Activities (IA)* у периоду 2015-2019. године. Члан је координационог одбора (*Management Committee*) *COST* акције *PROBE* (*PROfiling the atmospheric Boundary layer at European scale*) која је у току (2019-2023). Део је тима који се бави даљинским мерењима лидар системом у Београду, који је део европске мреже лидар система *EARLINET* (*European Aerosol Research Lidar Network*).

Главне теме рада Маје Кузманоски су истраживања оптичких карактеристика атмосферских аеросола применом даљинских мерења и моделирањем, као и анализа утицаја атмосферских аеросола на квалитет ваздуха. Кандидаткиња је аутор или коаутор 10 радова објављених у међународним часописима, једног поглавља у истакнутој монографији међународног значаја и више саопштења на међународним конференцијама.

3. ПРЕГЛЕД НАУЧНЕ АКТИВНОСТИ КАНДИДАТКИЊЕ

Напомена: Звездицом (*) су означени радови публиковани у периоду након претходног реизбора у звање

Научно-истраживачки рад кандидаткиње, Маје Кузманоски, одвија се у области атмосферске физике и физике животне средине. Њена досадашња научна активност усмерена је на две теме: (1) оптичке карактеристике атмосферских аеросола и њихова улога у климатском систему и (2) загађење животне средине и утицај атмосферских аеросола на квалитет ваздуха.

У периоду пре ангажовања у Институту за физику у Београду, истраживања кандидаткиње су била усмерена на област оптичких карактеристика и радијативних ефеката атмосферских аеросола. Истраживања су базирана на подацима о физичким и оптичким карактеристикама аеросола добијеним даљинским мерењима санфотометром и лидаром, као и *in situ* мерењима у току две експерименталне кампање организоване са циљем карактеризације аеросола у југоисточној Азији и јужној Африци, због њиховог значајног утицаја на регионалну и глобалну климу. Кандидаткиња је радила на моделирању карактеристика атмосферских аеросола, валидацији модела поређењем са мерењима, као и на анализи конзистентности различитих метода мерења коришћењем модела као везе између различитих мерених карактеристика аеросола. Кандидаткиња је рачунала расподеле аеросола по димензијама на основу мерених зависности оптичке дебљине слоја аеросола од таласне дужине. Затим је радила на моделирању оптичких карактеристика аеросола на основу израчунатих и мерених расподела аеросола по димензијама и индекса преламања честица добијеним на основу њиховог хемијског састава. Разматран је утицај начина на који су апсорбујуће и неапсорбујуће компоненте аеросола помешане у честицама на оптичке карактеристике аеросола. Кандидаткиња је вршила процену радијативних ефеката аеросола на основу моделираних и мерених оптичких карактеристика честица. На основу описаних истраживања кандидаткиња је 2005. године одбранила докторску дисертацију на Универзитету Нови Јужни Велс у Сиднеју, у Аустралији. Резултати истраживања су приказани у четири рада и на неколико међународних конференција:

- **Kuzmanoski, M.**, M. A. Box, B. Schmid, P. B. Russell, and J. Redemann, Case study of modeled aerosol optical properties during the SAFARI 2000 campaign, Applied Optics, 46, 5263-5275 (2007).
- **Kuzmanoski, M.**, M. A. Box, G. P. Box, B. Schmid, J. Wang, P. B. Russell, H. H. Jonsson, and J. H. Seinfeld, Aerosol properties computed from aircraft-based observations during the ACE-Asia campaign: 1. Aerosol size distributions retrieved from optical thickness measurements, Aerosol Science and Technology, 41, 202-216 (2007).

- **Kuzmanoski, M.**, M. A. Box, B. Schmid, G. P. Box, J. Wang, P. B. Russell, D. Bates, H. H. Jonsson, E. J. Welton, and J. H. Seinfeld, Aerosol properties computed from aircraft-based observations during the ACE-Asia campaign: 2. A case study of lidar ratio closure, Aerosol Science and Technology, 41, 231-243 (2007).
- Box, M. A., G. P. Box, M. J. Kay, **M. Kuzmanoski**, G. Taha, and D. Cohen, Physical, chemical and radiative properties of aerosols in Sydney, Australia, Australian Meteorological Magazine, 51, 223-228 (2002).

У оквиру Националног пројекта ИИИ 43007 истраживања Маје Кузманоски су првобитно била фокусирана на испитивање загађења земљишта. Кандидаткиња је била ангажована на калибрацији енергетски дисперзивног рендгенског спектрометра (*EDXRF*) за анализу садржаја тешких метала у земљишту. Применом *EDXRF* спектрометрије анализирала је садржај тешких метала у узорцима земљишта из паркова у урбаном делу Београда, будући да повишена концентрација тешких метала у земљишту може имати штетан ефекат на околину, као и на здравље људи. Поред тога, кандидаткиња је вршила поређење релативне заступљености појединих тешких метала у земљишту паркова са одговарајућим резултатима претходне анализе садржаја тешких метала у ваздуху на истим локацијама. Резултати су објављени у једном раду и на неколико конференција.

- **Kuzmanoski, M.**, M. Todorović, M. Aničić Urošević, and S. Rajšić, Heavy metal content of soil in urban parks of Belgrade, Hemijska Industrija 68, 643-651 (2014).

У оквиру ове теме, Маја Кузманоски је била коментор при изради мастер рада „Испитивање загађености тешким металима земљишта паркова урбаног дела Београда *XRF* спектрометријом“ одбрањеног на Хемијском факултету 2013. године.

Кандидаткиња је такође била ангажована на испитивању загађења ваздуха и процени ризика по здравље људи услед хроничне изложености тешким металима у ваздуху. Применом *US EPA* (*US Environmental Protection Agency*) модела вршила је процену изложености људи тешким металима који се налазе у саставу PM10 честица у ваздуху и анализу ефеката садржаја тешких метала на здравље људи. Резултати ових истраживања су објављени у:

- Vuković, G., M. Aničić Urošević, I. Razumenić, **M. Kuzmanoski**, M. Pergal, S. Škrivanj, and A. Popović, Air quality in urban parking garages (PM10, major and trace elements, PAHs): Instrumental measurements vs. Active moss biomonitoring, Atmospheric Environment, 85, 31-40 (2014).
- Todorović, M., M. Perišić, **M. Kuzmanoski,** A. Stojić, A. Šoštarić, Z. Mijić, and S. Rajšić, Assessment of PM10 pollution level and required source emission reduction in Belgrade area, Journal of Environmental Science and Health, Part A, 50, 1351-1359 (2015).

У периоду након претходног реизбора у звање, кандидаткиња је започела истраживања утицаја сахарског песка, као природног аеросола, на квалитет ваздуха. У оквиру сарадње

са колегама из Института за нуклеарне науке "Винча", иницирала је кампању мерења различитих карактеристика атмосферских аеросола паралелном применом неколико уређаја у дворишту Института за физику, у току пролећа 2019. године. За време вишедневних епизода сахарског песка и у периоду након сваке епизоде вршена су мерења вертикалних профила аеросола лидар системом, затим мерења расподела честица по димензијама, као и узорковање PM10 и PM2.5 честица ради анализе њихових масених концентрација и елементног састава. Део резултата је до сада објављен у једном научном раду. Кандидаткиња је раду допринела анализом података о концентрацијама и елементном саставу узоркованих PM10 и PM2.5 честица у току епизода сахарског песка. Анализа је вршена са циљем утврђивања скупа елемената, као и односа концентрација елемената, који се могу повезати са доприносом песка узоркованим честицама у току посматраних епизода. Резултати анализе су затим у раду коришћени при интерпретацији резултата биомониторинга квалитета ваздуха помоћу маховина, вршеног паралелно са узорковањем PM честица.

- *Aničić Urošević M., **M. Kuzmanoski**, T. Milićević, I. Kodranov, K. Vergel, and A. Popović, Moss bag sensitivity for the assessment of airborne elements at suburban background site during spring/summer season characterized by Saharan dust intrusions, Air Quality, Atmosphere & Health (2022) https://doi.org/10.1007/s11869-022-01161-8.

Маја Кузманоски се такође бави истраживањима оптичких карактеристика атмосферских аеросола методама даљинске детекције. Учествује у мерењима и анализи података мерења лидар системом у Београду, који је део EARLINET мреже, европске мреже ових уређаја. Анализом детектованог сигнала добија се информација о висини планетарног граничног слоја и вертикалног профила оптичких карактеристика атмосферских аеросола (коефицијената екстинкције и расејања под углом 180°). Висина планетарног граничног слоја је важан параметар који утиче на ниво загађења ваздуха. Мерења лидар системом, вршена за време делимичног помрачења Сунца у марту 2015. године, коришћена су за проучавање динамике планетарног граничног слоја, упоредо са променама других параметара: метеоролошки параметри, УВ зрачење, концентрација атмосферских јона и озона у приземном слоју. Комбиновањем мерења помоћу лидар система са мерењима санфотометром у оквиру EARLINET и AERONET мрежа ових уређаја, може се добити информација о вертикалном профилу концентрације аеросола, као и посебно пустињског песка, потребна за верификацију резултата нумеричких модела. Део резултата истраживања у којима су примењена мерења лидар системом објављен је у два рада, као и на међународним конференцијама. У оквиру ове теме, Маја Кузманоски је коментор при изради докторске дисертације Луке Илића, студента докторских студија на Физичком факултету Универзитета у Београду.

- *Ilić, L., A. Jovanović, **M. Kuzmanoski**, L. Lazić, F. Madonna, M. Rosoldi, M. Mytilinaios, E. Marinou, and S. Ničković, Mineralogy sensitive immersion freezing parameterization in DREAM, Journal of Geophysical Research Atmospheres, 127, e2021JD035093, 2022. http://dx.doi.org/10.1029/2021JD035093.
- *Ilić L., **M. Kuzmanoski,** P. Kolarž, A. Nina, V. Srećković, Z. Mijić, J. Bajčetić, and M. Andrić, Changes of atmospheric properties over Belgrade, observed using remote sensing and in situ methods during the partial solar eclipse of 20 March 2015, Journal of Atmospheric and Solar-Terrestrial Physics, 171, 250-259, 2018.

Поред тога, кандидаткиња је вршила анализу података мерења лидар системом у Београду у оквиру *ACTRIS COVID-19 Near Real-time measurement campaign* експерименталне кампање, одржане у мају 2020. године са циљем испитивања утицаја рестриктивних мера у Европи почетком пандемије COVID-19 на оптичке карактеристике атмосферских аеросола. Ово је један од експеримената организованих и да би се показала примена мерења у оквиру EARLINET мреже за време ванредних ситуација.

4. ЕЛЕМЕНТИ ЗА КВАЛИТАТИВНУ АНАЛИЗУ НАУЧНОГ ДОПРИНОСА

4.1. Квалитет научних резултата

4.1.1. Научни ниво и значај резултата, утицај научних радова

Маја Кузманоски је аутор или коаутор 10 радова у међународним часописима са ISI листе, од тога 5 радова у часописима категорије М21, 2 рада у часописима категорије М22 и 3 рада у часописима категорије М23. У периоду након претходног покретања поступка за реизбор у звање, кандидаткиња је објавила 3 рада, од тога 1 рад у часопису категорије М21 и 2 рада у часописима категорије М22.

Најзначајнији рад Маје Кузманоски је:

Kuzmanoski, M., M. A. Box, B. Schmid, G. P. Box, J. Wang, P. B. Russell, D. Bates, H. H. Jonsson, E. J. Welton, and J. H. Seinfeld,
Aerosol properties computed from aircraft-based observations during the ACE-Asia campaign: 2. A case study of lidar ratio closure,
Aerosol Science and Technology, 41, 231-243 (2007)
doi:10.1080/02786820601146977
(М21, ИФ 2.905, цитиран 4 пута по Scopus бази, без аутоцитата)

Рад проистиче из докторске дисертације кандидаткиње. У раду је кандидаткиња моделирала однос коефицијената екстинкције и расејања под углом 180°, који је важан параметар при анализи мерења лидар системом како би се добиле квантитативне информације о аеросолима. У прорачунима су коришћене расподеле аеросола по

димензијама израчунате на основу даљинских мерења, као и мерене расподеле. Индекс преламања је био у складу са хемијским саставом честица, при чему је коришћена претпоставка о интерном мешању различитих компоненти. Вршена је анализа поређења моделираних вредности са вредностима добијеним на основу комбинованих мерења лидар системом и санфотометром. Анализом су обухваћена три типа аеросола различитих карактеристика. Показана је осетљивост резултата на ограничен опсег радијуса честица у случају расподеле аеросола по димензијама израчунате на основу даљинских мерења, као и на претпоставку о начину мешања компоненти честица. Ова анализа доприноси бољем разумевању и интерпретацији мерења аеросола помоћу лидар система. Кандидаткиња је дала кључни допринос раду моделирањем карактеристика аеросола и поређењем са мерењима. Самостално је извршила је прорачуне расподела аеросола по димензијама на основу даљинских мерења, моделирала оптичке карактеристике аеросола, испитивала осетљивост моделираних карактеристика на различите претпоставке и вршила анализу поређења са доступним мерењима.

4.1.2. Позитивна цитираност научних радова кандидаткиње

Подаци о цитираности радова кандидаткиње на дан 7. марта 2022. године су сумирани у табели:

База података	Број цитата	Број цитата без самоцитата	Хиршов индекс
Scopus	93	82	3
Web of Science	76	75	4

Подаци о цитираности са интернет страница Scopus и Web of Science база су дати након списка свих радова.

4.1.3. Параметри квалитета часописа

За процену квалитета часописа у којима су радови кандидаткиње објављени у наставку су приказане категорије часописа, њихов импакт фактор (ИФ), као и импакт фактор нормализован по импакту цитирајућег чланка (СНИП) (наведена је најбоља вредност из периода до две године уназад од године објављивања рада). Подвучени су импакт фактори часописа у којима су објављени радови након претходног реизбора у звање.

У категорији М21 (врхунски међународни часопис) кандидаткиња је објавила радове у следећим часописима:

- 1 рад у *Journal of Geophysical Research: Atmospheres* - ИФ 4.261, СНИП 1.27
- 1 рад у *Atmospheric Environment* - ИФ 3.281, СНИП 1.67

- 2 рада у *Aerosol Science and Technology* - ИФ 2.905, СНИП 1.21 (за сваки од радова)
- 1 рад у *Applied Optics* - ИФ 1.717, СНИП 1.71

У категорији М22 (истакнути међународни часопис) кандидаткиња је објавила радове у следећим часописима:

- 1 рад у *Air Quality, Atmosphere and Health* - ИФ 3.763, СНИП 1.18
- 1 рад у *Journal of Atmospheric and Solar-Terrestrial Physics* - ИФ 1.802, СНИП 1.06

У категорији М23 (међународни часопис) кандидаткиња је објавила радове у следећим часописима:

- 1 рад у *Journal of Environmental Science and Health, Part A* - ИФ 1.276 , СНИП 0.71
- 1 рад у *Australian Meteorological Magazine* - ИФ 1.209
- 1 рад у *Hemijska Industrija* - ИФ 0.562, СНИП 0.53

Укупан ИФ радова кандидаткиње је 23.681, а након претходног реизбора у звање 9.826.

Додатни библиометријски параметри у вези са објављеним радовима кандидаткиње након претходног реизбора у звање сумирани су у следећој табели:

	ИФ	М	СНИП
Укупно	9.826	18	3.51
Усредњено по чланку	3.275	6	1.17
Усредњено по аутору	1.326	2.347	0.470

4.1.4. Степен самосталности и степен учешћа у реализацији радова у научним центрима у земљи и иностранству

Маја Кузманоски је водећи аутор на 4 објављена рада, други аутор на 2 рада и трећи аутор на 2 рада. Кандидаткиња је значајно допринела конципирању и писању ових радова.

У радовима из области оптичких карактеристика аеросола, који су резултат њене докторске дисертације, кандидаткиња је дала кључни допринос осмишљавањем теме рада, моделирањем карактеристика аеросола, анализом поређења са мерењима, као и самим писањем радова.

Међу радовима објављеним након претходног реизбора у звање, у два експериментална рада кандидаткиња је дала допринос анализи података мерења и интерпретацији резултата, док је у раду који је резултат нумеричког моделирања и експерименталног рада кандидаткиња дала допринос анализи поређења резултата модела и мерења.

4.2. Ангажованост у формирању научних кадрова

Маја Кузманоски је 2013. године била коментор при изради мастер тезе Тијане Љубеновић, студенткиње мастер студија на Хемијском факултету Универзитета у Београду.

Прилог: насловна страна и захвалница мастер тезе Тијане Љубеновић

Кандидаткиња је коментор при изради докторске дисертације Луке Илића, студента докторских студија на Физичком факултету Универзитета у Београду.

Прилог: записник са седнице ННВ Физичког факултета Универзитета у Београду

4.3. Нормирање броја коауторских радова, патената и техничких решења

Међу радовима објављеним након претходног реизбора у звање, у једном раду категорије М21 (под редним бројем 1 на списку публикација у овој категорији) и четири саопштења на конференцијама (категорија М34, под редним бројем 2, 4, 5 и 8 на списку публикација у овој категорији) су комбинована експериментална истраживања са нумеричким моделирањем. Остали радови и саопштења на конференцијама засновани су у потпуности на експерименталном раду. Сви радови се рачунају са пуном тежином у односу на 7 коаутора.

Одговарајуће нормирање на основу броја коаутора зе извршено за 1 рад категорије М21 (9 аутора) и један рад категорије М22 (8 аутора).

4.4. Учешће у пројектима, потпројектима и пројектним задацима

Кандидаткиња је учествовала на националном пројекту ИИИ 43007 “Истраживање климатских промена и њиховог утицаја на животну средину-праћење утицаја, адаптација и ублажавање”, финансираном од стране Министарства просвете, науке и технолошког развоја Републике Србије, као и на три међународна пројекта:

- 2014-2015: *ACTRIS* (*Aerosols, Clouds, and Trace gases Research InfraStructure Network)* у оквиру EU FP7 програма (No 262254)
- 2015-2019: *ACTRIS-2* (*Aerosols, Clouds, and Trace gases Research InfraStructure Network Integrated Activities)* у оквиру *EU H2020* програма (No 654109)
- 2016-2018: *GEO-CRADLE* (*Coordinating and integRating state-of-the-art Earth Observation Activities in the regions of North Africa, Middle East, and Balkans and Developing Links with GEO related initiatives towards GEOSS*) у оквиру *EU H2020* програма (No 690133)

Прилог: копија дела уговора пројекта GEO-CRADLE са списком учесника; потврде руководиоца тима Института за физику у Београду у оквиру пројеката ACTRIS и ACTRIS-2 о учешћу кандидаткиње у овим пројектима

Кандидаткиња је тренутно учесник и члан координационог одбора (*Management Committee*) *COST* акције *PROBE* (*PROfiling the atmospheric Boundary layer at European scale*) која је у току (2019-2023).

Прилог: копија интернет странице COST акције PROBE

4.5. Активност у научним и научно-стручним друштвима

4.5.1. Рецензије научних радова

Маја Кузманоски је била рецензент једног рада у *Journal of Geophysical Research: Atmospheres* (2010. године) и два рада у *Atmospheric Pollution Research* (2016. и 2020. године).

Прилог: потврде уредника часописа

4.5.2. Организација научних скупова

Кандидаткиња је била члан Организационог одбора међународне конференције *18th International Conference on Photoacoustic and Photothermal Phenomena* (*ICPP18*), одржане од 6. до 10. септембра 2015. године у Новом Саду.

Прилог: извод књиге апстраката са наведеним саставом научног организационог одбора

4.6. Утицајност научних резултата

Утицајност научних резултата кандидата је наведена у одељцима 3 и 4.1 овог документа. Пун списак радова је дат у одељку 6, а подаци о цитираности са интернет страница база *Scopus* и *Web of Science* су дати након списка свих радова кандидаткиње.

4.7 Конкретан допринос кандидата у реализацији радова у научним центрима у земљи и иностранству

Од три рада објављена након претходног реизбора у звање, један је урађен у сарадњи са колегама из иностранства (Грчка и Италија), а два су урађена у сарадњи са колегама из земље. Маја Кузманоски је имала кључни допринос у сва три рада. Кандидаткиња је допринела одабиру методологије и интерпретацији резултата, као и конципирању и писању ових публикација. У раду категорије М21 о улози песка у формирању облачног леда, који је резултат нумеричког моделирања и експерименталног рада, кандидаткиња

дала допринос анализи поређења резултата модела и мерења. У два рада категорије М22 кандидаткиња је дала допринос експерименталном раду и анализи података мерења.

4.8. Међународна сарадња

Кандидаткиња учествује у међународној сарадњи у оквиру *EARLINET* (*European Aerosol Research Lidar Network*) мреже лидар станица. У оквиру те сарадње учествовала је у експерименталној кампањи *ACTRIS COVID-19 NRT lidar measurement campaign*.

Прилог: копија интернет странице EARLINET мреже; извод извештаја са првим резултатима експерименталне кампање

5. ЕЛЕМЕНТИ ЗА КВАНТИТАТИВНУ ОЦЕНУ НАУЧНОГ ДОПРИНОСА КАНДИДАТКИЊЕ

Остварени М-бодови кандидаткиње у периоду након претходног реизбора у звање:

Категорија	М бодова по раду	Број радова	Укупно М бодова	Нормирани број М бодова
М21	8	1	8	5.714
М22	5	2	10	9.167
М33	1	3	3	3
М34	0.5	9	4.5	4.5

Поређење оствареног броја М-бодова са минималним условима потребним за реизбор у звање научни сарадник:

Минимални број М бодова	Неопходно	Остварено	Остварено, нормирано
Укупно	16	25.5	22.381
М10+М20+М31+М32+М33+М41+М42	10	21	17.881
М11+М12+М21+М22+М23	6	18	14.881

6. СПИСАК ПУБЛИКАЦИЈА ПО КАТЕГОРИЈАМА

МОНОГРАФИЈЕ, МОНОГРАФСКЕ СТУДИЈЕ, ТЕМАТСКИ ЗБОРНИЦИ, ЛЕСКИКОГРАФСКЕ И КАРТОГРАФСКЕ ПУБЛИКАЦИЈЕ МЕЂУНАРОДНОГ ЗНАЧАЈА (М10)

Поглавље у истакнутој монографији међународног значаја (М13)

Радови објављени пре претходног реизбора у звање

1. Tomašević, M., Z. Mijić, M. Aničić, A. Stojić, M. Perišić, **M. Kuzmanoski**, M. Todorović, and S. Rajšić,
Air Quality Study in Belgrade: Particulate Matter and Volatile Organic Compounds as Threats to Human Health, In: Air Pollution: Sources, Prevention and Health Effects, Editor: Rajat Sethi, Nova Science Publishers, NY, USA, p. 315-346 (2013).
ISBN: 978-1-62417-735-4
https://www.novapublishers.com/catalog/product_info.php?products_id=38962&osCsid=cc956b5e1008d06c56c891f47982d91c

РАДОВИ ОБЈАВЉЕНИ У НАУЧНИМ ЧАСОПИСИМА МЕЂУНАРОДНОГ ЗНАЧАЈА (М20)

Рад у врхунском међународном часопису (М21)

Радови објављени након претходног реизбора у звање

1. Ilić, L., A. Jovanović, **M. Kuzmanoski**, L. Lazić, F. Madonna, M. Rosoldi, M. Mytilinaios, E. Marinou, and S. Ničković,
Mineralogy sensitive immersion freezing parameterization in DREAM,
Journal of Geophysical Research:Atmospheres, 127, e2021JD035093 (2022).
http://dx.doi.org/10.1029/2021JD035093.
(IF 4.261, M_{norm}=5.714)

Радови објављени пре претходног реизбора у звање

1. Vuković, G., M. Aničić Urošević, I. Razumenić, **M. Kuzmanoski**, M. Pergal, S. Škrivanj, and A. Popović,
Air quality in urban parking garages (PM10, major and trace elements, PAHs): Instrumental measurements vs. Active moss biomonitoring,
Atmospheric Environment, 85, 31-40 (2014). http://dx.doi.org/10.1016/j.atmosenv.2013.11.053.
(IF 3.281)

2. **Kuzmanoski, M.**, M. A. Box, B. Schmid, P. B. Russell, and J. Redemann,
Case study of modeled aerosol optical properties during the SAFARI 2000 campaign,
Applied Optics, 46, 5263-5275 (2007).
doi: 10.1364/AO.46.005263
(IF 1.717)

3. **Kuzmanoski, M.**, M. A. Box, G. P. Box, B. Schmid, J. Wang, P. B. Russell, H. H. Jonsson, and J. H. Seinfeld,
Aerosol properties computed from aircraft-based observations during the ACE-Asia campaign: 1. Aerosol size distributions retrieved from optical thickness measurements,
Aerosol Science and Technology, 41, 202-216 (2007).
doi:10.1080/02786820601126789
(IF 2.905)

4. **Kuzmanoski, M.**, M. A. Box, B. Schmid, G. P. Box, J. Wang, P. B. Russell, D. Bates, H. H. Jonsson, E. J. Welton, and J. H. Seinfeld,
Aerosol properties computed from aircraft-based observations during the ACE-Asia campaign: 2. A case study of lidar ratio closure,
Aerosol Science and Technology, 41, 231-243 (2007).
doi:10.1080/02786820601146977
(IF 2.905)

Рад у истакнутом међународном часопису (М22)

Радови објављени након претходног реизбора у звање

1. Aničić Urošević M., **M. Kuzmanoski,** T. Milićević, I. Kodranov, K. Vergel, and A. Popović, Moss bag sensitivity for the assessment of airborne elements at suburban background site during spring/summer season characterized by Saharan dust intrusions,
Air Quality, Atmosphere and Health (2022).
https://doi.org/10.1007/s11869-022-01161-8.
(IF 3.763, M=5)

2. Ilić L., **M. Kuzmanoski,** P. Kolarž, A. Nina, V. Srećković, Z. Mijić, J. Bajčetić, and M. Andrić,
Changes of atmospheric properties over Belgrade, observed using remote sensing and in situ methods during the partial solar eclipse of 20 March 2015,
Journal of Atmospheric and Solar-Terrestrial Physics, 171, 250-259 (2018).
doi: 10.1016/j.jastp.2017.10.001
(IF 1.790, M_{norm}=4.167)

Рад у међународном часопису (М23)

Радови објављени пре претходног реизбора у звање

1. Todorović, M., M. Perišić, **M. Kuzmanoski,** A. Stojić, A. Šoštarić, Z. Mijić, and S. Rajšić, Assessment of PM10 pollution level and required source emission reduction in Belgrade area, Journal of Environmental Science and Health, Part A, 50, 1351-1359 (2015).
doi:10.1080/10934529.2015.1059110
(IF 1.276)

2. **Kuzmanoski, M.**, M. Todorović, M. Aničić Urošević, and S. Rajšić,
Heavy metal content of soil in urban parks of Belgrade,
Hemijska Industrija 68, 643-651 (2014).
doi: 10.2298/HEMIND131105001K
(IF 0.562)

3. Box, M. A., G. P. Box, M. J. Kay, **M. Kuzmanoski**, G. Taha, and D. Cohen,
Physical, chemical and radiative properties of aerosols in Sydney, Australia,
Australian Meteorological Magazine, 51, 223-228 (2002).
(IF 1.209)

ЗБОРНИЦИ МЕЂУНАРОДНИХ НАУЧНИХ СКУПОВА (М30)

Саопштење са међународног скупа штампано у целини (М33)

Радови објављени након претходног реизбора у звање

1. **Kuzmanoski M.**, L. Ilić, M. Todorović, and Z. Mijić,
A study of a dust intrusion event over Belgrade, Serbia,
Proceedings of the 6th WeBIOPATR Workshop and Conference, September 6-8, 2017,
Belgrade, Serbia, p. 103-108 (2019).

2. Mijić, Z., L. Ilić, **M. Kuzmanoski,**
Raman lidar for atmospheric aerosol profiling in Serbia,
Proceedings of the 49th International October Conference on Mining and Metallurgy, Bor,
October 18-21, 2017, Bor, Serbia, p. 65 - 68.

3. Mijić Z., M. Perišić, L. Ilić, A. Stojić, **M. Kuzmanoski,**
Air mass transport over Balkan region identified by atmospheric modeling and aerosol lidar technique,
Proceedings of the 49th International October Conference on Mining and Metallurgy, October 18 - 21, 2017, Bor, Serbia, p. 69 - 72.

Радови објављени пре претходног реизбора у звање

1. **Kuzmanoski M.**, L. Ilić, and Z. Mijić,
Aerosol remote sensing study of a Saharan dust intrusion episode in Belgrade, Serbia,
Proceedings of the XIX International Eco-Conference 2015, September 23-25, 2015, Novi Sad,
Serbia, p. 73-80.

2. Mijić Z., M. Perišić, A. Stojić, **M. Kuzmanoski,** and L. Ilić,
Estimation of atmospheric aerosol transport by ground-based remote sensing and modeling,
Proceedings of the XIX International Eco-Conference 2015, September 23-25, 2015, Novi Sad,
Serbia, p. 375-382.

3. Todorović, M., **M. Kuzmanoski**, and T. Ljubenović,
Horizontal distribution of heavy metal concentrations in urban park soil,
Physical Chemistry 2014: Proceedings of the 12th International Conference on Fundamental and Applied Aspects of Physical Chemistry, September 22-26, 2014, Belgrade, Serbia, p. 921-924.

4. Mijić, Z., **M. Kuzmanoski**, D. Nicolae, and L. Belegante,
The use of hybrid receptor models and ground-based remote sensing of particulate matter for identification of potential source regions,
Proceedings of the 4th WeBIOPATR Workshop and Conference, October 2-4, 2013, Belgrade, Serbia, p. 52-59.

5. Todorović, M., M. Perišić, **M. Kuzmanoski**, and A. Šoštarić,
Health risk assessment of trace metals associated with PM10 in Belgrade district,
Proceedings of the 4th WeBIOPATR Workshop and Conference, October 2-4, 2013, Belgrade, Serbia, p. 205-208.

6. Vuković, G., M. Aničić Urošević, **M. Kuzmanoski**, M. Tomašević, M. Pergal, S. Škrivanj, and A. Popović,
Health risk assessment of pollutants (PAHs and heavy metals) associated with PM10 in urban parking garages,
Proceedings of the 4th WeBIOPATR Workshop and Conference, October 2-4, 2013, Belgrade, Serbia, p. 171-175.

7. **Kuzmanoski, M.**, M. Todorović, M. Aničić Urošević, S. Rajšić, and M.Tasić,
XRF analysis of heavy metal content in soil samples using MINIPAL 4 spectrometer,
Proceedings of the 11th International Conference on Fundamental and Applied Aspects of Physical Chemistry (Volume II), September 24-28, 2012, Belgrade, Serbia, p. 660-662.

8. Box, G. P., G. Taha, and **M. Kuzmanoski**,
Long-term atmospheric monitoring in Sydney using an MFRSR,
Proc. IEEE International Geoscience and Remote Sensing Symposium (IGARSS'01), 1, p. 81-83, 2001.

Саопштење са међународног скупа штампано у изводу (М34)

Радови објављени након претходног реизбора у звање

1. Milićević T., D. Mutavdžić, M. Aničić Urošević, **M. Kuzmanoski,** I. Kodranov, A. Popović, and D. Relić,
Health risk assessment for residents and workers based on toxic and carcinogenic element content from PM2.5 in Belgrade suburban area,
Book of Abstracts of the 21st European Meeting on Environmental Chemistry EMEC21, November 30 - December 3, 2021, Novi Sad, Serbia, p. 134.

2. Ilić L., E. Marinou, A. Jovanović, **M. Kuzmanoski**, and S. Ničković,
Ice nucleating particle concentrations in Dust Regional Atmospheric Model (DREAM),
EGU General Assembly 2021, Vienna, Austria, April 2021. https://doi.org/10.5194/egusphere-egu21-7754

3. Mijić Z., **M. Kuzmanoski,** and L. Ilić,
Study on tropospheric aerosols change during the COVID-19 lock-down period: experience from EARLINET measurement campaign,
Book of Abstracts of the 8th International WeBIOPATR Workshop & Conference, Belgrade, Serbia, November 2021. p. 54.

4. Ilić L., A. Jovanović, **M. Kuzmanoski,** F. Madonna, M. Rosoldi, E. Marinou, and S. Ničković,
Mineralogy sensitive ice nucleation parameterizations in Dust Regional Atmospheric Model (DREAM),
EGU General Assembly 2020, Vienna, Austria, May 2020,
https://doi.org/10.5194/egusphere-egu2020-15857

5. Ilić L., A. Jovanović, **M. Kuzmanoski** and S. Ničković,
Modeling of immersion freezing initiation on mineral dust in Dust Regional Atmospheric Model (DREAM),
Book of Abstracts of the 7th International WeBIOPATR Workshop & Conference, Belgrade, Serbia, October 2019. p. 69.

6. Mijić Z., A. Jovanović, **M. Kuzmanoski,** and L. Ilić,
Climatology of satellite derived aerosol optical depth over Belgrade region, Serbia,
Book of Abstracts of the 7th International WeBIOPATR Workshop & Conference, Belgrade, Serbia, October 2019. p. 74.

7. Jovanović A., L. Ilić, **M. Kuzmanoski,** and Z. Mijić,
Case study of the vertical distribution of Saharan dust over Belgrade,
Book of Abstracts of the 7th International WeBIOPATR Workshop & Conference, Belgrade, Serbia, October 2019. p. 80.

8. Ilić L., B. Cvetković, G. Pejanović, S. Petković, **M. Kuzmanoski,** and S. Ničković,
Modeling of mineral composition effects on ice nucleation due to dust in Dust Regional Atmospheric Model (DREAM),
EGU General Assembly 2018, Vienna, Austria, April 2018, Geophysical Research Abstracts Vol. 20, EGU2018-16921, 2018.

9. Z.Mijić, L. Ilić, **M. Kuzmanoski,**
Vertical Raman LIDAR profiling of atmospheric aerosol optical properties over Belgrade, Book of Abstracts PHOTONICA2017, The Sixth International School and Conference on Photonics, Belgrade, Serbia, 28. Aug - 01. Sep, 2017, p. 210.

Радови објављени пре претходног реизбора у звање

1. **Kuzmanoski M.**, S. Ničković, and L. Ilić,
Spatial distribution of mineral dust single scattering albedo based on DREAM model,
Geophysical Research Abstracts, Vol. 18, EGU2016-4425, 2016, EGU General Assembly, Vienna, Austria, April 2016.

2. Ilić L., **M. Kuzmanoski**, and Z. Mijić,
Planetary boundary layer and elevated aerosol layer height estimation from lidar signal in Belgrade,
Book of Abstracts of the 5th International WeBIOPATR Workshop & Conference, Belgrade, Serbia, October 2015. p. 47.
https://www.vin.bg.ac.rs/webiopatr/#Workshop/Abstracts-and-papers

3. Todorović M., M. Perišić, **M. Kuzmanoski**, and A. Šoštarić,

Health risk assessment of trace metals associated with PM10 in Belgrade district,
5th International WeBIOPATR Workshop & Conference, Belgrade, Serbia, October 2015. p. 41.
https://www.vin.bg.ac.rs/webiopatr/#Workshop/Abstracts-and-papers

4. Mijić, Z., **M. Kuzmanoski**, A. Stojić, A. Žekić, S. Rajšić, M. Tasić,
Investigation of regional transport and health risk effects of metals in PM2.5 air particulate matter in Belgrade,
Book of Abstracts of the 3rd International WeBIOPATR Workshop & Conference, Belgrade, Serbia, November 2011. p. 51.
https://www.vin.bg.ac.rs/webiopatr/#About

5. Schmid, B., H. Guan, **M. Kuzmanoski**, P. Pilewskie, A. Bucholtz, A. McComiskey, S. McFarlane, and B. Magi,
The Sensitivity of Shortwave Radiative Forcing and Heating Rates to the Aerosol Vertical Profile,
DOE ARM Science Team Meeting, Norfolk, USA, March 2008.

6. Schmid, B., H. Guan, A. McComiskey, S. McFarlane, **M. Kuzmanoski**, P. Pilewskie, B. Magi,
The Sensitivity of Shortwave Radiative Forcing and Heating Rates to the Aerosol Vertical Profile,
AGU Fall Meeting, San Francisco, USA, December 2007.

7. **Kuzmanoski, M.**, M. A. Box, B. Schmid, P. B. Russell, B. Holben , and J. Redemann,
Modeled aerosol optical properties during the SAFARI 2000 campaign,
AGU Fall Meeting, San Francisco, USA, December 2006.

8. **Kuzmanoski, M.**, M. A. Box, B. Schmid, J. Redemann, P. B. Russell, and B. Holben,
Case studies of modeled properties of biomass burning aerosol during SAFARI 2000,
EGU General Assembly 2006, Vienna, Austria, April 2006.

9. **Kuzmanoski, M.**, M. A. Box, B. Schmid, G. P. Box, J. Wang, P. B. Russell, D. Bates, H. H. Jonsson, E. J. Welton, and J. H. Seinfeld,
A case study of aerosol optical properties and radiative effects computed from airborne measurements during the ACE-Asia campaign,
AGU Fall Meeting, San Francisco, USA, December 2005.

10. **Kuzmanoski, M.**, M. A. Box, G. P. Box, B. Schmid, P. B. Russell, J. Redemann, J. M. Livingston, J. Wang, R. C. Flagan, J. H. Seinfeld,
Aerosol size distributions retrieved from sunphotometer measurements during ACE-Asia: Intercomparison of two retrieval methods,
10th National Conference, Australian Meteorological and Oceanographic Society, Perth, Australia, February 2003.

11. **Kuzmanoski, M.**, M. A. Box, G. P. Box, B. Schmid, P. B. Russell, J. Redemann, J. M. Livingston, J. Wang, R. C. Flagan, and J. H. Seinfeld,
Aerosol size distributions during ACE-Asia: Retrievals from optical thickness and comparisons with in-situ measurements,
AGU Fall Meeting, San Francisco, USA, December 2002.

12. **Kuzmanoski, M.**, M. A. Box, G. P. Box, B. Schmid, P. B. Russell, J. Redemann, J. M. Livingston, J. Wang, R. C. Flagan, and J. H. Seinfeld,
Size distributions of aerosols during ACE-Asia,
Western Pacific Geophysics Meeting, Wellington, New Zealand, July 2002.

13. **Kuzmanoski, M.**, G. Box, M. Box, P. Russell, and B. Schmid,
Aerosol properties from international field campaigns,
9th National Conference, Australian Meteorological and Oceanographic Society, Melbourne, Australia, February 2002.

14. **Kuzmanoski, M.**, G. Taha, M. J. Kay, G. P. Box, and M. A. Box,
Radiative effects of aerosols in Sydney, Australia,
8th National Conference, Australian Meteorological and Oceanographic Society, Hobart, Australia, February 2001.

ЗБОРНИЦИ СКУПОВА НАЦИОНАЛНОГ ЗНАЧАЈА (М60)

Саопштење са скупа националног значаја штампано у изводу (М64)

Радови објављени пре претходног реизбора у звање

1. Todorović, M., **M. Kuzmanoski**, M. Aničić Urošević, T. Ljubenović, S. Rajšić, and M. Tasić: Heavy metal content in Belgrade urban parks (poster presentation), Book of Abstracts, 6th Symposium Chemistry and Environmental Protection, May 21-24, 2013, Vršac, Serbia, p. 322-323.

2. Perišić, M., M. Todorović, A. Stojić, **M. Kuzmanoski**, and S. Rajšić: Health risk assessment of VOCs in Belgrade semi-urban area, Book of Abstracts, 6th Symposium Chemistry and Environmental Protection, May 21-24, 2013, Vršac, Serbia, p. 378-379.

МАГИСТАРСКЕ И ДОКТОРСКЕ ТЕЗЕ (М70)

Одбрањена докторска дисертација (М71)

Maja Kuzmanoski, “Physical and optical properties of aerosols from field campaigns”, PhD thesis, University of New South Wales, 2005.

Citation overview

Back to document results

Export Print

This is an overview of citations for the documents you've selected.

Document *h*-index : 4 View *h*-graph

9 cited documents

+ Add to list

Date range: 2018 to 2022 Exclude self citations of all authors Exclude citations from books Update

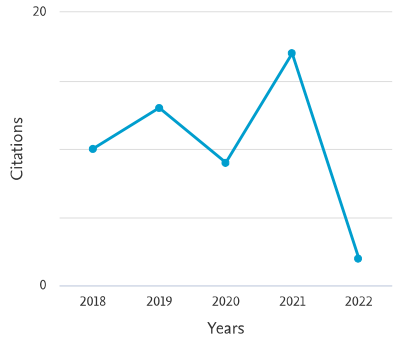

Sort on: Date (newest)

Page Remove

	Documents	Citations	<2018	2018	2019	2020	2021	2022	Subtotal	>2022	Total
		Total	**42**	**10**	**13**	**9**	**17**	**2**	**51**	0	**93**
1	Moss bag sensitivity for the assessment of airborne elements...	2022							0		0
2	Changes of atmospheric properties over Belgrade, observed us...	2018			1	1	1		**3**		**3**
3	Assessment of PM $_{10}$ pollution level and required ...	2015	3				1		**1**		**4**
4	[Heavy metal content of soil in urban parks of Belgrade, Sad...	2014	5	3	3	5	4		**15**		**20**
5	Air quality in urban parking garages (PM_{10}, major...	2013	20	6	9	3	11	2	**31**		**51**
6	Case study of modeled aerosol optical properties during the ...	2007	4						0		**4**
7	Aerosol properties computed from aircraft-based observations...	2007	5						0		**5**
8	Aerosol properties computed from aircraft-based observations...	2007	4	1					**1**		**5**
9	Long-term atmospheric monitoring in Sydney using an MFRSR	2001	1						0		**1**

Citation overview

Self citations of all authors are excluded. ×

Back to document results Export Print

This is an overview of citations for the documents you've selected. Document *h*-index : 3 View *h*-graph

9 cited documents + Add to list

Date range: 2018 to 2022 Exclude self citations of all authors Exclude citations from books Update

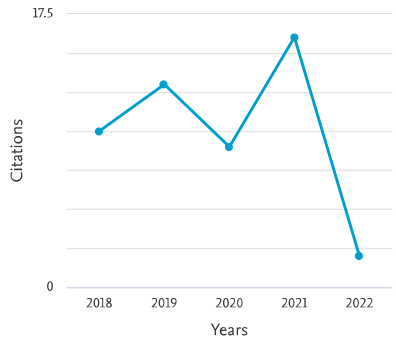

Sort on: Date (newest)

Page Remove

	Documents	Citations	<2018	2018	2019	2020	2021	2022	Subtotal	>2022	Total
		Total	32	10	13	9	16	2	50	0	82
1	Moss bag sensitivity for the assessment of airborne elements...	2022							0		0
2	Changes of atmospheric properties over Belgrade, observed us...	2018			1	1			2		2
3	Assessment of PM $_{10}$ pollution level and required ...	2015	1				1		1		2
4	[Heavy metal content of soil in urban parks of Belgrade, Sad...	2014	5	3	3	5	4		15		20
5	Air quality in urban parking garages (PM_{10}, major...	2013	16	6	9	3	11	2	31		47
6	Case study of modeled aerosol optical properties during the ...	2007	3						0		3
7	Aerosol properties computed from aircraft-based observations...	2007	4						0		4
8	Aerosol properties computed from aircraft-based observations...	2007	2	1					1		3

	Documents	Citations	<2018	2018	2019	2020	2021	2022	**Subtotal**	>2022	**Total**
		Total	**32**	**10**	**13**	**9**	**16**	**2**	**50**	0	**82**
☐	9 Long-term atmospheric monitoring in Sydney using an MFRSR	2001	1						0		**1**

Display: 20 results per page

BACK TO SEARCH RESULTS

Citation Report

Kuzmanoski, M. (Author)

Analyze Results Create Alert

Export Full Report

Publications

8
Total

From 1996 to 2022

Citing Articles

76 Analyze
Total

75 Analyze
Without self-citations

Times Cited

76
Total

9.5
Average per item

75
Without self-citations

4

H-Index

Times Cited and Publications Over Time

DOWNLOAD

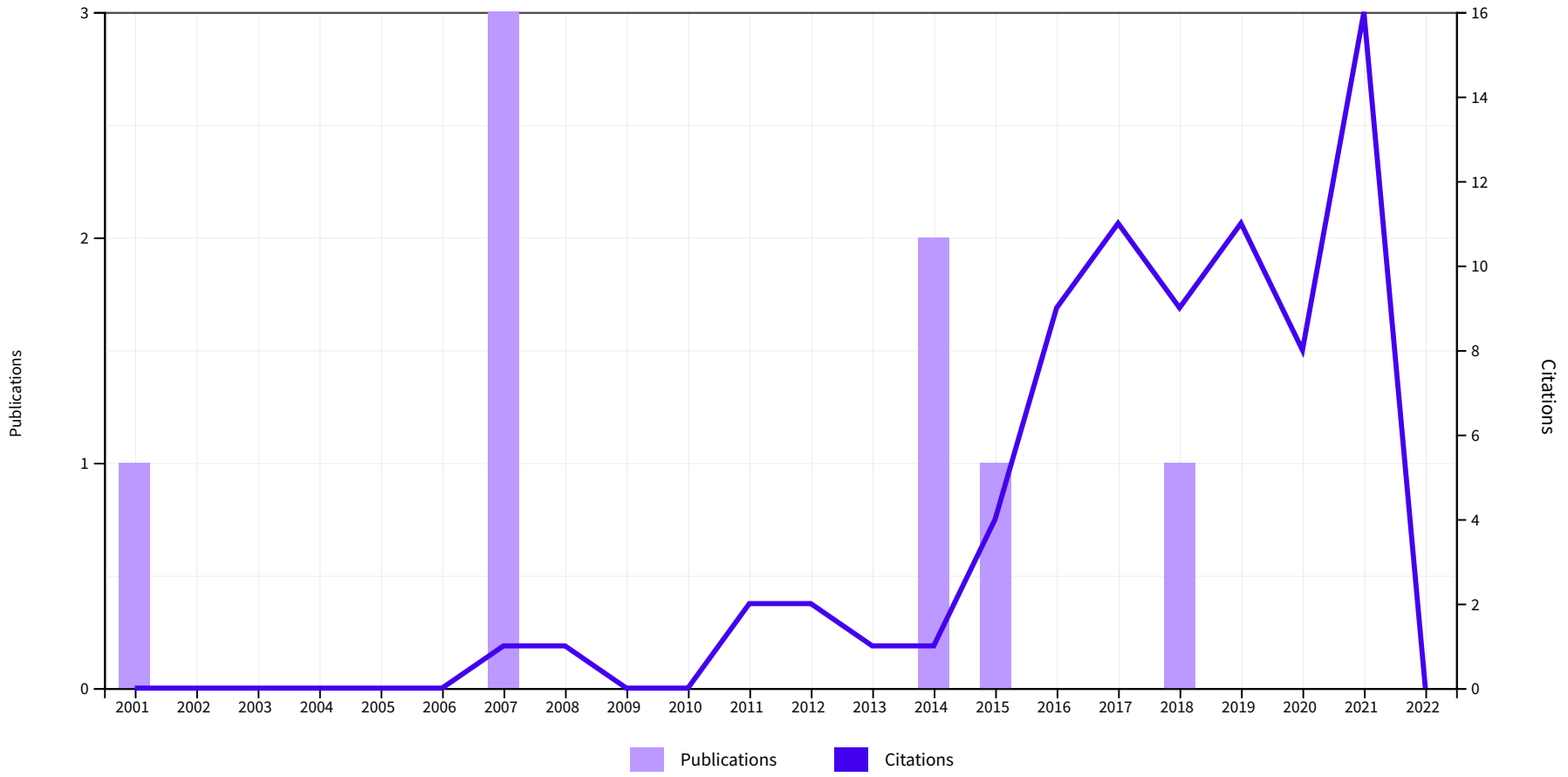

8 Publications

Sort by: **Citations: highest first**

1 of 1

		Citations						
		Back				Forward	Average per year	Total
		2018	2019	2020	2021	2022		
	Total	9	11	8	16	0	4.75	76
1	Air quality in urban parking garages (PM10, major and trace elements, PAHs): Instrumental measurements vs. active moss biomonitoring Vukovic, G; Urosevic, MA; (...); Popovic, A Mar 2014 | ATMOSPHERIC ENVIRONMENT 85 , pp.31-40	5	7	4	11	0	4.78	43

38

2	Heavy metal content of soil in urban parks of Belgrade Kuzmanoski, MM; Todorovic, MN; (...); Rajsic, SF Sep-oct 2014 | HEMIJSKA INDUSTRIJA 68 (5) , pp.643-651	4	3	3	2	0	2	18
3	Changes of atmospheric properties over Belgrade, observed using remote sensing and in situ methods during the partial solar eclipse of 20 March 2015 Ilic, L; Kuzmanoski, M; (...); Andric, M Jun 2018 | JOURNAL OF ATMOSPHERIC AND SOLAR-TERRESTRIAL PHYSICS 171 , pp.250-259	0	1	1	2	0	0.8	4
4	Aerosol properties computed from aircraft-based observations during the ACE-Asia campaign: 2. A case study of lidar ratio closure Kuzmanoski, M; Box, MA; (...); Seinfeld, JH Mar 2007 | AEROSOL SCIENCE AND TECHNOLOGY 41 (3) , pp.231-243	0	0	0	0	0	0.25	4
5	Assessment of PM10 pollution level and required source emission reduction in Belgrade area Todorovic, MN; Perisic, MD; (...); Rajsic, SF Nov 10 2015 | JOURNAL OF ENVIRONMENTAL SCIENCE AND HEALTH PART A-TOXIC/HAZARDOUS SUBSTANCES & ENVIRONMENTAL ENGINEERING 50 (13) , pp.1351-1359	0	0	0	1	0	0.38	3
6	Aerosol properties computed from aircraft-based observations during the ACE-Asia campaign: 1. Aerosol size distributions retrieved from optical thickness measurements Kuzmanoski, M; Box, MA; (...); Seinfeld, JH Feb 2007 | AEROSOL SCIENCE AND TECHNOLOGY 41 (2) , pp.202-216	0	0	0	0	0	0.19	3
7	Long-term atmospheric monitoring in Sydney using an MFRSR Box, G; Taha, G and Kuzmanoski, M IEEE International Geoscience and Remote Sensing Symposium 2001 | IGARSS 2001: SCANNING THE PRESENT AND RESOLVING THE FUTURE, VOLS 1-7, PROCEEDINGS , pp.81-83	0	0	0	0	0	0.05	1
8	Case study of modeled aerosol optical properties during the SAFARI 2000 campaign Kuzmanoski, M; Box, MA; (...); Redemann, J Aug 1 2007 | APPLIED OPTICS 46 (22) , pp.5263-5275	0	0	0	0	0	0	0

Citation Report Publications Table

УНИВЕРЗИТЕТ У БЕОГРАДУ

Студентски трг 1, 11000 Београд, Република Србија
Тел.: 011 3207400; Факс: 011 2638912; E-mail: officebu@rect.bg.ac.yu

Београд, 07.11.2007.
Број: 06-613-1822/4
JJ

На основу члана 104. став 9. Закона о високом образовању ("Службени гласник РС", број 76/05), члана 11. Правилника о признавању страних високошколских исправа ("Гласник Универзитета у Београду", број 129/06) и одлуке Комисије Универзитета за признавање страних високошколских исправа број: 06-613-1822/3 од 24.10.2007., доносим

Р Е Ш Е Њ Е

ПРИЗНАЈЕ СЕ диплома **Универзитета Нови Јужни Велс у Сиднеју, Аустралија** од 15.12.2005. године на коме је **Маја Кузманоски** стекла образовање као диплома докторских студија са научним звањем **доктор физичких наука.**

О б р а з л о ж е њ е

Универзитету у Београду и Физичком факултету обратила се Маја Кузманоски рођена 18.05.1973. год. у Београду, Србија, захтевом за признавање дипломе Универзитета Нови Јужни Велс у Сиднеју, Аустралија, на коме је именована стекла звање доктора наука.

Стручни органи Факултета размотрили су све списе предмета и предложили Комисији Универзитета доношење одлуке, којом се предметна диплома признаје као диплома докторских студија са научним звањем доктор физичких наука, што је Комисија Универзитета прихватила.

Са изложеног, одлучено је као у изреци овог решења.

ПОУКА О ПРАВНОМ ЛЕКУ:
Ово решење је коначно у управном поступку, па се против њега може покренути управни спор код Врховног суда Србије, у року од 30 дана од дана пријема решења.

Р Е К Т О Р

Проф. др Бранко Ковачевић

Prevod sa engleskog na srpski jezik

UNIVERZITET NEW SOUTH WALES

Ovime se potvrđuje da je Savet na današnji dan dodelio

MAJI KUZMANOSKI

diplomu

DOKTORA NAUKA

Rektor

(potpis nečitak)

Prorektor

(potpis nečitak)

Robert J King (svr.)
Zamenik Prorektora (Univezitet)
Upisničar i Zamenik Direktora

Ovlašćenjem Saveta, ova diploma se
overava pečatom Univerziteta
na dan 15. decembra 2005.

Prevod sa engleskog na srpski jezik

UNIVERZITET NEW SOUTH WALES

Prepis Ocena

MAJA KUZMANOSKI (2264233)

TITULA

PhD	Doktor nauka
Oblast:	Fizika
Završila:	6. oktobra 2005
Diploma dodeljena:	15. decembra 2005

PODACI O TEZI

PhD	Doktor nauka
Naslov teze:	Fizička i optička svojstva aerosola u eksperimentalnim kampanjama

KRATAK PREGLED UPISANIH SEMESTARA

Semestar		Profesija	Program
Semestar 2	2000	Istraživanje	2930 Fizika –Msc
Semestar 1	2001	Istraživanje	1890 Fizika -PhD
Semestar 2	2001	Istraživanje	1890 Fizika –PhD
Semestar 1	2002	Istraživanje	1890 Fizika -PhD
Semestar 2	2002	Istraživanje	1890 Fizika –PhD
Semestar 1	2003	Istraživanje	1890 Fizika -PhD
Semestar 2	2003	Istraživanje	1890 Fizika –PhD
Semestar 1	2004	Istraživanje	1890 Fizika –PhD
Semestar 2	2004	Istraživanje	1890 Fizika –PhD

DETALJI O UPISANIM SEMESTRIMA

ISTRAŽIVANJE 2930 FIZIKA –Msc

Semestar 2 2000
Drugi deo
Phys 9103 Istraživački rad iz fizike –redovno Nastavak istraživanja

ISTRAŽIVANJE 1890 FIZIKA –PhD

Semestar 1 2001
Deo prvi
Phys 9103 Istraživački rad iz fizike –redovno Nastavak istraživanja

Semestar 2 2001
Deo drugi

Phys 9103	Istraživački rad iz fizike –redovno	Nastavak istraživanja

Semestar 1 2002
Deo prvi

Phys 9103	Istraživački rad iz fizike –redovno	Nastavak istraživanja

Semestar 2 2002
Deo drugi

Phys 9103	Istraživački rad iz fizike –redovno	Nastavak istraživanja

Semestar 1 2003
Deo prvi

Phys 9103	Istraživački rad iz fizike –redovno	Nastavak istraživanja

Semestar 2 2003
Deo drugi

Phys 9103	Istraživački rad iz fizike –redovno	Nastavak istraživanja

Semestar 1 2004
Deo prvi

Phys 9103	Istraživački rad iz fizike –redovno	Nastavak istraživanja

Semestar 2 2004
Deo drugi

Phys 9103	Istraživački rad iz fizike –redovno	Nastavak istraživanja

Robert J King (svr.)
Zamenik Prorektora (Univezitet)
Upisničar i Zamenik Direktora
13. decembar 2005.

Potvrđujem da je ovaj DOKUMENT tačno preveden sa engleskog jezika na srpski jezik od strane sudskog tumača za engleski jezik pri Okružnom sudu u Beogradu.

Rešenje broj: 74-57/86-03
Datum: 28. juni 2007.
Br. 487/2007

STALNI SUDSKI TUMAČ ZA ENGLESKI JEZIK PRI OKRUŽNOM SUDU U BEOGRADU
JASNA FILIPOVIĆ-BOJIĆ

JASNA FILIPOVIĆ-BOJIĆ
Svetogorska 4, Beograd
Telefon: 3239-053

Република Србија
МИНИСТАРСТВО ЗА НАУКУ И ТЕХНОЛОШКИ РАЗВОЈ
Комисија за стицање научних звања

Број:06-00-75/70
22.12.2010. године
Б е о г р а д

На основу члана 22. става 2. члана 70. став 5. Закона о научноистраживачкој делатности ("Службени гласник Републике Србије", број 110/05 и 50/06 – исправка и 18/10), члана 2. става 1. и 2. тачке 1 – 4.(прилози) и члана 38. Правилника о поступку и начину вредновања и квантитативном исказивању научноистраживачких резултата истраживача ("Службени гласник Републике Србије", број 38/08) и захтева који је поднео

Институт за физику у Београду

Комисија за стицање научних звања на седници одржаној 22.12.2010. године, донела је

ОДЛУКУ
О СТИЦАЊУ НАУЧНОГ ЗВАЊА

Др Маја Кузманоски
стиче научно звање
Научни сарадник

у области природно-математичких наука - физика

О Б Р А З Л О Ж Е Њ Е

Институт за физику у Београду

утврдио је предлог број 1331/1 од 14.09.2010. године на седници научног већа Института и поднео захтев Комисији за стицање научних звања број 1339/1 од 23.09.2010. године за доношење одлуке о испуњености услова за стицање научног звања ***Научни сарадник***.

Комисија за стицање научних звања је по предходно прибављеном позитивном мишљењу Матичног научног одбора за физику на седници одржаној 22.12.2010. године разматрала захтев и утврдила да именована испуњава услове из члана 70. став 5. Закона о научноистраживачкој делатности ("Службени гласник Републике Србије", број 110/05 и 50/06 – исправка и 18/10), члана 2. става 1. и 2. тачке 1 – 4.(прилози) и члана 38. Правилника о поступку и начину вредновања и квантитативном исказивању научноистраживачких резултата истраживача ("Службени гласник Републике Србије", број 38/08) за стицање научног звања ***Научни сарадник***, па је одлучила као у изреци ове одлуке.

Доношењем ове одлуке именована стиче сва права која јој на основу ње по закону припадају.

Одлуку доставити подносиоцу захтева, именованом и архиви Министарства за науку и технолошки развој у Београду.

ПРЕДСЕДНИК КОМИСИЈЕ
Др Станислава Стошић-Грујичић,
научни саветник

МИНИСТАР
Божидар Ђелић

Република Србија
МИНИСТАРСТВО ПРОСВЕТЕ, НАУКЕ И ТЕХНОЛОШКОГ РАЗВОЈА
Комисија за стицање научних звања

Број:660-01-00011/538
30.03.2016. године
Б е о г р а д

На основу члана 22. става 2. члана 70. став 5. и члана 86. став 1. и 2. Закона о научноистраживачкој делатности ("Службени гласник Републике Србије", број 110/05 и 50/06 – исправка и 18/10), члана 50. став 1. Закона о изменама и допунама Закона о научноистраживачкој делатности ("Службени гласник Републике Србије", број 112/15), члана 2. става 1. и 2. тачке 1 – 4.(прилози), члана 31. став 1., члана 37. и 38. Правилника о поступку и начину вредновања и квантитативном исказивању научноистраживачких резултата истраживача ("Службени гласник Републике Србије", број 38/08) и захтева који је поднео

Институт за физику у Београду

Комисија за стицање научних звања на седници одржаној 30.03.2016. године, донела је

ОДЛУКУ
О СТИЦАЊУ НАУЧНОГ ЗВАЊА

Др Маја Кузманоски
стиче научно звање
Научни сарадник
Р е и з б о р

у области природно-математичких наука - физика

О Б Р А З Л О Ж Е Њ Е

Институт за физику у Београду

утврдио је предлог број 1286/1 од 22.09.2015. године на седници Научног већа Института и поднео захтев Комисији за стицање научних звања број 1322/1 од 01.10.2015. године за доношење одлуке о испуњености услова за реизбор у научно звање ***Научни сарадник***.

Комисија за стицање научних звања је по претходно прибављеном позитивном мишљењу Матичног научног одбора за физику на седници одржаној 30.03.2016. године разматрала захтев и утврдила да именована испуњава услове из члана 70. став 5. и члана 86. став 1. Закона о научноистраживачкој делатности ("Службени гласник Републике Србије", број 110/05 и 50/06 – исправка и 18/10), члана 2. става 1. и 2. тачке 1 – 4.(прилози), члана 31. став 1., 37. и 38. Правилника о поступку и начину вредновања и квантитативном исказивању научноистраживачких резултата истраживача ("Службени гласник Републике Србије", број 38/08) за реизбор у научно звање ***Научни сарадник***, па је одлучила као у изреци ове одлуке.

Доношењем ове одлуке именована стиче сва права која јој на основу ње по закону припадају.

Одлуку доставити подносиоцу захтева, именованој и архиви Министарства просвете, науке и технолошког развоја у Београду.

ПРЕДСЕДНИК КОМИСИЈЕ
Др Станислава Стошић-Грујичић,
научни саветник

С. Стошић-Грујичић

МИНИСТАР
Др Срђан Вербић

Република Србија
МИНИСТАРСТВО ПРОСВЕТЕ,
НАУКЕ И ТЕХНОЛОШКОГ РАЗВОЈА
Комисија за стицање научних звања

Број:660-01-00001/643
27.09.2017. године
Б е о г р а д

На основу члана 22. став 2. члана 70. став 4. и члана 86. ст. 1. и 2. Закона о научноистраживачкој делатности ("Службени гласник Републике Србије", број 110/05 и 50/06 – исправка, 18/10 и 112/15), члана 3. ст. 1. и 3., члана 32. став 1., члана 35. став 1. и члана 40. Правилника о поступку, начину вредновања и квантитативном исказивању научноистраживачких резултата истраживача ("Службени гласник Републике Србије", број 24/16, 21/17 и 38/17) и захтева који је поднео

Институт за физику у Београду

Комисија за стицање научних звања на седници одржаној 27.09.2017. године, донела је

ОДЛУКУ
О СТИЦАЊУ НАУЧНОГ ЗВАЊА

Др Маја Кузманоски
стиче научно звање
Научни сарадник
Р е и з б о р

у области природно-математичких наука - физика

О Б Р А З Л О Ж Е Њ Е

Институт за физику у Београду

утврдио је предлог број 1936/1 од 15.11.2016. године на седници Научног већа Института и поднео захтев Комисији за стицање научних звања број 1980/1 од 24.11.2016. године за доношење одлуке о испуњености услова за реизбор у научно звање ***Научни сарадник***.

Комисија за стицање научних звања је по претходно прибављеном позитивном мишљењу Матичног научног одбора за физику на седници одржаној 27.09.2017. године разматрала захтев и утврдила да именована испуњава услове из члана 70. став 4. и члана 86. ст. 1. и 2. Закона о научноистраживачкој делатности ("Службени гласник Републике Србије", број 110/05 и 50/06 – исправка, 18/10 и 112/15), члана 3. ст. 1. и 3., члана 32. став 1., члана 35. став 1. и члана 40. Правилника о поступку, начину вредновања и квантитативном исказивању научноистраживачких резултата истраживача ("Службени гласник Републике Србије", број 24/16, 21/17 и 38/17) за реизбор у научно звање ***Научни сарадник***, па је одлучила као у изреци ове одлуке.

Доношењем ове одлуке именована стиче сва права која јој на основу ње по закону припадају.

Одлуку доставити подносиоцу захтева, именованој и архиви Министарства просвете, науке и технолошког развоја у Београду.

ПРЕДСЕДНИК КОМИСИЈЕ

Др Станислава Стошић-Грујичић,
научни саветник

МИНИСТАР

Младен Шарчевић

JGR Atmospheres

RESEARCH ARTICLE
10.1029/2021JD035093

Mineralogy Sensitive Immersion Freezing Parameterization in DREAM

Luka Ilić[1,2], Aleksandar Jovanović[1], Maja Kuzmanoski[1], Lazar Lazić[3], Fabio Madonna[4], Marco Rosoldi[4], Michail Mytilinaios[4], Eleni Marinou[5,6,7], and Slobodan Ničković[1,8]

[1]Institute of Physics Belgrade, University of Belgrade, Belgrade, Serbia, [2]Now at Barcelona Supercomputing Center, Barcelona, Spain, [3]Faculty of Physics, University of Belgrade, Belgrade, Serbia, [4]Consiglio Nazionale delle Ricerche – Istituto di Metodologie per l'Analisi Ambientale (CNR-IMAA), Potenza, Italy, [5]Institute for Astronomy, Astrophysics, Space Applications and Remote Sensing (IAASARS), National Observatory of Athens (NOA), Athens, Greece, [6]Department of Physics, Aristotle University of Thessaloniki (AUTH), Thessaloniki, Greece, [7]Institut für Physik der Atmosphäre, Deutsches Zentrum für Luft- und Raumfahrt, Oberpfaffenhofen, Germany, [8]Republic Hydormeteorological Service of Serbia, Beograd, Serbia

Key Points:

- Mineralogy-sensitive setup predicts spatial distribution of ice nucleating particle concentrations (INPC) in a dust plume in Mediterranean
- Mineralogy-sensitive prediction of INPC is within the range of mineralogy-indifferent ones and in agreement with measurements below −20°C
- Feldspar content in a dust plume affects ice initiation by around 6% at −35°C, and up to 17% at −25°C, but sedimentation reduces this effect

Supporting Information:

Supporting Information may be found in the online version of this article.

Correspondence to:

L. Ilić,
luka.ilic@ipb.ac.rs

Citation:

Ilić, L., Jovanović, A., Kuzmanoski, M., Lazić, L., Madonna, F., Rosoldi, M., et al. (2022). Mineralogy sensitive immersion freezing parameterization in DREAM. *Journal of Geophysical Research: Atmospheres*, *127*, e2021JD035093. https://doi.org/10.1029/2021JD035093

Received 19 APR 2021
Accepted 7 FEB 2022

Abstract Dust aerosols are abundant in the atmosphere and are very efficient ice nucleating particles at temperatures below −15°C. Depending on temperature, dust particles containing certain minerals (i.e., feldspar and quartz) are the most active as ice nuclei. A mineralogy-sensitive immersion freezing parameterization for ice nucleating particle concentration (INPC) is implemented in Dust Regional Atmospheric Model (DREAM) for the first time. Additionally, four mineralogy-indifferent parameterizations are implemented, two for immersion freezing and two for deposition nucleation. Dust concentration and its feldspar and quartz fractions are forecasted by DREAM for a dust episode in the Mediterranean in April 2016. DREAM results are compared with vertical profiles of cloud-relevant dust concentrations and INPC from ground-based lidar measurements in Potenza, Italy and Nicosia, Cyprus. INPC predictions are also compared with vertical profiles of ice crystal number concentration (ICNC) from satellite observations for two overpasses over the dust plume. The model successfully simulates the evolution and vertical extent of the dust plume. Mineralogy-sensitive and mineralogy-indifferent INPC parameterization results generally differ by about an order of magnitude. Forecasted INPC and observed ICNC values differ by an order of magnitude for all parameterizations. Feldspar fraction increase within a dust plume during transport can increase INPC by around 6% at −35°C, and up to 17% at −25°C, but sedimentation can reduce this effect. Over the Atlantic, mineralogy-sensitive parameterization predicts horizontal distribution of clouds with higher probability of success, while in the Mediterranean; the results for different parameterizations show lower variability.

Plain Language Summary Supercooled water droplets in clouds can freeze at temperatures around −37°C. Dust particles immersed in water droplets can enhance formation of ice crystals at higher temperatures. The efficiency of dust particles in ice initiation has been attributed to the presence of ice-active minerals, such as feldspar and quartz. In this work, we use a computer model (DREAM) to calculate how mineral dust particles from Sahara and Middle East are lifted and transported by the atmospheric flow. The model, includes equations that predict ice initiation depending on dust concentration and mineral composition, temperature and humidity. Atmospheric remote sensing observations from lidar and radar ground-based and satellite platforms provide information about vertical structures of dust plumes, their horizontal extent, and estimations of the dust particle and ice crystal concentrations in the atmosphere. We simulate a dust plume development in Mediterranean in April 2016 and compare results with data from lidar stations (in Potenza, Italy and Nicosia, Cyprus) and from satellites. DREAM successfully predicts horizontal and vertical extent of the dust plume and provides good estimations of ice initiation. Feldspar, the most efficient mineral in ice initiation, is mostly present in larger particles and can be more easily deposited during atmospheric transport.

1. Introduction

Interaction between aerosols and clouds is one of major sources of uncertainty in climate modeling and numerical weather prediction (Boucher et al., 2013). Particles in the atmosphere have a large influence on the physical properties of clouds and their interaction with radiation, latent heat release, precipitation and cloud electrification

(Kanji et al., 2017; Lohmann & Feichter, 2005). Aerosols, interacting with clouds, serve as cloud condensation nuclei (CCN) or ice nucleating particles (INP). Homogeneous freezing of supercooled liquid droplets in the atmosphere becomes increasingly important with decreasing temperature, while the droplets can be supercooled to temperatures below about −37°C (Herbert et al., 2015; Ickes et al., 2015). These temperature conditions and high ice saturation ratios are usually reached only in the upper troposphere. In higher temperatures, clouds typically glaciate at lower supercooling by heterogeneous nucleation on INPs (Hoose & Möhler, 2012; Murray et al., 2012; Pruppacher & Klett, 1997; Vali et al., 2015). Heterogeneous ice nucleation can take place directly on the aerosol surface by deposition of water vapor molecules through the deposition nucleation process. Near the water saturation level, water can condense in particle pores and freeze at low temperatures by the pore condensation and freezing mechanism (Marcolli, 2014; Wagner et al., 2016). Above the water saturation, supercooled droplets are formed and can freeze by an aerosol particle immersed in the droplet by the immersion freezing (Madonna et al., 2009). A particle colliding with the droplet can induce contact nucleation (Vali et al., 2015). Finally, particles can act as CCN and INP, at almost the same time and at the same temperature which is named condensation freezing.

Findings from field experiments, modeling and laboratory studies suggest that mineral dust particles are very efficient INPs even in regions distant from the desert sources (Cziczo et al., 2013; Hoose & Möhler, 2012; Murray et al., 2012). The sources of mineral dust transported to the Mediterranean basin are mainly located in the Sahara Desert (Tegen & Fung, 1994). The significance of mineral dust in ice initiation has led to the development of parameterizations of ice nucleation due to dust particles by mechanism of immersion freezing and deposition nucleation (DeMott et al., 2015; Niemand et al., 2012; Schrod et al., 2017; Ullrich et al., 2017). These parameterizations provide the dust ice nucleating particle concentration (INPC) as a function of cloud-relevant dust concentrations and meteorological parameters, without an explicit differentiation of the dust mineral components.

Furthermore, several studies focus on the influence of dust mineral composition on its ice nucleating ability (Atkinson et al., 2013; Harrison et al., 2016, 2019; Zolles et al., 2015). Atkinson et al. (2013) developed an INPC parameterization applicable in atmospheric models for several minerals typically present in dust. They used the parameterization based on these results in the Global Model of Aerosol Processes (GLOMAP) model (Mann et al., 2010) and showed that feldspar-containing particles are among the most important ice nuclei at temperatures lower than −15°C. Vergara-Temprado et al. (2017) found that feldspar particles are prevailing INPs near terrestrial sources, while marine organic aerosol (Wilson et al., 2015) are dominant INP in remote ocean locations. Further investigation confirmed that K-feldspars are generally very efficient ice nuclei although some alkali feldspars may have high nucleating abilities with implications on INPC prediction (Harrison et al., 2016). Quartz, as a major component of atmospheric mineral dust (Glaccum & Prospero, 1980), has been studied as a potential INP contributor and has proven to be active as an INP as well (Holden et al., 2019, 2021; Zolles et al., 2015). Harrison et al. (2019) analyzed the relative importance of quartz to feldspars in immersion ice nucleation, and as a result, developed new INP parameterizations for feldspar and quartz concentrations. Boose et al. (2016) found correlation between ice nucleating ability of nine desert dust samples and K-feldspar concentrations. Based on their findings, they suggest that improvement in numerical dust model INPC predictions should be achieved by simulations of feldspar and quartz concentrations in the atmosphere and use of relevant mineralogy-sensitive INP parameterizations.

Mineralogy-indifferent INPC parameterizations have been applied in weather models to estimate the INPC abundance in the atmosphere (Nickovic et al., 2016; Niemand et al., 2012). Furthermore, only a few weather or climate models forecast dust concentration and routinely use it in an online INPC calculation (e.g., Hande et al., 2015; Nickovic et al., 2016; Su & Fung, 2018). The INPC estimations for a small fraction of these models have been compared with ground-based in situ concentration measurements (Atkinson et al., 2013; Niemand et al., 2012; Vergara-Temprado et al., 2017) and with vertical profiles of cloud ice retrieved from ground-based or satellite observations (Nickovic et al., 2016; Su & Fung, 2018).

Remote sensing measurements are a crucial information source for the validation of model results. Ground based lidars and cloud radars with high temporal and vertical resolution can be used to investigate the relationship between aerosols and clouds (Illingworth et al., 2007; Seifert et al., 2010) and have been used frequently for model evaluations (e.g., Tsikerdekis et al., 2017; Solomos et al., 2017, 2019; Georgoulias et al., 2018; Konsta et al., 2018; Kampouri et al., 2021; Varlas et al., 2021). Aerosol optical depth from the Aerosol Robotic Network (AERONET; Holben et al., 1998) has been used to validate dust models (Basart et al., 2012; Gama

et al., 2015) and is routinely used in the frame of Sand and Dust Storm Warning Advisory and Assessment System (SDS-WAS) project (WMO, http://www.wmo.int/sdswas). Synergistic lidar and AERONET data are used with methodologies developed within the European Aerosol Research Lidar Network (EARLINET; Pappalardo et al., 2014) to provide dust-relevant lidar profiles (total dust, fine or coarse mode concentrations) which are suitable for the evaluation of dust models (Binietoglou et al., 2015). Binietoglou et al. (2015) used coarse-spheroid concentrations derived with the LIRIC algorithm (Lidar-Radiometer Inversion Code; Chaikovsky et al., 2016) to evaluate four regional dust transport models. POLIPHON approach (Polarization Lidar Photometer Networking) has been developed to provide dust concentrations (Ansmann et al., 2011, 2012). Papayannis et al. (2014) retrieved and intercompared lidar-derived dust mass concentrations from two different synergistic methodologies, LIRIC and POLIPHON, highlighting the advantage of POLIPHON to provide dust concentration profiles in cloud-free conditions and in presence of thin clouds, as it does not require spatio-temporally collocated lidar and AERONET measurements. In recent years, the POLIPHON method has been extended to derive cloud-relevant aerosol concentrations from lidar measurements, used then as input in mineralogy-indifferent INPC parameterizations (Ansmann, Mamouri, Hofer, et al., 2019; Mamouri and Ansmann, 2015, 2016; Marinou et al., 2019). Marinou et al. (2019) performed inter-comparison of lidar-derived cloud-relevant dust concentrations with in situ measurements on-board un-manned aerial systems. Particle concentrations show good agreement within the measurement uncertainties for the majority of analyzed cases. In this study, we implement for the first time a mineralogy-sensitive INPC parameterization into a regional coupled atmosphere dust numerical model. We implement the feldspar and quartz parameterizations (Harrison et al., 2019) in the DREAM model (Nickovic et al., 2016) and perform simulations for a Saharan dust episode in the Mediterranean during April 2016. Using the model results, we quantify the relative contribution of feldspar and quartz to total INPC and compare these results with parameterizations that do not explicitly take mineral composition into consideration. We compare the model results with the retrieval of remote sensing observations performed during the INUIT-BACCHUS-ACTRIS experiment (Mamali et al., 2018; Marinou et al., 2019; Schrod et al., 2017).

The paper starts with the description of the DREAM model and INPC parameterizations implemented in the model in Section 2.1. It is followed by Section 2.2 with a description of the observational datasets and algorithms used. In Section 3.1 the model is compared with vertical profiles of dust mass, number and surface area concentrations from the ground-based lidars. INPC parameterizations used in the model are also compared in this section. In Section 3.2 the model results are compared with ice crystal number concentrations (ICNC) retrieved from DARDAR (raDAR/liDAR) products (Delanoë & Hogan, 2010) in the cross-section of the dust plume in the Mediterranean Basin. In Section 3.3 we show the horizontal distribution of mineral fractions and the integrated INPC profiles output from the DREAM model. The paper concludes with summary and conclusions.

2. Methodology

2.1. Modeling

2.1.1. Dust Regional Atmospheric Model (DREAM)

The Dust Regional Atmospheric Model (DREAM) (Nickovic, 2005; Nickovic et al., 2001; Pejanovic et al., 2012; Vukovic et al., 2014) is an atmospheric dust cycle model, including emission, horizontal and vertical turbulent mixing, large scale transport and deposition. DREAM forecasts are part of the SDS-WAS project. DREAM is coupled with the Nonhydrostatic Mesoscale Model (NMM), as an atmospheric driver, so that they share the same time step and dust is transported as a passive tracer. It is possible for the DREAM model to assimilate ECMWF (European Centre for Medium-Range Weather Forecasts) dust analysis in the initial dust field (Binietoglou et al., 2015). The DREAM model used in this study does not assimilate the dust field. Instead, DREAM was initiated with dust concentrations set to zero ("cold-start") several days before the studied period. Thus allowing the model to develop meaningful dust concentration field at the date considered as the effective model start ("warm up") (Nickovic et al., 2016). Dust emission parameterization includes a viscous sub-layer between the surface and the lowest model layer (Janjic, 1994) in order to parameterize the turbulent vertical transfer of dust into the lowest model layer following different turbulent regimes (laminar, transient and turbulent mixing). Dust productive areas are at grid points which are described as barren and arid soils. After the emission, dust is transported by horizontal and vertical advection and horizontal and vertical turbulent diffusion processes described by the atmospheric model. The wet dust removal is proportional to the rainfall rate (Nickovic et al., 2001). Rainfall can be produced by convective cloud scheme (Janjic, 1994) and by the Ferrier et al. (2002) grid-scale cloud

microphysics scheme in NMM. The Ferrier et al. (2002) scheme is not aerosol-friendly, which means that it does not take forecasted aerosol concentrations as an input to cloud process calculations. The dry deposition on the Earth surface is parameterized according to the scheme of Georgi (1986). This scheme includes processes of deposition by surface turbulent diffusion and Brownian diffusion, gravitational settlement, and interception and impaction on the surface roughness elements. Particles are distributed in 8 size bins with effective radii of 0.15, 0.25, 0.45, 0.78, 1.3, 2.2, 3.8 and 7.1 μm. Size limits of the 8 bins are: 0.1–0.18, 0.18–0.3, 0.3–0.6 and 0.6–1.0 μm, for the clay fraction, and 1.0–1.8, 1.8–3.0, 3.0–6.0 and 6.0–10.0 μm, for the silt fraction (Pérez et al., 2006). A version of the DREAM model has been also developed to simulate mineral fractions of dust aerosol (Nickovic et al., 2001, 2013). Ratios of eight minerals typical for dust are specified on the model grid at dust sources based on GMINER30 gridded database (Nickovic et al., 2012). GMINER30 provides mineral fractions of illite, kaolinite, smectite, calcite, quartz and hematite in clay size fraction. For the silt, size fraction, feldspar, gypsum, calcite, quartz and hematite mineral fractions are available in the database.

In this study the DREAM model was set up with a domain covering Saharan and Middle Eastern dust sources and dust transport in the Mediterranean (Figure S1 in the Supporting Information S1). The model is run with 0.1×0.1 horizontal resolution and 28 vertical levels. Dust-productive areas are defined using USGS (United States Geological Survey) land cover data combined with sources originating from sediments in paleo-lake and riverine beds (Ginoux et al., 2001; Nickovic et al., 2016). Grid points identified as dust-productive are overlapped with dust mineral composition data from GMINER30 database. Dust source masks are calculated by multiplying the silt and clay fractions in model grid points (Nickovic et al., 2001) by mineral fractions based on GMINER30 data in those grid points. Mineral fractions of dust, in our case those for feldspar and quartz, and total dust mass concentrations in the atmosphere are simulated for each of the 8 size bins (Nickovic et al., 2016). The particle number concentrations with radius greater than 250 nm and the surface area concentrations are calculated using the modeled effective radii for each size bin and mineral fraction. The clay fraction in GMINER30 does not include feldspar, although there is observational evidence of its presence in the atmosphere (Kandler et al., 2009). To estimate feldspar fraction in clay, we use the same quartz-to-feldspar ratio as considered for silt-sized particles (Atkinson et al., 2013). Samples from feldspar group of minerals can have different ice nucleation abilities, depending on the source (Harrison et al., 2016). Boose et al. (2016) found that in their samples, at temperatures above −23°C ice-nucleating activity can be attributed to K-feldspar. At lower temperatures, quartz and sum of all feldspars should be considered. Dust source masks, feldspar and quartz source masks in the model domain are shown in Figure S1 in the Supporting Information S1.

2.1.2. Ice Nucleating Particle Concentration Parameterizations

There are several dust-dependent INPC parameterizations for immersion freezing at or above water saturation (DeMott et al., 2015; Niemand et al., 2012; Ullrich et al., 2017) and deposition nucleation at ice supersaturation (Steinke et al., 2015; Ullrich et al., 2017). Furthermore, mineralogy-sensitive parameterizations for the immersion freezing regime are available by Atkinson et al. (2013) and Harrison et al. (2019). In this work, we use three different model setups to parameterize the INPC for immersion and deposition freezing.

In this study, we use the mineralogy-sensitive parameterization by Harrison et al. (2019) (H19i) to address immersion freezing and the mineralogy-indifferent deposition nucleation parameterization (Ullrich et al., 2017) (U17d). This setup is addressed as H19i_U17d herein. H19i quantifies INPC for feldspar and quartz minerals. In order to quantify the importance of feldspar and quartz as INPs, the mineralogy-sensitive immersion freezing parameterization is used under the assumption of external mixing of particles consisting of different minerals. The concentration of each mineral fraction forecasted by DREAM directly influences the number of particles available for ice initiation in each size bin (Atkinson et al., 2013). Using dust, feldspar and quartz concentrations, total INPC can be calculated as a sum for all size bins. Harrison et al. (2019) proposed a nucleation site density parameterization for quartz, K-feldspar, plagioclase and albite. They found that their parameterization for K-feldspar is a better representati of INPC related to dust than those by Niemand et al. (2012) and Atkinson et al. (2013). In this study we apply the INPC parameterizations for the K-feldspar, plagioclase and albite fractions separately (Harrison et al., 2019). INPC contribution of feldspar is then calculated as the sum of the INPC contributions from the three types of feldspar represented in the parameterizations. The GMINER30 database used in this work provides information about feldspar fraction at dust productive areas. It does not include the detailed information about fractions of K-feldspar, plagioclase and albite in dust sources. We assume that based on compiled measurement data (Atkinson et al., 2013), K-feldspar accounts for 35% of total feldspar, with 65% being plagioclase. We

consider albite to be a part of plagioclase as it is often done when discussing atmospheric mineral dust content (Harrison et al., 2019). Following the parameterization by Harrison et al. (2019), we consider albite to be 10% of plagioclase. Having in mind these feldspar components, and the fact that GMINER30 does not differentiate between them, in the further text, we refer to them as feldspar. Harrison et al. (2019) parameterizations for quartz and feldspar minerals with valid temperature ranges and standard deviations for log (n_s(T)) (n_s is in units of cm^{-2}) given in brackets, are the following:

Quartz: (−10.5 °C to −37.5 °C; σ=0.8);

$$\log\left(n_s(T)\right) = -1.709 + \left(2.66 \times 10^{-4} T^3\right) + \left(1.75 \times 10^{-2} T^2\right) + \left(7 \times 10^{-2} T\right) \quad (1)$$

K−feldspar: (−3.5 °C to −37.5 °C; σ=0.8)

$$\log\left(n_s(T)\right) = -3.25 + (-0.793T) + \left(-6.91 \times 10^{-2} T^2\right) + \left(-4.17 \times 10^{-3} T^3\right) + \left(-1.05 \times 10^{-4} T^4\right)\left(-9.08 \times 10^{-7} T^5\right) \quad (2)$$

plagioclase feldspar: (−12.5 °C to −38.5 °C; σ=0.5);

$$\log\left(n_s(T)\right) = \left(-3.24 \times 10^{-5} T^4\right) + \left(-3.17 \times 10^{-3} T^3\right) + \left(-0.106 T^2\right) + (-1.71T) - 12.00 \quad (3)$$

Albite: (−6.5 °C to −35.5 °C; σ=0.7);

$$\log\left(n_s(T)\right) = \left(3.41 \times 10^{-4} T^3\right) + \left(1.89 \times 10^{-2} T^2\right) + \left(-1.79 \times 10^{-2} T\right) - 2.29 \quad (4)$$

Additionally, we use the setup of DREAM presented in Nickovic et al. (2016) (D15i_S15d), which is also used in daily operational dust and INPC forecasts in Republic Hydrometeorological Service of Serbia. In that model, the immersion parameterization by DeMott et al. (2015) and the deposition nucleation parameterization by Steinke et al. (2015) (S15d) are used. In another mineralogically indifferent setup, we use the parameterizations provided by Ullrich et al. (2017) (U17) to address the immersion freezing and deposition nucleation (U17i and U17d, respectively). U17i and U17d, as well as S15d parameterizations, are based on laboratory studies performed within the AIDA cloud chamber (Aerosol Interaction and Dynamics in the Atmosphere) of the Karlsruhe Institute of Technology. U17i and U17d are based on desert dust samples collected from Sahara, Taklamakan Desert, Canary Islands and Israel. S15d parameterization is based on dust samples which showed an enhanced freezing efficiency in the deposition mode. The INPC parameterizations have been applied without any mathematical smoothing at the transition temperatures between immersion freezing and deposition nucleation parameterizations (Nickovic et al., 2016). Marinou et al. (2019) analysis of five cases in the Mediterranean showed that the U17d parameterization is able to provide dust INPC results in agreement with in situ observations, while S15d parameterization overestimates the dust INPC abundance 3–4 orders of magnitude. For immersion mode, D15i INPC comparisons with in situ measurements show agreement within 1–2 orders of magnitude, while U17i show agreement within 2–3 orders of magnitude. When collocated ice crystal number concentrations (ICNC) were considered, the INPC predicted from the D15i and U17i parameterizations were in the lower and upper bounds of the observed ICNC.

All the INPC parameterizations with their valid temperature ranges and input parameters used in this study are summarized in Table 1. The parameterizations described above have been used in the model in three different setups:

1. The H19i_U17d setup, which is mineralogy-sensitive in immersion freezing mode, uses H19i parameterization for immersion freezing and U17d for the deposition mode;
2. The setup described by Nickovic et al. (2016), which uses D15i and S15d parameterizations for immersion freezing and deposition, respectively, and is denoted as D15i_S15d;
3. The third setup is based on immersion freezing parameterization U17i and deposition nucleation parameterization U17d from Ullrich et al. (2017), and is denoted as U17i_U17d.

In order to evaluate the expected contribution of feldspar and quartz to INPC in the model, as a result of mineralogy-sensitive model setup, we analyze their fractions in the source masks of the model domain (Figure S2 in the Supporting Information S1). The mean fractions and standard deviations for feldspar and quartz fractions in clay and silt, based on dust source grid points in the model domain, are shown in Table S1 in the Supporting

Table 1
Ice Nucleating Particle Concentrations Parameterizations Used in This Study, With References, List of Input Parameters, Temperature Ranges in Which the Parameterizations are Used

Parameterization	Reference	Freezing mode	Input parameters	T range [°C]
H19i	Harrison et al. (2019)	Immersion	K-feldspar S_d, T plagioclase S_d, Talbite S_d, Tquartz S_d, T	−37.5 to −3.5−38.5 to −12.5−35.6 to −6.5−37.5 to −10.5
D15i	DeMott et al. (2015)	Immersion	Dust n_{250}, T	−36.0 to −5.0
S15d	Steinke et al. (2015)	Deposition	Dust S_d, T	−55.0 to −36.0
U17i	Ullrich et al. (2017)	Immersion	Dust S_d, T	−30.0 to −14.0
U17d	Ullrich et al. (2017)	Deposition	Dust S_d, T	−67.0 to −33.0

Information S1. The mass size distribution at the sources is assumed to be monomodal lognormal (Pérez et al., 2006; Zender et al., 2003), as used in DREAM. The INPC fraction has been calculated based on H19i for quartz fraction (H19iQ) and feldspar fraction (H19iF). Additionally, H19iF is calculated for the case in which there is no feldspar in the clay fraction. When analyzing quartz contribution, it should be noted that the H19iQ parameterization should be considered as an upper limit in quartz contribution to INPC: it is valid for freshly milled quartz while the active sites on quartz are removed upon exposure to air and water (Harrison et al., 2019; Zolles et al., 2015). In this analysis, feldspar is the dominant INP source, with the highest fraction of feldspar INPs at around −25°C as expected due to K-feldspar activity. At higher temperatures quartz contributes to about 7% of INPC. At temperatures above −10.5°C, parameterization for quartz is not defined. At temperatures below −25°C, quartz contribution becomes increasingly important with decrease of temperature. This contribution is up to 30% at −35°C when feldspar is present in clay particles, and increases to 51% under the assumption of no feldspar in clay particles. These results agree with findings of Boose et al. (2016). They show that at temperatures between the homogeneous freezing limit and −33°C quartz can be a significant contributor to INPC.

2.2. Observations

2.2.1. Aerosol Observations and Retrievals

Data from two ground-based lidar measurement sites, at Potenza, Italy and Nicosia, Cyprus, are considered in our study. MUSA (Multiwavelength System for Aerosol) is a mobile multi-wavelength Raman lidar system located in the CNR-IMAA Atmospheric Observatory (CIAO) in Tito Scalo, 6 km far from Potenza, Southern Italy, on the Apennine Mountains (40.60 N, 15.72 E, 760 m a.s.l.) (Madonna et al., 2011). The site is in a plain surrounded by low mountains (<1,100 m a.s.l.). The PollyXT-NOA lidar system (Baars et al., 2016; Engelmann et al., 2016) is a multiwavelength Raman lidar system of the National Observatory of Athens (NOA). During spring 2016, and for the objectives of the INUIT-BACHUSS-ACTRIS experiment, the system was collecting measurements at The Cyprus institute in Nicosia (35.14 N, 33.18 E; 181 m a.s.l.). Both instruments operate within EARLINET (European Aerosol Research Lidar Network) and in the frame of the European ACTRIS-RI (Aerosols, Clouds, and Trace gases Research Infrastructure). Measurements performed during the presence of thick dust layers above the stations are used in this study. Specifically, we use the observations on 18 April 2016 in Potenza and the observations on 21 April 2016 in Nicosia. Vertical profiles of particle backscatter coefficient and linear depolarization ratio at 532 nm have been retrieved: using (a) the EARLINET Single Calculus Chain (SCC) (D'Amico et al., 2016; Mattis et al., 2016) with a vertical resolution of 60 m and temporal integration of 100 min for the Potenza lidar; (b) using the PollyNET algorithm (Baars et al., 2016) with a temporal integration of 30 min and vertical resolution of 7.5 m for the PollyXT-NOA lidar. The different integration time in the lidar observations is due to the need to keep a balance between the homogeneity of the observed aerosol layer in the selected time window and the signal-to-noise ratio for the lidar retrievals.

The profiles of concentrations of dust particles with radii >250 nm (n_{250}) and dust dry particle surface area concentrations (S_d) are calculated from the aerosol extinction coefficient profiles using the POLIPHON algorithm and AERONET-based parameterizations. POLIPHON algorithm can be applied to lidar profiles from both ground based and spaceborne instruments and, using the particle depolarization ratio signature of dust, is able to separate the contribution of mineral dust from the total aerosol load. In the first step, the algorithm

uses the profiles of thelinear particle depolarization ratio to separate dust and non-dust backscatter profiles by means of physical thresholds of dust and non-dust particles (0.31 ± 0.04 for dust and 0.05 ± 0.03 for the non-dust component; Ansmann et al., 2011; Baars et al., 2016; Freudenthaler et al., 2009; Groß et al., 2011; Groß et al., 2013; Haarig et al., 2017; Müller et al., 2007; Veselovskii et al., 2016) according to the dust separation method described (among others) by Tesche et al. (2009) and Groß et al. (2011). Then, the vertical profiles of dust backscattering coefficient is converted to dust extinction coefficient assuming appropriate values of dust lidar ratio (45 ± 10 sr for Saharan dust at 532 nm; Müller et al., 2007; Nisantzi et al., 2015; Tesche et al., 2011; Veselovskii et al., 2016). The parameters used for the conversion of particle extinction coefficients into cloud-relevant dust number, surface area and volume concentrations are based on AERONET measurements and described by Ansmann, Mamouri, Bühl, et al. (2019), Ansmann, Mamouri, Hofer, et al. (2019). POLIPHON algorithm is applied to the lidar profiles from Potenza and Nicosia taking into consideration the conversion factors for North African and Cyprus AERONET sites, respectively. Uncertainties in the SCC retrieved products, as well as in dust and non-dust linear depolarization ratio, dust lidar ratio and conversion factors have been propagated through all the steps of the POLIPHON algorithm. The uncertainties in the products are as follows: the dust extinction coefficients can be obtained with uncertainty of the order of 20%–40%, while the uncertainty in the microphysical parameters is of the order of 20%–50% for the dust component (Marinou et al., 2019). To provide INPC estimations, meteorological parameters (i.e., temperature and humidity) are also required as input. For the lidar retrievals, these parameters are used from the operational systems GDAS (Global Data Assimilation System) of the National Weather Service's National Centers for Environmental Prediction (NCEP) Ansmann, Mamouri, Hofer, et al., 2019; Marinou et al., 2019).

Additionally, in situ measurements of INP samples, collected using UAVs during the INUIT-BACHUSS-ACTRIS experiment, and analyzed with the FRIDGE (FRankfurt Ice nucleation Deposition freezinG Experiment) INP counter (Schrod et al., 2016, 2017) are used in comparison with the modeled INPC. A detailed presentation and description of the UAV-FRIDGE data from this campaign is provided in Schrod et al. (2017), and for the samples used in our work in Marinou et al. (2019). In brief, FRIDGE is an isostatic diffusion chamber, which allows measurements at temperatures down to −30°C and relative humidity up to water supersaturation. And encompass ice nucleation by deposition nucleation plus condensation/immersion freezing. Measurements during an intercomparison experiment with controlled laboratory settings showed that the method compares well to other INP counters for various aerosol types (DeMott et al., 2018). The errors of the INP measurements used were estimated to be ∼20% considering the statistical reproducibility of an individual sample, for the samples used here.

2.2.2. Cloud Radar Observations and Cloudnet Retrievals

CIAO is a Cloudnet station (Stephens et al., 2002; https://cloudnet.fmi.fi) equipped with near infrared ceilometers (Vaisala CT25k and Jenoptik CHM15k), a microwave radiometer (Radiometrics MP3014) and a Ka-band pulsed polarimetric Doppler radar (Metek Mira 36). All datasets from these instruments are processed using the Cloudnet algorithm (Illingworth et al., 2007), interpolated on the radar time and height resolution on a common grid of 30 s and 30 m in height. By exploiting the synergy between lidar and radar, for each range gate the various target types, such as hydrometeors forming clouds and precipitation (liquid droplets, ice crystals, drizzle, rain), aerosols and insects are categorized. The target categorization is a fundamental input to retrieve liquid water content (LWC) and ice water content (IWC) profiles, with the same resolution of observations. IWC is estimated using the approach by Hogan et al. (2006) from radar reflectivity and temperature from the ECMWF forecast model using a power relationship between IWC and radar reflectivity at 36 GHz. The formula is only applied when the target is composed of ice, according to the target categorization. The retrieval is not reliable above rain or melting ice when attenuation cannot be estimated accurately.

2.2.3. Satellite Products and the DARDAR Retrieval

The DARDAR retrieval uses collocated CloudSat, CALIPSO, and MODIS measurements to provide an ice cloud retrieval product (Delanoë et al., 2014) on a 60 m vertical and 1.1 km horizontal resolution. DARDAR ice crystal concentration product (DARDAR-Nice) offers satellite retrievals of ice crystal concentration profiles obtained from combined lidar-radar measurements (Delanoë & Hogan, 2010). This product is limited to ice clouds with an IWC larger than 10^{-8} kg m^{-3}. Particle size distribution is integrated from 3 minimum size thresholds corresponding to particles larger than 5, 25 and 100 μm. Retrievals obtained within mixed-phase clouds are flagged and have larger uncertainties. DARDAR-Nice has been evaluated against theoretical considerations and a large

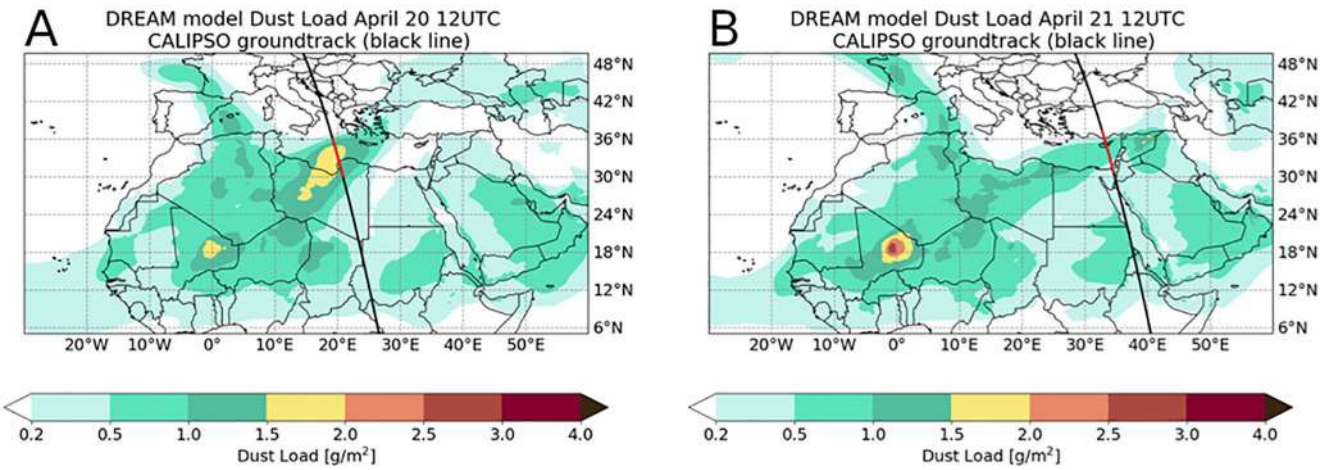

Figure 1. Dust Regional Atmospheric Model simulated dust load (shaded contours) and A-Train constellation track (black and red line) for 20 April at 12UTC during overpass A (a) and 21 April at 12UTC during overpass B (b). Red part of the satellite track indicates the cross section used in the comparisons with DARDAR products.

amount of in situ measurements and its estimates are expected to have uncertainties from 25% up to 50% (Sourdeval et al., 2018). Concerning the overestimation of ICNC in cloud parcels warmer than about −30°C, due to the assumption of a monomodal gamma particle size distribution (PSD) shape in the current method, can increase the uncertainties by an additional 50%. Following the results of Marinou et al. (2019), which show that DARDAR-Nice falls between D15i and U17i INPC estimations derived from POLIPHON results, we compare the DREAM INPC predictions with DARDAR ICNC products in mixed-phase clouds. To examine how the model predicts the horizontal distribution of cold clouds, the ice water path (IWP) from the CLAAS-2 data set was used (Nickovic et al., 2016). A comprehensive evaluation of CLAAS-2 results is presented in Benas et al. (2017). Cloud properties are retrieved from the SEVIRI (Spinning Enhanced Visible and InfraRed Imager) instrument onboard METEOSAT second generation (MSG). SEVIRI data are available with 15 min temporal and ∼4 km spatial resolution (Stengel et al., 2014). In order to ensure the homogeneity of the data set, the solar SEVIRI channels of MSG-1, MSG-2 and MSG-3 were inter-calibrated (Meirink et al., 2013) with MODIS Aqua before applying the cloud retrievals.

3. Results and Discussion

The efficiency of dust as INP is investigated for the case of dust advection above the Mediterranean between 18 and 21 April, 2016 (Figure 1 and Figure S3 in the Supporting Information S1). The outputs from the DREAM model are compared against the ground-based measurements at Potenza on 18 April and at Nicosia on 21 April 2016. Both ground-based sites observed the Saharan dust during this period, along with occasional formation of mixed-phase and cold clouds. The dust plume overpassed Potenza first and then Nicosia, after being advected eastward. Comparison with satellite observations of the dust plume on 20 and 21 April is performed, as well. In the first part of the analysis, we use aerosol subtyping products from CALIPSO and ground-based lidar measurements to qualitatively evaluate the DREAM dust forecast and its implications on INPC estimations. In the second part we compare the INPCs predicted from the DREAM model with the retrieved DARDAR-Nice product.

Figure 1 shows the dust plume, as simulated by the DREAM model, and the two A-train satellite overpasses (A and B) during the episode. The overpass A was on 20 April at 12 UTC over central-south Mediterranean and the overpass B was on 21 April at 12 UTC over Cyprus. In Figure 2, the dust mass concentration from the DREAM model is compared to CALIPSO aerosol subtype products for the two overpasses. CALIPSO detected both the dust particles and clouds present in the top of the dust layers in both cases. Additional presence of some pollution in the dust layers of overpass B is also observed. The DREAM model successfully forecasted the dust advection (in space, top height and time) as shown in the vertical cross sections of the dust plume. CALIPSO products show that there are also marine and dusty-marine (marine and dust) particles present in the lower troposphere of overpass A.

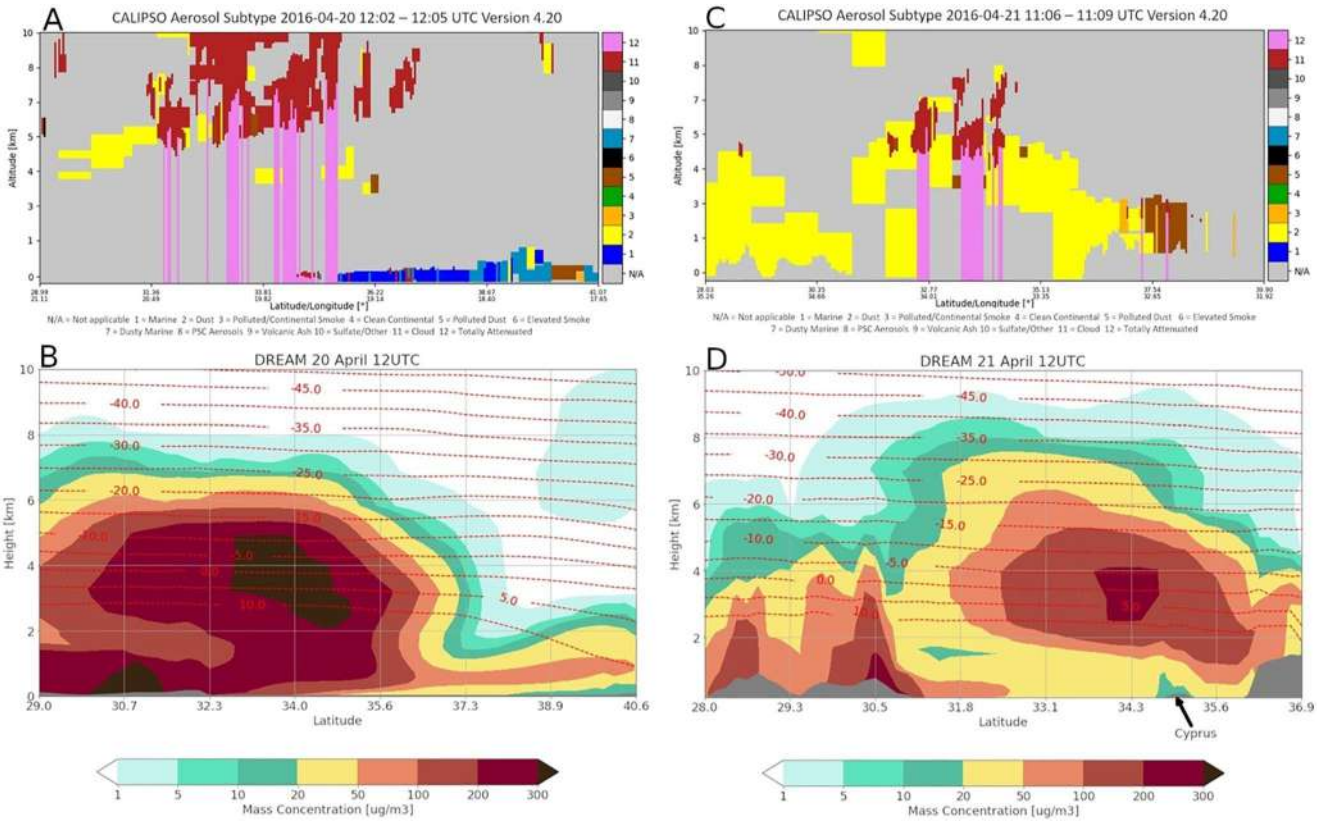

Figure 2. CALIPSO aerosol subtype and cloud presence products (a and c) and Dust Regional Atmospheric Model vertical cross section of dust concentrations (b and d) with isotherms (dashed red lines), along the satellite path during overpass A on 20 April and during overpass B on 21 April.

3.1. Comparison With POLIPHON Concentrations

DREAM predictions of mineral dust concentration have been compared against POLIPHON dust retrievals for three cases: above Potenza on 18 April at 15 UTC (Po) (Figure 3 and Figure S4 in the Supporting Information S1), and above Nicosia on 21 April at 3 UTC (Ni 1) and at 15 UTC (Ni 2) (Figure 5 and Figure S7 in the Supporting Information S1). DREAM outputs are available every 3h, therefore we used the nearest DREAM output in time to the POLIPHON products. Since the maximum possible difference between measurement times and DREAM output time is less than 3 hr, for each studied case we estimate the variability of the DREAM model results is represented by the profiles from ±3 hr of the observation times. The uncertainties of POLIPHON products are described in the previous section. Table 2 provides quantitative comparison of vertical profiles of dust concentration and their geometrical properties. We calculate the center of mass (CoM), the correlation coefficient as a function of height, the column mass concentration and its peak concentration from mass concentration profiles from both DREAM and POLIPHON. As model and lidar data are available on different vertical resolutions, we linearly interpolate POLIPHON products and DREAM outputs to 100 m vertical resolution. The comparison metrics calculated from interpolated values vary by less than 1% from the calculations on native resolutions. Due to the presence of clouds, some POLIPHON profiles do not have data at height levels above 6 km: therefore, we derive the evaluation metrics based on data points where both DREAM and POLIPHON are available. Additionally, we provide CoM and column mass concentrations for the whole DREAM vertical extent. We apply mineralogy-indifferent INPC parameterizations D15i, S15d, U17i and U17d to POLIPHON retrievals and DREAM dust concentrations. The total dust concentration simulated in all the three experiments is the same, since it is based on the same sources. Total dust concentration is used as input to mineralogy-indifferent parameterizations. Feldspar and quartz concentrations are used as input to mineralogy-sensitive parameterization. Additionally, we apply mineralogy-sensitive H19i parameterization to DREAM feldspar and quartz concentrations. Mamali et al. (2018) found agreement within uncertainty limits between POLIPHON retrievals of dust concentration and optical particle counter (OPC) measurements aboard unmanned aerial vehicles (UAV) within dust layers mixed

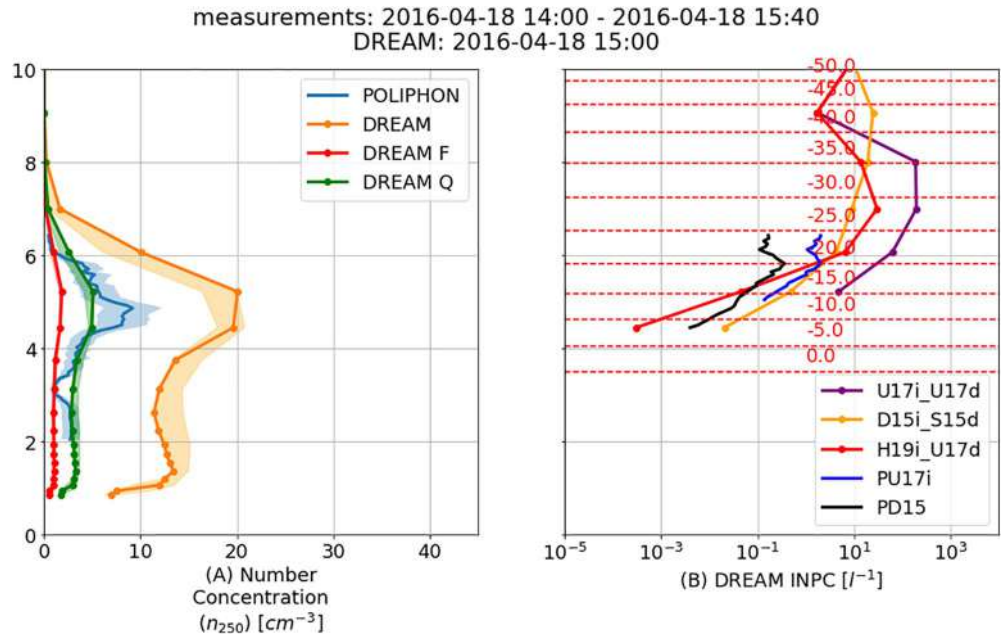

Figure 3. POLIPHON and Dust Regional Atmospheric Model profiles of dust n_{250} number concentration (a). F and Q indicate feldspar and quartz concentrations. Ice nucleating particle concentration for the three model setups and two immersion parameterizations used with POLIPHON data (b), for 18 April 2016 at 15UTC above Potenza station.

with near spherical particles and continental/pollution particles. They consider that the two techniques can be used interchangeably and systematically with numerical models. Marinou et al. (2019) reported that DeMott et al. (2015) and Ullrich et al. (2017) parameterizations applied to POLIPHON retrievals agree within the uncertainty range in the immersion range and within one order of magnitude for deposition range, with the results derived from UAV measurements. Based on these findings we compare DREAM and POLIPHON cloud-relevant dust concentrations and INPC. The results are discussed for each case in the next section.

3.1.1. Potenza, April 18

During the first hours of the lidar measurements in Potenza on 18 April, a thick Saharan dust layer was detected, between 4 and 6 km a.s.l. (above sea level), with clouds embedded in it, while cirrus clouds were present during the complete measurement period at altitudes between 7.5 and 12 km (Figure S5a in the Supporting Information S1). Figure 3 shows comparison of vertical profiles of dust concentrations and INPC from POLIPHON and DREAM on 18 April. DREAM simulation of the dust episode above Potenza starting on 16 April until 19 April is shown in Figure S5b in the Supporting Information S1. It is evident that although the maximum dust concentrations are observed at height of 5 km, dust is present even at lower heights with concentrations of ∼30% to the peak concentration. Potenza lidar, located at 760 m asl, provides measurements from 2 to 6 km.

Maximum dust concentrations during the lidar measurements are simulated at the height of 5 km in agreement with the lidar range corrected signal (RCS) (Table 2, Figure 3). DREAM dust concentration profiles variability (±3 hr) results in dust CoM, column mass concentration and the peak concentration variabilities of 3%, 20% and 15% respectively. CoM comparisons and correlation coefficients show that the model successfully simulated the altitude of transported dust and its vertical distribution. When all the DREAM data points are included in the CoM calculation, the CoM is found at a lower height. In the Potenza case, the model overestimated both the column mass concentration and the peak concentration. Therefore, DREAM reasonably simulates the vertical extent but overestimates dust particle concentrations, and INPC, when compared with the results from lidar measurements. Figure 3 shows that the three DREAM INPC setups differ within one to two orders of magnitude in immersion range at temperatures lower than −20°C. At higher temperatures, the mineralogy-sensitive setup H19i_U17d underestimates INPC in comparison to D15i_S15d and U17i_U17d setups, as expected based on results presented in Figure S2 in the Supporting Information S1. Vertical profiles of feldspar and quartz fractions are analyzed (Figure S10 in the Supporting Information S1). Feldspar content is highest at 6 km height,

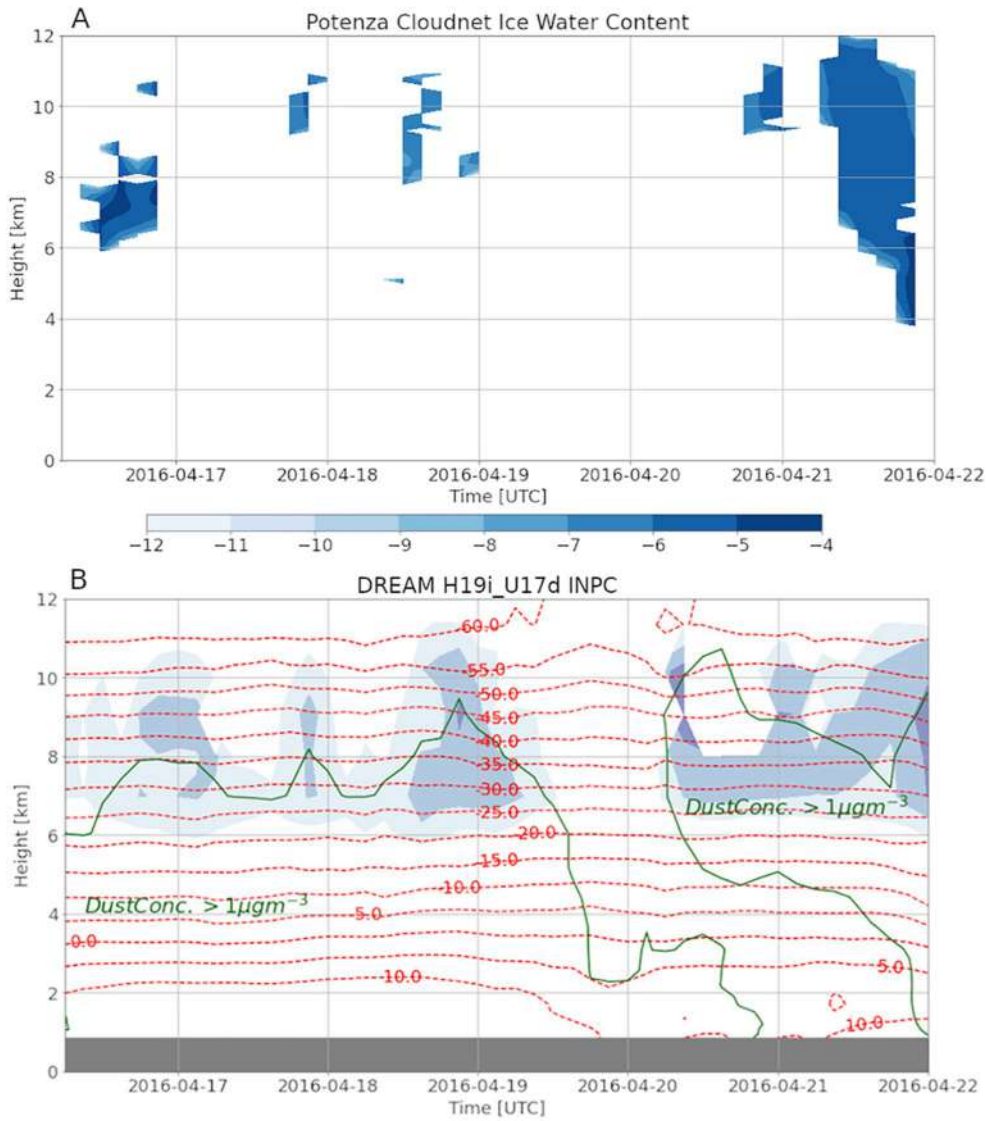

Figure 4. Ice water content retrieved in Potenza using the Cloudnet retrieval scheme coarsegrained to model resolution (a) and DREAM H19i_U17d INPC (b) from 16–22 April. Green contour line represents 1 μg/m^3 dust mass concentration.

accounting for 21% of total dust mass concentration and declines to about 16% near the surface. Quartz, which is less efficient than feldspar as an INP source, takes up a larger fraction of dust at lower heights. Potenza lidar provides retrievals up to 6 km height, and is used only in estimation of immersion mode INPC at temperatures higher than −25°C, at altitudes around maximum dust concentration. Overestimation of dust concentrations by DREAM compared to POLIPHON is around 100% (Table 2) and produces corresponding differences of one order of magnitude for INPC values predicted by D15i (setup D15i_S15d) and two orders of magnitude in INPC values for U17i (setup U17i_U17d). It should be noted that it has been shown that day-to-day variability of fine-mode dust mixing ratio is associated with ice occurrence frequency in clouds of 5%–10% (Villanueva et al., 2020). Additionally, difference in freezing efficiency of dust on Northern and Southern hemispheres was attributed to different mineral content of dust and specifically feldspar at −15°C.

Figure 4 shows the DREAM INPC (H19i_U17d) prediction (B) collocated with the Cloudnet IWC products in Potenza (A) for the period of 16–22 April. This is a qualitative analysis exploring DREAM INPC as an indicator of presence of dust in appropriate atmospheric conditions for cloud development. The presence of dust-laden air masses was found to berelated to cloud development above the Potenza station during the measurement period. During this period, two Saharan dust plumes reached Potenza. Due to westerly flow, the first one reached the

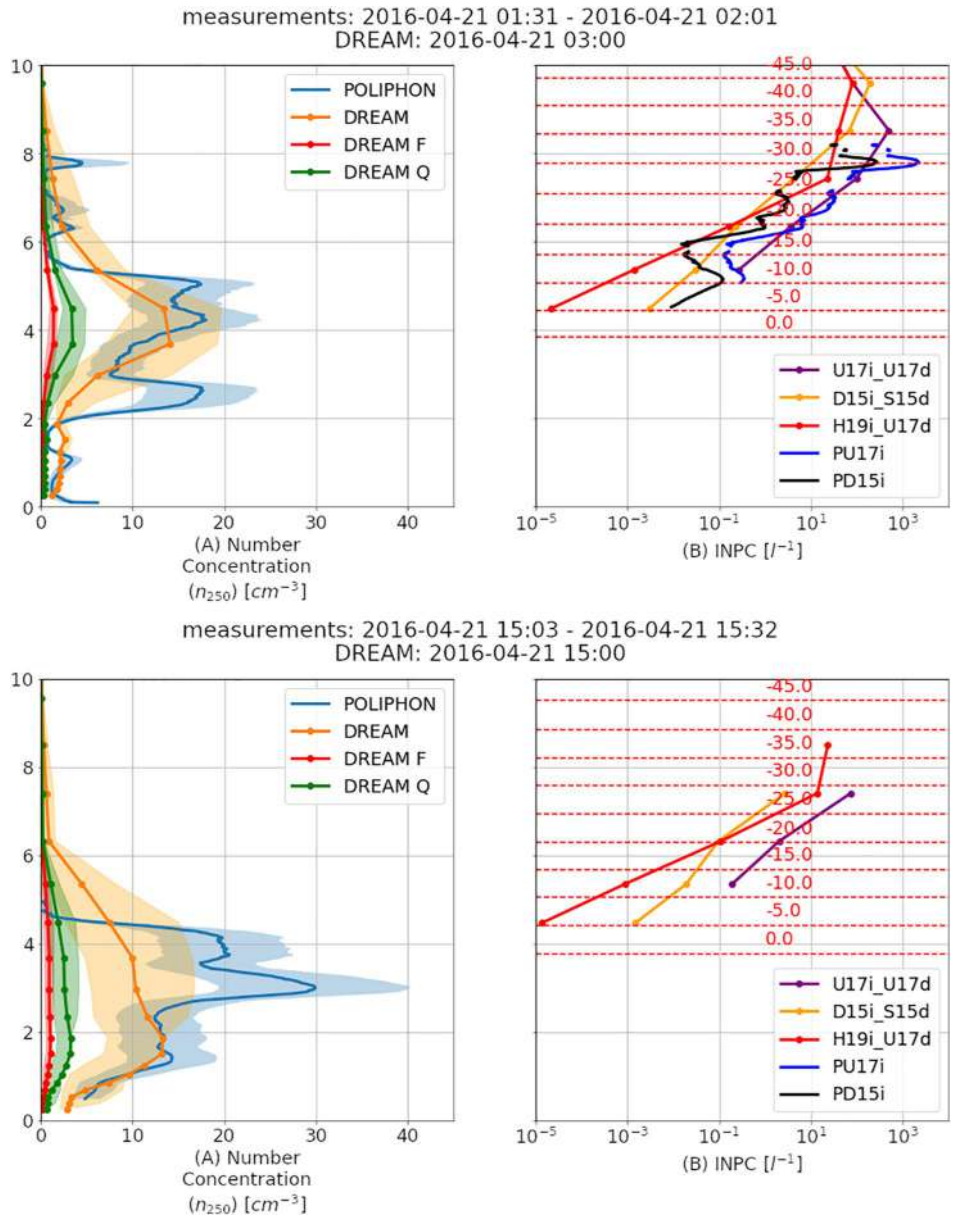

Figure 5. POLIPHON and Dust Regional Atmospheric Model profiles of dust n_{250} number concentration (a). F and Q indicate feldspar and quartz concentrations. Ice nucleating particle concentration for the three model setups and two immersion parameterizations used with POLIPHON data (b), on 21 April at 3 UTC (Ni1) and on 21 April at 15 UTC (Ni2) at Nicosia.

Mediterranean on 14 April and was above Potenza on 16 April, with INPC production (according to the DREAM model) coinciding with observed clouds above 6 km. The dust plume was transported northward on 17 April, reducing the dust concentrations. Cirrus cloud development on 17 April was not indicated by INPC predicted by the model. On 18 April, the observed clouds and the predicted INPC are vertically co-located. On 19–20 April, advection of a drier air mass from northwest, with no dust present, was predicted by the model. Thus dust-related INPC were not predicted in that period. On 21–22 April, another dust plume reached Potenza, influencing pre-frontal cloud development.

3.1.2. Nicosia, April 21

DREAM simulated the height of dust layer, its gradual altitude descent and intrusion in the planetary boundary layer after 12UTC on 21 April over Nicosia in agreement with the lidar measurements (Figure S6 in the

Table 2
POLIPHON (P) and DREAM (D) Comparison Metrics (Center of Mass, Column Mass Concentration, Peak Concentration and Correlation Coefficient) for the Three Lidar Cases Above Potenza (Po; 18 April at 15 UTC) and Nicosia (Ni 1; 21 April at 3 UTC) (Ni 2; 21 April at 15 UTC) (Ni 2; April 21 at 15)

	Center of mass [m]			Column mass concentration [g/m^2]			Peak concentration [μg/m^3]		Correlation coefficient
Location	P	D	D-all	P	D	D-all	P	D	
Po	4412 (4393,4422)	4310	3556	0.16 (0.11,0.21)	0.64	0.82	87 (60,114)	205	0.92
Ni 1	3778 (3597,3864)	4133	4143	0.45 (0.29,0.61)	0.32	0.32	155 (105,205)	119	0.79
Ni 2	2819 (2797,2831)	2857	2841	0.56 (0.42,0.63)	0.49	0.50	263 (177,349)	134	0.84

Note. D-all represents the metrics for the whole DREAM profile (not limited to data points where POLIPHON products are available). Lower and upper values due to the uncertainties of POLIPHON (coming from the natural variability and the retrievals uncertainties) are given in brackets.

Supporting Information S1). In Figure 5, the DREAM model is compared with the Nicosia observations on 21 April. For the 3UTC profiles (Ni1), dust layer CoM from DREAM is higher than from POLIPHON (Table 2), as the model did not predict the dust layer at 2.5 km height. DREAM dust CoM showed variability of 3%. For the 15UTC profiles (Ni2), CoM is correctly positioned in the model but with larger variability of 11%. Correlation coefficients reveal that the main vertical structure of the dust plume was well represented by the model in both cases. Due to lower DREAM vertical resolution, in comparison with POLIPHON, some features of the dust layers might not be resolved by the model because of the complex vertical structure of the observed aerosol and the coarser horizontal and vertical resolution of the model. DREAM peak concentrations show variability of 65% and 90% for Ni1 and Ni2, respectively. The model underestimated both peak concentrations and the concentrations of the layer below 3 km for Ni1 and between 2.5 and 4.5 km for Ni2. Nevertheless, for the rest of the altitudes DREAM simulated column mass concentrations are within the uncertainties of the POLIPHON retrievals. Considering that the model data are representative for the model gridbox of 0.1 × 0.1, while the POLIPHON profiles are representative for the atmospheric column directly above the measurement point, this is a very good agreement. We need to point here that only the dust concentrations at altitudes above 4 km contributed to the INPC concentrations in this case, as temperatures at lower heights are above 0°C. A systematic model performance study from Binietoglou et al. (2015) indicated that four evaluated dust models (including the DREAM model used in this study) simulate systematically lower total amount of dust relative to the LIRIC profiles. In that study, it was suggested that this could be caused by insufficient dust source strength, overestimated deposition and wet scavenging parameters, or a combination of these effects. Data set used in the study was not sufficient to discriminate between these factors. The mass concentration from the four models showed significant correlation with the measured one. Additionally, it was concluded that DREAM predicted sufficiently well the concentration values. Better performance of DREAM could be attributed to the assimilation scheme used in that study only by that model. In both Nicosia cases we see similar agreement in the three INPC setups at temperatures below −20°C, with differences of up to an order of magnitude. H19i_U17d INPC falls between D15i_S15d and U17i_U17d. Feldspar mass fraction profiles show values greater than 20% at altitudes above 5 km (Figure S8 in the Supporting Information S1). As in the Potenza case, quartz contribution is increased between 4 and 5 km but has a minor role in the INPC. In the Ni1 case, Nicosia observations are available at altitudes which enable the use of D15i and U17i_U17d INPC parameterizations. The results differ from those obtained using the same parameterizations in the DREAM model, within one order of magnitude (Figure 5). INPC values estimated by POLIPHON show larger vertical variability compared to the model due to the higher resolution of lidar measurements.

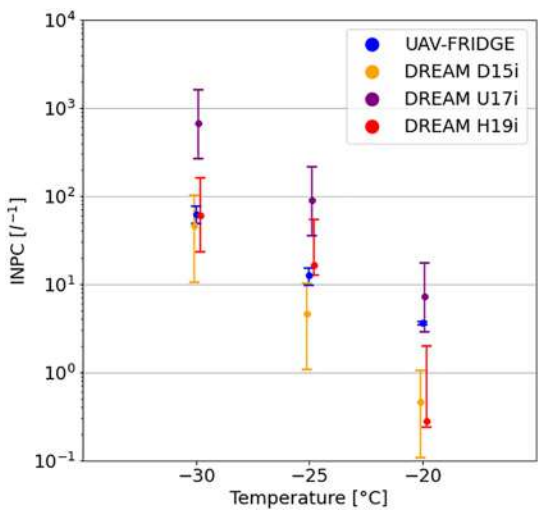

Figure 6. Ice nucleating particle concentration prediction by Dust Regional Atmospheric Model on 21 April 2016 and the UAV-FRIDGE measurements (Marinou et al., 2019; Schrod et al., 2017) for immersion freezing (as a function of temperature). The data points are slightly shifted from the actual temperature for clearer presentation.

Additionally, we compare the model results with collocated in time UAV-FRIDGE INPC measurements above Cyprus, described in more detail by Schrod et al. (2016) and Marinou et al. (2019). Figure 6 presents the results of the comparison between the DREAM INPC and the in situ measurements in the immersion freezing temperature range, for the mineralogy

sensitive and mineralogy indifferent parameterizations. The UAV samples were collected at 2.5 km height and for the analysis they were exposed to water saturation of 101% and temperatures at which the immersion freezing is expected. UAV-FRIDGE data and uncertainties presented in this paper are adopted from Marinou et al. (2019). We use mineral dust concentrations from the model at the same latitude, longitude and height at which the UAV samples were collected. These concentrations are used as input to the D15i, U17i and H19i parameterizations at the same thermodynamic conditions used in the FRIDGE. The DREAM results are presented with typical uncertainties of the INPC parameterizations (Harrison et al., 2019; Marinou et al., 2019). The variability of DREAM results described by the +3h and −3h profiles would introduce variability in INPC estimations of 27%, 30% and 33% for H19i, D15i and U17i, respectively (not shown in the plot).

At −30°C and −25°C, the H19i parameterization predicts INPC values between those of the mineralogy indifferent parameterizations, D15i and U17i, similarly to the results presented in the comparisons with POLIPHON (Figure 3 and Figure 5), and in a very good agreement with the UAV-FRIDGE measurements (within their uncertainties). However, at −20°C, H19i underestimates INPC in comparison to D15i parameterization and UAV-FRIDGE measurements. The analysis performed by Marinou et al. (2019) showed that dust is the dominant contributor to INPC in this case of 21 April, and suggested that for dust D15i is applicable in immersion temperature range, while in the deposition nucleation regime U17d results agree well with in situ observations. The DREAM results of D15i underestimate INPC in comparison with FRIDGE measurements. It should be noted that at 2.5 km height, DREAM underestimated the cloud-relevant dust concentrations in comparison with POLIPHON retrievals (Figure 5b), contributing to INPC underestimations. D15i parameterization is based on particle concentration as input, and it is not affected by changes in particles size. On the other hand, H19i predictions are influenced by particle size and mineral composition of dust. At the temperatures used in the FRIDGE experiment (≥−30°C), quartz contribution to INPC is expected to be small, so the most of the H19i INPC can be attributed to feldspar. Majority of feldspar is present in the silt particles while its efficiency as an INP source is reduced with increase of temperature. We assume that sedimentation of silt particles leads to an underestimation of H19i prediction of INPC when compared to D15i at −20°C. It should be noted that in this case, relative contribution of silt particles to total dust particle concentration is smaller than in the mean particle size distribution at the sources in the model domain. DREAM results of H19 show closer agreement with UAV-FRIDGE results at −25°C and −30°C, in comparison with the results of the mineralogy-indifferent parameterizations, but the sensitivity to mineral composition contributed to underestimation at −20°C in this case.3.2 Comparison with the DARDAR product.

We compare the vertical extent and distribution of INPC from the DREAM model with the ICNC from the DARDAR-Nice product for two cases, shown in Figure 1. A recently published closure study presented the relationship between the INPC and ICNC in clouds at temperature ranges which promote immersion freezing and deposition nucleation mechanisms, based on ground-based active remote sensing (Ansmann, Mamouri, Bühl, et al., 2019; Ansmann, Mamouri, Hofer, et al., 2019). In the three closure experiments, in which clouds formed in Saharan dust layers, the estimated INPC and ICNC values agreed within an order of magnitude. Marinou et al. (2019) found that DARDAR-Nice estimates were between INPC values derived from dust profiles based on CALIPSO measurements for two immersion parameterizations (D15i and U17) and within the errors of the two parameterizations. At temperatures between −3°C and −8°C secondary ice production (SIP) processes can be present in clouds, as well, and contribute to the ICNC (Field et al., 2017; Hallett & Mossop, 1974). Due to the strong INPC dependence on temperature, high INPC values are expected close to the top of the upper aerosol–cloud layers. Additionally, liquid droplets can be supercooled to temperatures around −37°C. We assume that the ice crystals which nucleate close to the cloud top and then grow and fall through the lower layers of clouds. Since this version of the model does not include a microphysics scheme fully coupled with aerosols, we discuss the use of the INPC parameterizations as a proxy for ICNC estimation and whether the mineralogy-sensitive parameterization presents a considerable improvement in INPC estimation.

Vertical cross sections of DARDAR-Nice during the overpass B have been previously compared by Marinou et al. (2019) with the neighboring INPC profiles based on CALIPSO observations. They used the CALIPSO L2 version 4 (V4) aerosol profile products and considered only quality-assured retrievals (Marinou et al., 2017; Tackett et al., 2018). Besides the parameterizations used in our study, they also included soot contributions to INPC based on parameterizations by DeMott et al. (2010) and Ullrich et al. (2017). They concluded that the lidar-derived dust INPC can be used to estimate the minimum and maximum boundary of the ICNC in the clouds

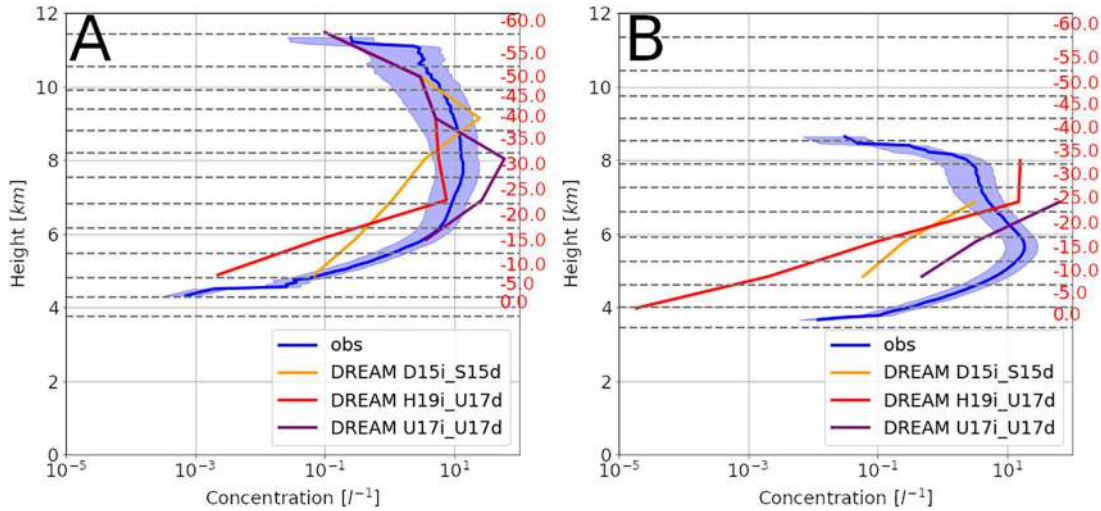

Figure 7. Comparison of Dust Regional Atmospheric Model simulated Ice nucleating particle concentration profiles using three model setups and DARDAR-Nice product on 20 April, 12UTC during overpass A (a) and on 21 April, 12UTC during overpass B (b). Solid blue line represents DARDAR ICNC for $D > 25$ μm; while the shaded blue area indicates $D > 100$ μm (lower limit) and $D > 5$ μm (upper limit) values.

formed in their presence when immersion is the dominant mechanism. DREAM INPC results in this case agree with their INPC estimations within an order of magnitude. Overpass A cross section has not been analyzed in this way due to the presence of clouds in dust containing profiles, therefore not satisfying the quality assurance criteria. Based on these results we consider DREAM INPC comparison with DARDAR-Nice.

In this study, vertical cross sections of the DARDAR-Nice products are used to calculate the mean ICNC vertical profiles (Figure 7). DARDAR can have some pixels misclassified as ice instead of mixed-phase clouds (Villanueva et al., 2020). In analyzed cases, all the profiles were classified as mixed-phase clouds. Average DARDAR-Nice product is calculated for ice crystal diameters greater than 5 μm, 25 and 100 μm. The relative uncertainties in the individual profiles in the overpass A are in the ranges: 15%–83%, 14%–79%, 10%–85% for the mentioned diameters. In the overpass B, the uncertainties are in the ranges: 27%–72%, 28%–68%, 33%–57%. These uncertainties are not presented in Figure 7. To calculate average INPC profiles from the DREAM model, the satellite track was used to locate nearest model grid points to the locations of observed clouds.

Mean simulated dust concentration profiles along the marked part of the satellite tracks of Figure 1 shows that there is significantly less dust in the atmosphere during the overpass B (Figure S10 in the Supporting Information S1). Peak concentrations decreased from 253 μg m^{-3} to 184 μg m^{-3} and integrated dust load decreased from 1.1 g m^{-2} to 0.7 g m^{-2}. However, at heights between 6 and 8 km, where the immersion freezing is likely to occur, there is more dust in the overpass B. Additionally, the model predicts a cooler atmosphere than in overpass A, shifting the immersion range to lower altitudes. The mineral composition of dust in the immersion range is changed during transport (Figure S9 in theSupporting Information S1). Overall, these changes in mineral composition would make the dust produce around 6% higher INPC at −35°C and up to 17% percent higher at −25°C. However, the total mass in silt bins was significantly reduced, mainly through deposition of larger particles, reducing this effect.

In Figure 7a we see that DREAM INPC parameterizations provide a good proxy of the vertical extent and distribution of the DARDAR ICNC in the mixed phase and cirrus clouds in overpass A. In the top of the cloud, where we assume that ice crystal nucleate, agreement is observed between the three model setups and the observations. The mineralogy-sensitive setup (H19i_U17d) shows the maximum INPC in the immersion mode, at −25°C, in the temperature range where K-feldspar is the dominant INP source. At temperatures higher than −25°C, H19i_U17d differs by an order of magnitude from the ICNC values. D15i_S15d setup estimates peak in INPC in the deposition mode and underestimates concentrations in immersion mode by an order of magnitude. U17i_U17d differs from the ICNC values by an order of magnitude, although it overestimates the maximum concentration value.

Table 3
Evaluation of DREAM INPC - DARDAR ICNC Comparison for Three Model Setups

	The overpass A			The overpass B		
	H19i_U17d	D15i_S15d	U17	H19i_U17d	D15i_S15d	U17
Mean difference [l^{-1}]	−4.1	−2.2	11.1	−1.3	−10.5	7.0
Root Mean Square Difference [l^{-1}]	4.9	7.6	19.0	10.7	12.1	25.6

In overpass case B (Figure 7b), DARDAR-Nice product shows a much smaller vertical extent, not completely covered by all three model setups, likely because of the coarser model vertical resolution. The model has 28 vertical levels based on the hybrid pressure-sigma coordinate (Janjic, 2003), having vertical resolution of several hundreds of meters in the immersion temperature range. It is possible that the temperature representative of a model grid box is too low to predict INPs based on immersion parameterization. In this case the highest altitude with forecasted INPs is limited by immersion parameterization and model vertical resolution. Additionally, DARDAR-Nice product, predicts ICNC at heights where homogenous nucleation is possible (around and below −37°C)

In overpass case B, DREAM estimates larger INPC than in overpass case A because of the larger dust mass concentrations in the immersion temperature range above 6 km. For this case, the efficiency of dust as an INP is affected by the physical aging (Figure S9 in the Supporting Information S1) and in the different contribution of quartz and feldspar fractions to total dust concentration. H19i_U17d- and U17i_U17d-predicted INPC depends on ice nucleation active surface-site density and dust particle size bin effective diameter, while the INP fraction in each size bin is dependent only on temperature. The particles in the two silt size bins with the effective radii of 1.3 and 2.2 μm are very efficient as INPs at temperatures below −30°C (Niemand et al., 2012). Additionally, in the mineralogy-sensitive H19i_U17d setup, the smaller contribution of feldspar influenced the reduction of INP activity of dust at temperatures lower than −25°C. In case of overpass B, U17i_U17d predicts a smaller INP fraction of total dust concentration than in overpass case A due to the warmer temperature at same heights (Figure S2 in the Supporting Information S1). The difference in INPC estimation between overpasses A and B, based on D15i parameterization is caused by the difference in total particle concentrations indicated by higher dust concentration in the immersion temperature range (Figure S10 in the Supporting Information S1) and lower dust concentration in silt bins (Figure S9 in the Supporting Information S1). At temperatures higher than −20°C, more ICNC are retrieved in comparison to the higher altitudes and to the estimated INPC. A possible explanation for the higher ICNC at lower altitudes could be that the ice crystals in these clouds nucleate close to the cloud top (where the lowest temperatures are observed) and that afterward the crystals grow and fall through the lower heights of the clouds formed (Ansmann, Mamouri, Bühl, et al., 2019; Marinou et al., 2019). Since the model simulates only dust aerosols, it is possible that additional INPs at higher temperatures are from biogenic sources (Nickovic et al., 2016; O'Sullivan et al., 2018; Welti et al., 2018; Sanchez-Marroquin et al., 2021). Table 3 shows the evaluation of applicability of the three INP parameterization setups in DREAM, with the DARDAR ICNC as a reference in the two studied cases. As discussed previously, H19i_U17d and U17i_U17d INPC capture the general shape of the ICNC profile in overpass A. D15i_S15d shows the lowest bias, while positioning the peak concentrations above the observed maximum of INPC. U17i_U17d predicts one order of magnitude more INPC compared to ICNC. These results are in agreement with the results by Marinou et al. (2019) of comparison of lidar-derived INPC with DARDAR-derived ICNC for the two immersion freezing parameterizations (D15i and U17). It should be noted that in study of Price et al. (2018) in Atlantic, an INPC parameterization by Niemand et al. (2012) overestimated INPC in comparison to samples collected in aircraft measurements. U17i uses some of the same data as the parameterizations by Niemand et al. (2012) and is on average producing n_s values a factor 1.64 times higher. In overpass B, DREAM is less successful in predicting the shape of the ICNC profiles and this inevitably largely affects the comparison. D15i INPC prediction is below the ICNC, U17i_U17d predicts INPC in a limited altitude range, and H19i_U17d INPC decreases sharply at lower altitudes. We follow the assumption that the conditions were not favorable for the SIP and introduce the hypothesis that the ICNC can reach the values of up to INPC (Marinou et al., 2019). The differences presented in Table 3 show that observed ICNC values are within the range of the uncertainties of the parameterizations introduced in the H19i_U17d setup in the case A. The setup uncertainties are described in Equations 1–4 and in Marinou et al. (2019). In the case B, DREAM results indicate INPC underestimation. In both cases (A and B), H19i_U17d had most success in predicting

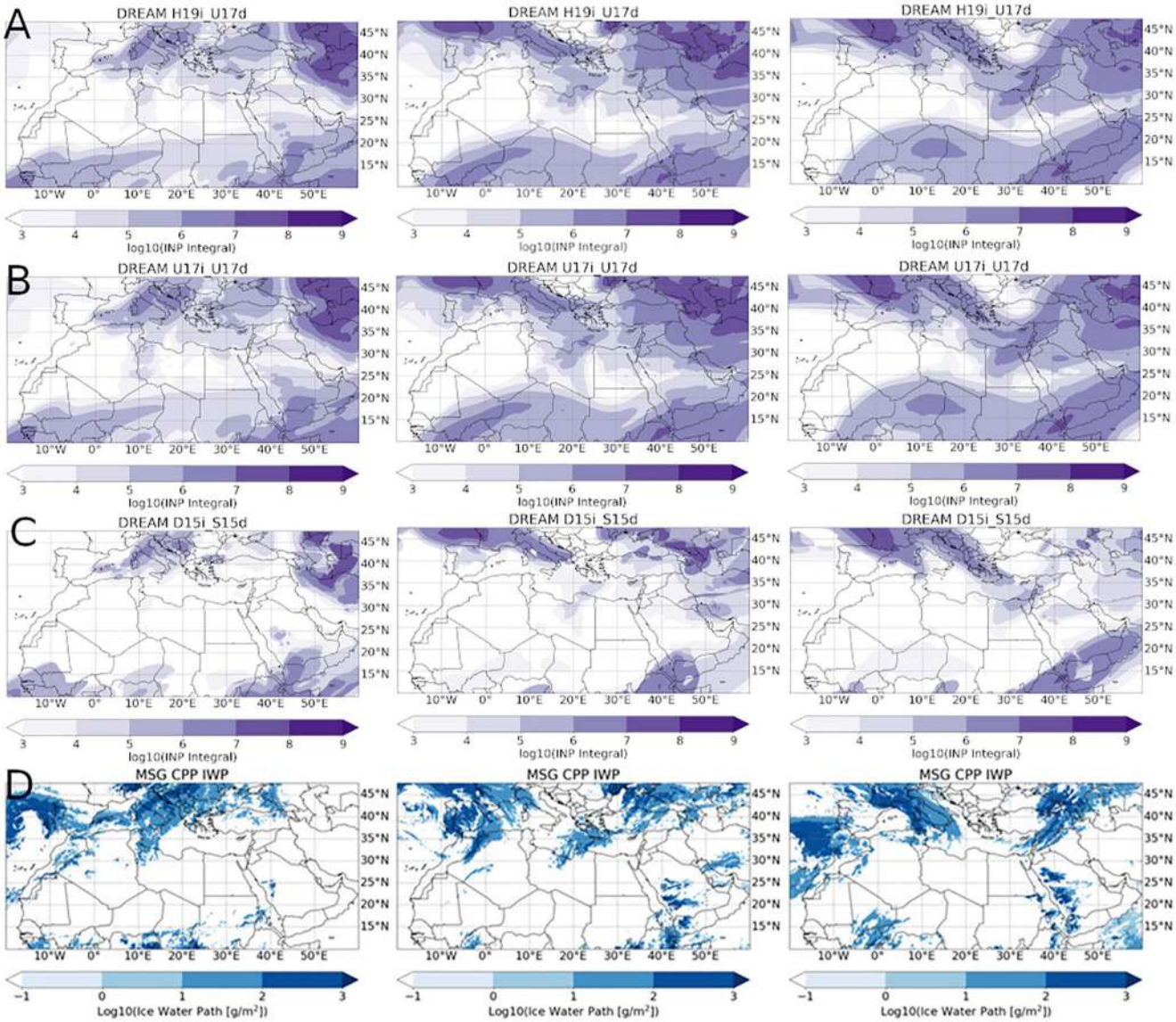

Figure 8. Dust Regional Atmospheric Model simulated integrated Ice nucleating particle concentration values for H19i_U17d (a) U17i_U17d (b) and D15i_S15d (c) setups. MSG IWP product (d) on 18 April, 15UTC, 20 April, 12UTC and 21 April. 12UTC.

vertical extent and the shape of the profile. Additionally, it shows the least root mean square difference when compared to ICNC.

3.2. Comparison With MSG Ice Water Path

DREAM mineral fractions and INPC values are compared with the MSG IWP product in order to discuss the performance of DREAM INPC setups on the prediction of horizontal patterns of ice clouds (Figure 8 and Figure S11 in the Supporting Information S1). The INPC parameterizations are used to predict conditions for ice-initiation in clouds in the presence of dust particles. The qualitative comparison between DREAM INPC and MSG IWP uses the overlap between areas with predicted INP and observed cloud ice as an indicator of useful prediction. Mineral fractions have been presented for mean concentrations in the immersion temperature range. Dust mass can locally consist of 30% feldspar in Europe and Mediterranean. In the three presented cases, lower feldspar concentrations reach the north-eastern part of the model domain, due to deposition of silt particles. In those areas quartz fraction is above 60%. The three INP setups differ from each other up to two orders of magnitude

in the vertically integrated profiles. The largest differences are present in the south of model domain, to the west over the Atlantic and in the north east near Caspian Sea. H19i_U17d INPC is generally between the U17i_U17d and D15i_S15d values. H19i_U17d and U17i_U17d predict INPC over the Atlantic in the first two cases, but miss the clouds between 30°N and 40°N in the last case. South of 30°N, H19i_U17d overestimates the production of clouds. In southern parts of Europe and in the Mediterranean, the forecast patterns match the observed ones. The INPC in the northeast part of the model domain is overestimated. U17i_U17d has similar patterns partly because they rely on the same deposition parameterization. In these areas of "false alarm" (Nickovic et al., 2016), where INPC is predicted but no clouds are observed, the values of H19i_U17d and U17i_U17d are similar in the south. In the Caspian Sea region, U17i_U17d predicts slightly higher values, due to lower feldspar contribution in the H19i_U17d. D15i_S15d predicts the lowest concentrations and, therefore, smaller "false alarm" areas, but also shows less probability of predicting observed clouds over the Atlantic.

4. Summary and Conclusions

For the first time, a mineralogy-sensitive INPC parameterization has been implemented in an operational, regional dust-atmosphere coupled model. A dust episode in the Mediterranean in April 2016 with dust plumes reaching Potenza and Nicosia was analyzed. Atmospheric transport of feldspar and quartz minerals was simulated using mineralogy-sensitive emission and transport schemes based on mineralogy of the dust sources. External mixing of dust is assumed in the model. Dust forecast profiles have been compared with POLIPHON lidar retrievals of particle number, surface area and mass concentrations. DREAM INPC predictions have been compared with vertical profiles of POLIPHON INPC and DARDAR ICNC product for two A-train satellite overpasses of dust plume. Horizontal distribution of INPs was evaluated using MSG-SEVIRI IWP product. The main limitation of the current version of the model is that, while DREAM is fully coupled in terms of dust transport and INPC predictions, dust concentrations are not coupled with the cloud microphysics scheme. This limits the possibilities of model verification in terms of INPC direct comparisons with ICNC or IWP. Nevertheless, a useful comparison can be made between modeled INPC and ICNC values derived from remote sensing observations.

We found that the DREAM model successfully simulates the evolution and vertical distribution of the dust plume. In the vertical profiles, the three INPC setups (mineralogy-sensitive H19i_U17d and mineralogy-indifferent D15i_S15d and U17i_U17d) differ by about an order of magnitude. H19i_U17d presents a sharp maximum in INPC at −25°C due to feldspar activity and sharper decrease of INPC at temperatures higher than −20°C. We found agreement within an order of magnitude between forecasted INPC and observed ICNC values for all model setups. In the two presented cases, the H19i_U17d model setup was closest to predicting the shape and extent of the ICNC vertical profiles. Analysis of the vertical profiles of presented cases showed that variations in feldspar content due to atmospheric circulation can change the productivity of dust as an INP by 6% at −35°C and up to 17% at −25°C. This effect can easily be reduced by physical aging of dust through deposition of silt particles, where most of the feldspar mass is present.

Vertically integrated values of INPC have shown that U17i_U17d and H19i_U17d model setups have higher probability to predict the presence of cold clouds than D15i_S15d over the Atlantic and Mediterranean. However, they show differences in predicted INPC over Atlantic and the Caspian Sea region due to differences in feldspar content.

The presented results strengthen the conclusions from previous in situ and laboratory studies of the importance of including mineral composition of dust into INPC prediction by numerical models. In comparison to mineralogy indifferent setups, where INP production in the immersion range changes over time due to particle concentration or (in case of U17i_U17d) shows some additional variability due to particle size, the mineralogy-sensitive setup provides a more detailed view on dust effectiveness and INPC prediction. It shows potential to be a better proxy than mineralogy-indifferent parameterizations for ice initiation in numerical models based on predictions of vertical extent and structure of cloud ice concentration and probability of success in predicting presence of clouds based on IWP retrievals.

Model results agreement with measurements, presented here, gives confidence in possibilities of INPC prediction and INPC estimation in areas where observations are sparse. Using mineralogy-sensitive parameterizations is a step forward in quantifying the role dust plays as INP. Further analysis with long-term simulations and a dust model with fully coupled microphysics scheme would provide better insight into the effectiveness of these model

setups and overcome some of the limitations of this study. In such a model, dust and potentially other aerosol contribution to INPC could be calculated and used as an input parameter to microphysics scheme. Additionally, other aerosol types, such as biogenic particles contribute to INPC at higher temperatures than dust and including them in the model is another aspect of future model development. Experimental campaigns, especially with aircraft in situ measurements of dust and INPC would significantly refine the current parameterizations and improve possibilities of model verification.

Conflict of Interest

The authors declare no conflicts of interest relevant to this study.

Data Availability Statement

We thank EARLINET (https://www.earlinet.org/, last access: 12 December 2020), ACTRIS (https://www.actris.eu, last access: 12 December 2020) and PollyNET (http://polly.tropos.de, last access: 15 March 2021) for the data collection, calibration, processing and dissemination. We thank the PollyNet group for their support during the development and operation of the PollyXT-NOA lidar system. We are grateful to the AERIS/ICARE Data and Services Center for generating and storing the DARDAR products and for providing access to the CALIPSO data used and their computational center (http://www.icare.univ-lille1.fr/, last access: 8 August 2019). We thank the NASA CloudSat Project and NASA/LaRC/ASDC for making available the CloudSat and CALIPSO products, respectively, which are used to build the synergetic DARDAR products.

Acknowledgments
Authors LI, AJ, and MK acknowledge funding provided by the Institute of Physics Belgrade, through the grant by the Ministry of Education, Science, and Technological Development of the Republic of Serbia. EM is grateful to Dr. Jean Sciare for hosting the PollyXT-NOA lidar in the Cyprus institute during the INUIT-BACCHUS-ACTRIS experiment. We are grateful to Jann Schrod and Bingemer Heinz G. for the provision of UAV-FRIDGE measurement data. The INUIT-BACCHUS-ACTRIS experiment received support from the Deutsche Forschungsgemeinschaft (Grant Nos. 1525, INUIT), the European Union's Seventh Frame-work Program (Grant Nos. 603445, BACCHUS), the European Union's Horizon 2020 research and innovation program (654109,ACTRIS-2). EM was funded by the European Research Council (Grant Nos. 725698, D-TECT) and by a DLR VO-R young investigator group and the Deutscher Akademischer Austauschdienst (Grant No. 57370121).

References

Ansmann, A., Mamouri, R.-E., Bühl, J., Seifert, P., Engelmann, R., Hofer, J., et al. (2019). Ice-nucleating particle versus ice crystal number concentrationin altocumulus and cirrus layers embedded in Saharan dust:a closure study. *Atmospheric Chemistry and Physics*, *19*, 15087–15115. https://doi.org/10.5194/acp-19-15087-2019

Ansmann, A., Mamouri, R.-E., Hofer, J., Baars, H., Althausen, D., & Abdullaev, S. F. (2019). Dust mass, cloud condensation nuclei, and ice-nucleating particle profiling with polarization lidar: Updated POLIPHON conversion factors from global AERONET analysis. *Atmospheric Measurement Techniques*, *12*, 4849–4865. https://doi.org/10.5194/amt-12-4849-2019

Ansmann, A., Seifert, P., Tesche, M., & Wandinger, U. (2012). Profiling of fine and coarse particle mass: Case studies of Saharan dust and Eyjafjallajökull/Grimsvötn volcanic plumes. *Atmospheric Chemistry and Physics*, *12*, 9399–9415. https://doi.org/10.5194/acp-12-9399-2012

Ansmann, A., Tesche, M., Seifert, P., Groß, S., Freudenthaler, V., Apituley, A., et al. (2011). Ash and fine-mode particle mass profiles from EARLINET-AERONET observations over central Europe after the eruptions of the Eyjafjallajökull volcano in 2010. *Journal of Geophysical Research*, *116*, D00U02. https://doi.org/10.1029/2010JD015567

Atkinson, J. D., Murray, B. J., Woodhouse, M. T., Whale, T. F., Baustian, K. J., Carslaw, K. S., et al. (2013). The importance of feldspar for ice nucleation by mineral dust in mixed-phase clouds. *Nature*, *498*, 355–358. https://doi.org/10.1038/nature12278

Baars, H., Kanitz, T., Engelmann, R., Althausen, D., Heese, B., Komppula, M., et al. (2016). An overview of the first decade of PollyNET: An emerging network of automated Raman-polarization lidars for continuous aerosol profiling. *Atmospheric Chemistry and Physics*, *16*, 5111–5137. https://doi.org/10.5194/acp-16-5111-2016

Basart, S., Pérez, C., Nickovic, S., Cuevas, E., & Baldasano, J. M. (2012). Development and evaluation of the BSC-DREAM8b dust regional model over Northern Africa, the Mediterranean and the Middle East. *Tellus B: Chemical and Physical Meteorology*, *64*, 18539. https://doi.org/10.3402/tellusb.v64i0.18539

Benas, N., FinkensieperFamilyNamePrefix, S., Stengel, M., ZadelhofffamilyNamePrefix, G.-J., Hanschmann, T., Hollmann, R., & Meirink, J. F. (2017). The MSG-SEVIRI-based cloud property data record CLAAS-2. *Earth System Science Data*, *9*, 415–434. https://doi.org/10.5194/essd-9-415-2017

Binietoglou, I., Basart, S., Alados-Arboledas, L., Amiridis, V., Argyrouli, A., Baars, H., et al. (2015). A methodology for investigating dust model performance using synergistic EARLINET/AERONET dust concentration retrievals. *Atmospheric Measurement Techniques*, *8*, 3577–3600. https://doi.org/10.5194/amt-8-3577-2015

Boose, Y., Welti, A., Atkinson, J., Ramelli, F., Danielczok, A., Bingemer, H. G., et al. (2016). Heterogeneous ice nucleation on dust particles sourced from nine deserts worldwide – Part 1: Immersion freezing, Atmos. *Chemical Physics*, *16*, 15075–15095. https://doi.org/10.5194/acp-16-15075-2016

Boucher, O., Randall, D. A., Artaxo, P., Bretherton, C. S., Feingold, G., Forster, P. M., et al. (2013). Clouds and aerosols. In T. F. Stocker, D. Qin, G.-K. Plattner, M. Tignor, S. K. Allen, A. Nauels, et al. (Eds.), *Climate change 2013: The physical science basis. Contribution of working group I to the fifth assessment report of the intergovernmental panel on climate Change, 25edited* (pp. 571–657). Cambridge University Press.

Chaikovsky, A., Dubovik, O., Holben, B., Bril, A., Goloub, P., Tanré, D., et al. (2016). Lidar-radiometer inversion Code (LIRIC) for the retrieval of vertical aerosol properties from combined lidar/radiometer data: Development and distribution in EARLINET, atmos. *Measurement Techniques*, *9*, 1181–1205. https://doi.org/10.5194/amt-9-1181-2016

Cziczo, D., Froyd, K. D., Hoose, C., Jensen, E. J., Diao, M., Zondlo, M. A., et al. (2013). Clarifying the dominant sources and mechanisms of cirrus cloud formation. *Science*, *340*, 1320–1324. https://doi.org/10.1126/science.1234145

D'Amico, G., Amodeo, A., Mattis, I., Freudenthaler, V., & Pappalardo, G. (2016). EARLINET Single Calculus Chain – Technical – Part 1: Pre-processing of raw lidar data. *Atmospheric Measurement Techniques*, *9*, 491–507

Delanoë, J., & Hogan, R. J. (2010). Combined CloudSat-CALIPSO-MODIS retrievals of the properties of ice clouds. *Journal of Geophysical Research*, *115*, D00H29. https://doi.org/10.1029/2009JD012346

Delanoë, J. M. E., Heymsfield, A. J., Protat, A., Bansemer, A., & Hogan, R. J. (2014). Normalized particle size distribution for remote sensing application. *Journal of Geophysical Research: Atmospheres*, *119*, 4204–4227. https://doi.org/10.1002/2013JD020700

DeMott, P. J., Möhler, O., Cziczo, D. J., Hiranuma, N., Petters, M. D., Petters, S. S., et al. (2018). The fifth international workshop on ice nucleation phase 2 (FIN-02): Laboratory intercomparison of ice nucleation measurements. *Atmospheric Measurement Techniques*, *11*, 6231–6257. https://doi.org/10.5194/amt-11-6231-2018

DeMott, P. J., Prenni, A. J., Liu, X., Kreidenweis, S. M., Petters, M. D., Twohy, C. H., et al. (2010). Predicting global atmospheric ice nuclei distributions and their impacts on climate. *Proceedings of the National Academy of Sciences*, *107*, 11217–11222. https://doi.org/10.1073/pnas.0910818107

DeMott, P. J., Prenni, A. J., McMeeking, G. R., Sullivan, R. C., Petters, M. D., Tobo, Y., et al. (2015). Integrating laboratory and field data to quantify the immersion freezing ice nucleation activity of mineral dust particles. *Atmospheric Chemistry and Physics*, *15*, 393–409. https://doi.org/10.5194/acp-15-393-2015

Engelmann, R., Kanitz, T., Baars, H., Heese, B., Althausen, D., Skupin, A., et al. (2016). The automated multiwavelength Raman polarization and water-vapor lidar PollyXT: The neXT generation. *Atmospheric Measurement Techniques*, *9*, 1767–1784. https://doi.org/10.5194/amt-9-1767-2016

Ferrier, B. S., Jin, Y., Lin, Y., Black, T., Rogers, E., & DiMego, G. (2002). Implementation of a new grid-scale cloud and precipitation scheme in the NCEP Eta model. In *15th conference on numerical weather prediction* (pp. 280–283). American Meteorological Society.

Field, P. R., Lawson, R. P., Brown, P. R. A., Lloyd, G., Westbrook, C., Moisseev, D., et al. (2017). Secondary ice production: Current state of the science and recommendations for the future. *Meteorological Monographs*, *58*, 7–17. Retrieved from https://journals.ametsoc.org/view/journals/amsm/58/1/amsmonographs-d-16-0014.1.xml

Freudenthaler, V., Esselborn, M., Wiegner, M., Heese, B., Tesche, M., Ansmann, A., et al. (2009). Depolarization ratio profiling at several wavelengths in pure Saharan dust during. *SAMUM 2006, Tellus B*, *61*, 165–179. https://doi.org/10.1111/j.1600-0889.2008.00396.x

Gama, C., Tchepel, O., Baldasano, J. M., Basart, S., Ferreira, J., Pio, C., et al. (2015). Seasonal patterns of Saharan dust over Cape Verde-a combined approach using observations and modelling. *Tellus B: Chemical and Physical Meteorology*, *67*, 24410. https://doi.org/10.3402/tellusb.v67.24410

Georgi, F. (1986). A particle dry-deposition parameterization scheme for use in tracer transport models. *Journal of Geophysical Research*, *91*, 9794–9806.

Georgoulias, A. K., Tsikerdekis, A., Amiridis, V., Marinou, E., Benedetti, A., Zanis, P., et al. (2018). A 3-D evaluation of the MACC reanalysis dust product over Europe, northern Africa and Middle East using CALIOP/CALIPSO dust satellite observations. *Atmospheric Chemistry and Physics*, *18*, 8601–8620. https://doi.org/10.5194/acp-18-8601-2018

Ginoux, P., Chin, M., Tegen, I., Prospero, J., Holben, B., Dubovik, O., & Lin, S. J. (2001). Sources and distributions of dust aerosols simulated with the GOCART model. *Journal of Geophysical Research*, *106*(D17), 20255–20273. https://doi.org/10.1029/2000jd000053

Glaccum, R. A., & Prospero, J. M. (1980). Saharan aerosols over the tropical north atlantic—mineralogy. *Marine Geology*, *37*, 295–321. https://doi.org/10.1016/0025-3227(80)90107-3

Groß, S., Esselborn, M., Abicht, F., Wirth, M., Fix, A., & Minikin, A. (2013). Airborne high spectral resolution lidar observation of pollution aerosol during EUCAARI-LONGREX. *Atmospheric Chemistry and Physics*, *13*, 2435–2444. https://doi.org/10.5194/acp-13-2435-2013

Groß, S., Tesche, M., Freudenthaler, V., Toledano, C., Wiegner, M., Ansmann, A., et al. (2011). Characterization of Saharan dust, marine aerosols and mixtures of biomass burning aerosols and dust by means of multi-wavelength depolarization and Raman lidar measurements during SAMUM 2. *Tellus B: Chemical and Physical Meteorology*, *63*, 706–724. https://doi.org/10.1111/j.1600-0889.2011.00556.x

Haarig, M., Ansmann, A., Gasteiger, J., Kandler, K., Althausen, D., Baars, H., et al. (2017). Dry versus wet marine particle optical properties: RH dependence of depolarization ratio, backscatter, and extinction from multiwavelength lidar measurements during SALTRACE. *Atmospheric Chemistry and Physics*, *17*, 14199–14217. https://doi.org/10.5194/acp-17-14199-2017

Hallett, J., & Mossop, S. C. (1974). Production of secondary ice crystals during the riming process. *Nature*, *249*, 26–28. https://doi.org/10.1038/249026a0

Hande, L. B., Engler, C., Hoose, C., & Tegen, I. (2015). Seasonal variability of Saharan desert dust and ice nucleating particles over Europe. *Atmospheric Chemistry and Physics*, *15*, 4389–4397. https://doi.org/10.5194/acp-15-4389-2015

Harrison, A. D., Lever, K., Sanchez-Marroquin, A., Holden, M. A., Whale, T. F., Tarn, M. D., et al. (2019). The ice-nucleating ability of quartz immersed in water and its atmospheric importance compared to K-feldspar. *Atmospheric Chemistry and Physics*, *19*, 11343–11361. https://doi.org/10.5194/acp-19-11343-2019

Harrison, A. D., Whale, T. F., Carpenter, M. A., Holden, M. A., Neve, L., O'Sullivan, D., et al. (2016). Not all feldspars are equal: A survey of ice nucleating properties across the feldspar group of minerals. *Atmospheric Chemistry and Physics*, *16*, 10927–10940. https://doi.org/10.5194/acp-16-10927-2016

Herbert, R. J., Murray, B. J., Dobbie, S. J., & Koop, T. (2015). Sensitivity of liquid clouds to homogenous freezing parameterizations. *Geophysical Research Letters*, *42*(5), 1599–1605. https://doi.org/10.1002/2014GL062729

Hogan, R. J., Mittermaier, M. P., & Illingworth, A. J. (2006). The retrieval of ice water content from radar reflectivity factor and temperature and its use in evaluating a Mesoscale model. *Journal of Applied Meteorology and Climatology*, *45*, 301–317. https://doi.org/10.1175/jam2340.1

Holben, B. N., Eck, T. F., Slutsker, I., Tanré, D., Buis, J. P., Setzer, A., et al. (1998). Aeronet – a federal instrument network and data archive for aerosol charac- terization. *Remote Sensing of Environment*, *66*, 1–16. https://doi.org/10.1016/S0034-4257(98)00031-5

Holden, M. A., Campbell, J. M., Meldrum, F. C., Murray, B. J., & Christenson, H. K. (2021). Active sites for ice nucleation differ depending on nucleation mode. *Proceedings of the National Academy of Sciences*, *118*(18), e2022859118. https://doi.org/10.1073/pnas.2022859118

Holden, M. A., Whale, T. F., Tarn, M. D., O'Sullivan, D., Wal-shaw, R. D., Murray, B. J., et al. (2019). High-speed imaging of ice nucleation in waterproves the existence of active sites. *Science Advances*, *5*, eaav4316. https://doi.org/10.1126/sciadv.aav4316

Hoose, C., & Möhler, O. (2012). Heterogeneous ice nucleation on atmospheric aerosols: A review of results from laboratory experiments. *Atmospheric Chemistry and Physics*, *12*, 9817–9854. https://doi.org/10.5194/acp-12-9817-2012

Ickes, L., Welti, A., Hoose, C., & Lohmann, U. (2015). Classical nucleation theory of homogeneous freezing of water: Thermodynamic and kinetic parameters. *Physical Chemistry Chemical Physics*, *17*(8), 5514–5537. https://doi.org/10.1039/C4CP04184D

Illingworth, A. J., Hogan, R. J., O'Connor, E. J., Bouniol, D., Brooks, M. E., Delanoe, J., et al. (2007). Cloudnet - Continuous evaluation of cloud profiles in seven operational models using ground-based observations. *Bulletin of the American Meteorological Society*, *88*, 883–898. https://doi.org/10.1175/bams-88-6-883

Janjic, Z. I. (1994). The step-mountain Eta coordinate model: Further developments of the convection, viscous sublayer, and turbulence closure schemes. *Monthly Weather Review*, *122*, 927–945.

Janjic, Z. I. (2003). A nonhydrostatic model based on a new approach. *Meteorology and Atmospheric Physics*, *82*, 271–285. https://doi.org/10.1007/s00703-001-0587-6

Kampouri, A., Amiridis, V., Solomos, S., Gialitaki, A., Marinou, E., Spyrou, C., et al. (2021). Investigation of volcanic emissions in the mediterranean: "The Etna-antikythera connection". *Atmosphere*, *12*, 40. https://doi.org/10.3390/atmos12010040

Kandler, K., Schütz, L., Deutscher, C., Ebert, M., Hofmann, H., Jäckel, S., et al. (2009). Size distribution, mass concentration, chemical and mineralogical composition and derived optical parameters of the boundary layer aerosol at Tinfou, Morocco, during SAMUM 2006. *Tellus B: Chemical and Physical Meteorology*, *61*, 32–50. https://doi.org/10.1111/j.1600-0889.2008.00385.x

Kanji, Z. A., Ladino, L. A., Wex, H., Boose, Y., Burkert-Kohn, M., Cziczo, D. J., & Krämer, M. (2017). Overview of ice nucleating particles. *Meteorological Monographs*, *58*. https://doi.org/10.1175/amsmonographs-d-16-0006.110.1175/AMSMONOGRAPHS-D-16-0006.1

Konsta, D., Binietoglou, I., Gkikas, A., Solomos, S., Marinou, E., Proestakis, E., et al. (2018). Evaluation of the BSC-DREAM8b regional dust model using the 3D LIVAS-CALIPSO product. *Atmospheric Environment*, *195*, 46–62. https://doi.org/10.1016/j.atmosenv.2018.09.047

Lohmann, U., & Feichter, J. (2005). Global indirect aerosol effects: A review. *Atmospheric Chemistry and Physics*, *5*, 715–737. https://doi.org/10.5194/acp-5-715-2005

Madonna, F., Amodeo, A., Boselli, A., Cornacchia, C., Cuomo, V., D'Amico, G., et al. (2011). CIAO: The CNR-IMAA advanced observatory for atmospheric research. *Atmospheric Measurement Techniques*, *4*, 1191–1208. https://doi.org/10.5194/amt-4-1191-2011

Madonna, F., Russo, F., Ware, R., & Pappalardo, G. (2009). Mid-tropospheric supercooled liquid water observation consistent with nucleation induced by a mountain lee wave. *Geophysical Research Letters*, *36*, L18802. https://doi.org/10.1029/2009GL039545

Mamali, D., Marinou, E., Sciare, J., Pikridas, M., Kokkalis, P., Kottas, M., et al. (2018). Vertical profiles of aerosol mass concentration derived by unmanned airborne in situ and remote sensing instruments during dust events. *Atmospheric Measurement Techniques*, *11*, 2897–2910. https://doi.org/10.5194/amt-11-2897-2018

Mamouri, R. E., & Ansmann, A. (2015). Estimated desert-dust ice nuclei profiles from polarization lidar: Methodology and case studies. *Atmospheric Chemistry and Physics*, *15*, 3463–3477. https://doi.org/10.5194/acp-15-3463-2015

Mamouri, R. E., & Ansmann, A. (2016). Potential of polarization lidar to provide profiles of CCN- and INP-relevant aerosol parameters. *Atmospheric Chemistry and Physics*, *16*, 5905–5931. https://doi.org/10.5194/acp-16-5905-2016

Mann, G. W., Carslaw, K. S., Spracklen, D. V., Ridley, D. A., Manktelow, P. T., Chipperfield, M. P., et al. (2010). Description and evaluation of GLOMAP-mode: A modal global aerosol microphysics model for the UKCA composition-climate model. *Geoscientific Model Development*, *3*, 519–551. https://doi.org/10.5194/gmd-3-519-2010

Marcolli, C. (2014). Deposition nucleation viewed as homogeneous or immersion freezing in pores and cavities. *Atmospheric Chemistry and Physics*, *14*, 2071–2104. https://doi.org/10.5194/acp-14-2071-2014

Marinou, E., Amiridis, V., Binietoglou, I., Tsikerdekis, A., Solomos, S., Proestakis, E., et al. (2017). Three-dimensional evolution of Saharan dust transport towards Europe based on a 9-year EARLINET-optimized CALIPSO dataset. *Atmospheric Chemistry and Physics*, *17*, 5893–5919. https://doi.org/10.5194/acp-17-5893-2017

Marinou, E., Tesche, M., Nenes, A., Ansmann, A., Schrod, J., Mamali, D., et al. (2019). Retrieval of ice-nucleating particle concentrations from lidar observations and comparison with UAV in situ measurements. *Atmospheric Chemistry and Physics*, *19*, 11315–11342. https://doi.org/10.5194/acp-19-11315-2019

Mattis, I., D'Amico, G., Baars, H., Amodeo, A., Madonna, F., & Iarlori, M. (2016). EARLINET Single Calculus Chain – Technical – Part 2: Calculation of optical products. *Atmospheric Measurement Techniques*, *9*, 3009–3029. https://doi.org/10.5194/amt-9-3009-2016

Meirink, J. F., Roebeling, R. A., & Stammes, P. (2013). Inter-calibration of polar imager solar channels using SEVIRI. *Atmospheric Measurement Techniques*, *6*, 2495–2508. https://doi.org/10.5194/amt-6-2495-2013

Müller, D., Ansmann, A., Mattis, I., Tesche, M., Wandinger, U., Althausen, D., & Pisani, G. (2007). Aerosol-type-dependent lidar ratios observed with Raman lidar. *Journal of Geophysical Research*, *112*, D16202. https://doi.org/10.1029/2006JD008292

Murray, B. J., O'Sullivan, D., Atkinson, J. D., & Webb, M. E. (2012). Ice nucleation by particles immersed in supercooled cloud droplets. *Chemical Society Reviews*, *41*, 6519–6554. https://doi.org/10.1039/c2cs35200a

Nickovic, S. (2005). Distribution of dust mass over particle sizes: Impacts on atmospheric optics. *Forth ADEC Workshop - Aeolian Dust Experiment on Climate Impact*, (Vol. *26–28*, pp. 357–360). Nagasaki.

Nickovic, S., Cvetkovic, B., Madonna, F., Rosoldi, M., Pejanovic, G., Petkovic, S., & Nikolic, J. (2016). Cloud ice caused by atmospheric mineral dust – Part 1: Parameterization of ice nuclei concentration in the NMME-DREAM model. *Atmospheric Chemistry and Physics*, *16*, 11367–11378. https://doi.org/10.5194/acp-16-11367-2016

Nickovic, S., Kallos, G., Papadopoulos, A., & Kakaliagou, O. (2001). A model for prediction of desert dust cycle in the atmosphere. *Journal of Geophysical Research*, *106*, 18113–18130. https://doi.org/10.1029/2000jd900794

Nickovic, S., Vukovic, A., & Vujadinovic, M. (2013). Atmospheric processing of iron carried by mineral dust. *Atmospheric Chemistry and Physics*, *13*, 9169–9181. https://doi.org/10.5194/acp-13-9169-2013

Nickovic, S., Vukovic, A., Vujadinovic, M., Djurdjevic, V., & Pejanovic, G. (2012). Technical Note: High-resolution mineralogical database of dust-productive soils for atmospheric dust modeling. *Atmospheric Chemistry and Physics*, *12*, 845–855. https://doi.org/10.5194/acp-12-845-2012

Niemand, M., Moehler, O., Vogel, B., Vogel, H., Hoose, C., Connolly, P., et al. (2012). A particle-surface area based parametrization of immersion freezing on desert dust particles. *Journal of the Atmospheric Sciences*, *69*, 3077–3092. https://doi.org/10.1175/jas-d-11-0249.1

Nisantzi, A., Mamouri, R. E., Ansmann, A., Schuster, G. L., & Hadjimitsis, D. G. (2015). Middle East versus Saharan dust extinctionto-backscatter ratios. *Atmospheric Chemistry and Physics*, *15*, 7071–7084. https://doi.org/10.5194/acp-15-7071-2015

O'Sullivan, D., Adams, M. P., Tarn, M. D., Harrison, A. D., Vergara-Temprado, J., Porter, G. C., et al. (2018). Contributions of biogenic material to the atmospheric ice-nucleating particle population in North Western Europe. *Scientific Reports*, *8*(1), 13821. https://doi.org/10.1038/s41598-018-31981-7

Papayannis, A., Nicolae, D., Kokkalis, P., Binietoglou, I., Talianu, C., Belegante, L., et al. (2014). Optical, size and mass properties of mixed type aerosol in Greece and Romania as observed by synergy of lidar and sunphotometers in combination with model simulation: A case study. *The Science of the Total Environment*, *500–501*, 277–294. https://doi.org/10.1016/j.scitotenv.2014.08.101

Pappalardo, G., Amodeo, A., Apituley, A., Comeron, A., Freudenthaler, V., Linné, H., et al. (2014). EARLINET: Towards an advanced sustainable European aerosol lidar network. *Atmospheric Measurement Techniques*, *7*, 2389–2409. https://doi.org/10.5194/amt-7-2389-2014

Pejanovic, G., Nickovic, S., Petkovic, S., Vukovic, A., Djurdjevic, V., Vujadinovic, M., & Dacic, M. (2012). *Dust operational forecast system with assimilation of dust analysed data, Regional Conference on Dust and Dust Storms* (pp. 20–22).

Pérez, C., Nickovic, S., Pejanovic, G., Baldasano, J. M., & Özsoy, E. (2006). Interactive dust-radiation modeling: A step to improve weather forecasts. *Journal of Geophysical Research*, *111*, D16206. https://doi.org/10.1029/2005JD006717

Price, H. C., Baustian, K. J., McQuaid, J. B., Blyth, A., Bower, K. N., Choularton, T., & Murray, B. J. (2018). Atmospheric ice-nucleating particles in the dusty tropical Atlantic. *Journal of Geophysical Research: Atmospheres*, *123*, 2175–2193. https://doi.org/10.1002/2017JD027560

Pruppacher, H. R., & Klett, J. D. (1997). *Microphysics of clouds and precipitation* (2nd ed., p. 954). Kluwer Academic.

Sanchez-Marroquin, A., West, J. S., Burke, I. T., McQuaid, J. B., & Murray, B. J. (2021). Mineral and biological ice-nucleating particles above the south east of the British isles. *Environmental Sciences: Atmos.*, *1*, 176–191. https://doi.org/10.1039/d1ea00003a

Schrod, J., Danielczok, A., Weber, D., Ebert, M., Thomson, E. S., & Bingemer, H. G. (2016). Re-evaluating the Frankfurt isothermal static diffusion chamber for ice nucleation. *Atmospheric Measurement Techniques*, *9*, 1313–1324. https://doi.org/10.5194/amt-9-1313-2016

Schrod, J., Weber, D., Drücke, J., Keleshis, C., Pikridas, M., Ebert, M., et al. (2017). Ice nucleating particles over the Eastern Mediterranean measured by unmanned aircraft systems. *Atmospheric Chemistry and Physics*, *17*, 4817–4835. https://doi.org/10.5194/acp-17-4817-2017

Seifert, P., Ansmann, A., Mattis, I., Wandinger, U., Tesche, M., Engelmann, R., et al. (2010). Saharan dust and heterogeneous ice formation: Eleven years of cloud observations at a central European EARLINET site. *Journal of Geophysical Research*, *115*, D20201. https://doi.org/10.1029/2009JD013222

Solomos, S., Abuelgasim, A., Spyrou, C., Binietoglou, I., & Nickovic, S. (2019). Development of a dynamic dust source map for NMME-DREAM v1.0 model based on MODIS normalized difference vegetation index (NDVI) over the arabian peninsula, geosci. *Model Dev*, *12*, 979–988. https://doi.org/10.5194/gmd-12-979-2019

Solomos, S., Ansmann, A., Mamouri, R.-E., Binietoglou, I., Patlakas, P., Marinou, E., & Amiridis, V. (2017). Remote sensing and modelling analysis of the extreme dust storm hitting the Middle East and eastern Mediterranean in September 2015. *Atmospheric Chemistry and Physics*, *17*, 4063–4079. https://doi.org/10.5194/acp-17-4063-2017

Sourdeval, O., Gryspeerdt, E., Krämer, M., Goren, T., Delanoë, J., Afchine, A., et al. (2018). Ice crystal number concentration estimates from lidar–radar satellite remote sensing – Part 1: Method and evaluation. *Atmospheric Chemistry and Physics*, *18*, 14327–14350. https://doi.org/10.5194/acp-18-14327-2018

Steinke, I., Hoose, C., Möhler, O., Connolly, P., & Leisner, T. (2015). A new temperature- and humidity-dependent surface site density approach for deposition ice nucleation. *Atmospheric Chemistry and Physics*, *15*, 3703–3717. https://doi.org/10.5194/acp-15-3703-2015

Stengel, M., Kniffka, A., Meirink, J. F., Lockhoff, M., Tan, J., & Hollmann, R. (2014). CLAAS: The CM SAF cloud property data set using SEVIRI. *Atmospheric Chemistry and Physics*, *14*, 4297–4311. https://doi.org/10.5194/acp-14-4297-2014

Stephens, G. L., Vane, D. G., Boain, R. J., Mace, G. G., Sassen, K., Wang, Z., et al. (2002). The Cloudsat missionand the A–train. *B. Am.Meteorol. Soc.*, *83*, 1771–1790. https://doi.org/10.1175/bams-83-12-1771

Su, L., & Fung, J. C. H. (2018). Investigating the role of dust in ice nucleation within clouds and further effects on the regional weather system over east asia – Part 1: Model development and validation. *Atmospheric Chemistry and Physics*, *18*, 8707–8725. https://doi.org/10.5194/acp-18-8707-2018

Tackett, J. L., Winker, D. M., Getzewich, B. J., Vaughan, M. A., Young, S. A., & Kar, J. (2018). CALIPSO lidar level 3 aerosol profile product: Version 3 algorithm design. *Atmospheric Measurement Techniques*, *11*, 4129–4152. https://doi.org/10.5194/amt-11-4129-2018

Tegen, I., & Fung, I. (1994). Modeling of mineral dust in the atmosphere: Sources, transport,and optical thickness. *Journal of Geophysical Research*, *99*(D11), 22897–22914. https://doi.org/10.1029/94jd01928

Tesche, M., Ansmann, A., Müller, D., Althausen, D., Engelmann, R., Freudenthaler, V., & Groß, S. (2009). Vertically resolved separation of dust and smoke over Cape Verde using multiwavelength Raman and polarization lidars during Saharan Mineral Dust Experiment 2008. *Journal of Geophysical Research*, *114*, D13202. https://doi.org/10.1029/2009jd011862

Tesche, M., Groß, S., Ansmann, A., Müller, D., Althausen, D., Freudenthaler, V., & Esselborn, M. (2011). Profiling of Saharan dust and biomass-burning smoke with multiwavelength polarization Raman lidar at Cape Verde. *Tellus B: Chemical and Physical Meteorology*, *63*, 649–676. https://doi.org/10.1111/j.1600-0889.2011.00548.x

Tsikerdekis, A., Zanis, P., Steiner, A. L., Solmon, F., Amiridis, V., Marinou, E., et al. (2017). Impact of dust size parameterizations on aerosol burden and radiative forcing in RegCM4. *Atmospheric Chemistry and Physics*, *17*, 769–791. https://doi.org/10.5194/acp-17-769-2017

Ullrich, R., Hoose, C., Möhler, O., Niemand, M., Wagner, R., Höhler, K., et al. (2017). A new ice nucleation active site parameterization for desert dust and soot. *Journal of the Atmospheric Sciences*, *74*, 699–717. https://doi.org/10.1175/jas-d-16-0074.1

Vali, G., DeMott, P. J., Möhler, O., & Whale, T. F. (2015). Technical note: A proposal for ice nucleation terminology. *Atmospheric Chemistry and Physics*, *15*, 10263–10270. https://doi.org/10.5194/acp-15-10263-2015

Varlas, G., Marinou, E., Gialitaki, A., Siomos, N., Tsarpalis, K., Kalivitis, N., et al. (2021). Assessing sea-state effects on sea-salt aerosol modeling in the lower atmosphere using lidar and in-situ measurements. *Remote Sensing*, *13*(4), 614. https://doi.org/10.3390/rs13040614

Vergara-Temprado, J., Murray, B. J., Wilson, T. W., O'Sullivan, D., Browse, J., Pringle, K. J., et al. (2017). Contribution of feldspar and marine organic aerosols to global ice nucleating particle concentrations. *Atmospheric Chemistry and Physics*, *17*, 3637–3658. https://doi.org/10.5194/acp-17-3637-2017

Veselovskii, I., Goloub, P., Podvin, T., Bovchaliuk, V., Derimian, Y., Augustin, P., et al. (2016). Retrieval of optical and physical properties of African dust from multiwavelength Raman lidar measurements during the SHADOW campaign in Senegal. *Atmospheric Chemistry and Physics*, *16*, 7013–7028. https://doi.org/10.5194/acp-16-7013-2016

Villanueva, D., Heinold, B., Seifert, P., Deneke, H., Radenz, M., & Tegen, I. (2020). The day-to-day co-variability between mineral dust and cloud glaciation: A proxy for heterogeneous freezing. *Atmospheric Chemistry and Physics*, *20*, 2177–2199. https://doi.org/10.5194/acp-20-2177-2020

Vukovic, A., Vujadinovic, M., Pejanovic, G., Andric, J., Kumjian, M. R., Djurdjevic, V., et al. (2014). Numerical simulation of "an American haboob. *Atmospheric Chemistry and Physics*, *14*, 3211–3230. https://doi.org/10.5194/acp-14-3211-2014

Wagner, R., Kiselev, A., Möhler, O., Saathoff, H., & Steinke, I. (2016). Pre-activation of ice-nucleating particles by the pore condensation and freezing mechanism. *Atmospheric Chemistry and Physics*, *16*, 2025–2042. https://doi.org/10.5194/acp-16-2025-2016

Welti, A., Müller, K., Fleming, Z. L., & Stratmann, F. (2018). Concentration and variability of ice nuclei in the subtropical maritime boundary layer. *Atmospheric Chemistry and Physics*, *18*, 5307–5320. https://doi.org/10.5194/acp-18-5307-2018

Wilson, T. W., Ladino, L. A., Alpert, P. A., Breckels, M. N., Brooks, I. M., Browse, J., et al. (2015). A marine biogenic source of atmospheric ice-nucleating particles. *Nature*, *525*, 234–238. https://doi.org/10.1038/nature14986

Zender, C. S., Bian, H., & Newman, D. (2003). Mineral dust entrainment and deposition (DEAD) model: Description and 1990s dust climatology. *Journal of Geophysical Research*, *108*(D14), 4416. https://doi.org/10.1029/2002JD002775

Zolles, T., Burkart, J., Häusler, T., Pummer, B., Hitzenberger, R., & Grothe, H. (2015). Identification of ice nucleation active sites on feldspar dust particles. *The Journal of Physical Chemistry A*, *119*, 2692–2700. https://doi.org/10.1021/jp509839x

Air Quality, Atmosphere & Health
https://doi.org/10.1007/s11869-022-01161-8

Moss bag sensitivity for the assessment of airborne elements at suburban background site during spring/summer season characterized by Saharan dust intrusions

Mira Aničić Urošević[1] · Maja Kuzmanoski[1] · Tijana Milićević[1] · Igor Kodranov[2] · Konstantin Vergel[3] · Aleksandar Popović[2]

Received: 27 October 2021 / Accepted: 19 January 2022

Abstract
Moss transplants of *Hypnum cupressiforme* and *Sphagnum girgensohnii* were tested for efficiency in detection of airborne element pollution at a suburban background site during short time exposure of 15 days (twelve consecutive periods) and during prolonged exposure from one to six months. Concomitantly, particulate matter (PM10, PM2.5) was sampled during three identified Saharan dust episodes, while MERRA-2 data were used for estimation of dust concentration at ground level to which the moss bags were exposed during 15-day periods. The concentrations of 22 potentially toxic elements were measured in the moss and PM10 samples. The results showed that 15-day bag exposure at the background location could not provide a measurable and reliable signature of the elements in the moss transplants, except for Al, V, As, Ga, Y, and Tb, unlike the extended moss bag exposure of a couple of months. These were also the only elements whose concentrations were increased multifold in PM10 samples during the most intense dust episode, which was also recorded by *S. girgensohnii* bags exposed in the corresponding 15-day period. The ratio of crustal elements (Ca/Al, Mg/Al) in PM10 and moss samples (3-month exposed) was in line of those reported for dust transported from western Africa. The V/Al, Ga/Al, and Tb/Al concentration ratio values in PM10 and *S. girgensohnii* samples were higher for dust days contrary to the As/Al ratio, which could be used to distinguish between dust and fossil fuel combustion pollution sources. The moss bag technique could be used as a simple tool for tracking long-range transported elements, but after prolonged moss bag exposure (3 months).

Keywords Air Pollution · Element Content · Active Moss Biomonitoring · Bag Exposure Period · Saharan Dust Intrusion

Introduction

Particulate matter (PM) air pollution is recognized as one of the major threats to human health (Cohen et al. 2017; WHO 2016). The chemical composition of airborne PM depends on the geological background of the region and anthropogenic emission sources. Although natural sources are highly involved in PM composition, anthropogenic sources are mainly responsible for the adverse constituents of PM (carcinogenic and toxic elements, polycyclic aromatic hydrocarbon, etc.).

The air in urban areas is, almost by default polluted, since numerous anthropogenic sources of pollution run all the time at a local level. Long-range transport of air pollutants adds to the locally emitted pollution. Furthermore, specific urban topography contributes to poor ventilation and dilution of air pollution (Harrison and Hester 2009). Therefore, the urban population is chronically exposed to a certain level of ambient air pollution, so-called background air pollution (Gómez-Losada et al. 2018).

Regulatory air pollution monitoring is mainly oriented to measurements of air pollutants at presumable 'hot spots' of pollution, while background air pollution is measured at a limited number of monitoring stations due to economic constraints. The background air pollution is mostly estimated

✉ Mira Aničić Urošević
mira.anicic@ipb.ac.rs

[1] Institute of Physics Belgrade, University of Belgrade, Pregrevica 118, 11080 Belgrade, Serbia

[2] Faculty of Chemistry, University of Belgrade, Studentski trg 12 – 16, 11000 Belgrade, Serbia

[3] Frank Laboratory of Neutron Physics, Joint Institute for Nuclear Research, Joliot Curie 6, 141980 Dubna, Russian Federation

using different statistical models processing the available monitoring and meteorological data (DEFRA 2014; Gómez-Losada et al. 2018). In some cases, the background contribution might be a dominant portion of total pollutant concentration in situ (DEFRA 2014). Note the total pollution at the site represents the sum of transported and locally emitted pollutant concentrations. For example, Saharan dust can be transported far away from the source area influencing aerosol concentration and its chemical composition even at distant locations. The dust intrusion along the Mediterranean, especially during the spring and summer season (April–October), significantly contributes to particulate matter (PM) content loading in Southern and Eastern Europe (Ganor et al. 2010; Alastuey et al. 2016) subsequently adding to the deterioration of air quality. Relatively high contents of crustal (Al, Si, Ti, Fe, and K), trace (Mn, Rb, V, Cr, Sc, Be), and rare earth elements characterized dust-related samples (Querol et al. 2019).

Besides expensive instrumental methods, biomonitoring represents a valuable approach to evaluate the ambient pollution, with the advantage of low-cost sampling of systematically distributed organisms or their parts (Markert et al. 2003 and references therein). Atmospheric deposition of PM and its-bound pollutants (major, minor, and rare earth elements) has been successfully monitored by using cryptogams—mosses and lichens (Rühling and Tyler 1969; Berg and Steinnes 1997; Aničić Urošević et al. 2017b, a and references therein). Since cryptogams do not have a developed cuticle, root, and vascular system, they rely largely on atmospheric deposition for nourishment. Moreover, these organisms can be used as so-called active biomonitors (moss transplants) with the possibility of a precise definition of sampling site and time. The 'bag technique' has been widely used and tested in air pollution biomonitoring due to the simplicity of the biomonitor-form, easily applicable in any experimental design, which represents a time-integrated response to persistent air pollutants in a scale of several months (Goodman and Roberts 1971; Ares et al. 2012; Aničić Urošević and Milićević 2020 and references therein).

Moss bag technique has been widely used for air pollution monitoring of potentially toxic elements, and it has been tested for that purpose in different (micro)environments, industrial (Ares et al. 2011; Salo and Mäkinen 2014; De Agostini et al. 2020), urban (Culicov and Yurukova 2006; Adamo et al. 2011; Vuković et al. 2015; Hu et al. 2018), and agricultural (Milićević et al. 2017; Demková et al. 2017), but mainly at those sites with high air pollution. However, moss bag ability to record background air pollution has only been investigated in a few studies, in the rural area (Capozzi et al, 2016a), agricultural area (Milićević et al. 2021), and urban botanical garden (Aničić Urošević et al. 2017b, a).

From our previous biomonitoring study (Vuković et al. 2015), we obtained information about the air pollution zoning during the summer season in the urban area of Belgrade (Serbia), a variety of air pollution on a small scale (Vuković et al., 2016), and the sites that could represent the urban background of air pollution (Aničić Urošević et al. 2017b, a). In these studies, element concentrations in the moss bags showed clear distinction between areas (zones) and sites (crossroad, two- and one-lane street) with different levels of pollution, exhibiting capability to reveal the polluted environment. In the study by Vuković et al. (2015) clear differences between results for industrial and areas with high or moderate traffic flow, residential areas and parks were shown. The study by Aničić Urošević et al. (2017b, a) concentrations of several analyzed elements (Sb, Cr, Al, and V) showed significantly lower values in moss bags exposed at locations in the inner part of the Botanical garden in Belgrade and at the garden boundary close to high traffic flow. In addition, the study Aničić et al. (2009a) showed the increase of element concentrations in moss *Sphagnum girgensohnii* with exposure time, starting from 15 days up to 5 months. Significant enrichment of the elements was also recorded after 15-day exposure, and it was higher than the initial element concentration in the unexposed moss material. An optimal moss bag exposure time should be as short as possible due to practical reasons (to keep biomonitor's vitality, to record a short-time or accidental pollution events). To achieve a measurable pollution signature in the biomonitor at the background sites, the proposed minimal periods of moss bag exposure from three weeks (Capozzi et al. 2016b) up to two months (Aničić Urošević et al. 2017b, a) indicate the methodological discrepancy in the literature. It is still unknown if shortly exposed moss bags of several weeks can reflect the accidental and slight changes in ambient element content caused by anthropogenic or natural (e.g., desert dust intrusion) sources. Studying the moss bag exposure is especially important in the conditions of relatively low suburban background pollution, rarely monitored regularly, to which every citizen is chronically exposed. In addition, the moss bag technique has never been used for monitoring of long-range transported desert dust intrusion.

In our study, two moss species were used as biomonitors: *Hypnum cupressiforme* Hedw. and *Sphagnum girgensohnii* Russow. The former is widely present in Serbia, and the latter, the most recommended for biomonitoring of air pollutants (Ares et al. 2012; González and Pokrovsky 2014), is an endemic species in the south and middle European countries that are often under the influence of long-range transported desert dust from Sahara.

The aims of this study are *i)* to search for the measurable element signature in two moss species exposed at a suburban background site for different periods of exposure; *ii)* to examine the extent to which reduction of direct wet and dry atmospheric deposition influence the element content in the exposed moss bags; *iii)* to test whether moss bag technique

can detect elements that characterize Saharan dust intrusions common for spring/summer season in the study area.

Materials and Methods

Study area

The study was carried out in the inner courtyard of the Institute of Physics Belgrade (φ = 44° 51' N, λ = 20° 23' E, H_s = 92 m), situated on the right bank of the Danube in Zemun, a suburb of Belgrade (Serbia). The site is protected from road traffic, and during the summer season represents the place with presumably lower air pollution (a suburban background) than in other seasons of the year (Vuković et al. 2015). This study was performed from April to October 2019 due to lack of activity of heating pollution sources in a spring/summer season.

The climate of Belgrade is mild and generally warm—moderate-continental with a yearly temperature average of 10.9 ºC and annual precipitation in the interval from 540 to 820 mm (Republic Hydrometeorological Service of Serbia, http://www.hidmet.gov.rs/eng/meteorologija/klimatologija_srbije.php). The prevailing wind is N–NW, but the specific 'Košava' wind (SE–ESE) blows with an annual frequency of 26% and an average speed of 4 m s^{-1} (Unkašević et al. 1999). The meteorological data specifically for the studied period are presented in Figure S1 (Supplementary material).

(Bio)monitoring

Both studied moss species were collected at sites remote from anthropogenic pollution sources: *H. cupressiforme* in a national park of Serbia and *S. girgensohnii* in a pristine area in Russia where the species is widely present. The green upper part of the collected mosses was cleaned from extraneous materials, washed thrice with bidistilled water, air-dried, and used for the bag preparations (Ares et al. 2012; Vuković et al., 2016; Aničić Urošević et al. 2017b, a). A portion of such prepared material was kept in the laboratory conditions and used as a control sample for measurement of the initial element content in the moss, necessary for an assessment of net element content after the bag exposure. Polyethylene net bags of dimensions 7 × 7 cm were filled with the moss material and exposed at the studied site free hanging (Vuković et al. 2015). Each moss species were exposed in duplicate, at open space, and under the improvised roof, for twelve consecutive 15-day periods starting from April to October 2019 (summer, non-heating season). Such a design was used to enable differentiation of the influence of atmospheric deposition to the moss enrichment by elements, especially in the case of precipitation events during the episodes of Saharan dust. In addition, the wash-off effect to the element content in moss bags during intense precipitation events could be avoided using an improvised roof. The bags were also exposed to one-, two-, three-, four-, five-, and six-month periods to be sure about achieving element enrichment in the moss tissue. After exposure, the moss samples were air-dried, and duplicated moss samples were homogenized and kept under stable laboratory conditions until the chemical analysis.

Particulate matter monitoring

At the studied site, particulate matter (PM) was sampled daily during the episodes of Saharan dust evidenced from April to October 2019 by forecasting models, and for several days after each episode. Specifically, 24-h samples of PM10 and PM2.5 were collected by the referent particle sampler (Sven Leckel MVS6, Germany) upon the procedure prescribed by the European Standard for determining the suspended particulate matter in ambient air (EN 12,341:2014). Quartz fiber filters (Frisenette ApS, Denmark) were used for the particle collection. The mass concentrations of the suspended particulate matter were determined following the standard gravimetric measurement method (EN 12,341:2014).

Identification of dust episodes and dust surface concentrations

Long-range transported aerosols, such as the Saharan dust over the Mediterranean, are characteristic of the spring and summer seasons (Israelevich et al. 2012). In this study, to identify dust episodes affecting the sampling location, we relied on World Meteorological Organization's Sand and Dust Storm Warning Advisory and Assessment System (SDA-WAS) ensemble forecast (Terradellas et al. 2016), available on https://sds-was.aemet.es/forecast-products/dust-forecasts/ensemble-forecast. It involves a larger number of models (global or regional) which have different characteristics (differences are in horizontal and vertical resolution, assimilation, dust emission, and deposition parameterizations). Dust optical depth from model simulations is evaluated against AERONET (Holben et al. 1998) aerosol retrievals. SDS-WAS Regional Center for Northern Africa, Middle East, and Europe calculates multi-model mean and median dust optical depth and surface concentrations. In addition to model results, MODIS Aerosol products (aerosol optical depth and Angstrom exponent) were used to confirm dust presence over the study area (https://worldview.earthdata.nasa.gov). Three major dust episodes, which lasted for several days, were identified during this period: 23–27 April, 26–30 May, and 8–15 June of 2019.

The Modern-Era Retrospective Analysis for Research and Applications version 2 (MERRA-2) data for dust surface

concentration have been used in this work. MERRA-2 is the most recent atmospheric reanalysis of the modern satellite era provided by NASA's Global Modeling and Assimilation Office (GMAO, https://gmao.gsfc.nasa.gov/reanalysis/MERRA-2/). It is based on Goddard Earth Observing System version 5 (GEOS-5) atmospheric general circulation model and Goddard Chemistry, Aerosol, Radiation and Transport (GOCART) aerosol module. The model resolution is 0.5° × 0.625° (latitude by longitude), with 72 vertical levels. It provides a mass mixing ratio of five aerosol species (dust, sea salt, black carbon, organic carbon, and sulfate). Details on aerosol data assimilation systems are described in Randles et al. (2017). Dust concentrations at the studied site in this work were averaged over 15-day periods of moss bag exposure and used as complementary information in discussion of dust contribution to the element content in moss bag samples.

Chemical analysis of moss and PM10 samples

Both types of studied samples, mosses (≈0.3 g) and filters with collected PM10, were digested with 7 mL of 65% HNO_3 (Merck, p.a.) and 1 mL of 30% H_2O_2 (Merck) in Teflon vessels for 45 min in a microwave digester (Speed Wave, XPERT, Products + Instruments GmbH, Berghof, Germany). After filtration through the filter papers (*Blue Ribbon, Grade* 15 (2–3 pm), Ø125 mm, *FIORONI*), the dissolved samples were diluted with ultrapure water (18 MΩ x cm) up to the volume of 50 mL in volumetric flasks (Vuković et al. 2015; Aničić et al. 2017).

The concentrations of 12 elements (Al, Ba, Ca, Fe, K, Mg, Mn, Ni, P, S, Sr, and Zn) were determined by inductively coupled plasma-optical emission spectrometry, ICP-OES (iCAP 6500 Duo, Thermo Scientific, UK), while the content of 10 elements (V, Cr, Co, Cu, As, Cd, Pb, Ga, Y, Tb) was measured by inductively coupled plasma-mass spectrometry (ICP-MS, iCAP Q, Thermo Scientific, UK). A Multi-Element Plasma Standard Solution 4, Specpure (Alfa Aesar GmbH & Co KG, Germany) and low-level Elements Calibration Stock, US EPA Method Standard (VHG Labs, Manchester) were used for the calibration of the analytical devices. This procedure was regularly used for the determination of the element concentrations in the moss samples in many of our biomonitoring studies (Aničić Urošević and Milićević 2020 and references therein). The methodology for the determination of the element concentrations by ICP-OES and ICP-MS was described in detail (with all limits of detection and limit of quantifications) by Milićević 2018.

The analytical quality of the element detection was checked by the analysis of the analytical blank samples, and the reference materials, moss *Pleurozium schreberi* (Brid.) Mitt. M2 and M3 (Finnish Forest Research Institute; Steinnes et al. 1997), and aquatic plant (BCR-670), per each microwave bench (after every 11 samples). The recoveries of the element concentrations in the reference materials were in the range of 82–132%. The precision of analysis was estimated by the variation coefficient of three replicates of 20% moss samples; the relative standard deviation (RSD) of the replicate samples was within ± 11% for the measured elements. The initial element content was measured in four control subsamples of both studied mosses, and RSD varied up to 10%, except for Cr, Zn, Y and Tb (up to 18%). For filters with PM10, a blank Quartz fiber filter was used for the analytical quality control.

Data processing

Software Statistica 8.0 (StatSoft Inc, Tulsa, OK, USA) was used for the data processing. The control of the moss bag experiment was not only the initial element content ($C_{initial}$) in the unexposed moss material, but the limit of quantification of the moss bag technique (LOQt) was calculated following the equation:

$$\mathrm{LOQt} = x\mathrm{C}i + 1.96\mathrm{sC}i \quad (1)$$

where $x\mathrm{C}i$ is the mean value of the initial concentration in the unexposed moss (control samples) for each element determined, while $\mathrm{sC}i$ is the corresponding standard deviation. Calculation of the LOQ_T enables clear distinction of the element concentrations in the exposed and unexposed moss material; thus, the 'noise' associated with the methodology of moss bag technique is already included in data interpretation. The strict definition of LOQ coming from analytical chemistry, which defines LOQ as $10\mathrm{sC}i$, can be detracted in the active moss biomonitoring to $1.96\mathrm{sC}i$ due to a normal element distribution in the unexposed moss material (Ares et al. 2015).

For testing differences between the element concentrations in the samples of the same moss species under the roof (R) and at open space (O), we applied the sign test (a nonparametric test), due to the relatively small sample size. In addition, differences between the element concentrations between two moss species (*H. cupressiforme* and *S. girgensohnii*) were tested by Wilcoxon matched paired test. To determine significant differences in the elemental concentrations between different periods of the moss bag exposure, Mann–Whitney U test was used. To assess the specific associations and origin of the elements, Spearman's correlation analysis between the element concentrations was done. All tests were performed at the confidence level of $p < 0.05$.

As a measure of moss capability for the element accumulation, relative accumulation factors (RAF) were calculated according to the equation:

$$\mathrm{RAF} = (C_{exposed} - C_{initial})/C_{initial} \quad (2)$$

where the element concentration in the moss after exposure ($C_{exposed}$) was reduced and divided by its concentration in the moss before exposure ($C_{initial}$).

Enrichment factors (EF) (Bargagli et al. 1995) of the elements in the mosses were calculated according to the typical crustal values (Mason 1966) and local topsoil values (Aničić et al. 2007) using the formula:

$$EF = (E/R)_{moss}/(E/R)_{E.crust/topsoil} \quad (3)$$

where E represents a particular element in the sample and R represents a referent element (Al was used as a referent element for other measured elements in the natural background, such as the Earth's crust or local topsoil. If EF is close to unity, then crustal material is likely to be a predominant source of the element (E) in the studied sample (moss), while EF values higher than one suggest the contribution of non-crustal sources (Bergamaschi et al. 2002; Berg et al. 1994; Wang et al. 2005).

Results and Discussion

H. cupressiforme vs. S. girgensohnii

H. cupressiforme moss is widely present species in the studied climate, while *S. girgensohnii*, although highly recommended for biomonitoring purpose, rather represents an endemic species in the study area. Hence, we intend to test both species and their interchangeable use at the studied suburban background site, with relatively low air pollution confirmed by previous PM measurements (Vuković et al. 2015). The initial element concentrations in the unexposed moss material represent one of the factors influencing the efficiency of element entrapment by moss and expected to differ in the two moss species. In this study, both moss species were collected from the pristine areas selected for the purpose of all our active biomonitoring studies (Aničić et al. 2009a, 2009b; Vuković et al. 2015; Milićević et al. 2017; Aničić Urošević et al. 2017b, a; Aničić Urošević and Milićević 2020 and references therein). The measurements showed that the initial element concentrations in the mosses were at a similar level to those measured in the previous surveys. However, the values in the moss *S. girgensohnii* were lower than in *H. cupressiforme*, except for Mg, Mn, and K (Table S1, Supplementary material). This difference in element composition between the mosses can be a consequence of their morphological features and growth rates (Zechmeister 1995) and environmental pollution of the pristine/background areas. *H. cupressiforme* represents pleurocarpous moss with a spread carpet-like thallus in tight contact with the substrate and a relatively low growth rate, which are predispositions for increased element content. Conversely, *S. girgensohnii*, whose thallus is growing upright, achieves typically high biomass with low element enrichment (Mohamed, 2014). In addition to specific morpho-physiological and ion-binding preferences (Brown 1982; González and Pokrovsky 2014; Varela et al. 2015; Glime 2017), the lower initial element content in *S. girgensohnii* suggesting that cation-exchange sites were not saturated with basic cations, which possibly influenced better element adsorption capacity in comparison with *H. cupressiforme* species (see discussion in Section 3.4). The indication of more efficient entrapment of elements by moss with low initial element content was also shown in previous research (Culicov and Yurukova 2006; González and Pokrovsky 2014). In present research, low standard deviations (SD) of the initial element concentrations measured for the *S. girgensohnii* subsamples, except for Ni, Sr and Pb, testify about more homogeneity of the initially used moss material for the bag preparation, contrary to *H. cupressiforme*. The uniformity of initial moss material very likely influenced the element concentrations in the exposed moss bags, especially in case of short exposure time. Although short-time exposed moss bags (15-day exposure time) showed low element enrichment, variations of element content in *H. cupressiforme* bags were notable between consecutive 15-day exposure periods which can be influenced by pronounced variations of the initial element concentrations (SD) in the unexposed material of this moss (Fig. 1, Table S1). It should be noted that the initial element concentrations are indicated in Fig. 1 and Table S1. Since the unexposed *S. girgensohnii* material showed to be more homogenous and with lower initial element content than *H. cupressiforme*, this species can be considered as more reliable for testing the short-time moss exposure periods providing better replicability of the results.

The prolongation of bag exposure (up to six months) usually led to higher and more stable element enrichment in the tissue of both moss species, diminishing the influence of variability of the initial element content. The element enrichment in *H. cupressiforme* gradually increased with prolongation of exposure time, reaching a kind of plateau after the third month. Moss *S. girgensohnii* samples were also characterized by an increase of the element concentrations with time, but with a sharp decrease of the concentrations in two- and four-month exposed moss samples. These periods of the year (June–August) were characterized by increased air temperature and several days of intense precipitation events, which, as will be discussed in more detail in Section 3.3, represent unfavored environmental conditions for capture and keeping of airborne elements (Figure S1).

Besides different initial element content in the studied mosses and different thallus form number of ion-binding sites on the membrane surface could influence differences in the element uptake during the moss exposure. Still, correlation analysis applied to all exposure periods showed a

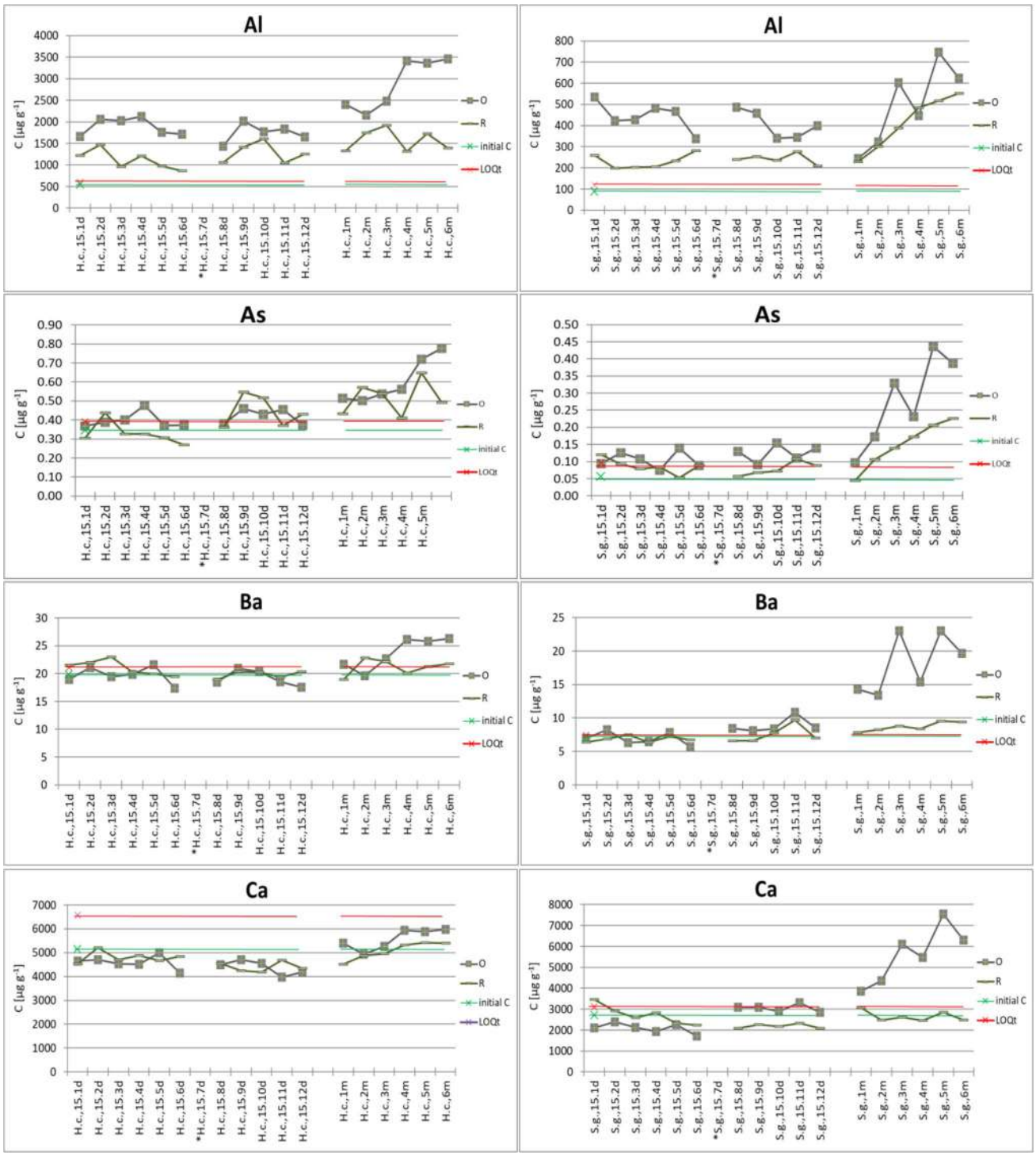

Fig. 1 The element concentrations (µg g^{-1}) measured in the moss *H. cupressiforme* (H.c.) and *S. girgensohnii* (S.g.) samples exposed for twelve 15-day consecutive periods (15.1–15.12d), one-, two-, three-, four-, five-, and six-month periods (1 m, 2 m, 3 m, 4 m, 5 m, 6 m, respectively) at open space (O) and under the roof (R) during the spring/summer season 2019; the element concentration in the unexposed moss material (initial C); limit of quantification for the moss bag technique (LOQt); *excluded data due to unforeseen local emission—landscaping and mowing a surrounding lawn

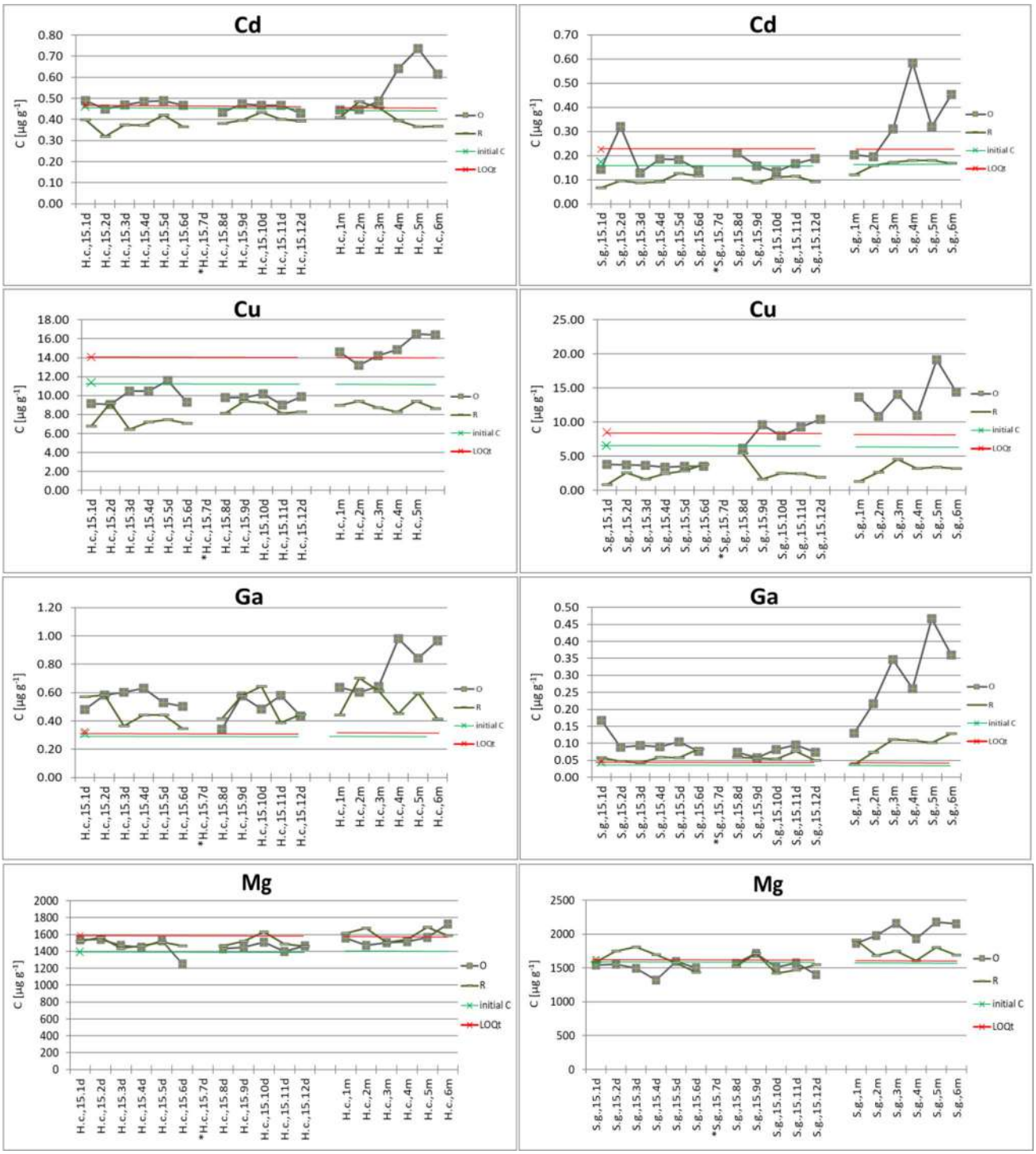

Fig. 1 (continued)

good correlation of V, As ($r > 0.89$), Ba, Ca, Ga ($r > 0.7$), Zn, Cd ($r > 0.6$), Co, Mg, Tb, and Y ($r > 0.5$) concentrations between the two studied moss species, exposed at open space (Fig. 2). This finding suggests a possible comparable use of *H. cupressiforme* and *S. girgensohnii* for biomonitoring of the above-mentioned elements, particularly V and As.

Moss element concentrations vs. exposure time

An optimal moss bag exposure time is also one of the crucial variables influencing a reliable signature of elements in the moss, especially at a background site with a relatively low airborne element burden. The optimal duration of moss bag

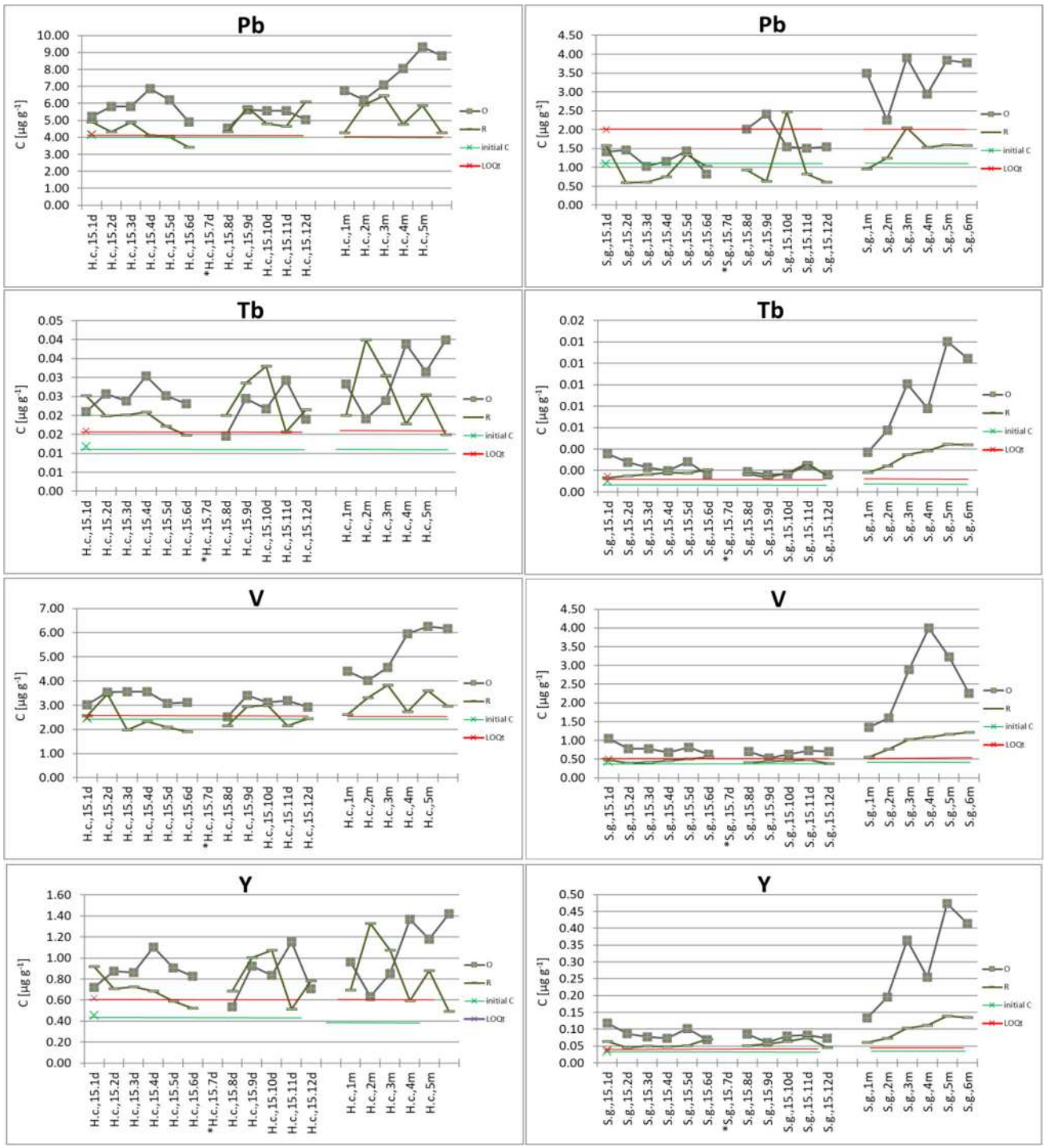

Fig. 1 (continued)

exposure has often been tested in diversely polluted environments. However, previous studies mainly considered longer moss bag exposure times, lasting from a month to several months, but the most often in the condition of increased ambient pollution, around industrial sources or in urban areas (Ares et al. 2012). In addition, the majority of our moss bag studies (e.g., Vuković et al. 2015, 2016) were performed in the urban area of Belgrade city, which is characterized by increased level of air pollution in comparison with a rural or remote areas, that guarantee the remarkable element enrichment in the moss material during exposure. Here, in this study, we focus on testing the applicability of the moss bag

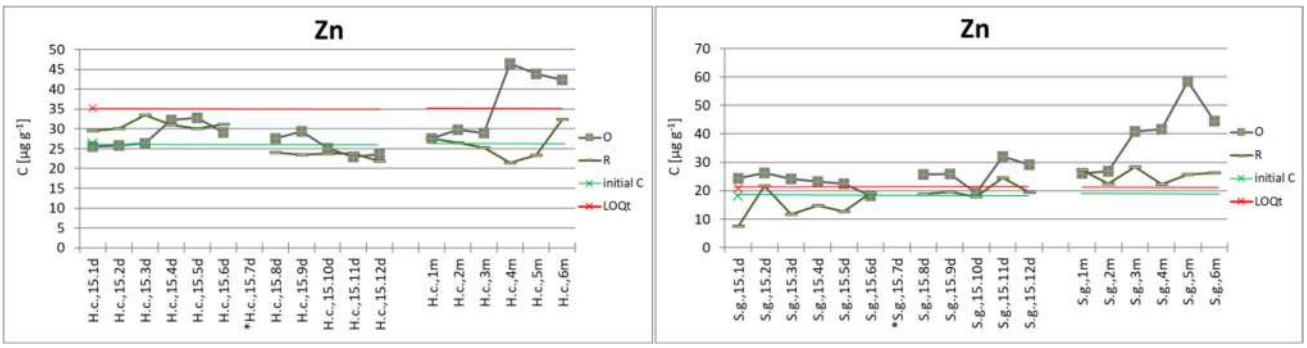

Fig. 1 (continued)

technique in research of dynamics of airborne PTEs at the suburban background site, during a period of expected intrusions of long-range transported dust. The possibility of an accidental influence of remote emissions to the studied site set a challenge for testing a short-time bag exposure, bearing in mind that these events usually last up to several days. Recent research by Capozzi et al. (2016b) showed that three weeks of *Pseudoscleropodium purum* bag exposure in a rural (unpolluted) area were not enough to achieve a consistent signal of the PTEs in the moss, above the LOQt, while only a small difference occurred between six and 12 weeks of bag exposure. Despite this conclusion, we followed our previous experience regarding different periods of moss bag exposure at suburban background site that the significant accumulation of the PTEs in *S. girgensohnii* bags was found after two weeks of exposure (Aničić et al. 2009a). Hence, in this study, we have defined 15 days as the minimal moss bag exposure time. Although the LOQt criterion was not applied in Aničić et al. (2009a), the moss element uptake after 15-day bag exposure appeared meaningful.

Figure 1 presents the element concentrations in the two moss species that were exposed in the bags for different periods of time (from 15 days to six months) at the study site. The level of element load in the exposed mosses was studied considering the initial element content in unexposed moss material, and the LOQt (defined in Section 2.6). The latter is a stricter criterion for overcoming a possible error associated with an effect of averaging the initial element content in the unexposed moss material. Element concentrations in both mosses were increased with the prolongation of exposure, achieving the highest values after several months, not necessarily after the longest moss exposure of six months. In addition, not all the elements showed the same temporal dynamics of concentration change in the mosses, which certainly depends on their presence in the ambient, the initial element concentrations in moss, the morpho-physiological characteristics of the used mosses, the affinity for ion-exchange sites on cell membranes, etc. (Varela et al. 2015; Ares et al. 2012). The database for all elements determined in the moss bag samples after different exposure times is provided in the Supplementary material (Table S1).

The presented results indicate that 15-day period of moss exposure was not enough for achieving a reliable signature of the majority of measured elements in the moss tissue of both studied species, since the accumulated element concentrations were close to their initial element content. With the prolongation of bag exposure (from one to six months), the element enrichment in the tissue of both moss species has become more defined, i.e., were increasing with time.

Considering the shortest periods of 15 days, the elements that were significantly enriched in both exposed mosses (above the LOQt) were, particularly Al, but to some extent As, Ga, Tb, V, and Y, while Pb and Zn were enriched only in *H. cupressiforme* and *S. girgensohnii*, respectively (Fig. 1). The total concentrations of these elements significantly correlated with each other, but with higher correlation coefficients in *H. cupressiforme* ($r > 0.8$) than in *S. girgensohnii* ($r > 0.6$). The correlation of net accumulated element concentrations (after excluding the initial values) will be discussed in more detail in Section 3.4. Most of these elements are typical soil constituents (Kabata-Pendias 2011), and the resuspension process and meteorological conditions can contribute to their increased content in the air, especially during dry spring/summer season. Note that the two moss species in the consecutive 15-day exposure periods showed different trend of the element variation in the studied ambient. The possible explanation lays in their different morpho-physiological features and the initial elements content, discussed in the Section 3.1. However, in the seventh 15-day period (15.7.d), unexpectedly high concentrations of all the elements were measured in the mosses, particularly in *S. girgensohnii* samples. This peak of the element concentrations was likely related to an unforeseen local emission—landscaping and mowing of a surrounding lawn, which caused strong local topsoil resuspension, and hence we decided to exclude this data due to non-representativity.

An extended moss bag exposure (from one to six months) was used in addition, as a proven method to

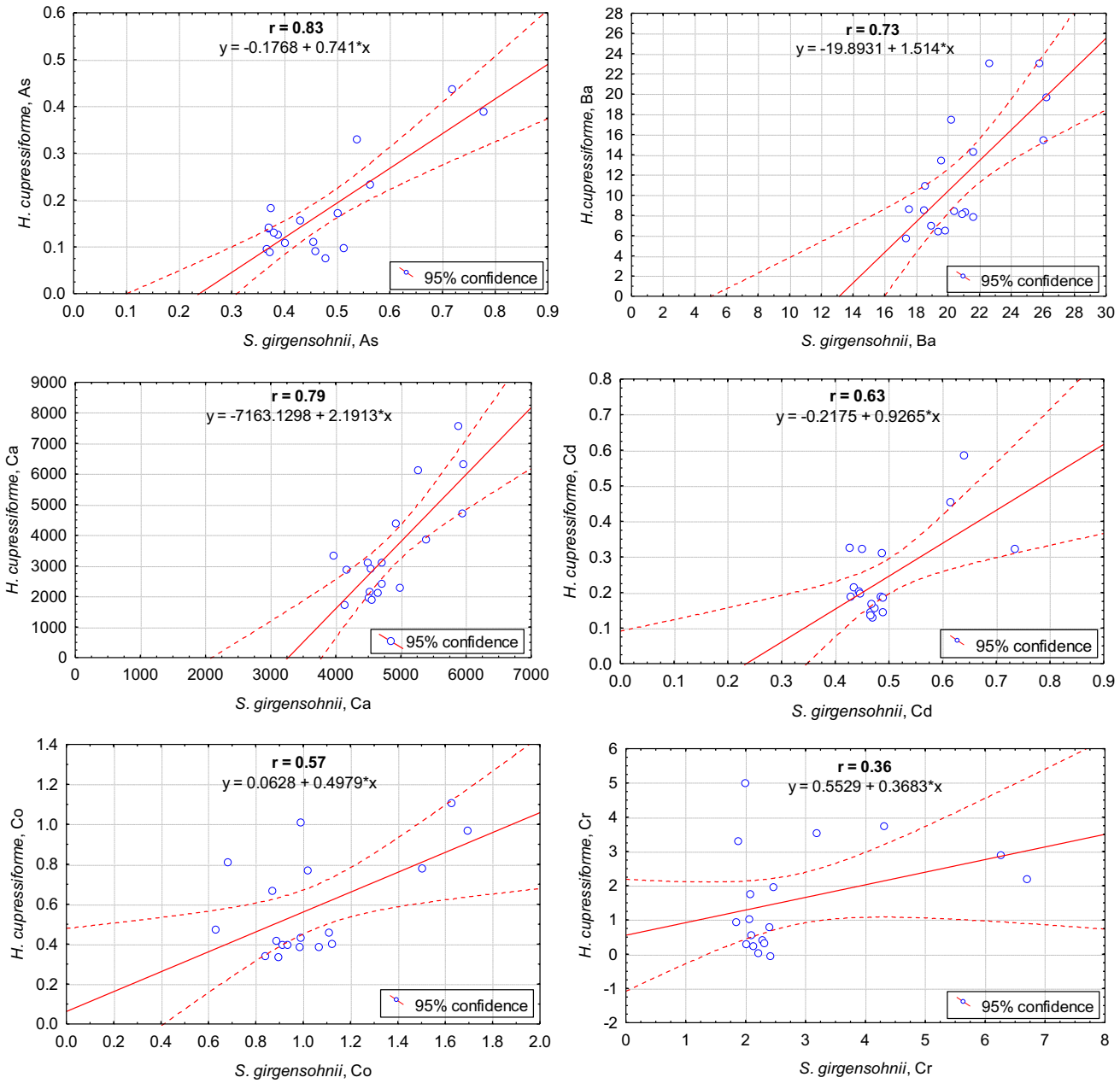

Fig. 2 Correlation between corresponding element concentrations (As, Ba, Ca, Cd, Co, Cr, Ga, Mg, Tb, V, Y, Zn) measured in two moss species *H. cupressiforme* and *S. girgensohnii*

achieve the stable pollutant signature in the mosses at the sampling site. The moss element content has increased with the bag exposure time, and statistically significant element enrichment in comparison with LOQt values was achieved after two–three months for both studied species (Fig. 1, Table S1). A similar conclusion was reached in the previous study (Aničić et al. 2009a), in which only the *S. girgensohnii* bags were exposed from 15 days up to five months at the same suburban site, but on the roof terrace of the Institute, which is more traffic-oriented, unlike the sampling site in this study, which is in the inner courtyard. In comparison with the previous study, enrichment of *S. girgensohnii* tissue by the PTEs was less pronounced in the present study, especially for Fe and Pb (possibly due to the phase-out of leaded gasoline in the meantime). For some other elements (Ba, Ca, Co, Sr, V), it looks like an enrichment plateau was reached after six months of exposure (Figure S2). It is worth noting that the consecutive 15-day periods of the moss exposure in the present study gave evidence that there was no uniform element

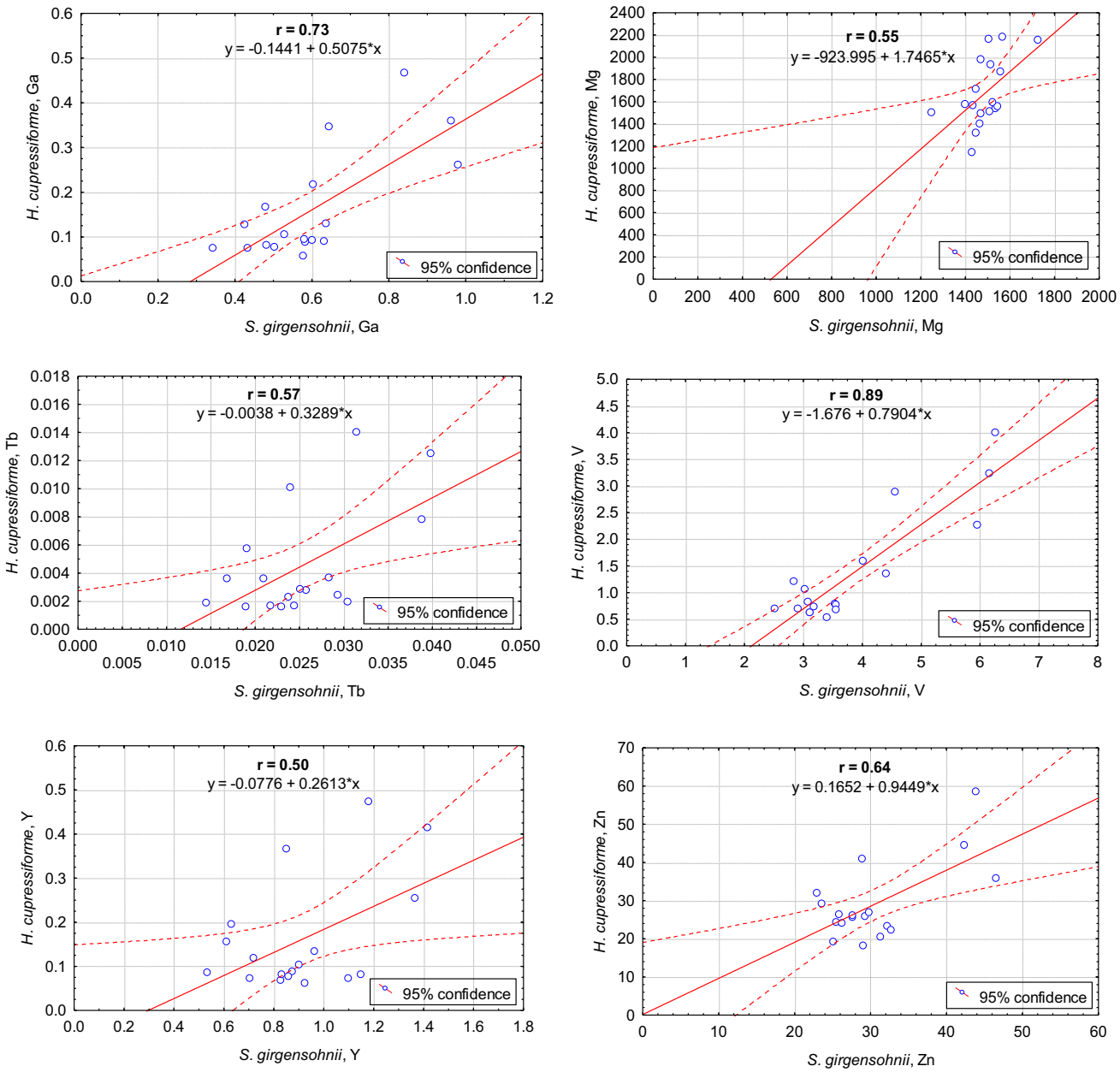

Fig. 2 (continued)

enrichment with time in the mosses. Also, the element content in the moss bag exposed for prolonged periods is not a simple sum of its content during shorter 15-day exposures. The cumulative element content in the moss after several months of exposure represents a dynamic equilibrium between adsorption and release of the PTEs in favorable (humidity) or unfavorable (strong wind and intensive precipitation events) conditions. Salo and Mäkinen (2019) showed that bags of ectohydric moss species *Sphagnum papillosum* collected PM more efficiently in humid conditions. Furthermore, the loss of coarse particles from the moss surface is inevitable in long-term bag exposure, while smaller size particles (classes < 2.5 μm) are more efficiently entrapped and kept on rough moss surface (Tretiach et al. 2011). The comparison of two-month element enrichment in the mosses from this study with the previous summer study regarding air pollution zoning in Belgrade, using the same biomonitors (Vuković et al. 2015) showed that the majority of the analyzed elements from this study were in the concentration range estimated for the residential zones. The residential zones in the previous study were recognized as less polluted than the typical urban ones (with intense traffic flow). The exceptions are Co, Cr, Cu, and V, whose concentrations in this study

exceed the levels found in the residential zones and were at the level characteristic for the typical urban zones.

Extension of exposure time did not lead to increased concentrations of all measured PTEs in the moss tissue. Namely, concentrations of a couple of macroelements (K, P) in the exposed moss bags were lower than the initial content in the unexposed mosses (Table S1). For some other elements (Mn, S), strong depletion of the concentrations was recorded in the 15-day exposed bags of both species, but with slight increase with extension of exposure time. Note that at the same time, depletion of these elements was less pronounced in the bags exposed under the roof than those exposed at open space. This phenomenon was also recorded in the previous study (Aničić et al. 2009a) for a studied moss *S. girgensohnii* exposed at open space. The above-mentioned elements are physiologically active macroelements, and they were probably leaching from moss transplants due to the cell-membrane damage and its interruptions caused by changing the moss native ambient (Spagnuolo et al. 2011). Still, this depletion was less pronounced in the moss samples set under the roof that provided some kind of shadow enabling more favorable microenvironmental conditions for the exposed mosses. However, the lack of the above-mentioned element accumulation in the exposed moss bags is evident, which does not favor the use of the mosses for biomonitoring of these macroelements. Further discussion will be predominantly focused on the elements that were accumulated above the LOQt in the exposed moss tissue.

Moss bags at open space vs. moss bags under roof

Exposure of the moss bags under the roof was aimed at diminishing the influence of wet and dry atmospheric deposition of aerosols to the element content. The moss samples under the roof receive airborne pollutants mainly by wind or fog. The moss bags hung under the improvised roof showed the lack of substantial element accumulation after the 15-day exposures, which remained at a similar level with prolongation of the bag exposure (Fig. 1). The total element concentrations in the moss samples exposed at open space were usually higher than those in the moss bags that were hung under the roof, especially for longer periods of bag exposure (> 2 months). This indicates the important effect of wet and dry deposition on element content in exposed moss samples. Namely, wet deposition can contribute to the more efficient sorption of elements from the solution, while intense precipitation events cause wash-off of particles from the exposed mosses. Calculated for all tested periods of the moss bag exposure, the difference between mosses at open space and those under the roof was statistically significant ($p < 0.05$) for Al, Fe, K, Li, Mn, P, S, V, Cr, Cu, Cd, Pb in *H. cupressiforme*, and Ba, Fe, P, Pb, S, Zn, V, Cr, Co, Cu, As, Cd, Ga, Y, Tb in *S. girgensohnii*. In a laboratory experiment (González and Pokrovsky 2014), both mosses *S. girgensohnii* and *H. cupressiforme* demonstrated very fast adsorption kinetics in metal solution, and steady-state element concentration is achieved in several minutes, remaining constant for a longer time. It suggests that the element-binding from the rain solution in real conditions had predominance over the moss wash-off effects by precipitation. However, increase of rainfall intensity possibly influences particle removal from biomonitor (leaf) surface (Zhou et al. 2021). The field study estimating metal uptake efficiency from precipitation in moss (Čeburnis and Valiulis 1999) showed that the best retained elements were Pb, Ni, Cu and V, and significantly lower uptake for Cd, Cr, Fe and Zn, while Mn always leached from the mosses. The similar pattern of the element uptake was obtained in this study. Although average precipitation during our study was relatively low, in May, June, and at the beginning of August there were a couple of days with increased precipitation, > 20 mm day^{-1} (Figure S1). Still, the rain wash-off effect of the moss bags exposed for 15 days at open space is hardly observed due to the mainly low element accumulation rate during this minimal bag exposure (around the LOQt). However, for the moss bags exposed for two and four months (especially *S. girgensohnii* bags), the drop in the element enrichment of moss tissue is observed, which could be explained by the mentioned days with increased precipitation. For the moss bags exposed under the roof, the reduction of direct wet and dry deposition during the extended periods of exposure substantially decreased the element enrichment in the mosses. Thus, further discussion will be only focused on the element concentrations in the moss bags exposed at open space.

Relative accumulation factors (RAFs) and enrichment factors (EFs)

The results show that both moss species testify about the presence the certain elements in the studied environment, particularly in their prolonged exposure. To exclude the influence of initial element content on comparison of the studied moss species, we calculated relative element accumulation in the mosses (Table S2). The RAF values of the elements in *S. girgensohnii* were mostly higher than in *H. cupressiforme*, probably due to the lower initial tissue load of the elements like Sr, Mn, Cd, Ni, Ca, and Cu, and the opposite for Mg. Expectedly, in the samples exposed in 15-day periods, the average RAF values for the majority of the elements in both moss species were close to zero or negative, especially in *H. cupressiforme*, while longer bag exposure provided the moss RAF increase. However, even for the 15-day exposure periods significant accumulation of several elements (Al, Ni, V, Pb, Ga, Y, Tb, As) in *S. girgensohnii* is indicated by the average RAF values (4.1, 5.1, 0.7, 0.9, 1.1, 1.5, 1.3 and 1.0, respectively). Most of

these elements are in focus of the analysis presented in Section 3.5. The prominent average RAFs (> 1) for prolonged bag exposure (one to six months) were reached for Al (4.3 and 4.7), Fe (6.8 and 0.9), Ni (2.3 and 4.5), V (1.1 and 4.8), As (0.7 and 3.9), Ga (1.5 and 5.8), Y (1.4 and 8.1) and Tb (1.6 and 8.2) in *H. cupressiforme* and *S. girgensohnii*, respectively. RAF values in the moss bags under the roof were substantially lower than those in the corresponding samples exposed at open space. The correlation of RAF values between elements was stronger in the case of *H. cupressiforme* than in *S. girgensohnii* (Figure S3), which is probably a consequence of strong soil element signature in the pleurocarpous *H. cupressiforme* species coming from its source habitat.

To recognize the effects of soil resuspension, enrichment factors (EFs) were calculated following the element abundance in the local topsoil and their values in the Earth's crust (Table S3), which indicates that the rest of the moss enrichment with elements is probably originating from other, mostly anthropogenic, sources. The enrichment of the elements in the exposed mosses was calculated using net element concentrations (i.e., after subtraction of the initial element content in the mosses). In both moss species, Al, Ba, Fe, Ni, Zn, V, Cr, As, and Tb were enriched to some extent for all periods of the bag exposure, according to both scales, lithological and local topsoil. Calcium was enriched only in *S. girgensohnii* bags after prolonged exposure periods. For some elements (Pb, Ga, and Y), the concentration values in local topsoil were not available.

After short bag exposure of 15 days, the EFs of elements in the mosses were quite low, close to zero, except for Fe, As and Pb in both species and Ni, Zn and Cr in *S. girgensohnii*. The longer bag exposure resulted in higher element EF values. The element enrichment was again higher for *S. girgensohnii* than *H. cupressiforme*, with average EFs of up to 60 (Zn) and 10 (Pb); and maximal EFs of up to 100 (Pb) and 12 (Pb), respectively (Fig. 3).

The element EFs in the mosses calculated according to the Earth's crust values were always higher than those estimated concerning the element composition of local topsoil. Note that for all exposure periods of both mosses the values of $EF_{E.crust}$ were prominent for As and Zn, while their $EF_{topsoil}$ values were substantially lower, especially for As (a factor of 7–8 lower). For As, the possible explanation could be a peculiarity of the naturally increased As content in Balkan soil (Dangić and Dangić 2007). Even some rare (Tb, Y) and trace (Ga) elements were slightly enriched in the mosses after exposure. Besides the resuspension of local soil, the high airborne content of some trace (Mn, V, Cr) and rare earth elements (REEs) can be desert dust-related (Querol et al. 2019). Thus, we assume that besides the local soil resuspension, the moss bag technique may give a signature of some long-range transported elements. Although the element EF values were relatively low, after excluding the influence of the initial element content and the impact of the element content from the local topsoil, even this not high enrichment of the elements in the mosses ($EF_{topsoil}$) is meaningful and could be associated with local anthropogenic sources and/or remote aerosol sources (e.g., Saharan dust intrusions).

Moss element enrichment vs. ground PM measurements during Saharan dust episodes

In the conditions of presumably low seasonal air pollution at the suburban background site, the influence of possible accidental emissions from some local or remote sources may result in the increase of element concentrations in the corresponding moss samples exposed in the series of twelve consecutive 15-day periods. In this study, three Saharan dust

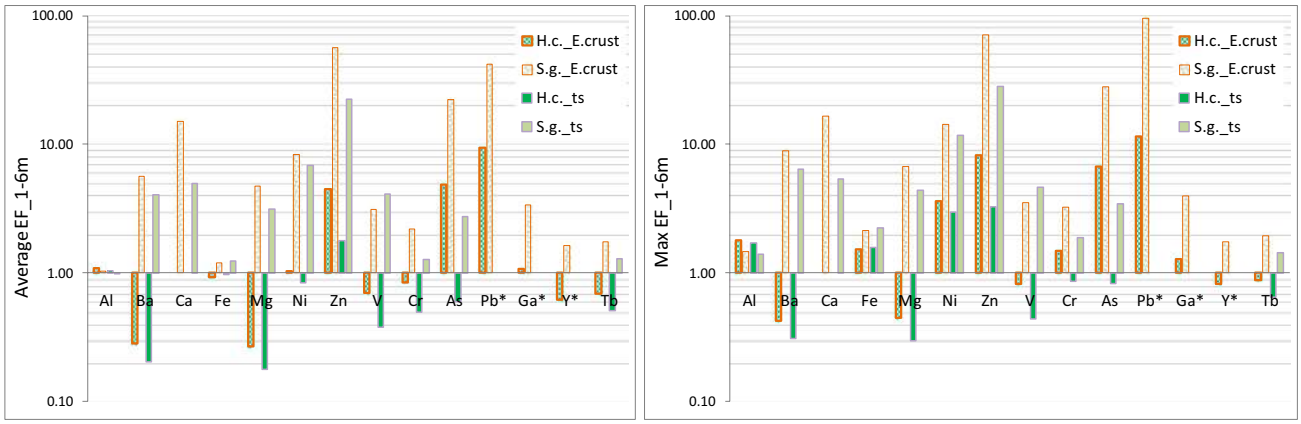

Fig. 3 Average and maximum EFs of the elements in *H. cupressiforme* (H.c.) and *S. girgensohnii* (S.g.) for exposure periods of 1–6 months calculated according to the Earth's crust (E. crust) and local topsoil element concentrations (ts); asterisk (*) means that the values for some elements were not available in the local topsoil

episodes (SDE), each lasting for several days, were identified over the study area within the period of April–October, 2019: 23–27 April (SDE1), 26–30 May (SDE2), and 8–15 June (SDE3) (Table 1). The potential influence of dust episodes on the moss element content was tested. It is noteworthy that elements characteristic for Saharan dust (Si, Al, Ca, K, Mg) are also major components of resuspended urban dust (Amato et al., 2009; 2016), including road dust, dust from construction works and local soil. Thus, analysis of PM samples corresponding to days after each SDE is necessary to make conclusions regarding the influence of Saharan dust (dust in further text) on particulate pollution. Additionally, the measurements of PM10 and PM2.5 mass concentrations were taken during each dust episode and several days after the episode. Here, we first discuss the results based on PM samples collected during dust episodes and then present the findings based on moss bag samples.

Outbreaks of Saharan dust affect particulate matter concentrations in Europe (Rodríguez et al. 2001; Alastuey et al. 2016). Alastuey et al. (2016) showed that the average dust load in PM10 concentrations was 0.5–10 μg m^{-3} at most sites of the European Monitoring and Evaluation Programme (EMEP) during the summer Saharan dust outbreaks. It should be noted that dust is transported within elevated layers and it does not necessarily contribute to PM concentration during all days of dust episode, as in a case study by Ajtai et al. (2020).

In our study, dust models suggest that dust load was particularly large during the SDE1 (Figure S5). Still, concomitantly performed measurements of PM2.5 and PM10 fractions (Table 1) at the study site showed relatively low mass concentrations, compared to the daily limit values of 25 μg m^{-3} and 50 μg m^{-3}, respectively, defined by the air quality standards (EEA, 2019; Directive 2008/50/EC). The average PM10 concentrations during the three measurement periods are lower than the average value of 37.52 μg m^{-3} reported for spring months of the 2003–2015 period in urban area of Belgrade (Stojić et al., 2016). Significant particle concentration in coarse (PM10—PM2.5) fraction is one of the general characteristics of dust contribution (Rodríguez et al. 2001; Alastuey et al. 2016; Dimitriou and Kassomenos 2018). The most prominent concentration of coarse fraction in this study was observed during SDE1, with the maximum of 22.5 μg m^{-3} reached on April 25, contributing to 62% of PM10 concentration. The least intense episode was SDE2, as suggested by models and measurements (Figure S5), with measured coarse particle concentration of up to 7.3 μg m^{-3} (44% of PM10 concentration).

Aluminum silicates represent one of the main mineral components of desert dust (Querol et al. 2019), and Al is often used as a tracer for dust. Elemental characterization of PM10 samples collected at the studied site showed that Al concentrations were increased by an order of magnitude during the SDE1 and somewhat less during the SDE3 (Fig. 4).

Querol et al. (2019) reported that, besides crustal elements, some trace (including V, Cr) and rare earth elements (including Tb) could show higher enrichment in PM samples collected on desert dust days, compared to non-dust days. Yttrium is not REE, but it is often associated with them, while Ga is often associated with Al and Zn ores (Kabata-Pendias 2010). Note that the analysis of PM is performed here as a guideline for examining a signature of dust in moss samples. Thus, we confine our interest to the elements that are significantly accumulated in moss samples.

In this study, besides Al, the concentration of V, As, Ga, Y, and Tb in the PM10 samples was markedly higher during the dust days, in comparison with non-dust days. The concentration of Al shows a strong correlation ($r^2 = 0.84$) with PM10 during non-dust days, with an average Al/PM10 mass ratio of 0.008 ± 0.002. Its content in PM10 increased during dust days, with maximum Al/PM10 ratio values of 0.034, 0.012, and 0.026 during SDE1, SDE2, and SDE3, respectively. It should be noted that the largest Al content in PM10 was observed during the SDE1, which was recognized as the most intense of the three observed episodes. The increased coarse fraction of particulate matter and increased contribution of Al content in PM10 indicate that dust contributed to PM10 during all three observed episodes, most prominently during SDE1. The increase of the element/PM10 concentration ratio during dust episodes was also observed in the case of V and Y, indicating their relation with dust. Both elements show lower correlation with PM10 concentration, compared to Al ($r^2 = 0.58$ and $r^2 = 0.77$ for V and Y, respectively), during non-dust days. The corresponding element fractions in PM10 were $(6 \pm 2) \times 10^{-5}$ for V and $(4 \pm 2) \times 10^{-6}$ for Y. These fractions increased during dust

Table 1 Average mass concentrations (μg m^{-3}) of PM2.5 and PM10 during three Saharan dust episodes and several days after the episodes, and daily limit values prescribed by the air quality standards

Saharan dust episode		PM10					PM2.5				
		Min	Max	Average	*SD*	Daily limit	Min	Max	Average	*SD*	Daily limit
I – Apr	22/04 – 01/05/2019	10	40	25	*12*	< 50	7	**28**	16	*7*	< 25
II – May	27/05 – 03/06/2019	3	21	11	*6*		3	13	7	*5*	
III – Jun	08/06 – 22/06/2019	15	49	29	*9*		9	**27**	18	*6*	

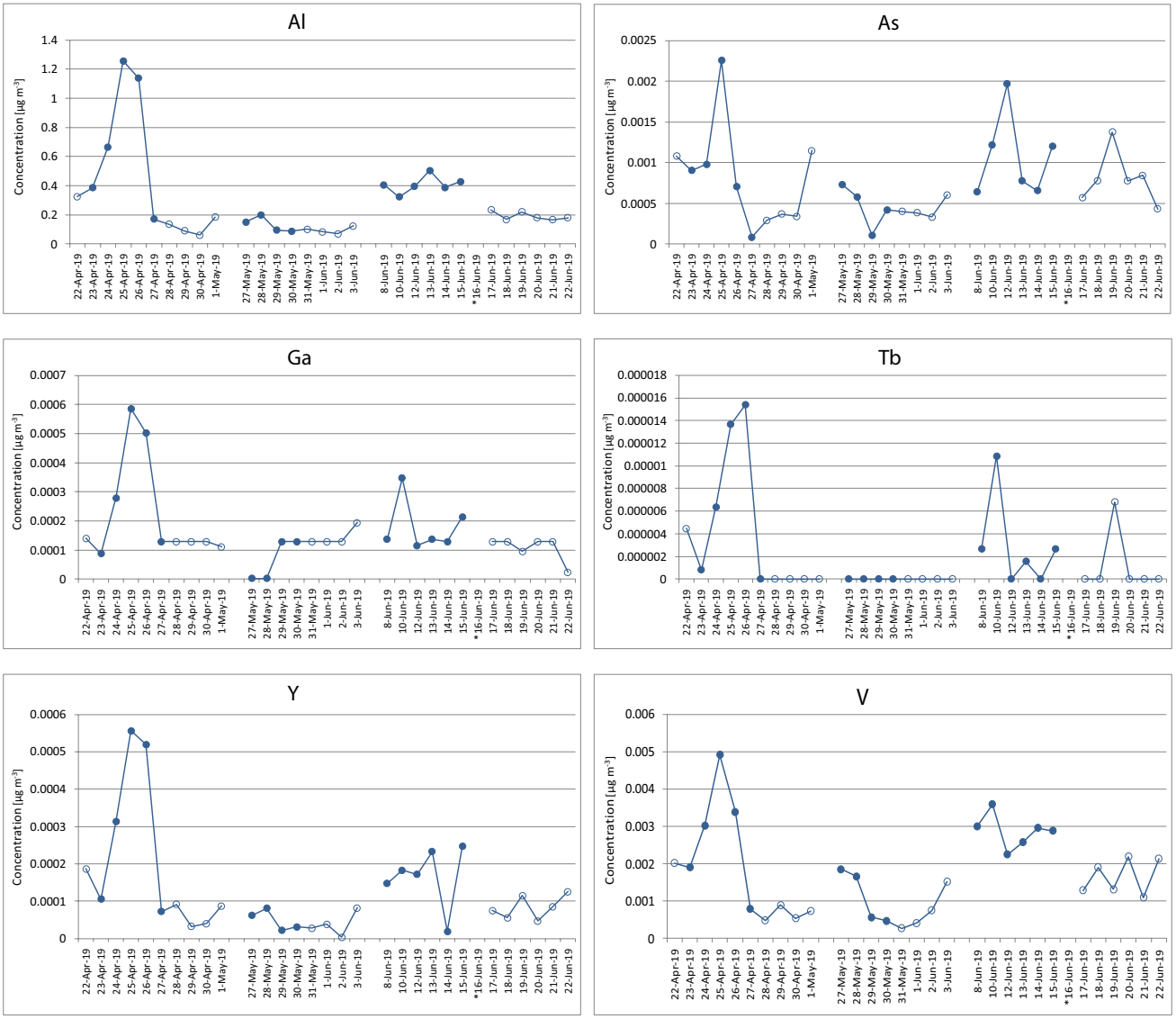

Fig. 4 The element concentrations (μg m^{-3}) in the PM10 samples collected during the days of the three episodes of Saharan dust and several days after at the studied site; open symbols correspond to non-dust days, while filled symbols are for dust days; asterisk (*) refers to the missed filter

days to $(11 \pm 3) \times 10^{-5}$ and $(8 \pm 3) \times 10^{-6}$ for V and Y, respectively. This suggests that dust contributed to the increase of concentrations of these elements.

Scheuvens et al. (2013) pointed out that concentration ratios of Ca/Al and Mg/Al in desert dust show variability across dust source regions. Furthermore, Querol et al. (2019) suggested that Ca/Al in PM can be used for distinguishing desert dust from urban dust contributions in urban environments, as these ratios are higher in the latter case. In this study, the above-mentioned ratios are analyzed in the collected PM10 samples during dust and non-dust days and the results are presented in Table S3. The average Ca/Al ratio during dust days was 3.4, with the maximum value of 5.8, while during non-dust days concentration of Ca was mainly below the detection limit. The results agree with those reported by Remoundaki et al. (2011) for PM10 samples collected in Athens during dust episodes originating from western Sahara and Algeria. The average $EF_{topsoil}$ for Ca was 2.5 (for dust days), suggesting the influence of additional, non-local sources.

The ratio of Mg/Al during dust days varied within the range of 0.03–0.80, with an average of 0.32. For two PM10 samples most affected by dust (as suggested by models, measured coarse fraction of PM, and Al fraction in PM10, described above), collected during SDE1, the values were 0.37 and 0.38. These are similar to the ratio obtained for local topsoil (0.39), as well as to the ratios reported for western Africa (Moreno et al. 2006; Scheuvens et al. 2013),

suggesting that Mg/Al ratio is not appropriate for distinguishing between influences of local soil resuspension and Saharan dust on PM10. The values of Ca/Al and Mg/Al during dust days are in line with those found by Djordjevic et al. (2019) for a larger number of Saharan dust events in 2012 and 2013.

Among other considered elements (which were also significantly accumulated in moss samples), As showed high $EF_{topsoil}$, with average values of 13.6 and 24.1 for dust and non-dust days, respectively. While concentrations of As in PM10 showed some peak values during dust episodes, particularly during SDE1, the average $EF_{topsoil}$ is smaller than that for non-dust days. This can be explained by decrease of As/Al ratio during dust days due to more significant increase of Al concentration (note that Al was the referent element in the calculation of $EF_{topsoil}$). High $EF_{topsoil}$ for As indicates that PM10 samples were affected by anthropogenic sources during both dust and non-dust days.

The average $EF_{topsoil}$ for V (5.1 during dust episodes and 6.2 during non-dust days) also indicates contribution from additional, probably mainly anthropogenic sources. These toxic elements, As and V, were likely petrol/diesel- and oil combustion-related pollutants, respectively (Pulles et al. 2012; Pacyna and Pacyna 2001) deposited generally in urban soils, whose particles have been transported by wind (Mach et al. 2021).

Gallium and Y were strongly correlated with Al ($r^2 = 0.82$ and $r^2 = 0.97$, respectively) during dust episodes. The mass ratio of Ga/Al was $(4 \pm 3) \times 10^{-4}$ during the dust days, while Ga concentrations during non-dust days were often below the detection limit. Yttrium showed similar Y/Al ratios for dust and non-dust days (ranging from 4.6×10^{-5} to 6.9×10^{-4}, and an average of 4.4×10^{-4}). These values were within the range of $(3.2—10.0) \times 10^{-4}$ obtained for Saharan dust samples, based on data by Moreno et al. (2006). We did not have information on Ga and Y concentration in local topsoil to calculate $EF_{topsoil}$.

The described analysis, performed to identify elements that should be considered in attempt to distinguish desert dust influence on elements in moss samples, revealed that the considered elements at the study site showed lower $EF_{topsoil}$ during dust days, in comparison with non-dust days. In case of As, the $EF_{topsoil}$ values indicate predominant anthropogenic origin of this element. Thus, As/Al ratios could be useful in making distinction between PM10 datasets dominantly influenced by anthropogenic pollution and those largely affected by urban or desert dust. The considered element ratios did not show clear distinction between dust and non-dust days.

When using moss bags for sampling Saharan dust, it should be noted that Saharan dust episodes could not be matched in advance with the series of minimal periods of moss bag exposure. The identified dust episodes lasted for several days, while the minimal period of moss bag exposure was 15 days. Thus, to better understand to what amount of dust the moss bags were exposed during 15-day periods, we averaged MERRA-2 predictions of dust concentrations at ground level over these periods (Figure S5). MERRA-2 data showed significant surface dust concentration during the SDE1, resulting in markedly higher average dust concentrations on April 15−30 (15.1d), compared to the other periods. While these concentrations are overestimated (in comparison with the measured PM10 concentrations), it should be noted that other models used for the identification of dust episodes (see Section 2.4) also predicted very intense SDE1. MERRA-2 data also showed increased dust concentrations in the first half of June (SDE3), but less than during SDE1. Lower surface dust concentration was predicted for SDE2. As discussed above, the PM10 and PM2.5 concentrations, as well as Al content in PM10, also indicated significantly higher dust load during SDE1, compared to SDE2 and SDE3. It should also be noted that the lowest MERRA-2 dust concentration values were predicted for the period July 16–31 (15.7d).

Based on discussions in the previous sections, here we consider only *S. girgensohnii* moss samples exposed at open space. EFs and ratios of element concentration ratios in moss samples discussed in this section are calculated based on net element concentrations. The concentrations of Al, V, Ga, Y, and Tb were significantly accumulated in the moss samples during the 15.1d period, corresponding to the most intense dust episode (SDE1) and it was particularly pronounced in *S. girgensohnii* (Fig. 1). These were the only elements (besides As) significantly accumulated in both studied mosses after a minimal period of the bag exposure. Still note that only extended moss bag exposure (> 2 months) at open space (O) provided the substantial enrichment of the elements in the mosses, far above their initial values, and their concentrations measured in the control bags exposed under the improvised roof (R). Average element EFs calculated for prolonged moss bag exposure (1-6 m) were relatively low, except for some PTEs As, Zn, Pb, V, Ni (up to 40) and trace elements Ga, Y, and Tb (up to 5) (Table S3). For further discussion, it should be noted that moss samples exposed during 15-day periods that include dust episodes are 15.1d (SDE1), 15.3d (SDE2), and 15.4d (SDE3).

Aluminum is the only element that was substantially accumulated in both studied mosses in all exposure periods, even in all 15-day exposed samples and the control bags exposed under the roof. Aluminum showed the largest difference between samples exposed at open space and the corresponding samples exposed under the roof. This may imply the significant contribution of atmospheric deposition of this element over its resuspension with local soil dust. There is increased Al concentration in the *S. girgensohnii* in the 15.1d period corresponding to SDE1. The

peak of Al content is also found in the 3-month exposed moss bags, which could be due to the cumulative contribution of all three dust episodes.

Except for Al, several trace elements, V, Ga, Y, and Tb, in *S. girgensohnii* showed a similar temporal trend of accumulation in the exposed bags, with increased concentrations during 15.1d period (that overlapped with SDE1), in comparison with the average for non-dust periods. Although present at a very trace level, these elements were also increased in the PM10 samples collected during the mentioned episode of Saharan dust (Fig. 4). However, concentrations of these elements were not significantly increased in moss samples during the other two periods affected by less intense Saharan dust episodes (15.3d and 15.4d).

Furthermore, we focus on the analysis of ratios of element content in collected samples (Table 2), and their comparison with the previously discussed results in PM10, as well as with values reported in the literature for dust sources.

Due to the low accumulation of Ca and Mg in 15-day exposed samples, the ratios of Ca/Al and Mg/Al are considered only for longer exposure periods (1–6 months). We consider *S. girgensohnii* samples exposed for three months, which is the period successfully used in the previous biomonitoring studies in urban areas (e.g., Aničić et al. 2009b, 2009a), and covers all three dust episodes analyzed here. Both Ca/Al and Mg/Al ratios in the mosses were somewhat larger than maximal values obtained in PM10 during dust-affected days. The value of the Mg/Al ratio obtained for the *S. girgensohnii* sample was 1.09, which is larger than the value in local topsoil and the values observed in PM10 (0.03–0.84), discussed earlier in this section. Values as large as 0.9 have been reported for dust in Morocco (Scheuvens et al. 2013). The ratio of Ca/Al after three months of exposure was 6.6. This value is somewhat larger than values obtained in PM10 in this study (0.9–5.8), described earlier in this section. Such large values have been reported for dust in Morocco (4.0–6.8) (Scheuvens et al. 2013), and PM10 in Athens (7.7) for dust transported from western Africa (Remoundaki et al. 2011; Scheuvens et al. 2013).

Ratios of V/Al, Ga/Al, and Tb/Al calculated for moss samples exposed in 15-day periods showed increased value for the period 15.1d (corresponding to SDE1) in comparison with the samples not affected by dust. Note that the corresponding ratios in PM10 showed increase during dust days. The ratio values in moss pertaining to 15.3d and 15.4d (SDE2 and SDE3), and Y/Al values for the three dust periods were within the ranges obtained for non-dust periods. The values of the ratios were larger for longer exposure time, by a factor ranging from 2.8 in case of As/Al, to 6.1 for V/Al. These values are closer to those corresponding to PM10 samples.

Among elements of dominantly anthropogenic origin, only As was accumulated above the LOQt in moss bag samples exposed in 15-day periods. The As/Al ratio was low for samples 15.1d and 15.4d (corresponding to SDE1 and SDE3, the most intense of the three dust episodes), in comparison with the other samples. The exception is the sample 15.9d, which is characterized by a lower accumulation of As, indicating insignificant influence of fossil fuel combustion. Relatively high concentration of Al in this sample, in the absence of Saharan dust indicates contribution of resuspended urban dust. This suggests that the As/Al ratio can potentially be used to distinguish between moss bag samples dominantly affected by dust (long-range transported or local) from those dominantly affected by fossil fuel combustion. However, this possibility should be explored in future experiments.

Besides the effect of ambient element concentrations, the enrichment of elements in the moss bags represents the balance between the particle capture by rough moss tissue and its removal by intense wind blow or precipitation wash-off. This is a possible reason for differences between ratios of element concentrations in PM10 and moss samples. Furthermore, some research (Tretiach et al. 2011) showed that mosses more efficiently entrap smaller particle classes, with efficiencies of 78.8 and 19.4% for < 2.5 and 2.5–10 µm, respectively, and only 0.2% for particles greater than 25 µm in diameter. Since desert dust predominantly contributes to coarse particle fractions, the mentioned findings could

Table 2 Ratio of concentrations of analyzed elements and Al in *S. girgensohnii* moss samples exposed during 15-day periods, and 1–6 months; non-dust samples are those exposed during 15.2d and 15.5d-15.12d periods

Date	Ca/Al	Mg/Al	V/Al ($\times 10^{-3}$)	As/Al ($\times 10^{-4}$)	Ga/Al ($\times 10^{-4}$)	Y/Al ($\times 10^{-4}$)	Tb/Al ($\times 10^{-5}$)
15-day exposure							
non-dust			0.8 ± 0.3	2.0 ± 0.8	1.2 ± 0.5	1.5 ± 0.5	0.3 ± 0.2
15.1d (SDE1)			1.4	0.9	2.8	1.9	0.6
15.3d (SDE2)			1.0	1.5	1.5	1.3	0.4
15.4d (SDE3)			0.6	0.5	1.2	1.0	0.2
1–6-month exposure							
average	6.8 ± 0.7	1.2 ± 0.4	5.1 ± 0.4	4.9 ± 1.2	6.2 ± 0.7	6.6 ± 0.5	1.9 ± 0.2
3-month expos	6.6	1.1	4.8	5.3	5.9	6.4	1.8

explain the absence of an unambiguous influence of the transported desert dust in the element content of the mosses. Still, the simplicity of the moss bag exposure that does not require electricity and technical maintenance should be considered as its comparative advantage over instrumental techniques for remote sites far from infrastructure, e.g., mountains. These sites are particularly suitable for monitoring desert dust transport due to the absence of pollution 'noise' caused by the local anthropogenic influence which is inevitable at the (sub)urban background sites. Further research could be directed to the investigation of moss bag potential for biomonitoring of elements characteristic for dust at rural/remote background sites, based on prolonged moss bag exposure of three months (in addition to 15-day exposure), as suggested by this study.

Conclusion

Mass concentrations of PM2.5 and PM10 recorded in the study site during the spring/summer season in 2019 were lower than the daily PM threshold values. In the conditions of such low particulate pollution, the moss bag technique showed a limitation in the element enrichment for the shortest period of bag exposure of 15 days. The majority of the examined elements, except Al, V, As, Ga, Y, and Tb, were not accumulated above the LOQt, which is considered as criteria for a valuable content of PTEs in a moss tissue. However, prolonged bag exposure of a couple of months led to stable element accumulation in the moss transplants. The moss bags exposed at open space were significantly more enriched with the elements than the moss bags that were exposed under the improvised roof. This suggests the predominant influence of bulk (dry and wet) atmospheric deposition to element accumulation in mosses over possible element wash-off effect during intense precipitations and element resuspension with local soil dust. Homogeneity of the pristine moss *S. girgensohnii* material recommends this species for active biomonitoring of the airborne elements, providing better replicability of the results, unlike *H. cupressiforme*. This is particularly important in case of short-term moss bag exposure (15 days), while prolonged exposure enables more significant element enrichment. Good correlation between the majority of the elements (V, As, Ba, Ca, Ga, Zn, Cd, Co, Mg, Tb, and Y) recommends the use of both moss species for the biomonitoring purpose, particularly for V and As.

The studied season was characterized by three Saharan dust episodes, each lasting for several days. MERRA-2 data showed particularly significant dust concentration at surface during the first episode that occurred in April (SDE1), as well as during the first 15-day moss exposure period. The PM measurements confirmed the increase of mass concentrations during dust days with the dominance of coarse particle fraction (PM10-PM2.5). The elemental characterization of the PM10 samples collected concomitantly with the dust episodes showed the substantial enrichment of Al, As, V, Ga, Y, and Tb, while element/PM10 concentration ratio indicated that the increase of Al, V and Y concentrations is partly related to dust. The same elements were significantly accumulated in the moss samples during the 15.1d period (corresponding to SDE1), especially in *S. girgensohnii*. The ratio of crustal elements (Ca/Al and Mg/Al) in moss samples (3-month exposed bags that covered all three SDEs) was somewhat larger than in PM10 samples taken during dust days; however, both were in line of those reported for dust from western Africa. The increase of V/Al, Ga/Al, and Tb/Al concentration ratio values was observed in PM10 for dust days and in *S. girgensohnii* moss samples for the period 15.1d, in comparison with the samples not affected by dust, contrary to the values of As/Al ratio that were smaller during SDE1. Additional analysis is needed to investigate the possibility of using these ratios to distinguish between moss bag samples dominantly affected by natural sources (desert dust) from those dominantly affected by anthropogenic pollution. Further research on the moss bag potential for biomonitoring of elements characteristic for desert dust at rural background sites should be based on extended period of moss bag exposure (3 months) in addition to 15-day exposure, in a long-term study covering multiple seasons characterized by dust intrusions. The extended period of exposure is necessary for the accumulation of a larger number of crustal elements in moss bag samples, which will allow a more detailed study of dust in moss bag samples. This pilot study points out the advantages of a multidisciplinary and multi-technique approach (model results, instrumental, and biomonitoring measurements) to the perception of air pollution issues.

Supplementary Information The online version contains supplementary material available at https://doi.org/10.1007/s11869-022-01161-8.

Acknowledgements The authors acknowledge funding provided by the Institute of Physics Belgrade and Faculty of Chemistry, through the grants by the Ministry of Education and Science of the Republic of Serbia (Institute of Physics Belgrade document: 0801-116/1 and Faculty of Chemistry contract number: 451-03-68/2020-14/200168), and bilateral cooperation between Institute of Physics Belgrade and Joint Institute for Nuclear Research, Dubna, Russia. The MERRA-2 data used in this study have been provided by the Global Modeling and Assimilation Office (GMAO) at NASA Goddard Space Flight Center.

Declarations

Ethics approval and consent to participate Not applicable.

Consent for publication Not applicable.

Availability of data and materials All data generated or analyzed during this study are included in this published article and its supplementary information files.

Competing interests The authors declare that they have no competing interests.

References

Adamo P, Giordano S, Sforza A, Bargagli R (2011) Implementation of air-borne trace element monitoring with devitalised transplants of *Hypnum cupressiforme* Hedw.: assessment of temporal trends and element contribution by vehicular traffic in Naples city. Environ Pollut 159:1620–1628

Ajtai N, Stefanie H, Mereut A, Radovici A, Botezan C (2020) Multi-Sensor Observation of a Saharan Dust Outbreak over Transylvania, Romania in April 2019. Atmosphere 11:364–378

Alastuey A, Querol X, Aas W, Lucarelli F, Pérez N, Moreno T, Cavalli F, Areskoug H, Balan V, Catrambone M, Ceburnis D, Cerro JC, Conil S, Gevorgyan L, Hueglin C, Imre K, Jaffrezo J-L, Leeson SR, Mihalopoulos N, Mitosinkova M, O'Dowd CD, Pey J, Putaud J-P, Riffault V, Ripoll A, Sciare J, Sellegri K, Spindler G, Yttri KE (2016) Geochemistry of PM10 over Europe during the EMEP intensive measurement periods in summer 2012 and winter 2013. Atmos Chem Phys 16:6107–6129

Amato F, Pandolfi M, Escrig A, Querol X, Alastuey A, Pey J, Perez N, Hopke PK (2009) Quantifying road dust resuspension in urban environment by multilinear engine: a comparison with PMF2. Atmos Environ 43:2770–2780

Amato F, Alastuey A, Karanasiou A, Lucarelli F, Nava S, Calzolai G, Severi M, Becagli S, Gianelle VL, Colombi C, Alves C, Custódio D, Nunes T, Cerqueira M, Pio C, Eleftheriadis K, Diapouli E, Reche C, Minguillón MC, Manousakas MI, Maggos T, Vratolis S, Harrison RM, Querol X (2016) AIRUSE-LIFE: a harmonized PM speciation and source apportionment in five southern European cities. Atmos Chem Phys 16:3289–3309

Aničić M, Frontasyeva MV, Tomašević M, Popović A (2007) Assessment of atmospheric deposition of heavy metals and other elements in Belgrade using moss biomonitoring technique and neutron activation analysis. Environ Monit Assess 129:207–219

Aničić M, Tomašević M, Tasić M, Rajšić S, Popović A, Frontasyeva MV, Lierhagen S, Steinnes E (2009a) Monitoring of trace element atmospheric deposition using dry and wet moss bags: Accumulation capacity versus exposure time. J Haz Mat 171:182–188

Aničić M, Tasić M, Frontasyeva MV, Tomašević M, Rajšić S, Mijić Z, Popović A (2009b) Active moss biomonitoring of trace elements with *Sphagnum girgensohnii* moss bags in relation to atmospheric bulk deposition in Belgrade Serbia. Environ Pollut 157:673–679

Aničić Urošević M, Vuković G, Jovanović P, Vujičić M, Sabovljević A, Sabovljević M, Tomašević M (2017a) Urban background of air pollution – Evaluation through moss bag biomonitoring of trace elements in Botanical garden. Urban for Urban Green 25:1–10

Aničić Urošević M, Vuković G, Tomašević M (2017b) Biomonitoring of Air Pollution Using Mosses and Lichens, A Passive and Active Approach, State of the Art Research and Perspectives. Nova Science Publishers, New York (**978-1-53610-212-3**)

Aničić Urošević M, Milićević T (2020) Moss bag biomonitoring of airborne pollutants as an ecosustainable tool for air protection management: Urban vs. agricultural scenario, Editors: Vertika Shukla and Narendra Kumar, Springer, pp 29 – 60

Ares Á, Fernández JA, Aboal JR, Carballeira A (2011) Study of the air quality in industrial areas of Santa Cruz de Tenerife (Spain) by active biomonitoring with *Pseudoscleropodium purum*. Ecotox Environ Safe 74:533–541

Ares Á, Aboal JR, Carballeira A, Giordano S, Adamo P, Fernández JA (2012) Moss bag biomonitoring: a methodological review. Sci Total Environ 432:143–158

Ares Á, Aboal JR, Carballeira A, Fernández JA (2015) Do moss bags containing devitalized *Sphagnum denticulatum* reflect heavy metal concentrations in bulk deposition? Ecol Indic 50:90–98

Bargagli R, Brown DH, Nelli L (1995) Moss biomonitoring with moss: Procedures for correcting for soil contamination. Environ Pollut 89:169–175

Berg T, Steinnes E (1997) Use of mosses (*Hylocomium splendens* and *Pleurozium schreberi*) as bio-monitors of heavy metal deposition: from relative to absolute deposition values. Environ Pollut 98:61–71

Berg T, Røyset O, Steinnes E (1994) Trace elements in atmospheric precipitation at Norwegian background stations (1989–1990) measured by ICP-MS. Atmos Environ 28(21):3519–3536

Bergamaschi L, Rizzio E, Valcuvia MG, Verza G, Profumo A, Gallorini M (2002) Determination of trace elements and evaluation of their enrichment factors in Himalayan lichens. Environ Pollut 120:137–144

Brown D (1982) Mineral nutrition, Bryophyte Ecology. Springer, pp 383–444

Capozzi F, Giordano S, Di Palma A, Spagnuolo V, de Nicola F, Adamo P (2016a) Biomonitoring of atmospheric pollution by moss bags: discriminating urban-rural structure in a fragmented landscape. Chemosphere 149:211–219

Capozzi F, Giordano S, Aboal RJ, Adamo P, Bargagli R, Boquete T, Di Palma A, Real C, Reski R, Spagnuolo V, Steinbauer K, Tretiach M, Varela Z, Zechmeister H, Fernandez AJ (2016b) Best options for the exposure of traditional and innovative moss bags: a systematic evaluation in three European countries. Environ Pollut 214:362–373

Čeburnis D, Valiulis D (1999) Investigation of absolute metal uptake efficiency from precipitation in moss. Sci Total Environ 226(2–3):247–253

Cohen A, Brauer M, Burnett R, Anderson HR, Frostad J, Estep K, Balakrishnan K, Brunekreef B, Dandona L, Dandona R, Feigin V, Freedman G, Hubbell B, Jobling A, Kan H, Knibbs L, Liu Y, Martin R, Morawska L, Pope CA III, Shin H, Straif K, Shaddick G, Thomas M, van Dingenen R, van Donkelaar A, Vos T, Murray CJL, Forouzanfar MH (2017) Estimates and 25-year trends of the global burden of disease attributable to ambient air pollution: an analysis of data from the Global Burden of Diseases Study 2015. Lancet 389:1907–1918

Culicov OA, Yurukova L (2006) Comparison of element accumulation of different moss and lichen-bags, exposed in the city of Sofia (Bulgaria). J Atmos Chem 55:1–12

Dangić A, Dangić J (2007) Arsenic in the soil environment of central Balkan Peninsula, southeastern Europe: occurrence, geochemistry, and impact. In: Bhattacharya, P, Mukherjee, B.B.A, Bundschuh, J, Zevenhoven, R, Loeppert, H.R. (Eds.), Arsenic in Soil and Groundwater Environment; Trace Metals and other Contaminants in the Environments 9, pp 207–236

De Agostini A, Cortis P, Cogoni A (2020) Monitoring of Air Pollution by Moss Bags around an Oil Refinery: A Critical Evaluation over 16 Years. Atmosphere 11(3):272–286

DEFRA—Department for Environment, Food and Rural Affairs (2014) Air Pollution Background Concentration Maps: A User Guide for Local Authorities, http://laqm.defra

Demková L, Bobulská L, Árvay J, Jezný T, Ducsay L (2017) Biomonitoring of heavy metals contamination by mosses and lichens

around Slovinky tailing pond (Slovakia). J Environ Sci Health A Tox Hazard Subst Environ Eng 52(1):30–36
Dimitriou K, Kassomenos P (2018) Day by day evolution of a vigorous two wave Saharan dust storm – Thermal and air quality impacts. Atmósfera 31(2):105–124
Directive 2008/50/EC of the European Parliament and of the council of 21 May 2008 on ambient air and cleaner air for Europe, Official Journal of the European Union, 1–44 (11/06/2008)
EEA (European Environment Agency) (2019) Air Quality in Europe - 2019 report, EEA Report No 10/2019 https://www.eea.europa.eu/publications/air-quality-in-europe-2019
EN 12341 (2014) Ambient air. Standard gravimetric measurement method for the determination of the PM10 or PM2.5 mass concentration of suspended particulate matter, Comite Europeen de Normalisation, https://infostore.saiglobal.com/en-us/Standards/EN-12341-2014-343607_SAIG_CEN_CEN_786527/
Ganor E, Osetinsky I, Stupp A, Alpert P (2010) Increasing trend of African dust, over 49 years, in the eastern Mediterranean. J Geophys Res 115(D7):1–7
Glime JM (2017) Water Relations: Movement. Chapt. 7–2. In: Glime, J. M. Bryophyte Ecology. Volume 1. Physiological 7–2–1 Ecology. Ebook sponsored by Michigan Technological University and the International Association of Bryologists. Last updated: 17 July 2020, http://digitalcommons.mtu.edu/bryophyte-ecology/
Gómez-Losada Á, Pires JCM, Pino-Mejías R (2018) Modelling background air pollution exposure in urban environments: Implications for epidemiological research. Environ Modell Softw 106:13–21
González GA, Pokrovsky SO (2014) Metal adsorption on mosses: Toward a universal adsorption model. J Colloid Interface Sci 415:169–178
Goodman GT, Roberts TM (1971) Plants and Soils as Indicators of Metals in the Air. Nature 231(5301):287–292
Harrison RM, Hester RE (2009) Air Quality in Urban Environments, Issues in Environmental Science and Technology, Royal Society of Chemistry Publishing, Cambridge, UK
Holben BN, Eck TF, Slutsker I, Tanré D, Buis JP, Setzer A, Vermote E, Reagan J, Kaufman Y, Nakajima T, Lavenu F, Jankowiak I, Smirnov A (1998) AERONET–A federated instrument network and data archive for aerosol characterization. Remote Sens Environ 66(1):1–16
Hu R, Yan Y, Zhou X, Wang Y, Fang Y (2018) Monitoring Heavy Metal Contents with *Sphagnum Junghuhnianum* Moss Bags in Relation to Traffic Volume in Wuxi, China. Int J Environ Res Public Health 15(2):374–386
Israelevich P, Ganor E, Alpert P, Kishcha P, Stupp A (2012) Predominant transport paths of Saharan dust over the Mediterranean Sea to Europe. J Geophys Res: Atmospheres 117(D2):1–11
Kabata-Pendias A (2010) Trace Elements in Soils and Plants (4th ed.). CRC Press, https://doi.org/10.1201/b10158
Mach T, Rogula-Kozłowska W, Bralewska K, Majewski G, Rogula-Kopiec P, Rybak J (2021) Impact of Municipal, Road Traffic, and Natural Sources on PM10: The Hourly Variability at a Rural Site in Poland. Energies 14:2654–2677
Markert BA, Breure AM, Zechmeister HG (2003) Definitions, strategies and principles for bioindications/biomonitoring of the environment. In: Breure AM, Zechmeister HG (eds) Markert BA. Bioindicators & Biomonitors, Elsevier Science Ltd, pp 3–41
Mason B (1966) Principles of Geochemistry. Wiley, New York
Milićević T, Aničić Urošević M, Vuković G, Škrivanj S, Relić D, Frontasyeva MV, Popović A (2017) Assessment of species-specific and temporal variations of major, trace and rare earth elements in vineyard ambient using moss bags. Ecotox Environ Saf 144:208–215
Milićević T, Aničić Urošević M, Relić D, Jovanović G, Nikolić D, Vergel K, Popović A (2021) Environmental pollution influence to soil-plant–air system in organic vineyard: bioavailability, environmental, and health risk assessment. Environ Sci Pollut Res 28:3361–3374
Milićević T (2018) An integrated approach to the investigation of potentially toxic elements and magnetic particles in the soil–plant–air system: bioavailability and biomonitoring, Doctoral Dissertation, UDC number: 504, Faculty of Chemistry, University of Belgrade, Republic of Serbia
Mohamed J (2014) Moss – Classification, Development and Growth and Functional Role, In Ecosystem. Nova Science Publishers, New York
Moreno T, Querol X, Castillo S, Alastuey A, Cuevas E, Herrmann L, Mounkaila M, Elvira J, Gibbons W (2006) Geochemical variations in aeolian mineral particles from the Sahara-Sahel Dust Corridor. Chemosphere 65:261–270
Pacyna JM, Pacyna EG (2001) An assessment of global and regional emissions of trace metals to the atmosphere from anthropogenic sources worldwide. Environ Rev 9(4):269–298
Pulles T, Denier van der Gon H, Appelman W, Verheul M (2012) Emission factors for heavy metals from diesel and petrol used in European vehicles. Atmos Environ 61:641–651
Querol X, Tobías A, Pérez N, Karanasiou A, Amato F, Stafoggia M, Pérez García-Pandoc C, Ginouxd P, Forastieree F, Gumye S, Mudue P, Alastuey A (2019) Monitoring the impact of desert dust outbreaks for air quality for health studies. Environ Internat 130:104867
Randles C, Da Silva A, Buchard V, Colarco P, Darmenov A, Govindaraju R, Smirnov A, Holben B, Ferrare R, Hair J (2017) The MERRA-2 aerosol reanalysis, 1980 onward. Part I: system description and data assimilation evaluation. J Climate 30:6823–6850
Remoundaki E, Bourliva A, Kokkalis P, Mamouri RE, Papayannis A, Grigoratos T, Samara C, Tsezos M (2011) PM10 composition during an intense Saharan dust transport event over Athens (Greece). Sci Total Environ 409:4361–4372
Rodríguez S, Querol X, Alastuey A, Kallos G, Kakaliagou O (2001) Saharan dust contributions to PM10 and TSP levels in Southern and Eastern Spain. Atmos Environ 35(14):2433–2447
Rühling Å, Tyler G (1969) Ecology of Heavy Metals—A Regional and Historical Study. Bot Notis 22: 248–259 Salo H, Mäkinen KJ (2014) Magnetic biomonitoring by moss bags for industry-derived air pollution in SW Finland. Atmos Environ 97:19–27
Salo H, Mäkinen KJ (2019) Comparison of traditional moss bags and synthetic fabric bags in magnetic monitoring of urban air pollution. Ecol Indic 104:559–566
Scheuvens D, Schütz L, Kandler K, Ebert M, Weinbruch S (2013) Bulk composition of northern African dust and its source sediments–A compilation. Earth-Sci Rev 116:170–194
Spagnuolo V, Zampella M, Giordano S, Adamo P (2011) Cytological stress and element uptake in moss and lichen exposed in bags in urban area. Ecotox Environ Safe 74:1434–1443
Stojić A, Stanišić Stojić S, Reljin I, Čabarkapa M, Šoštarić A, Perišić M, Mijić Z (2016) Comprehensive analysis of PM10 in Belgrade urban area on the basis of long-term measurements. Environ Sci Pollut Res 23:10722–10732
Terradellas E, Basart S, Cuevas E (2016) Airborne dust: From R&D to Operational forecast. AEMET, Madrid, NIPO: 281-16-007-3; WMO, Geneva, WMO/GAW Report No. 230; WMO/WWRP No. 2016-2
Tretiach M, Pittao E, Crisafulli P, Adamo P (2011) Influence of exposure sites on trace element enrichment in moss-bags and characterisation of particles deposited on the biomonitor surface. Sci Total Environ 409:822–830
Unkašević M, Mališić J, Tošić I (1999) Some aspects of the wind "Košava" in the lower troposphere over Belgrade. Meteorol Appl 6:69–80

Varela Z, Fernández JA, Real C, Carballeira A, Aboal JR (2015) Influence of the physicochemical characteristics of pollutants on their uptake in moss. Atmos Environ 102:130–135

Vuković G, Aničić Urošević M, Goryainova Z, Pergal M, Škrivanj S, Samson R, Popović A (2015) Active moss biomonitoring for extensive screening of urban air pollution: Magnetic and chemical analyses. Sci Total Environ 521–522:200–210

Vuković G, Aničić Urošević M, Škrivanj S, Milićević T, Dimitrijević D, Tomašević M, Popović A (2016) Moss bag biomonitoring of airborne toxic element decrease on a small scale: A street study in Belgrade. Serbia, Sci Total Environ 542:394–403

Wang X, Sato S, Xing B, Tamamura S, Tao S (2005) Source identification, size distribution and indicator screening of airborne trace metals in Kanayawa, Japan. J Aerosol Sci 36:197–210

World Health Organisation (WHO) (2016) Ambient air pollution: A global assessment of exposure and burden of disease Technical report, ISBN: 9789241511353 www.who.int/phe/publications/air-pollution-global-assessment/en/

Zechmeister HG (1995) Growth rates of five pleurocarpus moss species under various climatic conditions. J Bryol 18:455–468

Zhou S, Cong L, Liu Y, Xie L, Zhao S, Zhang Z (2021) Rainfall intensity plays an important role in the removal of PM from the leaf surfaces. Ecol Indic 128:107778–107787

Sitography:

Republic Hydrometeorological Service of Serbia, http://www.hidmet.gov.rs/eng/meteorologija/klimatologija_srbije.php

MODIS Aerosol products: https://worldview.earthdata.nasa.gov.

NASA's Global Modeling and Assimilation Office (GMAO): https://gmao.gsfc.nasa.gov/reanalysis/MERRA-2/

Journal of Atmospheric and Solar-Terrestrial Physics 171 (2018) 250–259

Contents lists available at ScienceDirect

Journal of Atmospheric and Solar-Terrestrial Physics

journal homepage: www.elsevier.com/locate/jastp

Changes of atmospheric properties over Belgrade, observed using remote sensing and in situ methods during the partial solar eclipse of 20 March 2015

L. Ilić [a,*], M. Kuzmanoski [a], P. Kolarž [a], A. Nina [a], V. Srećković [a], Z. Mijić [a], J. Bajčetić [b], M. Andrić [b]

[a] Institute of Physics Belgrade, University of Belgrade, Pregrevica 118, 11080, Belgrade, Serbia
[b] University of Defence, Military Academy, Generala Pavla Jurišića Šturma 33, 11000, Belgrade, Serbia

ARTICLE INFO

Keywords:
Solar eclipse
Lidar
Planetary boundary layer
Ground based observations

ABSTRACT

Measurements of atmospheric parameters were carried out during the partial solar eclipse (51% coverage of solar disc) observed in Belgrade on 20 March 2015. The measured parameters included height of the planetary boundary layer (PBL), meteorological parameters, solar radiation, surface ozone and air ions, as well as Very Low Frequency (VLF, 3–30 kHz) and Low Frequency (LF, 30–300 kHz) signals to detect low-ionospheric plasma perturbations. The observed decrease of global solar and UV-B radiation was 48%, similar to the solar disc coverage. Meteorological parameters showed similar behavior at two measurement sites, with different elevations and different measurement heights. Air temperature change due to solar eclipse was more pronounced at the lower measurement height, showing a decrease of 2.6 °C, with 15-min time delay relative to the eclipse maximum. However, at the other site temperature did not decrease; its morning increase ceased with the start of the eclipse, and continued after the eclipse maximum. Relative humidity at both sites remained almost constant until the eclipse maximum and then decreased as the temperature increased. The wind speed decreased and reached minimum 35 min after the last contact. The eclipse-induced decrease of PBL height was about 200 m, with minimum reached 20 min after the eclipse maximum. Although dependent on UV radiation, surface ozone concentration did not show the expected decrease, possibly due to less significant influence of photochemical reactions at the measurement site and decline of PBL height. Air-ion concentration decreased during the solar eclipse, with minimum almost coinciding with the eclipse maximum. Additionally, the referential Line-of-Sight (LOS) radio link was set in the area of Belgrade, using the carrier frequency of 3 GHz. Perturbation of the receiving signal level (RSL) was observed on March 20, probably induced by the solar eclipse. Eclipse-related perturbations in ionospheric D-region were detected based on the VLF/LF signal variations, as a consequence of Lyα radiation decrease.

1. Introduction

Abrupt change in the incoming solar radiation flux during solar eclipse induces disturbances in different atmospheric layers (Gerasopoulos et al., 2008; Aplin et al., 2016). These disturbances are not necessarily similar to those during sunset/sunrise, because of different time scales and initial conditions. They depend on a number of factors, including the percentage of sun obscuration, latitude, season, time of the day, synoptic conditions, terrain complexity and surface properties. Since solar energy impacts the atmosphere primarily by convection of heat from the ground, lower atmospheric layers are more influenced by changes in solar radiation. The layer of the atmosphere in direct interaction with the surface, thus directly influenced by the Earth's surface forcing, is called the planetary boundary layer (PBL). Since surface is also a source of humidity and pollutants, turbulence within the PBL is responsible for mixing and dispersion of pollutants, while air pollution concentrations in the PBL are generally higher than those in the free troposphere (Stull, 1988).

A number of studies have focused on the effect of solar eclipse on various atmospheric properties, mainly in PBL. Changes in meteorological parameters near the ground level were most extensively investigated, for several eclipse events (Anderson, 1999; Ahrens et al., 2001; Kolarž

* Corresponding author.
E-mail address: luka@ipb.ac.rs (L. Ilić).

https://doi.org/10.1016/j.jastp.2017.10.001
Received 31 March 2017; Received in revised form 16 August 2017; Accepted 3 October 2017
Available online 4 October 2017
1364-6826/

et al., 2005; Founda et al., 2007; Nymphas et al., 2009). The studies reported decrease in temperature and wind speed, changes in wind direction and increase in relative humidity, as a result of solar eclipse. The magnitude of these changes varied in different studies. Decrease in height of the PBL during solar eclipse was also observed (Kolev et al., 2005; Amiridis et al., 2007). The PBL quickly responds to surface forcing and its height can range from as low as a few hundred meters to a few kilometers. Diurnal cycle of the PBL height starts with the sunrise by heating of the surface and development of a convective boundary layer (CBL), reaching a steady state in the afternoon. The CBL remains as a residual layer until the development of a new mixing layer on the following day. A region of statically stable layer – the entrainment zone forms at the top of the PBL. It closely follows the PBL development, being shallow in the morning and thickening during the day due to intense turbulence and vigorous convection (Stull, 1988). During a solar eclipse, the change in the incoming radiation is more abrupt and affects the evolution of the PBL (Amiridis et al., 2007; Kolev et al., 2005), thus providing opportunity for investigating mechanisms involved in PBL evolution.

Some studies investigated eclipse-related changes in ozone concentration (Zerefos et al., 2001; Kolev et al., 2005; Zanis et al., 2001, 2007), due to its strong dependence upon the magnitude of UV flux (Bian et al., 2007). Tropospheric ozone (O_3)is the result of chemical reactions, mostly between nitrogen oxides (NOx), carbon monoxide (CO) and volatile organic compounds (VOCs), helped with UV radiation via process of photo-dissociation of O_3. Surface ozone concentrations were reported in literature to decrease during solar eclipse, with exception of unpolluted sites (Zanis et al., 2001, 2007).

Reported observations suggest increase in air ion (Kolarž et al., 2005; Aplin and Harrison, 2003 and references therein) and air radon concentrations (Gaso et al., 1994 and references therein) during solar eclipse, mainly attributed to PBL height decrease. Air ions are natural constituents of the atmosphere produced mostly by cosmic rays (20% of overall ionization) and natural radioactivity from soil (gamma decay of ^{40}K)and the air (^{222}Rn). The first two ionization sources mentioned above are nearly constant in time, and consequently changes of air ion generation areprimarily related to changes in Rn concentration. The background concentration of cluster air ions in lower troposphere vary from a few hundred to a few thousand ions cm^{-1}, with an average near-ground ionization rate of 10 ion pairs $cm^{-3}s^{-1}$. Air ions are neutralized mostly by ion-to-ion recombination and ion-aerosol attachment (Dolezalek, 1974). Their concentration changes diurnally: during the night, when the boundary layer conditions are stable concentrations are high, with maximum at dawn. During the day, with the development of convective boundary layer, air ion concentration decreases with minimum in the afternoon (Blaauboer and Smetsers, 1996). Radon and aerosol-carried Rn progenies are powerful air ionizers (energy of α particle decay is more than 5 MeV, while average ionization energy of air is 34 eV/ion pair) and thus the main source of cluster air ion pair production in the troposphere. Radon exhalation from the ground is determined by concentration of uranium, diffusion coefficients and porosity of soil layers on the way to surface (Ishimori et al., 2013). Average Rn concentration over the continents is 10 Bq m^{-3} (UNSCEAR, 1993).

The solar eclipse also influences ionosphere. In the upper part of this area variations in plasma frequencies are detected (Verhulst et al., 2016). Also, there are detected plasma variations in the lower ionosphere (see e.g. Guha et al., 2010; Maurya et al., 2014). One of the ways to register the variations of solar radiation impact within upper atmosphere is based on technology of radio waves which are reflected in ionosphere during propagation between emitters and receivers. Namely, the signal reflection height in the ionosphere and, consequently, parameters describing signal characteristics (propagation geometry, altitude distributions of refractive index and attenuation) depend on local plasma properties (primarily on electron density) (Bajčetić et al., 2015). Electron density declines during solar eclipse, similarly to sunset, resulting in increase of the reflection height of radio signals reflected on relevant atmospheric layer (Guha et al., 2010), as well as the occurrence of hydrodynamic waves (Nina and Čadež, 2013; Maurya et al., 2014). Because of that, the registered wave variations reflect the non-stationary physical and chemical conditions in the medium, along the considered wave trajectories, in real time. In addition to plasma parameters related to low ionosphere, several parameters describing signal propagation, like distance between transmitter and receiver, influence temporal changes in recorded signal characteristics. Because of that, the electron density decrease (or increase) can result in either increase and decrease of recorded amplitude (Grubor et al., 2008). Thus, only variation from the expected values is important for detection of influences of an event on low ionosphere.

The aim of this paper is to study atmospheric disturbances detected in Belgrade, induced by partial solar eclipse (51% coverage of solar disc) on March 20, 2015. Focusing on troposphere (mainly PBL) and ionosphere (D-region). For that purpose, four experimental setups were used to collect data, including lidar (Light Detection and Ranging) for measurement of PBL height and heights of elevated layers, AWESOME (Atmospheric Weather Electromagnetic System for Observation Modelling and Education) VLF/LF receiver (Cohen et al., 2010) and instruments for measurements solar radiation, meteorological parameters, concentrations of ozone, air ions and radon, and propagation of radio signals in troposphere.

The paper is organized as follows. In Section 2 we describe measurements and methods used in the study, and give overview of background conditions. The results are described in Section 3, and a conclusion of this study is given in Section 4.

2. Measurements and methods

2.1. UVradiation, ozone and air-ion measurements

UV-B erythemal radiation was measured using 501 biometer made by Solar light company, USA. Instrument was set on the roof of the Institute of Physics Belgrade (IPB), so that no obstacles entered the field of view. During the eclipse, data acquisition was set to 10 min. Global Sun radiation was measured by Republic Hydro-meteorological Service in Belgrade using Kipp&Zonen CMP6 pyranometer (http://www.kippzonen.com/Product/12/CMP6-Pyranometer), with 1-min data acquisition. Surface ozone measurements were conducted using Aeroqual monitor, series 500 (http://aeroqual.com/product/series-500-portable-air-pollution-monitor), made in New Zealand. The instrument was placed near UV 501 biometer and acquisition was set to 6 min. Air ions, temperature, pressure and relative humidity were measured using a Cylindrical Detector and Ion Spectrometer CDIS (Kolarž et al., 2011), made at IPB. The CDIS was placed 1 m above grassy surface (where the soil allows the radon exhalation), at IPB (44.86° N, 20.39° E, 89 m a.s.l.). Only positive air ion concentrations were measured since they have lower mobility than negative ions and consequently lower ion-to-aerosol attachment coefficient. Thus, they are less sensitive to air pollution and provide better picture of atmosphere processes. Radon was measured using continual radon measuring instrument RAD7, Durridge company, USA. Quality of continual Rn measurements is related to level of radon concentration and measuring period, i.e. counting events. The instrument was placed next to CDIS at the same level.

2.2. Measurements of meteorological parameters

The meteorological measurements were obtained at two semi-urban sites in Belgrade. One measurement site was located at IPB. At the site, temperature, relative humidity and atmospheric pressure at altitude 1 m above ground were measured. The meteorological measurements were also available from an automatic weather station collocated with a SYNOP station at Košutnjak, Belgrade (WMO no. 13275, 203 m a.s.l.), about 10 km away from the IPB site.

2.3. Detection of PBL height

A variety of methods can be used to quantify the PBL height, depending on available measurements (Emeis et al., 2008). Differences between PBL and free troposphere can be observed using vertical profiles of thermodynamic quantities and wind from radiosounding measurements. Lidar observations, using atmospheric aerosol as a tracer, can be used to determine heights of both PBL and elevated aerosol layers if present in the atmosphere.

In this study radiosounding and lidar measurements were used to determine PBL height. While radiosoudings are regularly available at 00UTC and 12UTC at the WMO station, providing meteorological data on mandatory and significant pressure levels, the advantage of lidar measurements is that they can be performed continuously with high vertical andtemporal resolutions. Data derived from lidarmeasurements can be used for detection and characterization of aerosols and PBL evolution, and allow for the detection of abrupt and smaller scale changes in the layer structure.

The lidar system at IPB, is a bi-axial system with combined elastic and Raman detection designed to perform continuous measurements of suspended aerosol particles in the PBL and the lower free - troposphere. It is based on the third harmonic frequency of a compact, pulsed Nd:YAG laser, emitting pulses of 65 mJ output energy at 355 nm with a 20 Hz repetition rate. The optical receiver is a Cassegrain reflecting telescope with a primary mirror of 250 mm diameter and a focal length of 1,250 mm. Photomultiplier tubes are used to detect elastic backscatter lidar signal at 355 nm and Raman signal at 387 nm. The detectors are operated both in the analog and photon-counting mode and the spatial raw resolution of the detected signals is 7.5 m. Averaging time of the lidar profiles during the March 2015 solar eclipse case was 1 min corresponding to 1,200 laser shots.

Lidar measurements can be used to estimate PBL height using different approaches (Sicard et al., 2006; Baars et al., 2008). In this study, the gradient method was used to determine the position of the strongest gradient of the aerosol vertical distribution, associated with the PBL height (Flamant et al., 1997). The height of a strong negative peak which can be identified as the absolute minimum of the range corrected signal's (RCS) derivative, determines the PBL top height. A strong negative gradient in lidar RCS is a result of decrease in aerosol backscatter due to decrease in aerosol concentration and humidity (Matthias et al., 2004). Our estimate of PBL height is based on lidar measurements at 355 nm. However, when available, measurements at larger wavelengths (i.e. 532 nm and 1,064 nm) are more appropriate for analysis of PBL height due to smaller relative contribution of molecular backscatter compared to 355 nm. Other local minima in the signal derivative, with absolute values above a specified threshold and with transition intervals including a minimum of five points, are associated with elevated aerosol layer top heights in the free troposphere (Flamant et al., 1997).

The Richardson number is used for PBL height estimation from radiosounding measurements. Radiosoundings are performed two times each day, at 00 and 12 UTC, at a weather station (Belgrade Košutnjak, WMO number 13275), 10 km away from the lidar measurement site at 203 m altitude. The Richardson number is defined as (Stull, 1988):

$$R_{ib} = \frac{g[z - z_0][\theta(z) - \theta(z_0)]}{\theta(z)\left[u(z)^2 + v(z)^2\right]} \quad (1)$$

where g is acceleration due to gravity, z_0 is the altitude of the weather station, $\theta(z)$ is the potential temperature and $u(z)$ and $v(z)$ are zonal and meridional components of the wind. The layers in which R_{ib} is above a critical value of 0.21 (Vogelezang and Holtslag, 1996; Menut et al., 1999) are considered to be above the PBL.

Since the data are available at discrete heights, at standard and significant pressure levels, the bulk Richardson number is used (Stull, 1988). Successful estimation of the PBL height from radiosounding measurements from stations in the WMO network, has been previously reported (Jeričević and Grisogono, 2006; Amiridis et al., 2007). Average uncertainty of the PBL height was estimated for March for a 10-year period from 2006 to 2015, from radiosounding profiles retrieved at 12 UTC. Typical resolutions varied from 100 m to 1,000 m, and the uncertainty of PBL height H was estimatedusing the following formula:

$$H = H_{estimated} \pm \frac{\Delta z}{2} \quad (2)$$

where Δz is the measurement resolution (Jeričević and Grisogono, 2006). It was calculated to be 180 m corresponding to the average vertical resolution of 350 m. On the eclipse day, the resolution and the uncertainty were estimated to be 150 m and 80 m, respectively.

2.4. Terrestrial line-of-sight radio communication measurement setup

The referential Line-of-Sight (LOS) radio link was set in the area of Belgrade, using the carrier frequency of 3 GHz, with the purpose of investigating solar eclipse contribution to receiving signal level (RSL) instability.

The transmitter was emitting non-modulated carrier, having the radio frequency (RF) output power level of 0 dBm. LOS link was established at the distance of 70 m. The signal was transmitted using the signal generator with the frequency stability of TCXO $\leq \pm 0.5$ ppm and signal level stability $\leq \pm 0.7$ dB which was housed at constant temperature. Antenna emitted horizontally polarized electromagnetic (EM) wave. The receiving system (Rx) was formed with Tektronix SA2600 spectrum analyser that was programmed to perform 1 kHz width spectral recording into 500 points. In this way, the generated signal spectrum at the receiving side could be reconstructed with an accuracy of 2 Hz, which made it possible to monitor temporal changes in the level of the received signal peak.

The measuring samples of the received signal level were recorded every 45 s equidistantly during continuous operation of the LOS link. On 20 March 2015, we made 480 recordings through 6 h, includingthe solar eclipse period.

2.5. Ionospheric observations

Global experimental setup for the low ionospheric observation is based on continuously emitting and receiving the VLF/LF signals by numerous worldwide-distributed VLF/LF transmitters and receivers, respectively. In this study, we based our analysis on D-region monitoring using the 37.5 kHz LF signal emitted by the NRK transmitter located in Grindavik (Iceland) and received at IPB by the AWESOMEVLF/LF receiver. This transmitter was chosen because the path of this signal passes through an area that was affected by a total eclipse.

2.6. Background conditions

The eclipse on March 20, 2015 started at 8:40 UTC, ended at 10:58 UTC, reaching maximum coverage of 51% at 9:48 UTC. In the days prior to the eclipse, the synoptic conditions were influenced by a cyclone moving to the east, over Balkans, followed by an increase in geopotential. Wind field was characterized by northwesterly flow shifting to northerly. On the day of the eclipse surface conditions were influenced by weak-gradient anticyclonic field. On the previous day, overcast skies with light rain in the evening were reported. From the morning of the March 20 and during the day, the sky was clear. The calm meteorological conditions provided good opportunity to observe possible eclipse-related changes in meteorological parameters near surface.

3. Results

3.1. Global and UV radiation

Primary effect of solar eclipse is reduction of solar radiation reaching the surface. In Fig. 1 diurnal variation of global sun radiation and UV-B erythemalradiation are shown for the day of the solar eclipse, and for three clear days after the eclipse. Solar eclipse on March 20 occurred during morning increase of both global and UV-B radiation due to sun elevation. Their attenuation was 48%, slightly smaller than the obscuration of the solar disc (51%). This difference could be due to diffuse solar irradianceknowing that UV-B radiation is the shortest wavelength reaching the surface and thus most prone to scattering. While the direct solar irradiance is reduced proportionally to the obscuration of solar disc during the eclipse, the diffuse irradiance is less affected due to contribution of multiple scattering from less shadowed part of the sky (Zerefos et al., 2001). They reported that the difference in reduction of diffuse and direct irradiance was more pronounced at shorter wavelengths.

3.2. Meteorological parameters

Meteorological measurements were analyzed to investigate the response of the air temperature, relative humidity and pressure at near-surface level to the eclipse. As mentioned in the previous section, the meteorological measurements were conducted at two locations: at IPB lidar measurement site and at Košutnjakstation, about10 km away. Diurnal cycle of the temperature was interrupted by the eclipse at both measurement sites (Fig. 2). Change in temperature increase rate was observed at both sites, with similar delay after the first contact. Higher temperatures were measured, and temperature decrease was more pronounced at IPB station, probably due to lower altitude and as a result of lower measurement height above ground. At this station, the temperature decreased during the eclipse, by 2.6 °C, at the rate of 0.043 °Cmin^{-1}, reaching minimum about 15 min after the maximum of the eclipse. At Košutnjakstation the temperature was almost constant after the first contact until the maximum of the eclipse, with an increase rate of 0.003 °wCmin^{-1}. After the eclipse maximum, it started increasing with increased downward radiation, at a higher rate of0.03 °C/min.To further investigate the effect of the eclipse on temperature, measurements available from Košutnjakstation on days following the eclipse were used. The rate of temperature change during the eclipse was compared to the rates recorded during the same period of day on three cloud-free days after the eclipse – March 21, 23 and 24. Increasing trend of maximum daily temperature was measured in this period. On the eclipse day, the increase rate from the first contact to the eclipse maximum (0.003 °Cmin^{-1})was very low in comparison to the rates of 0.016 °C min^{-1}, 0.025 °Cmin^{-1} and 0.032 °Cmin^{-1} for the same period on March 21, 23 and 24, respectively. After the eclipse maximum until the end of the eclipse, temperature increase rate of 0.025 °Cmin^{-1}was comparable to the corresponding rates on the three following days. Total increase in temperature during the eclipse was 2.0 °C, while the corresponding measured increase on March 21, 23 and 24, was 2.3 °C, 3.3 °C and 4.0 °C, respectively.

Relative humidity showed decreasing trend, typical for the beginning of the day and morning increase of temperature. During the eclipse, humidity was almost constant until the maximal obscuration of solar disc, and then it decreased by 10% at both locations (IPB and Košutnjak), in consistence with temperature increase. Until the maximal obscuaration, at IPB, the temperature was decreasing while the relative humidity was almost constant. It remains unclear whether its behaviour is an effect of eclipse.

The wind speed measured at the Košutnjak station followed atypical diurnal cycle, until the maximum of the eclipse, when both wind speed and gustiness dropped, and started increasing after the event (Fig. 3). Wind speed decreased from a maximum of 2.7 ms^{-1} to about 1.1 ms^{-1}at the end of the eclipse. The absolute minimum of wind speed and gusts was reached about 35 min after the last contact. Wind direction changed from northerly to northeasterly for the duration of the eclipse.

Pressure drop during the eclipse at Košutnjak station was 0.9 hPa (not shown here), which is most probably the consequence of the temperature

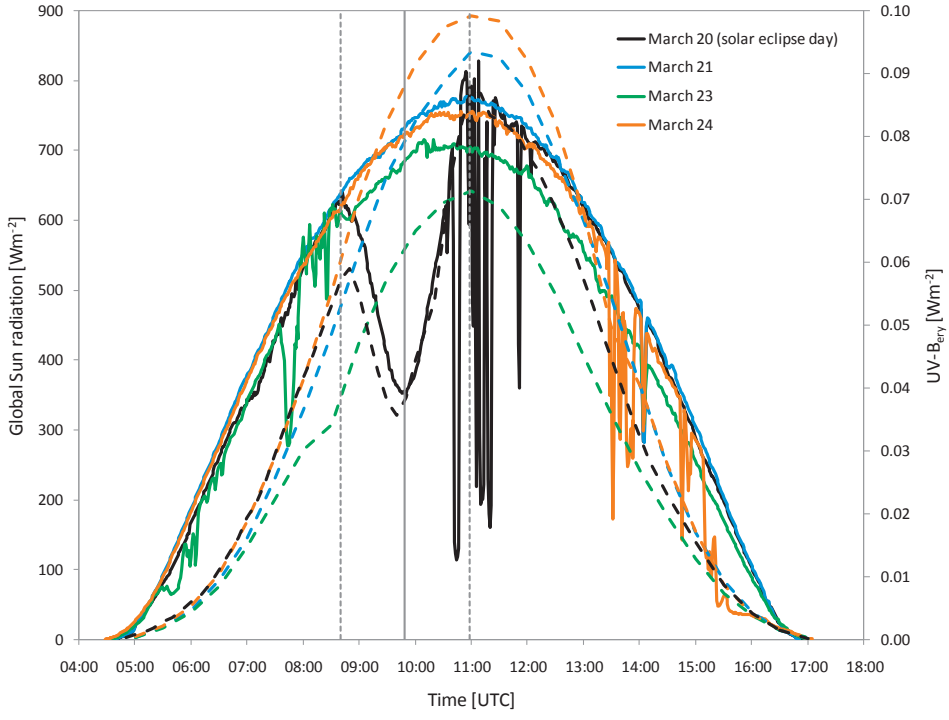

Fig. 1. Global Sun radiation (solid lines) and UV-B erythemal radiation (dashed lines) during partial Solar eclipse (March 20, 2015) and three clear days after the eclipse. Dotted vertical lines indicate beginning, maximum and end of the eclipse.

drop (Fig. 2). The pressure minimum was reached about 30 min after the eclipse maximum. Additional data, from radiosounding, provided information on vertical profiles of meteorological variables 1 h after the event. Up to the top of the PBL, the northerly wind speeds were relatively low, from 2 to 3.5 ms^{-1}. Air in the PBL was not very humid, with relative humidity of 35–60%.

These observed changes are generally in agreement with those reported in previous studies, related to eclipse events with larger obscuration of solar disc. The exception is relative humidity, which was almost constant until the eclipse maximum in this work, while it was reported to increase in previous studies. Anderson (1999) compiled data on near-surface temperature during selected total eclipse events, given in literature. These data showed temperature decrease of 2.0–3.6 °C, with minimal value coinciding with mid-eclipse (in one case), or reached with the time lag of 7–17 min. Foundaet al. (2007) presented observations at several sites in Greece, with different degrees of sun obscuration (74–100%) during solar eclipse in March 2007. Their results showed that temperature (measured at altitudes varying from 1.5 m to 17 m at different sites) decreased by 1.6–2.7 °C (3.9 °C at a site affected by low clouds), reaching minimal value 12–14 min after the mid-eclipse. Following the temperature response, the relative humidity was reported to increase by about 20% (Founda et al., 2007; Kolev et al., 2005). A decline in wind speed, after mid-eclipse, as a result of cooling the boundary layer and reduction of turbulent transport (Girard-Ardhuin et al., 2003) was also reported in literature (Anderson, 1999; Founda et al., 2007).

3.3. PBL evolution assessment from meteorological and lidar measurements

The presence of the residual layer, evolution of the PBL and aerosol layers in the free troposphere during the solar eclipse were observed using lidar measurements in Belgrade. For that purpose, the vertical profiles of the range-corrected analog signal at 355 nm, obtained from 10:15 UTC until 15:25 UTC with temporal resolution of 1 min, were analyzed, using the gradient method. The time series of range corrected signal (RCS) vertical profiles, along with heights of PBL and elevated aerosol layers are presented in Fig. 4.

The eclipse occurred before local noon, during the development of the mixing layer. In the morning, with surface heating, PBL started increasing from 600 m height to about 800 m above ground during the time period of about 2 h until the start of the eclipse at 8:40 UTC. The increase of the PBL height before the eclipse was steady and gradual. During this period, a layer was identified at height of about 1 km. This layer can be identified as the residual layer. With the beginning of the eclipse, the amount of solar radiation reaching the surface started decreasing (Fig. 1). This affected the change in surface temperature (Fig. 2), and therefore convective motion, with the effects diminishing with height. The PBL height decreased by about 200 m during the solar eclipse, reaching minimum 20 min after the maximum of the eclipse. This decrease in PBL height is similar to those reported in previous research (Amiridis et al., 2007; Kolev et al., 2005), for solar eclipse with larger solar disc obscuration. With passing of the eclipse, the PBL started gaining height until reaching the height of about 1700 m around 13 UTC. Stronger variations of PBL height observed after the eclipse can be attributed to stronger convective motions. In first minutes after the eclipse, shallow cumulus clouds formed with their base at the top of the PBL. A peak in PBL height, coinciding with peaks in temperature and wind speed measurements was observed during the later phase of the event. Depth of the entrainment zone followed the development of the PBL. It showed gradual increase before the eclipse, from low values of about 30 m, to variations in height of several tens of meters after the eclipse as a result of strong convective motions.

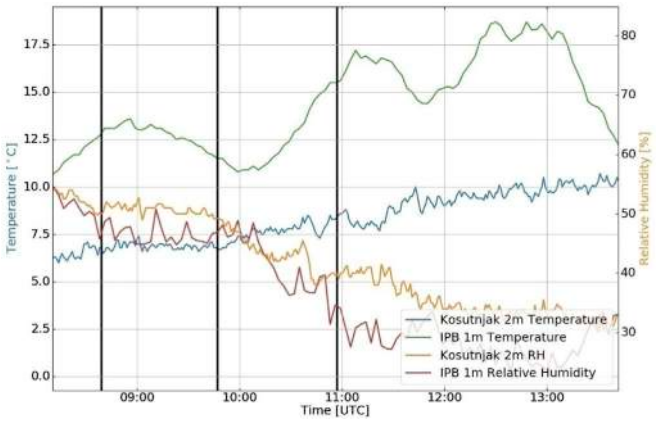

Fig. 2. Temperature and relative humidity. Vertical lines indicate beginning, maximum and end of the eclipse.

The PBL height value calculated as an hourly average around 12 UTC (soon after the end of the eclipse), was 1 500 ± 100 m, in agreement with the one estimated from radiosounding:1 600 ± 80 m.Small differences of results obtained from radiosounding and lidar measurements can be due to local effects at two measurement sites and differences in the methods used. The gradient method uses gradient in lidar RCS due to decrease in aerosol backscatter while the bulk Richardson number approach relies on thermodynamic properties. Different surface properties and elevations of measurement sites influence the heat and momentum fluxes contributing to the PBL development. Lidar is operated on a fixed location during the whole measurement period, providing information on vertical column of air directly above the instrument. Radiosounding profiles are affected by the horizontal drift of the instrument caused by wind and depend on whether the ascent is made in a thermal or between thermals (Stull, 1988). To further estimate impact of eclipse on PBL height we compared these values with the PBL heights calculated for March for a 10-year period from 2006 to 2015 from the radiosounding profiles taken at 12 UTC (excluding the profile on the day of the eclipse). The values estimated both from lidar (around 12 UTC) and radiosounding measurements made on the day of the eclipse fall within the inter-quartile range of the values for the 10-year reference period (Fig. 4).

The lidar measurements during solar eclipse also showed presence of aerosol layers in free troposphere, at altitudes up to 4 km.

3.4. Ozone and air-ion concentrations

Surface ozone measurements showed no significant decrease, as opposed to most other measured parameters, possibly indicating less significant influence of photochemical reactions at the IPB semi-urban measurement site (see Fig. 5). While a decrease of surface ozone concentration during solar eclipse is expected, this effect could be missing in less polluted areas, or it could be masked by air transport or decline of PBL height (Zanis et al., 2001, 2007). For an urban station in Thessaloniki, Zanis et al. (2001) reported that surface ozone concentration decreased by 10–15 ppbv during the solar eclipse in August 1999 (maximum sun obscuration 90%), with a half-hour delay in starting time of the decrease after the first contact. However, they did not observe any effect on surface ozone in an elevated rural station at Hohenpeissenberg (99.4% sun coverage). Measurements during the solar eclipse in March 2006, conducted in Greece, showed decrease of 5–10 ppb surface ozone in an urban site in Thessaloniki (about 70% sun obscuration), while no effect was observed in relatively unpolluted sites in Finokalia and Kastelorizo, with 82% and 86% solar obscuration, respectively (Zanis et al., 2007). In our study, the measurements were taken at semi-urban site, during solar eclipse event with 51% sun obscuration. It is also noteworthy that measurements conducted for few other days, after the solar eclipse, in the present study showed high time lag of ozone concentration peaks compared to UV radiation peak. This was also reported in Tie et al. (2007) and Bian et al. (2007).

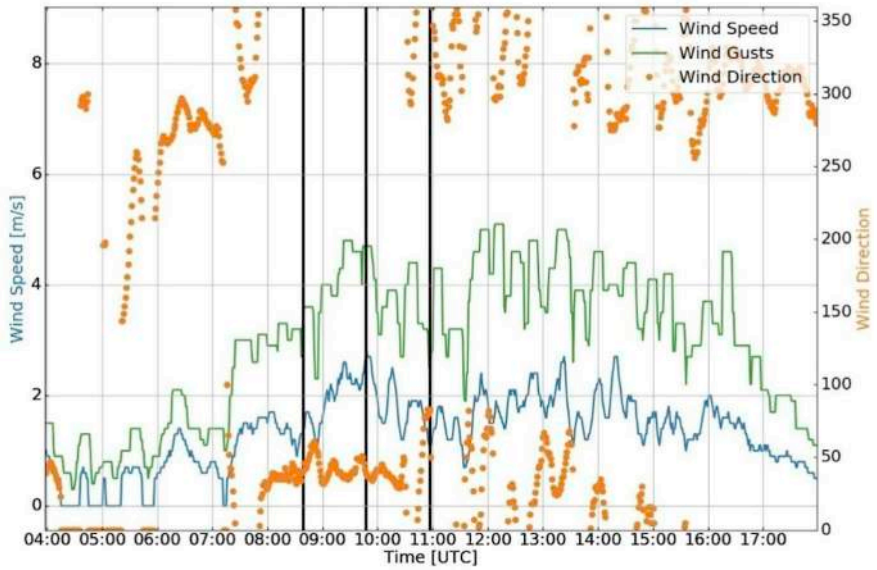

Fig. 3. Wind speed, gusts and direction. Vertical lines indicate beginning, maximum and end of the eclipse.

Radon concentrations measured during the eclipse (not shown here) were in the range between 0 and 15 Bq m^{-3} which is typical background for this part of the day. As shown in Fig. 6, air ion concentration decreased during the course of the day. The decrease was more intensive during the eclipse. After the eclipse, air ion concentration returned to its usual diurnal path to afternoon minimum. This could be explained by decrease of diffusion processes that are responsible for radon exhalation from the soil, as a result of cease of heating the surface during the eclipse. Differences were noted in air ion change during the eclipse in 1999 (97.7% sun obscuration), described in Kolarž et al. (2005) and that described in this study (51% sun obscuration).

3.5. Line-of-Sight radio communication receiving signal change

The observed RSL change during the time of solar eclipse was compared with the RSL change in few following days. The usual change of RSL in morning hours presented in Bajčetić et al. (2013) was confirmed during regular days, while, the pattern of signal level variation was quite different during the solar eclipse (Fig. 7, left panel).

Additionally, the observed meteorological variables were used to calculate the value of the air refractivity parameter (R) using (3), with the aim of the correlation between variation of that parameter and microwave RSL change (Fig. 7, right panel).

$$R = 77,6\frac{P}{T} + 3,73\cdot 10^5\frac{P_{vp}}{T^2}. \quad (3)$$

R is the value which describes the overall influence of the tropospheric medium on the radio wave propagation and depends on relative air pressure P, absolute temperature T and partially on water vapour pressure P_{vp} (Debye, 1957; Falodun and Ajewole, 2006).

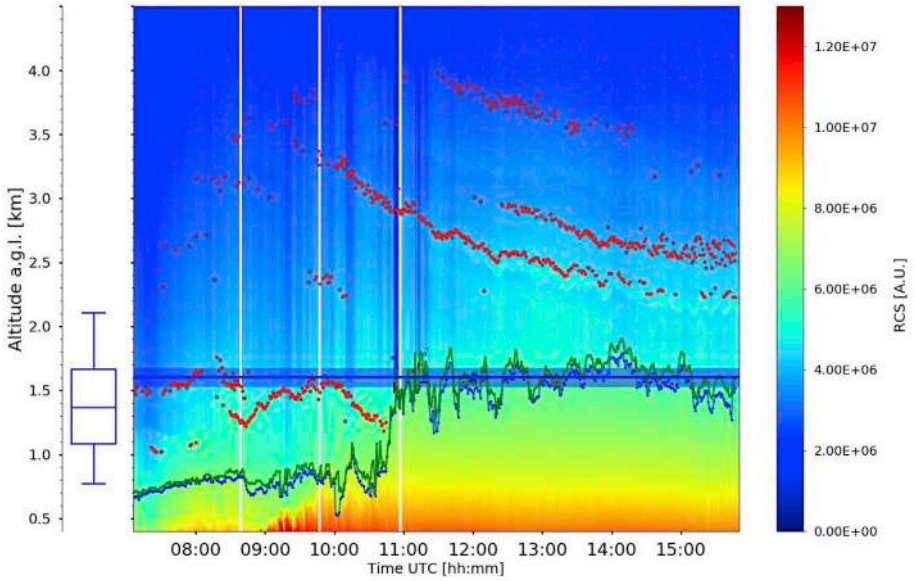

Fig. 4. Temporal evolution of PBL (blue line) and elevated aerosol layers (red dots). Colormaps represent the lidar RCS at 355 nm on March 20, 2015. White vertical lines indicate beginning, maximum and end of the eclipse. Box plot shows the median, first and third quartiles and 5th and 95th percentiles of PBL heights in March for period 2006–2015. (For interpretation of the references to colour in this figure legend, the reader is referred to the web version of this article.)

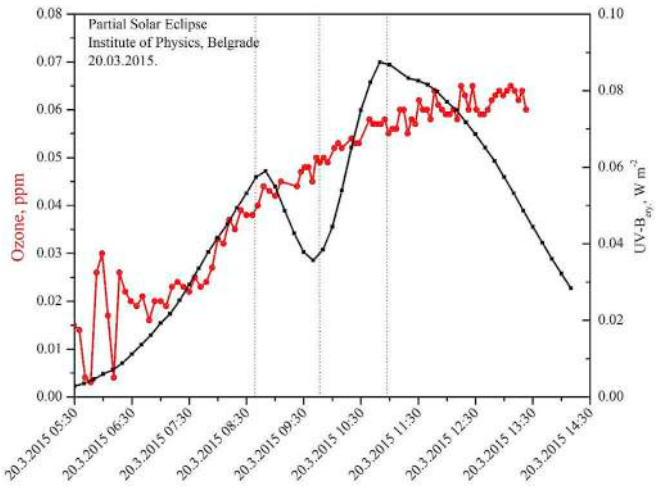

Fig. 5. Ozone and UV-B erythemal radiation during partial solar eclipse. Dotted vertical lines indicate beginning, maximum and end of the eclipse.

We normalized the measured values R_{xi} (i = 1,…, 480) of the air refractivity parameterto its mean value during the related day ($\overline{R}_x$), using Eq.2measured values R_{xi} of the air refractivity parameter, in order to emphasize the level of variation.

$$RSL = 100 \cdot \frac{R_{xi} - \overline{R}_x}{|\overline{R}_x|}. \quad (4)$$

Following the presented data in Fig. 8, it can be seen that there was meaningful correlation between RSL and R during the days after the solar eclipse, while their values change fairly independently on the day of the solar eclipse.

Analysing data presented in Fig. 8, it can be seen that before the period of solar eclipse, the disturbance manifested through the unusual *R* constant value until 08:40 is well correlated with the constant value of *RSL*. At the moment of solar eclipse maximum, the considerable *R* disturbance can be noticed, while this phenomenon does not reflect to the *RSL*. From 10:00, until the end of the solar eclipse, value of *R* varied within expected usual values, however *RSL* changed unusually.

This unusual RSL variation was possibly triggered by the solar eclipse event. In ordinary periods of measurements, the relative air pressure, absolute temperature and partially the pressure of the water vapour directly influence the permittivity of the air, causing the refraction of the electromagnetic wave, so the effects are noticeable as the RSL variation. However, during a solar eclipse event, it is not possible to consequently relate RSL and R. Considering the absolute amplitude variation of RSL, which was in the domain of 2,5 dB for the presented time periods, the sudden not so intense air permittivity perturbation within the area where LOS link was established did not have direct influence on the radio propagation at 3 GHz frequency. While RSLwas evidently slightly perturbedduring solar eclipse, there is not clear evidence that this perturbation is related to solar eclipse. The observed phenomena are not well presented in the literature for this particular scenario, and will be a subject of future analyses.

3.6. *Effects on the ionosphere and LF radio signal propagation*

The ionospheric perturbations were detected as variations of recorded NRK signal from Iceland. Generally, the temporal evolution of recorded signal can be used for detection of low ionospheric plasma perturbations; these changes in medium through which signal propagates affect wave reflection height, and consequently, propagation geometry and attenuation, resulting in variations of recorded signal characteristics.

The shapes of the temporal change depend on numerous parameters. Namely, in addition to periodic and sudden variations in the ionospheric plasma conditions, characteristics of signals like mutual locations of transmitter and receiver, power of transmitted signal, and geographical area through which the signal propagates, affect the recorded signal properties. For these reasons the dependencies between the ionospheric changes of electron density induced by radiation increase and VLF/LF signal amplitude are not monotonous, e.g. growth in the electron density does not necessarily cause amplification of recorded signal amplitudes (for detailed explanation see Nina et al., 2017). Thus, for detection of some sudden perturbationit is sufficient toobservechanges in temporal

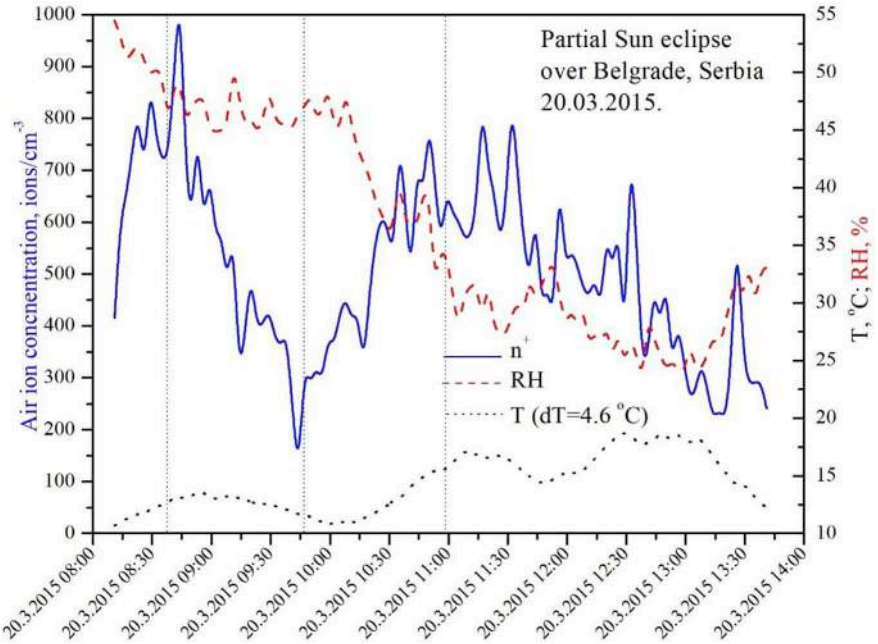

Fig. 6. Air ion concentration, temperature and relative humidity during partial solar eclipse. Dotted vertical lines indicate beginning, maximum and end of the eclipse.

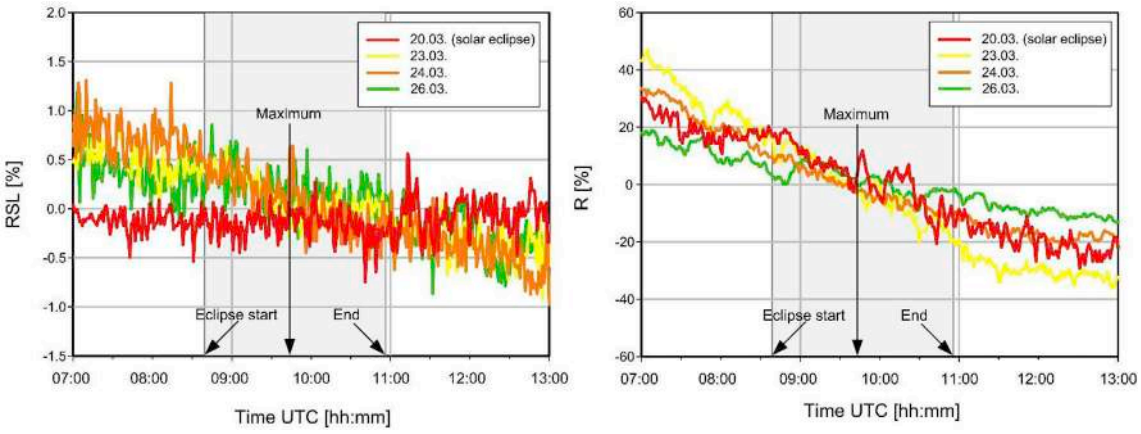

Fig. 7. Receiving signal level (*RSL*) and refractivity (R) variation. Shaded domains represent the time period when eclipse occurred.

evolution of signal characteristics.

Fig. 9 shows temporal variations of amplitude difference from its initial considered values, recorded by the AWESOME system at the Belgrade station on March 20, 2015 when solar eclipse occurred, and three days after that. The additional days are shown to visualize amplitude variation in solar eclipse period with respect to its shapes in other relevant periods without influence of the eclipse. The reason for choosing these particular days was relatively quiet conditions without significant traveling ionospheric disturbance resulting from atmospheric lightnings, and solar flares among other events. While amplitude variations are pronounced during the solar eclipse, they are practically within noise domains on the other three days. In the first period, a decrease in amplitude was observed, with the minimum occurring before the eclipse maximum. Further, the amplitude increased, exceeded the amplitude values during the first contact and reached the larger value approximately coincidently with the eclipse maximum time (indicated by a vertical line). Finally, it returned to the expected values, which are around initial values (this can be concluded from the three referent signals).

As explained in Section 1, electron density variation is most important for changes of plasma parameters which influence signal propagation. Its time variations depend on different electron gain and loss processes. The constituents of the low ionosphere can be ionized by γ, X and a part of UV photons. The most important solar influences on the ionization processes in the D-region in absence of large radiation increase, primarily as consequence of solar X-flares (Nina et al., 2012a,b) is coming from the solar Lyα line (121.6 nm) radiation (Swamy, 1991) whose presence is periodically intensified during the day. Bearing in mind that satellites did not register significant increase of intensity of X radiation, we can conclude that the signal variations are a consequence of Lyα radiation decrease. http://en.wikipedia.org/wiki/Solar_eclipse.

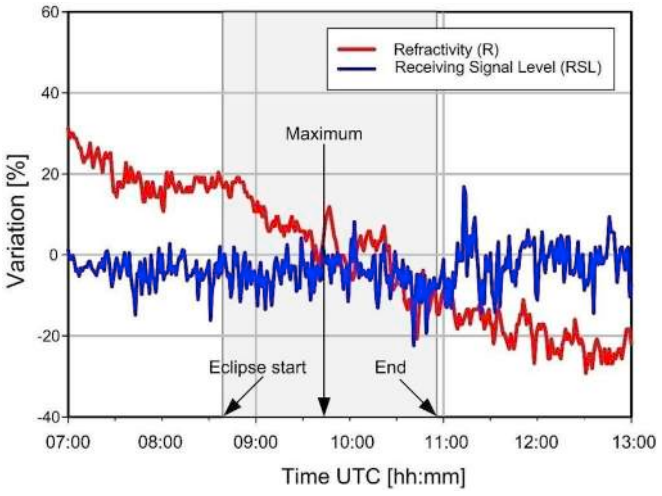

Fig. 8. *RSL* and R variation during solar eclipse. Shaded domains represent the time period when eclipse occurred.

4. Conclusions

Changes in atmospheric properties were observed during a partial solar eclipse (51%) on March 20, 2015 in Belgrade. For that purpose, four experimental setups were used to collect data, including lidar to derive PBL height and heights of elevated layers, AWESOME VLF/LF receiver (Cohen et al., 2010) and instruments for measurements of solar radiation, meteorological parameters, concentrations of ozone, air ions and radon and propagation of radio signals in troposphere. Although the solar eclipse was only partial, its influence on atmospheric properties in troposphere and ionosphere was noticeable. The detected changes in atmospheric parameters were generally similar, but weaker in intensity, to those reported in literature for solar eclipse events with larger obscuration of solar disc.

In troposphere, the influence of the eclipse was observed in meteorological surface parameters, and it was evident up to the top of the PBL. Eclipse-induced decrease in PBL height was 200 m, comparable to that reported in literature, with minimal value occurring 20 min after the eclipse maximum. The PBL height determined from 12 UTC radiosounding measurements (soon after the eclipse), showed that it was within the usual values for this location at that time of year. The meteorological parameters showed similar behavior at two measurement sites Košutnjak and IPB, respectively. The temperature change was more pronounced and abrupt at the –IPB station, probably due to lower measurement height, where it decreased by 2.6 °C, reaching minimum 15 min after the eclipse maximum. This temperature change is similar to those reported in literature for solar eclipse with larger obscuration of solar disc. At the Košutnjakstation the temperature was almost constant, until the eclipse maximum. Relative humidity was almost constant at both sites from the first contact until the eclipse maximum, as opposed to the increase reported in literature. The diurnal cycle then continued, with the increase in temperature and decrease in relative humidity at both sites. The 10-m wind speed and gusts decreased, reaching a minimum about 30 min after the eclipse. The wind direction changed from northerly to northeasterly for the duration of the event. Decrease of PBL height and the entrainment zone thickness were also observed during the eclipse, as a result of diminished surface heating. Ozone concentrations showed no decrease, as opposed to most results reported in literature, except for those reported for rural measurement sites. The possible reasons are less significant influence of photochemical reactions, decrease in PBL height or advection by changing wind during the event. Measured

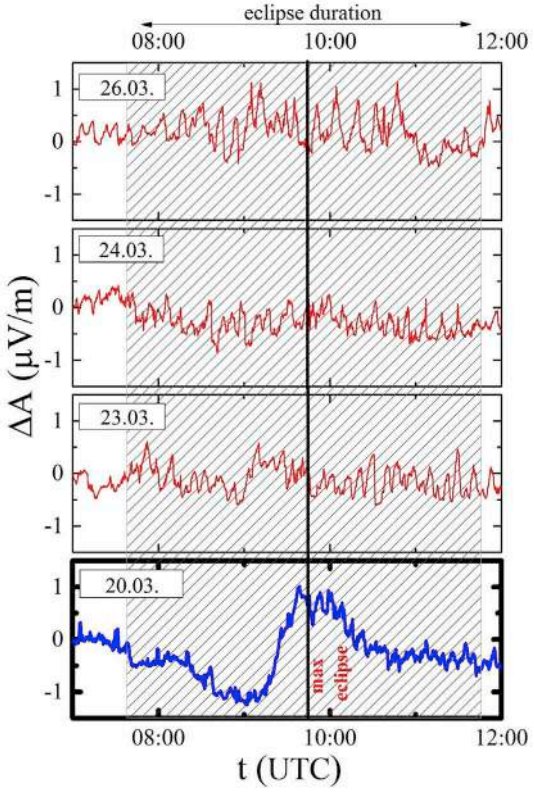

Fig. 9. The variations of amplitude difference from its initial considered values against the universal time (UT), recorded by the AWESOME system at the Belgrade station on March 20, 2015 when solar eclipseoccurred (lower panel) and three days after that (top panels). Shaded domains represent the time period when eclipse occurred (here we consider a whole period of eclipse because of long signal propagation path from Iceland to Serbia).

radon concentrations were typically low for this time of the day, while the air ion concentration sharply decreased.

The referential Line-of-Sight (LOS) radio link was set in the area of Belgrade, in order to investigate influence of the event on RSL instability. During the solar eclipse, an unusual pattern of the signal level variation was observed and different relationship between the RSL and the air refractivity parameter (R). Further analysis is needed to clearly relate the perturbation with solar eclipse which affected the atmospheric variables and therefore R.

Impact of the solar eclipse on the ionosphere was registered through changes of characteristics of radio waves which are reflected in ionosphere. The amplitude variations, were pronounced during the solar eclipse, and were at the expected values on the days after the event. Since satellite measurements did not show significant increase of intensity of X radiation, it was concluded that the signal variations are consequence of Lyα radiation decrease.

Acknowledgements

This research was realized as a part of projects no. III43007, no. III41011, no. III44002, no. 176002, no. P171020, no. III45003 financed by the Ministry of Education, Science and Technological Development of the Republic of Serbia within the framework of integrated and interdisciplinary research for the period 2011–2017. Also, this study is made within the COST project TD1403 and VarSITY project.

References

Ahrens, D., Moses, G.I., Lutz, J., Andreas, M., Helmut, M., 2001. Impacts of the solar eclipse of 11 August, 1999 on routinely recorded meteorological and air quality data in South-West Germany. Meteorol. Z. 10 (3), 215–223.

Amiridis, V., Melas, D., Balis, D.S., Papayannis, A., Founda, D., Katragkou, E., Giannakaki, E., Mamouri, R.E., Gerasopoulos, E., Zerefos, C., 2007. Aerosol Lidar observations and model calculations of the planetary boundary layer evolution over Greece, during the March 2006 total solar eclipse. Atmos. Chem. Phys. 7, 6181–6189. https://doi.org/10.5194/acp-7-6181-2007.

Anderson, J., 1999. Meteorological changes during a solar eclipse. Weather 54 (7), 207–215.

Aplin, K.L., Harrison, R.G., 2003. Meteorological effects of the eclipse of 11 August 1999 in cloudy and clear conditions. Proc. R. Soc. Lond. A 459, 353–371.

Aplin, K.L., Scott, C.J., Gray, S.L., 2016. Atmospheric changes from solar eclipses. Philosophycal Trans. R. Soc. A 374, 20150217.

Baars, H., Ansmann, A., Engelmann, R., Althausen, D., 2008. Continuous monitoring of the boundary-layer top with lidar. Atmos. Chem. Phys. 8, 7281–7296. https://doi.org/10.5194/acp-8-7281-2008.

Bajčetić, J., Andrić, M., Todorović, B., Pavlović, B., Suša, V., 2013. The correlation of geomagnetic component disturbances and 5 GHz LOS received signal daily variation. Microw. Rev. 19 (1).

Bajčetić, J.B., Nina, A., Čadež, V., Todorović, B.M., 2015. Ionospheric D-region temperature relaxation and its influences on radio signal propagation after solar X-flares occurrence. Therm. Sci. 19 (Suppl. 2), S299–S309.

Bian, H., Han, S., Tie, X., Sun, M., Liu, A., 2007. Evidence of impact of aerosols on surface ozone concentration in Tianjin, China. Atmos. Environ. 41, 4672–4681.

Blaauboer, R.O., Smetsers, R.C.G.M., 1996. Outdoor concentrations of the equilibrium-equivalent decay products of ^{222}Rn in The Netherlands and the effect of meteorological variables. Radiat. Prot. Dosim. 69, 7–18.

Cohen, M.B., Inan, U.S., Paschal, E.W., 2010. Sensitive broadband ELF/VLF radio reception with the AWESOME instrument. IEEE Trans. Geosci. Remote. 48, 3–17.

Debye, P., 1957. Polar Molecules. Dover Publications, New York.

Dolezalek, H., 1974. Electrical Processes in Atmospheres, Springer Verlag, Electrical Processes in Atmospheres. Springer Verlag.

Emeis, S., Schafer, K., Munkel, C., 2008. Surface-based remote sensing of the mixing-layer height – A review. Meteorol. Z. 17 (5), 621–630.

Falodun, S.E., Ajewole, M.O., 2006. Radio refractive index in the lowest 100-m layer of the troposphere in Akure, South Western Nigeria. J. Atmos. Sol.-Terr. Phys 236–243.

Flamant, C., Pelon, J., Flamant, P.H., Durand, P., 1997. Lidar determination of the entrainement zone thickness at the top of the unstable marine atmospheric boundary-layer. Boundary-Layer Meteorol. 83, 247–284.

Founda, D., Melas, D., Lykoudis, S., Lisaridis, I., Gerasopoulos, E., Kouvarakis, G., Petrakis, M., Zerefos, C., 2007. The effect of the total solar eclipse of 29 March 2006 on meteorological variables in Greece. Atmos. Chem. Phys. 7, 5543–5553. https://doi.org/10.5194/acp-7-5543-2007.

Gaso, M.I., Cervantes, M.L., Segovia, N., Espindola, V.H., 1994. Atmospheric radon concentration levels. Radiat. Meas. 23, 225–230.

Gerasopoulos, E., Zerefos, C.S., Tsagouri, I., Founda, D., Amiridis, V., Bais, A.F., Belehaki, A., Christou, N., Economou, G., Kanakidou, M., Karamanos, A., Petrakis, M., Zanis, P., 2008. The total solar eclipse of March 2006: overview. Atmos. Chem. Phys. 8, 5205–5220.

Girard-Ardhuin, F., Bénech, B., Campistron, B., Dessens, J., Jacoby-Koaly, S., 2003. Remote sensing and surface observations of the response of the atmospheric boundary layer to a solar eclipse. Boundary-Layer Meteorol. 106, 93–115.

Grubor, D.P., Šulić, D.M., Žigman, V., 2008. Classification of X-ray solar flares regarding their effects on the lower ionosphere electron density profile. Ann. Geophys. 26 (7), 1731–1740.

Guha, A., De, B.K., Roy, R., Choudhury, A., 2010. Response of the equatorial lower ionosphere to the total solar eclipse of 22 July 2009 during sunrise transition period studied using VLF signal. J. Geophys. Res. 115, A11302. https://doi.org/10.1029/2009JA015101.

Ishimori, Y., Lange, K., Martin, P., Mayya, Y.S., Phaneuf, M., 2013. Measurement and Calculation of Radon Releases from NORM Residues. International Atomic Energy Agency, Vienna.

Jeričević, A., Grisogono, B., 2006. The critical bulk richardson number in urban areas: verification and application in a numerical weather prediction model. Tellus A 58, 19–27. https://doi.org/10.1111/j.1600-0870.2006.00153.x.

Kolarž, P., Šekarić, J., Marinković, B.P., Filipović, D.M., 2005. Correlation between some of the meteorological parameters measured during the partial solar eclipse, 11 August, 1999. J. Atmos. Sol. Terr. Phys. 67, 1357–1364.

Kolarž, P., Miljković, B., Ćurguz, Z., 2011. Air-ion counter and mobility spectrometer. Nucl. Instrum. Methods Phys. Res. B 279, 219–222.

Kolev, N., Tatarov, B., Grigorieva, V., Donev, E., Simenonov, P., Umlensky, V., Kaprielov, B., Kolev, I., 2005. Aerosol Lidar and in situ ozone observations of the planetary boundary layer over Bulgaria during the solar eclipse of 11 August 1999. Int. J. Remote Sens. 26, 3567–3584.

Matthias, V., Balis, D., Bosenberg, J., Eixmann, R., Iarlori, M., Komguem, L., Mattis, I., Papayannis, A., Pappalardo, G., Perrone, M.R., Wang, X., 2004. Vertical aerosol distribution over Europe: statistical analysis of Raman lidar data from 10 European aerosol research lidar network (EARLINET) stations. J. Geophys. Res. 109, D18201. https://doi.org/10.1029/2004JD004638.

Maurya, Ajeet K., Phanikumar, D.V., Rajesh, Singh, Sushil, Kumar, Veenadhari, B., Kwak, Y.-S., Abhikesh, Kumar, Singh Abhay, K., Niranjan, Kumar K., 2014. Low-mid latitude D region ionospheric perturbations associated with 22 July 2009 total solar eclipse: wave-like signatures inferred from VLF observations. J. Geophys. Res. Space Phys. 119 (10), 8512–8523.

Menut, L., Flamant, C., Pelon, J., Flamant, P.H., 1999. Evidence of interaction between synoptic and local scales in the surface layer over the Paris area. Bound. Layer. Meteorol. 93, 269–286. https://doi.org/10.1023/A:1002013631786.

Nina, A., Čadež, V.M., 2013. Detection of acoustic-gravity waves in lower ionosphere by VLF radio waves. Geophys. Res. Lett. 4018, 4803–4807.

Nina, A., Čadež, V., Srećković, V., Šulić, D., 2012a. Altitude distribution of electron concentration in ionospheric D-region in presence of time-varying solar radiation flux. Nucl. Instrum. Methods. B 279, 110–113.

Nina, A., Čadež, V., Šulić, D., Srećković, V., Žigman, V., 2012b. Effective electron recombination coefficient in ionospheric D-region during the relaxation regime after solar flare from February 18, 2011. Nucl. Instrum. Methods. B 279, 106–109.

Nina, A., Čadež, V.M., Popović, Č.L., Srećković, A.V., 2017. Diagnostics of plasma in the ionospheric D-region: detection and study of different ionospheric disturbance types. Eur. Phys. J. D 71 (7). https://doi.org/10.1140/epjd/e2017-70747-0, 189, 1-12.

Nymphas, E.F., Adeniyi, M.O., Ayoola, M.A., Oladiran, E.O., 2009. Micrometeorological measurements in Nigeria during the total solar eclipse of 29 March, 2006. J. Atmos. Sol. Terr. Phys. 71 (12), 1245–1253.

Sicard, M., Pérez, C., Rocadenbosch, F., Baldasano, J.M., García-Vizcaino, D., 2006. Mixed-layer depth determination in the Barcelona Coastal area from regular lidar measurements: methods, results and limitations. Bound. Layer Meteorol. 119 (1), 135–157. https://doi.org/10.1007/s10546-005-9005-9.

Stull, R.B., 1988. An Introduction to Boundary Layer Meteorology. Kluwer Acad., Dordrecht, The Netherlands.

Swamy, A.B., 1991. A new technique for estimating D-region effective recombination coefficients under different solar flare conditions. Astrophys. Space Sci. 185 (1), 153–164.

Tie, X., Madronich, S., Li, G.H., Ying, Z.M., Zhang, R., Garcia, A., Lee-Taylor, J., Liu, Y., 2007. Characterizations of chemical oxidants in Mexico City: a regional chemical/dynamical model (WRF-Chem) study. Atmos. Environ. 41, 1989–2008.

United Nations Scientific Committee on the Effects of Atomic Radiation (UNSCEAR), 1993. Report to the General Assembly, with Scientific Annexes. New York.

Verhulst, T.G.W., Sapundjiev, D., Stankov, S.M., 2016. High-resolution ionospheric observations and modeling over Belgium during the solar eclipse of 20 March 2015 including first results of ionospheric tilt and plasma drift measurements. Adv. Space Res. 57 (No.11), 2407–2419. https://doi.org/10.1016/j.asr.2016.03.009.

Vogelezang, D.H.P., Holtslag, A.A.M., 1996. Evolution and model impacts of alternative boundary layer formulations. Bound. Layer. Meteorol. 81, 245–269. https://doi.org/10.1007/BF02430331.

Zanis, P., Zerefos, C.S., Gilge, S., Melas, D., Balis, D., Ziomas, I., Gerasopoulos, E., Tzoumaka, P., Kaminski, U., Fricke, W., 2001. Comparison of measured and modeled surface ozone concentrations at two different sites in Europe during the solar eclipse on August 11, 1999. Atmos. Environ. 35, 4663–4673.

Zanis, P., Katragkou, E., Kanakidou, M., Psiloglou, B., Karathanasis, S., Vrekoussis, M., Gerasopoulos, E., Lysaridis, I., Markakis, K., Poupkou, A., Amiridis, V., Melas, D., Mihalopoulos, N., Zerefos, C., 2007. Effects on surface atmospheric photo-oxidants over Greece during the total solar eclipse event of 29 March 2006. Atmos. Chem. Phys. Discuss. 7, 11399–11428.

Zerefos, C.S., Balis, D.S., Zanis, P., Meleti, C., Bais, A.F., Tourpali, K., Melas, D., Ziomas, I., Galani, E., Kourtidis, K., Papayannis, A., Gogosheva, Z., 2001. Changes in surface UV solar irradiance and ozone over the Balkans during the eclipse of 11 August 1999. Adv. Space Res. 27 (12), 1955–1963.

WeBIOPATR2017

Particulate Matter: Research and Management

Proceedings from the
6th WeBIOPATR
Workshop & Conference
Belgrade, Serbia
6.-8.9.2017

Milena Jovašević-Stojanović
and Alena Bartoňová, eds.

Belgrade 2019

The 6th WeBIOPATR Workshop and Conference,
Particulate Matter: Research and Management,
***WEBIOPATR2017 is organized by**:*

Vinča Institute of Nuclear Sciences, Serbia
Public Health Institute of Belgrade, Serbia
NILU Norwegian Institute for Air Research, Norway

The 6th WeBIOPATR Workshop and Conference,
Particulate Matter: Research and Management,
***WeBIOPATR2017 is supported by**:*

Ministry of Education, Science and Technological Development of

Republic of Serbia

PROCEEDINGS

The Sixth International WeBIOPATR Workshop & Conference
Particulate Matter: Research and Management
WeBIOPATR2017

6 - 8 September 2017
Belgrade, Serbia

Editors
Milena Jovašević-Stojanović
Alena Bartoňová

Publisher
Vinča Institute of Nuclear Sciences
Dr Zlatko Rakočević, Director
P.O. Box 522
11001 Belgrade, Serbia

Printed by
Vinča Institute of Nuclear Sciences

Number of copies
150

ISBN: 978-86-7306-152-8

Vinča Institute of Nuclear Sciences
www.vin.bg.ac.rs

SCIENTIFIC COMMITTEE

Dr Alena Bartoňová, Norway

Dr Bojan Radak, Serbia

Prof. Dr David Broday, Israel

Dr Med Elizabeta Paunović, Germany

Dr Maria Cruiz Min, Spain

Dr Milena Jovašević-Stojanović, Serbia

Prof. Dr Nenad Živković, Serbia

Prof. Dr Radim Šrám, Czech Republic

Dr Renata Kovačević, Serbia

Dr Slobodan Nićković, Serbia

Prof. Dr Simone Barreira Morais, Portugal

Zoran Mijić, Serbia

Prof. Dr Zoran Ristovski, Australia

Dr Zorana Jovanović-Andersen, Denmark

ORGANIZING COMMITTEE

Vinča Institute of Nuclear Sciences, Belgrade: Serbia
Dr Dragan Alavantić, Serbia
MS Ivan Lazović, Serbia
MS Maja Jovanović, Serbia (Secretary)
Dr Milena Jovašević-Stojanović (Co-chair)
Dr Miloš Davidović, Serbia (Secretary)
Dr Snežana Pašalić, Serbia

NILU - Norwegian Institute for Air Research, Kjeller
Dr Alena Bartoňová, Norway (Co-chair)

Public Health Institute of Belgrade, Belgrade
Dr Anka Cvetković, Serbia
MS Andrej Šoštarić, Serbia
Vesna Slapčević, Serbia

Ministry of Environmental Protection of RS
Ms Biljana Filipović, Serbia

Serbian Environmental Protection Agency
Mr Dejan Lekić, Serbia
Mr Tihomir Popović, Serbia

National Institute of Public Health "Dr Milan Jovanović-Batut", Belgrade
Dr Med Branislava Matić, Serbia

Military Medical Academy, Belgrade
Prof. Dr Jasmina Jović-Stošić, Serbia

Institute of Physics, Belgrade
Dr Mira Aničić Urošević, Serbia

Faculty of Occupational Protection, University of Niš
Prof. Dr Nenad Živković, Serbia

Medical Faculty, University of Niš
Prof. Dr Aleksandra Stanković, Serbia

Institute of Metallurgy and Mining, Bor
Dr Viša Tasić, Serbia

Mechanical Faculty, University of Belgrade
Prof. Dr Aleksandar Jovović, Serbia

CONFERENCE TOPICS

ATMOSPHERIC PARTICULATE MATTER - PHYSICAL AND CHEMICAL PROPERTIES

- *sources and formation of particulate matter*
- *particulate matter composition and levels outdoors and indoors*
- *environmental modeling*
- *nanoparticles in the environment*

PARTICULATE MATTER AND HEALTH

- *exposure to particulate matter*
- *health aspects of atmospheric particulate matter*
- *full chain approach*

PARTICULATE MATTER AND REGULATORY ISSUES

- *issues related to monitoring of particulate matter*
- *legislative aspects*
- *abatement strategies*

CONTENTS

5.3. A STUDY OF A DUST INTRUSION EVENT OVER BELGRADE, SERBIA

M. Kuzmanoski, L. Ilić, M. Todorović, Z. Mijić
Institute of Physics Belgrade, University of Belgrade, Belgrade, Serbia
maja.kuzmanoski@ipb.ac.rs

ABSTRACT

This paper is to present the results of aerosol measurements from a dust intrusion episode in Belgrade during the period of July 5-7, 2014. A vertical profile of the aerosol backscattering coefficient, obtained from ground-based LIDAR measurements in Belgrade, showed a distinct elevated dust layer at altitudes of 2-5 km on July 5, 2014. The altitude of the layer decreased later in the episode, with its centre of mass decreasing from approximately 4 km to below 3 km. On the last day of the episode, an entrainment of the dust layer into the planetary boundary layer was observed, consistent with the observed change of PM_{10} concentration at the surface level. The PM_{10} concentration increased by 15-17 μg m^{-3} at three monitoring sites in Belgrade, as the dust plume was settling down during the episode. The DREAM model simulations reproduced well the observed dust layer altitude. Dust surface concentrations from the model showed an increase of 11 μg m^{-3} during the episode. The difference from observed PM_{10} increase was attributed to contributions of other aerosol types to observations.

INTRODUCTION

Mineral dust is one of the most abundant components of the global aerosol burden (Kinne et al., 2006). Saharan dust originates from the world's primary dust source region, and can be transported over long distances (Prospero, 1999; Ansmann et al., 2003). It mixes with other aerosol types along the transport path, affecting their physical, optical and radiative properties. Mineral dust affects the Earth's radiative budget by scattering and absorbing solar and terrestrial radiation (direct effect), by modifying cloud properties due to their role in cloud formation (indirect effect) or by changing the thermal structure of the atmosphere (semi-direct effect). However, there is significant uncertainty in estimating role of dust in the Earth's climate system (IPCC, 2013). Dust impacts air quality, even at locations distant from the source region (Prospero, 1999), and has harmful effects on human health (Giannadaki et al., 2014). To address these problems, it is important to improve the understanding of dust properties on temporal and spatial scales. This requires the synergistic use of ground-based and satellite measurements, along with a regional dust model, for the analysis of dust spatial and temporal variability.

Here we present a case study of a dust intrusion episode observed in Belgrade from July 5-7, 2014. The analysis of the temporal variability of the dust layer was based on ground-based LIDAR measurements in Belgrade, while satellite measurements were used in the discussion of the spatial distribution of dust. Furthermore, the impact of the dust intrusion episode on PM_{10} concentrations in Belgrade was analysed. The measurement results were compared with results of Dust REgional Atmospheric Model DREAM (Ničković et al., 2001).

METHODOLOGY

The aerosol backscattering coefficient at 355 nm was derived from LIDAR measurements in Belgrade. A combined Raman elastic backscatter LIDAR has been operating at the Institute of Physics Belgrade since February 2014. It is based on the Nd:YAG laser operating at a fundamental wavelength of 1064 nm, and second and third harmonics at 532 and 355 nm. The laser pulses of 5 nm duration are transmitted at repetition rate of 20 Hz, with the output energies of 105, 45 and 65 mJ at these three wavelengths. The receiver is based on a 250 mm Cassegrain telescope in a biaxial arrangement, with adjustable field of view in the range from 0.5 to 3 mrad. Photomultiplier tubes are used to detect the backscatter signal in photon counting and analogue mode. The signals are detected at 355 and 387 nm, with a vertical resolution of 7.5 m and a temporal resolution of 1 minute. In this work we analysed the elastic backscatter signal at 355 nm. The analysis of the LIDAR signal to obtain the aerosol backscattering coefficient was performed using Fernald-Klett retrieval method (Fernald, 1984; Klett, 1985), assuming a LIDAR ratio value of 50 sr. Due to incomplete overlap of the laser and telescope fields of view, the LIDAR signal registering below 500 m was not considered in the analysis.

Daily PM_{10} mass concentrations at surface level, at three stations in Belgrade, were obtained from the State network for automatic monitoring of air quality (https://data.gov.rs/sr/datasets/kvalitet-vazdukha-u-republitsi-srbiji/).

Dust REgional Atmospheric Model DREAM (Ničković et al., 2001) embedded into the NCEP/NMME non-hydrostatic atmospheric model (Janjić et al., 2011) was used to provide horizontal and vertical distribution of dust concentration. The model domain covers Northern Africa, the Middle East and a large part of the European

continent, with a horizontal resolution of 1/5° (~ 30 km) and 28 vertical levels. It uses 8 particle size bins within the 0.1-10 μm radius range.

Additionally, we used an aerosol optical depth (AOD) at 550 nm from combined Deep Blue and Dark Target algorithms and the Deep Blue Ångström exponent (AE) at 412-470 nm products from the MODIS (Moderate Resolution Imaging Spetroradiometer) instrument aboard the NASA Aqua satellite. We used Collection 6, Level 3 data products. It should be noted, that the increase in AOD indicates an increase in aerosol load, while the AE parameter is used as a qualitative measure of particle size (the smaller AE values indicate predominantly coarse particles).

CALIOP (Cloud-Aerosol Lidar with Orthogonal Polarization) on board the CALIPSO satellite, was used to obtain vertical profiles of aerosols and clouds. It is an elastic backscatter LIDAR operating at two wavelengths: 532 nm and 1064 nm, with a depolarization channel at 532 nm. Here we used Level 2 Vertical Feature Mask product, which provides information on the aerosol types present in the detected layers (Omar et al., 2009).

Air-mass back trajectories ending at different altitudes over the LIDAR measurement site were calculated using the Hybrid Single-Particle Lagrangian Integrated Trajectory (HYSPLIT) model (Draxler and Hess, 1998; http://ready.arl.noaa.gov/HYSPLIT.php), with meteorological input from the Global Data Assimilation System (GDAS). The backtrajectories were used to provide an indication of the origin and pathways of air-masses arriving at altitudes of interest over Belgrade.

RESULTS AND DISCUSSION

We present an analysis of a dust episode that was observed over Belgrade from July 5-7, 2014. The beginning of the episode can be seen in MODIS data shown in Figure 1. MODIS values of AOD and AE indicate an increase of aerosol load and an increased contribution of coarse particles on July 5th compared to the previous day; this is typical for dust episodes.

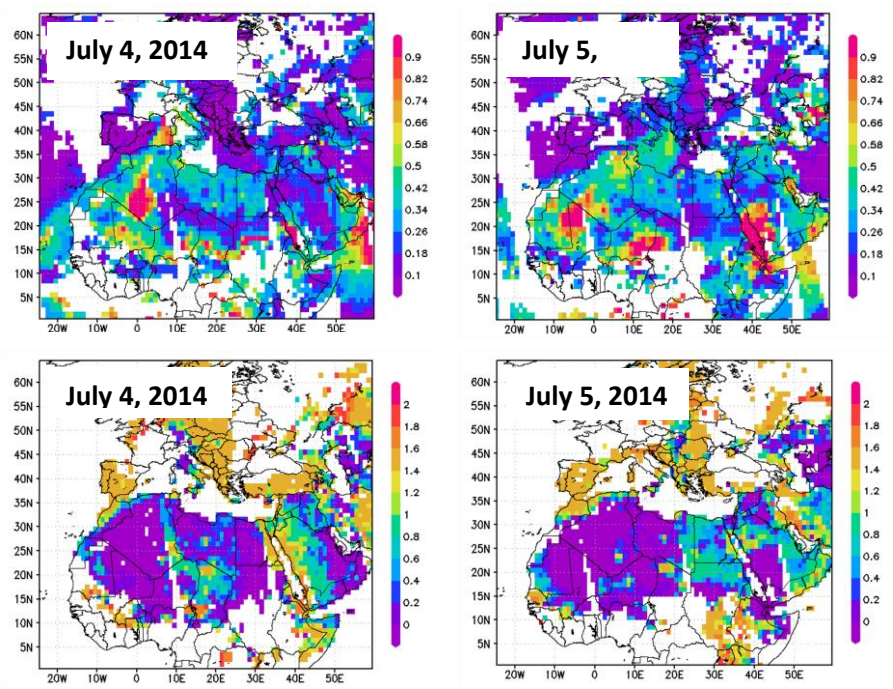

Figure 1. *MODIS aerosol data for July 4-5, 2014: (upper panels) MODIS aerosol optical depth (AOD) at 550 nm from combined Deep Blue and Dark Target algorithms; (lower panels) Deep Blue Angström exponent (AE) at 412-470 nm.*

The observed AOD at 550 nm over Belgrade increased from below 0.1 on July 4th, to about 0.3 on July 5th (the first day of the dust episode), with a decrease in the AE value from 1.4 to 0.4. Moderate AOD values were observed

over Belgrade during the dust episode. MODIS data also showed that the dust event affected parts of western and central Europe.

A close CALIPSO overpass over Belgrade occurred during the peak of the dust episode, on July 6th, at approximately 12 UTC. The CALIOP Vertical Feature Mask data, along the satellite ground track, is presented in Figure 2. We also showed the dust load over the area of interest and a vertical profile of the dust concentration along the CALIPSO ground track, resulting from DREAM model simulations. Both CALIOP data and the DREAM model results indicated that the dust plume extended north to Poland. The concentrations resulting from the model were largest around 40°N, at altitudes between 2 and 3 km, and decreased towards the north. At the part of the track within a 100 km distance from Belgrade, the DREAM model dust concentrations showeda maximum at a similar altitude range. CALIOP data suggested the presence of polluted dust (a mixture of pure dust with smoke or anthropogenic pollution) in this layer.

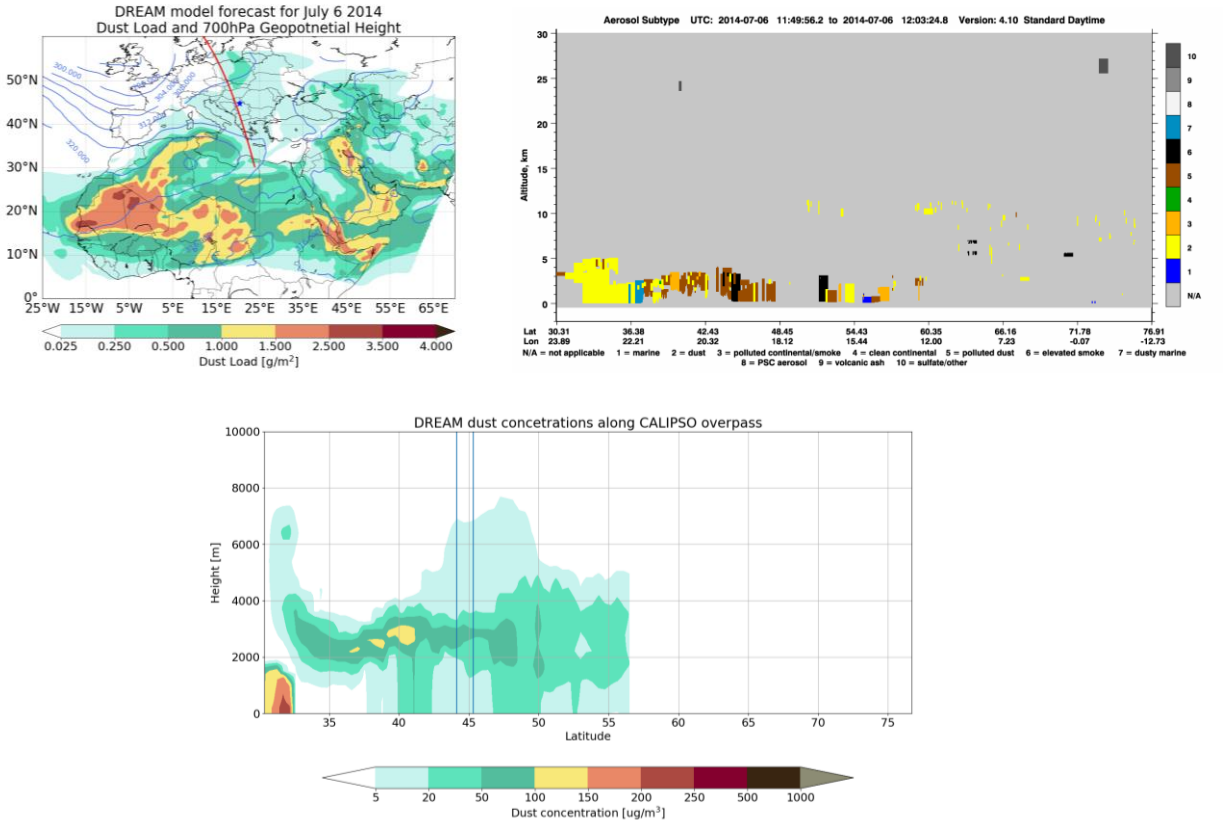

Figure 2. *(upper panels) Map of dust load calculated from DREAM model on July 6, 2014 at 12 UTC, with CALIPSO ground track and Belgrade LIDAR station marked; and the corresponding results of CALIOP aerosol classification. (lower panel) Dust concentration vertical profiles along the CALIPSO ground track obtained from DREAM model. Data between the two vertical lines corresponds to the part of the track within 100 km distance from Belgrade LIDAR station.*

Ground-based LIDAR measurements in Belgrade were analyzed to characterize the aerosol vertical profile during the dust episode. The profile of the aerosol backscattering coefficient showed a distinctly elevated aerosol layer on July 5th, at altitudes between approximately 2 and 5 km, with a maximum at about 4.5 km. It was identified as a dust layer, based on the air-mass backtrajectory was calculated to find the corresponding aerosol source region. Selected vertical profiles of the aerosol backscattering coefficient, and of the corresponding profiles of dust mass concentration obtained from DREAM model simulations, are presented in Figure 3. It should be noted that their comparison is only qualitative as we did not attempt to calculate the backscattering coefficient from the DREAM model results due to its high sensitivity to aerosol chemistry. The averaging of LIDAR signals for the analysis of the presented data was performed in 30minute intervals centered at the time of the model result. The dust layer boundaries were determined following the procedure described by Mona et al. (2006). The backscattering

coefficients showed that the layer descended during the course of the dust episode, and indicated an entrainment of dust into the PBL on July 7th. Dust mass concentrations resulting from the DREAM model showed a similar vertical pattern as the LIDAR measurements and a notable increase of dust concentration at altitudes below 2 km on July 7th.

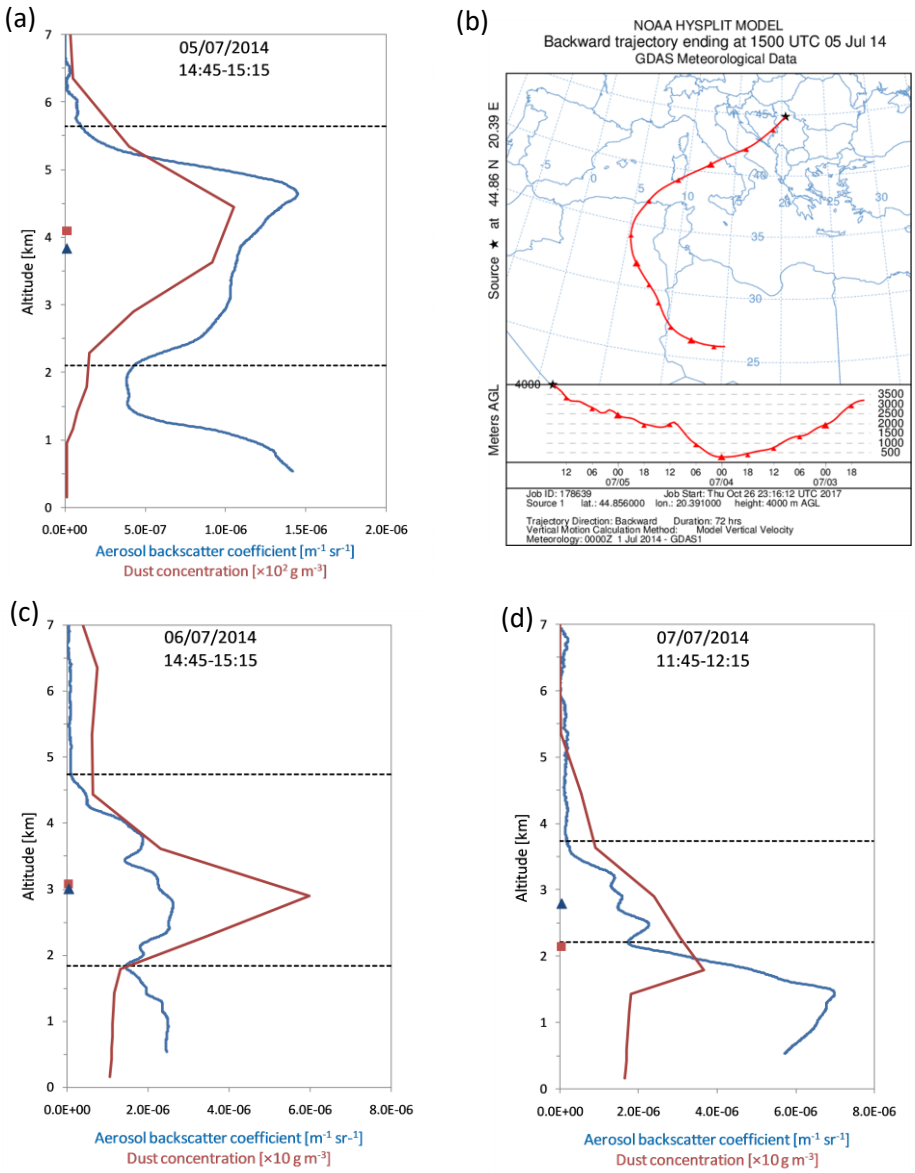

Figure 3. *(a, c, d) Vertical profile of aerosol backscattering coefficient from LIDAR measurements in Belgrade (blue line) and the corresponding profile of dust concentration from the DREAM model (red line); horizontal lines indicate dust layer base and top, while symbols show the positions of the dust layer's center of mass as calculated from LIDAR measurements and the DREAM model (b) 72hour airmass backtrajectory arriving at a 4 km altitude over Belgrade on July 5, 2014, at 15 UTC (corresponding to profile (a)).*

Figure 3 also shows altitudes of the dust layer center of mass, based on LIDAR measurements and the DREAM model. In the case of LIDAR measurements, it was calculated as a backscattering-coefficient-weighted altitude, according to:

$$z_c = \frac{\int_{z_b}^{z_t} z \cdot \beta(z) dz}{\int_{z_b}^{z_t} \beta(z) dz}$$

where z_b and z_t are the altitudes of the base and the top of the dust layer and $\beta(z)$ is the aerosol backscattering coefficient at altitude z. To minimize the effect of anthropogenic pollution, the center of mass from the LIDAR measurements was calculated only for the elevated layer. The dust's centre of mass from the DREAM model was calculated taking into account the entire dust profile.

Daily mass concentration of PM_{10} at ground level showed a similar trend at three air quality monitoring stations in Belgrade, with an increase during the dust episode (Figure 4). The increase started on July 6th, and the maximum was reached on July 7th, exceeding the 95th percentile of the summer (June, July and August) 2014 values. However, the daily limit value of 50 μg m^{-3}, set by the EU Air Quality Directive 2008/50/EC, was not exceeded. The increase of PM_{10} concentration is in agreement with the results of the LIDAR measurements, and the DREAM model, which indicated a settling of the dust plume (as shown in Figure 3). For comparison, daily average dust mass concentrations at the surface, obtained from the DREAM model, are also shown in Figure 4. They showed a similar trend as measured PM_{10} concentrations, increasing by 11 μg m^{-3} during the dust episode, while measured PM_{10} increased by 15 to 17 μg m^{-3} at the three monitoring stations. Larger measured PM_{10} concentrations, compared to surface dust concentrations from the model, were attributed to sources other than mineral dust.

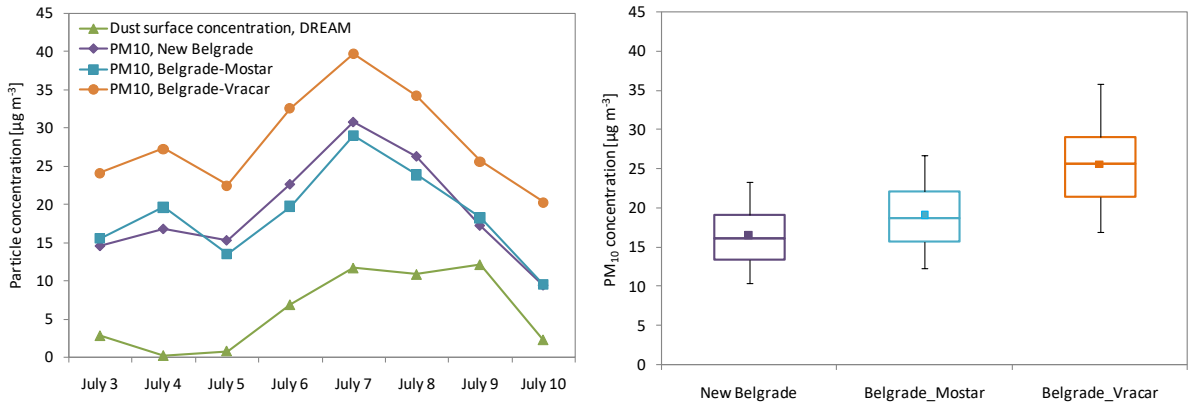

Figure 4. *(left panel) Daily average dust surface concentration values from the DREAM model and PM_{10} concentrations from three air quality monitoring stations in Belgrade. (right panel) Boxplot of PM_{10} concentrations during summer (June, July, August) of 2014 at three monitoring stations in Belgrade; the extent of the box indicates the 25th and 75th percentiles, the central line represents the median value, while the whiskers indicate the 5th and 95th percentiles; the points represent the mean values.*

CONCLUSION

We present analysis of a dust intrusion episode that was observed over Belgrade on July 5-7, 2014. The satellite measurements showed that the dust plume extended to western and central Europe. A distinctly elevated dust layer, extending at altitudes of approximately 2-5 km, was observed on July 5th using ground-based LIDAR in Belgrade. The layer altitude decreased during the dust episode, with the centre of mass altitude decreasing from approximately 4 km to below 3 km. The LIDAR measurements indicated entrainment of dust into the PBL on July 7th, the last day of the episode. The vertical distribution of dust and its temporal evolution over Belgrade was reproduced well by the DREAM model. The observed daily PM_{10} concentrations at three monitoring stations in Belgrade showed an increase of 15-17 μg m^{-3}, while dust was settling down during the episode as indicated by LIDAR measurements. Dust surface concentrations obtained from the DREAM model showed the same trend as measured PM_{10} concentrations, with a smaller increase (11 μg m^{-3}), during the episode: This difference was attributed to the contribution of other aerosol types to the observed PM_{10} concentrations.

ACKNOWLEDGEMENTS

This research was realized as a part of the project no. III43007, financed by the Ministry of Education, Science and Technological Development of the Republic of Serbia within the framework of integrated and interdisciplinary research for the period 2011-2020. The authors acknowledge support by the project GEO-CRADLE, Grant Agreement No. 690133, funded under European Union Horizon 2020 Programme. The authors gratefully acknowledge the NOAA Air Resources Laboratory (ARL) for the provision of HYSPLIT transport and dispersion

model and READY website (http://www.ready.noaa.gov), used in this publication. Analyses and visualizations of MODIS data used in this study were produced with the Giovanni online data system, developed and maintained by the NASA GES DISC. CALIPSO data were obtained from the NASA Langley Research Center Atmospheric Science Data Center.

REFERENCES

1. Ansmann, A., Bösenberg J., Chaikovsky, A., Comeron, A., Eckhardt, S., Eixmann, S. et al., 2003. Long-range transport of Saharan dust to northern Europe: The 11-16 October 2001 outbreak observed with EARLINET, Journal of Geophysical Research 108, 4783, doi:10.1029/2003JD003757.
2. Draxler, R. R. and Hess, G. D., 1998. An overview of the HYSPLIT 4 modeling system for trajectories, dispersion, and deposition, Australian Meteorology Magazine, 47, 295-308.
3. Fernald, F. G., 1984. Analysis of atmospheric lidar observations: some comments, Applied Optics 23,652-653.
4. Giannadaki, D., Pozzer, A., Lelieveld, J., 2014. Modeled global effects of airborne desert dust on air quality and premature mortality, Atmospheric Chemistry and Physics 14, 957-968.
5. IPCC: Climate Change 2013: The physical science basis. Contribution of Working Group I to the Fifth Assessment Report of the Intergovernmental Panel on Climate Change, edited by: Stocker, T.F., Qin, D., Plattner, G.-K., Tignor, M., Allen, S.K., Boschung, J., Nauels, A., Xia, Y., Bex, V., Midgley, P.M., Cambridge University Press, Cambridge, UK and New York, USA.
6. Janjić, Z. I., Gerrity Jr, J. P., Ničković, S., 2011. An alternative approach to non-hydrostatic modelling, Monthly Weather Review 129, 1164-78.
7. Kinne, S., Schulz, M., Textor, C., Guilbert, S., Balkansky, Y., Bauer, S. E. et al., 2006. An AeroCom initial assessment - optical properties in aerosol component modules of global models, Atmospheric Chemistry and Physics 6, 1815-1834.
8. Klett, J. D. 1985. Lidar inversion with variable backscatter/extinction ratios, Applied Optics 24, 1638-1643.
9. Mona, L., Amodeo, A., Pandolfi, M., Pappalardo, G., 2006. Saharan dust intrusions in the Mediterranean area: Three years of Raman lidar measurements, Journal of Geophysical Research, 111, D16203, doi:10.1029/2005JD006569.
10. Ničković, S., Kallos, G., Papadopoulos, A., Kakaliagou, O., 2001. A model for prediction of desert dust cycle in the atmosphere, Journal of Geophysical Research 106, 18113-18130.
11. Omar, A. H., Winker, D. M., Kittaka, C., Vaughan, M. A., Liu, Z., Hu, et al., 2009. The CALIPSO automated aerosol classification and Lidar Ratio Selection Algorithm, Journal of Atmospheric and Oceanic Technology 26, 1994-2014, doi:10.1175/2009JTECHA1231.1.
12. Prospero, J. M., 1999. Long-term measurements of the transport of African mineral dust to the southeastern United States: Implications for regional air quality, Journal of Geophysical Research 104, 15917-15927, doi:10.1029/1999JD900072.

CIP - Каталогизација у публикацији
Народна библиотека Србије, Београд

502.3:502.175(082)
66.071.9(082)
613.15(082)

INTERNATIONAL WeBIOPATR Workshop Particulate Matter: Research and Management (6; 2017; Beograd)

Proceedings [Elektronski izvor] /
The Sixth International WeBIOPATR Workshop & Conference Particulate Matter: Research and Management, WeBIOPATR2017, 6-8 September 2017, Belgrade;
editors Milena Jovašević-Stojanović and Alena Bartoňová. –
Belgrade: Vinča Institute of Nuclear Sciences, 2019
(Belgrade: Vinča Institute of Nuclear Sciences). -
1 elektronski optički disk (CD-ROM); 12 cm

Sistemski zahtevi: Nisu navedeni. –
Nasl. sa naslovne strane dokumenta. -
Tiraž 150. –
Bibliografija uz svaki rad.

ISBN 978-86-7306-152-8

a) Ваздух - Контрола квалитета - Зборници

b) Отпадни гасови – Штетно дејство - Зборници

c) Здравље - Заштита - Зборници

COBISS.SR-ID 278918412

WeBIOPATR

University of Belgrade
Technical Faculty in Bor and
Mining and Metallurgy Institute Bor

49th International October Conference on Mining and Metallurgy

PROCEEDINGS

Editors:
Nada Štrbac
Ivana Marković
Ljubiša Balanović

Bor Lake, Serbia
October 18-21, 2017

IOC 2017
International October Conference

PROCEEDINGS,
49th INTERNATIONAL OCTOBER CONFERNCE
on Mining and Metallurgy

Editors:
Prof. dr Nada Štrbac
Doc. dr Ivana Marković
Doc. dr Ljubiša Balanović
University of Belgrade, Technical Faculty in Bor

Technical Editor:
M. Sc. Uroš Stamenković
University of Belgrade, Technical Faculty in Bor

Publisher: University of Belgrade, Technical Faculty in Bor
For the publisher: Dean Prof. dr Nada Štrbac
Circulation: 200 copies

Printed by "Happy trend DOO", Zaječar, 2017

ISBN 978-86-6305-066-2

CIP - Каталогизација у публикацији - Народна библиотека Србије, Београд

622(082)
669(082)

INTERNATIONAL October Conference on Mining and Metallurgy (49 ; 2017 ; Bor Lake)
Proceedings / 49th International October Conference on Mining and Metallurgy - IOC 2017,
Bor Lake, Serbia, October 18-21, 2017;
[organized by] University of Belgrade, Technical Faculty Bor and Mining and Metallurgy Institute Bor;
editors Nada Štrbac, Ivana Marković, Ljubiša Balanović. - Bor : University of Belgrade, Technical Faculty,
2017 (Zaječar : Happy trend). - XXIII, 664 str. : ilustr. ; 25 cm

Tiraž 200. - Bibliografija uz svaki rad. - Registar.

ISBN 978-86-6305-066-2

a) Рударство - Зборници b) Металургија - Зборници

COBISS.SR-ID 246349324

Bor Lake, Serbia, October 18-21, 2017

SCIENTIFIC COMMITTEE

Prof. dr Nada Štrbac (Serbia) - president
Prof. dr Radoje Pantović (Serbia) - vice-president
Prof. dr Grozdanka Bogdanović (Serbia)- vice-president
Prof. dr Dragoslav Gusković (Serbia) - vice-president
Prof. dr Aleksandar Dimitrov (Macedonia)
Dr Ana Kostov (Serbia)
Dr Andrei Rotaru (Romania)
Prof. dr Anđelka Mihajlov (Serbia)
Prof. dr Batrić Pešić (USA)
Prof. dr Boštjan Markoli (Slovenia)
Prof. dr Boyan Boyanov (Bulgaria)
Prof. dr Branka Jordović (Serbia)
Prof. dr Carl Heinz Spitzer (Germany)
Prof. dr Costas Matis (Greece)
Prof. dr Dejan Tanikić (Serbia)
Prof. dr Desimir Marković (Serbia)
Prof. dr Dimitris Panias (Greece)
Prof. dr Dimitriu Sorin (Romania)
Prof. dr Dragan Manasijević (Serbia)
Prof. dr Duško Minić (Serbia)
Prof. dr Endre Romhanji (Serbia)
Prof. dr Fathi Habashi (Canada)
Prof. dr Guven Onal (Turkey)
Prof. dr György Kaptay (Hungary)
Prof. dr Heikki Jalkanen (Finland)
Prof. dr Iwao Katayama (Japan)
Prof. dr Jakob Lamut (Slovenia)
Prof. dr Jelena Penavin Škundrić (B&H)
Prof. dr Jožef Medved (Slovenia)
Prof. dr Karlo Raić (Serbia)
Prof. dr Kemal Delijić (Montenegro)
Prof. dr Krzystof Fitzner (Poland)
Prof. dr Luis Filipe Malheiros (Portugal)
Dr Magnus Ericsson (Sweden)
Prof. dr Milan Antonijević (Serbia)
Prof. dr Milan Trumić (Serbia)
Prof. dr Mile Dimitrijević (Serbia)
Prof. dr Mirjana Rajčić Vujasinović (Serbia)
Prof. dr Mirko Gojić (Croatia)
Dr Mile Bugarin (Serbia)
Dr Milenko Ljubojev (Serbia)
Dr Mirjam Jan-Blažić (Slovenia)
Dr Miroslav Sokić (Serbia)
Prof. dr Mirsada Oruč (B&H)
Dr Nadežda Talijan (Serbia)
Prof. dr Nenad Radović (Serbia)
Prof. dr Nenad Vušović (Serbia)
Prof. dr Nobuyuki Masuda (Japan)
Prof. dr Onuralp Yucel (Turkey)
Prof. dr Petr M. Solozhenkin (Russia)
Prof. dr Rodoljub Stanojlović (Serbia)
Prof. dr Sanda Krausz (Romania)
Prof. dr Seshadri Seetharaman (Sweden)
Dr Slavomir Hredzak (Slovakia)
Prof. dr Snežana Šerbula (Serbia)
Prof. dr Stoyan Groudev (Bulgaria)
Prof. dr Sulejman Muhamedagić (B&H)
Prof. dr Svetlana Ivanov (Serbia)
Dr Srećko Stopić (Germany)
Prof. dr Tamara Holjevac Grgurić (Croatia)
Prof. dr Tatjana Volkov-Husović (Serbia)
Prof. dr Tomaš Havlik (Slovakia)
Prof. dr Velizar Stanković (Serbia)
Prof. dr Velimir Radmilović (USA)
Prof. dr Vitomir Milić (Serbia)
Dr Vladan Ćosović (Serbia)
Prof. dr Vladimir Krstić (Canada)
Prof. dr Vladislav Kecojević (USA)
Prof. dr Vlastimir Trujić (Serbia)
Prof. dr Yong Du (China)
Prof. dr Zoran Marković (Serbia)
Prof. dr Žarko Radović (Montenegro)
Prof. dr Željko Kamberović (Serbia)
Prof. dr Živan Živković (Serbia)
Dr Walter Valery (Australia)
Dr Zvonko Gulišija (Serbia)

ORGANIZING COMMITTEE

Doc. dr Ivana Marković - president
Doc. dr Ljubiša Balanović - vice-president
Doc. dr Saša Stojadinović - vice-president
Prof. dr Svetlana Ivanov
Prof. dr Dragan Manasijević
Prof. dr Snežana Urošević
Dr Ana Kostov (IRM Bor)
Doc. dr Vesna Grekulović
Doc. dr Aleksandra Mitovski
Doc. dr Dejan Petrović
Doc. dr Milan Gorgievski
Doc. dr Ana Simonović
Doc.dr Tanja Kalinović
Doc.dr Marija Petrović Mihajlović
M.Sc. Uroš Stamenković
M.Sc. Oliver Marković
Slavica Stevanović, prof. engl.
Sandra Vasković, prof. engl.
Predrag Stolić, dipl. ing.
Dr Ana Radojević
M.Sc. Jelena Milosavljević

RAMAN LIDAR FOR ATMOSPHERIC AEROSOL PROFILING IN SERBIA

Zoran Mijić, Luka Ilić, Maja Kuzmanoski

Institute of Physics Belgrade, University of Belgrade, Pregrevica 118, 11080 Belgrade, Serbia

Abstract

Due to the large variability in space and time atmospheric aerosols are considered one of the major uncertainties in climate forcing and atmospheric processes affecting human health and environment. An advanced laser remote sensing technique – lidar is the most appropriate tool for providing range-resolved aerosol vertical distribution. Lidar measurements of aerosol optical properties with high spatial and temporal resolution give detailed information on the occurrence and development of aerosol structures. The characteristics of Raman lidar system at the Institute of Physics Belgrade and its potential for investigation of tropospheric aerosols will be discussed. Lidar case study measurements together with methodology for aerosol layer identification is presented.

***Keywords**: remote sensing, Raman lidar, aerosol vertical distribution*

1. INTRODUCTION

Atmospheric aerosols influence the energy balance of the Earth, the water cycle and atmospheric chemistry, playing a crucial role in climate change and air quality. Due to their short lifetime and the large variability in space and time, atmospheric aerosols are considered one of the major uncertainties in climate forcing and atmospheric processes [1]. For radiative studies, it is necessary to measure aerosol optical properties, size, morphology and composition as a function of time and space, with a high resolution in both domains to account for the large variability. Lidar (Light Detection And Ranging), an active remote sensing technique, represents the optimal tool to provide range-resolved aerosol optical parameters. The first observational lidar stations network called EARLINET (the European Aerosol Research Lidar Network) [2] was founded in 2000 to provide the long-term measurement series needed to build a climatology of aerosol optical properties at the continental scale. The main objectives of EARLINET are the establishment of a comprehensive and quantitative statistical data base of the horizontal and vertical distribution of aerosols on the European scale using a network of advanced laser remote sensing stations, and the use of these data for studies related to the impact of aerosols on a variety of environmental problems. The developments for the quality assurance strategy, the optimization of instruments and data processing, and the dissemination of data have contributed to a significant improvement of the network towards a more sustainable observing system. Several lidar techniques are suitable for aerosol studies and in the last ten years rapid progress in laser technology, measurement techniques, and data acquisition systems has contributed to a much wider use of these techniques for aerosol remote monitoring. In this paper the characteristics of Raman lidar system at the Institute of Physics Belgrade (IPB), the EARLINET joining lidar station, is presented together with several quality tests in order to assess the performance of a lidar system. Case study measurement together with gradient method used to determine heights of both planetary boundary layer (PBL) and elevated aerosol layers is discussed.

2. EXPERIMENTAL

Atmospheric probing by lidar is able to obtain time dependent three dimensional pictures of aerosol distributions. Typical lidar system can be divided into the three main components, transmitter, receiving and data acquisition unit (Figure 1-left panel). Raman lidar system at the IPB (44.860 N, 20.390 E) is bi-axial lidar system with combined elastic and Raman detection designed to perform continuous measurements of aerosols in the planetary boundary layer and the lower free troposphere (Figure 1-right panel). Transmitter unit is based on the third harmonic frequency of a water cooled, pulsed Nd:YAG laser, emitting pulses of 65 mJ output energy at 355 nm with a 20 Hz repetition rate. In order to improve the maximum range and the precision of the system the beam expander is used to reduce the laser beam divergence expanding the beam's diameter by 3 times. The optical receiving unit consists of two sub-units, a receiving telescope and wavelength separation unit. The optical receiver is a Cassegrain reflecting telescope with a primary mirror of 250 mm diameter and a focal length of 1250 mm. Photomultiplier tubes are used to detect elastic backscatter lidar signal at 355 nm and Raman signal at 387 nm (Nitrogen vibrational scattering). The detectors are operated both in the analog and photon-counting mode and the spatial raw resolution of the detected signals is 7.5 m. Averaging time of the lidar profiles is of the order of 1 min corresponding to 1200 laser shots. The Licel transient recorder is comprised of a fast transient digitizer with on board signal averaging, a discriminator for single photon detection and a multichannel scaler combined with preamplifiers for both systems. For analog detection, the signal is amplified according to the input range selected and digitized by a 12-Bit-20 MHz A/D converter. At the same time the signal part in the high frequency domain is amplified and a 250 MHz fast discriminator detects single photon events above the selected threshold voltage.

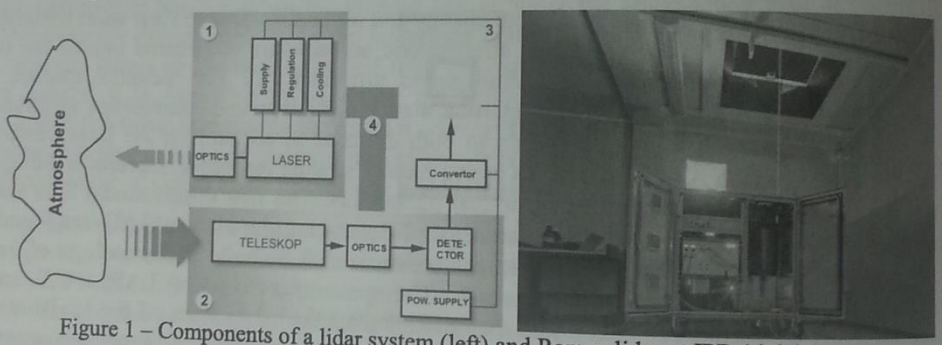

Figure 1 – Components of a lidar system (left) and Raman lidar at IPB (right)

Besides vertical profiles of aerosols backscatter and extinction coefficients lidar measurements can be used to estimate PBL height and aerosol elevated layers using different approaches [3]. In this study, the gradient method was used to determine the position of the strongest gradient of the aerosol vertical distribution, associated with the PBL height [4]. The height of a strong negative peak which can be identified as the absolute minimum of the range corrected signal's (RCS) derivative, determines the PBL top height. Other local minima in the signal derivative, with absolute values above a specified threshold and with transition intervals including a minimum of five points, are associated with elevated aerosol layer top heights in the free troposphere [4]. Differences between PBL and free troposphere can be also observed using vertical profiles of thermodynamic quantities and wind from radiosounding measurements. The bulk Richardson number is used for PBL height estimation from radiosounding measurements [5] at a weather station (Belgrade Košutnjak, WMO number 13275), 10 km away from the lidar measurement site.

3. RESULTS AND DISCUSSION

Within the lidar network, quality assurance program has been developed for both hardware and retrieval algorithms. One of the basic setup tests is system alignment since the incomplete overlap between the laser beam and the receiver field of view affects significantly lidar observations of particle optical properties.

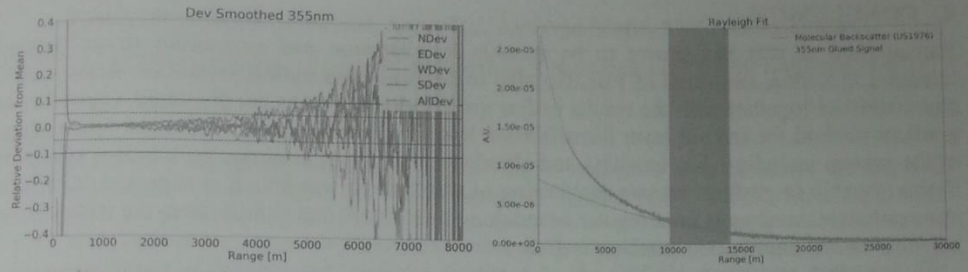

Figure 2 – Deviations of signals collected with four telescope sectors compared to the mean signal (left) and Rayleigh fit and fitting interval for 355 nm elastic channel, Raman lidar at IPB

Thus, quality assurance of the lidar measurement requires to test the alignment of the lidar system i.e. to determine overlap function. Procedure developed by Freudenthaler [6] involves a set of measurements with partially covered telescope (four sectors named N, E, W and S) so that each measurement is in fact collection of the backscattered light at a certain sector of the telescope. The deviation of each sector signal compared to the average of all signals below 10% is acceptable and from Figure 2 it is clear that the system is well aligned in the near field starting from 400 m. To assure lidar alignment in the far range the Rayleigh fit procedure can be used which is a normalization of the lidar signal to the calculated Rayleigh backscatter coefficient in a range where we assume clean conditions and where the calculated signal fits the lidar signal sufficiently good. From Figure 2–right panel it can be seen that the lidar system is well aligned up to the 12 km. Once the system is properly aligned it can be used for systematic aerosol measurements. In Figure 3 time series of RCS measured on July 6 2014 is presented.

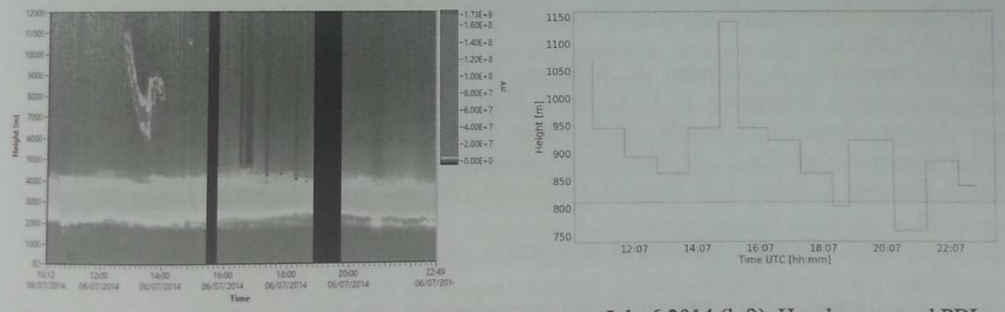

Figure 3 – Colormaps represent the lidar RCS at 355 nm on July 6 2014 (left). Hourly averaged PBL height (right). Horizontal red line represents PBL height retrieved from radiosounding at 00 UTC (dashed line) on July 7 2014

The gradient method was used to analyze the evolution of the PBL height during its diurnal cycle, and estimate elevated aerosol layer heights. Hourly averaged values of PBL show decrease of the PBL height from 1070 m to 860 m after the local noon (10 UTC). Significant increase in PBL height, reaching above 1100 m around 15 UTC can be attributed to strong convective motions which could have influenced formation of clouds between 16 UTC and 18 UTC, visible in the RCS plot. Gradient method shows decrease of the PBL heights until the end of the

measurement period to about 840 m. This value, is similar to the one estimated from 00 UTC radiosounding – 810 m. Two elevated aerosol layers were identified, one with its top reaching height of 2 – 2.2 km in the morning and reducing its height to below 1800 m in the afternoon. Another layer with top height ranging from 3.1 to 3.5 km was present during the whole measurement period.

4. CONCLUSION

Raman lidar at IPB has shown to be suitable for detection and monitoring aerosol layers' intrusion in Serbia, evolution of PBL but also to describe their optical properties. Basic system characteristics together with the results of few quality checks results are presented. Capability of gradient method for aerosol layer identification has been demonstrated. Additional optimization of the system including data handling and algorithm tests are in progress. As a unique system in Serbia capable to perform remote monitoring of atmospheric aerosols it is expected to perform systematic measurements on a regular schedule in near future and contribute to the collection of aerosol vertical distribution database in Europe.

ACKNOWLEDGEMENTS

This paper was realized as a part of the project III43007 financed by the Ministry of Education and Science of the Republic of Serbia within the framework of integrated and interdisciplinary research for the period 2011-2017. The publication was supported by the project GEO-CRADLE (Coordinating and integRating state-of-the-art Earth Observation Activities in the regions of North Africa, Middle East, and Balkans and Developing Links with GEO related initiatives towards GEOSS), Grant Agreement No. 690133, funded under European Union Horizon 2020 Programme - Topic: SC5-18b-2015, Integrating North African, Middle East and Balkan Earth Observation capacities in GEOSS.

REFERENCES

[1] T. F. Stocker, D. Qin, G.-K. Plattner, M. Tignor, S. K. Allen, J. Boschung, A. Nauels, Y. Xia, V. Bex, P. M. Midgley, IPCC: The Physical Science Basis, Contribution of Working Group I to the Fifth Assessment Report of the Intergovernmental Panel on Climate Change, Cambridge University Press, Cambridge, United Kingdom and New York, NY, USA, 2013.

[2] G. Pappalardo, A. Amodeo, A. Apituley, A. Comeron, V. Freudenthaler, H. Linné, A. Ansmann, J. Bösenberg, G. D'Amico, I. Mattis, L. Mona, U. Wandinger, V Amiridis, L. Alados Arboledas, D. Nicolae, M. Wiegner. Atmos. Meas. Tech. 7 (2014) 2389.

[3] S. Emeis, K. Schafer, C., Munkel Meteorologische Zeitschrift, 17(5) (2008) 621-630.

[4] C. Flamant, J. Pelon, P.H. Flamant, P. Durand., Boundary-Layer Meteorol. 83 (1997) 247-284.

[5] L. Menut, C. Flamant, J. Pelon, P. H. Flamant., Boundary-Layer Meteorol. 93 (1999) 269–286.

[6] V. Freudenthaler, Proceedings of 24th International Laser Radar Conference, 23-27 June, Boulder, USA, 2008.

University of Belgrade
Technical Faculty in Bor and
Mining and Metallurgy Institute Bor

49th International October Conference on Mining and Metallurgy

PROCEEDINGS

Editors:
Nada Štrbac
Ivana Marković
Ljubiša Balanović

Bor Lake, Serbia
October 18-21, 2017

IOC 2017
International October Conference

PROCEEDINGS,
49th INTERNATIONAL OCTOBER CONFERNCE
on Mining and Metallurgy

Editors:
Prof. dr Nada Štrbac
Doc. dr Ivana Marković
Doc. dr Ljubiša Balanović
University of Belgrade, Technical Faculty in Bor

Technical Editor:
M. Sc. Uroš Stamenković
University of Belgrade, Technical Faculty in Bor

Publisher: University of Belgrade, Technical Faculty in Bor
For the publisher: Dean Prof. dr Nada Štrbac
Circulation: 200 copies

Printed by "Happy trend DOO", Zaječar, 2017

ISBN 978-86-6305-066-2

CIP - Каталогизација у публикацији - Народна библиотека Србије, Београд

622(082)
669(082)

INTERNATIONAL October Conference on Mining and Metallurgy (49 ; 2017 ; Bor Lake)
Proceedings / 49th International October Conference on Mining and Metallurgy - IOC 2017, Bor Lake, Serbia, October 18-21, 2017;
[organized by] University of Belgrade, Technical Faculty Bor and Mining and Metallurgy Institute Bor;
editors Nada Štrbac, Ivana Marković, Ljubiša Balanović. - Bor : University of Belgrade, Technical Faculty, 2017 (Zaječar : Happy trend). - XXIII, 664 str. : ilustr. ; 25 cm

Tiraž 200. - Bibliografija uz svaki rad. - Registar.

ISBN 978-86-6305-066-2

a) Рударство - Зборници b) Металургија - Зборници

COBISS.SR-ID 246349324

Bor Lake, Serbia, October 18-21, 2017

SCIENTIFIC COMMITTEE

Prof. dr Nada Štrbac (Serbia) - president
Prof. dr Radoje Pantović (Serbia) - vice-president
Prof. dr Grozdanka Bogdanović (Serbia)- vice-president
Prof. dr Dragoslav Gusković (Serbia) - vice-president
Prof. dr Aleksandar Dimitrov (Macedonia)
Dr Ana Kostov (Serbia)
Dr Andrei Rotaru (Romania)
Prof. dr Anđelka Mihajlov (Serbia)
Prof. dr Batrić Pešić (USA)
Prof. dr Boštjan Markoli (Slovenia)
Prof. dr Boyan Boyanov (Bulgaria)
Prof. dr Branka Jordović (Serbia)
Prof. dr Carl Heinz Spitzer (Germany)
Prof. dr Costas Matis (Greece)
Prof. dr Dejan Tanikić (Serbia)
Prof. dr Desimir Marković (Serbia)
Prof. dr Dimitris Panias (Greece)
Prof. dr Dimitriu Sorin (Romania)
Prof. dr Dragan Manasijević (Serbia)
Prof. dr Duško Minić (Serbia)
Prof. dr Endre Romhanji (Serbia)
Prof. dr Fathi Habashi (Canada)
Prof. dr Guven Onal (Turkey)
Prof. dr György Kaptay (Hungary)
Prof. dr Heikki Jalkanen (Finland)
Prof. dr Iwao Katayama (Japan)
Prof. dr Jakob Lamut (Slovenia)
Prof. dr Jelena Penavin Škundrić (B&H)
Prof. dr Jožef Medved (Slovenia)
Prof. dr Karlo Raić (Serbia)
Prof. dr Kemal Delijić (Montenegro)
Prof. dr Krzystof Fitzner (Poland)
Prof. dr Luis Filipe Malheiros (Portugal)
Dr Magnus Ericsson (Sweden)
Prof. dr Milan Antonijević (Serbia)
Prof. dr Milan Trumić (Serbia)
Prof. dr Mile Dimitrijević (Serbia)
Prof. dr Mirjana Rajčić Vujasinović (Serbia)
Prof. dr Mirko Gojić (Croatia)
Dr Mile Bugarin (Serbia)
Dr Milenko Ljubojev (Serbia)
Dr Mirjam Jan-Blažić (Slovenia)
Dr Miroslav Sokić (Serbia)
Prof. dr Mirsada Oruč (B&H)
Dr Nadežda Talijan (Serbia)
Prof. dr Nenad Radović (Serbia)
Prof. dr Nenad Vušović (Serbia)
Prof. dr Nobuyuki Masuda (Japan)
Prof. dr Onuralp Yucel (Turkey)
Prof. dr Petr M. Solozhenkin (Russia)
Prof. dr Rodoljub Stanojlović (Serbia)
Prof. dr Sanda Krausz (Romania)
Prof. dr Seshadri Seetharaman (Sweden)
Dr Slavomir Hredzak (Slovakia)
Prof. dr Snežana Šerbula (Serbia)
Prof. dr Stoyan Groudev (Bulgaria)
Prof. dr Sulejman Muhamedagić (B&H)
Prof. dr Svetlana Ivanov (Serbia)
Dr Srećko Stopić (Germany)
Prof. dr Tamara Holjevac Grgurić (Croatia)
Prof. dr Tatjana Volkov-Husović (Serbia)
Prof. dr Tomaš Havlik (Slovakia)
Prof. dr Velizar Stanković (Serbia)
Prof. dr Velimir Radmilović (USA)
Prof. dr Vitomir Milić (Serbia)
Dr Vladan Ćosović (Serbia)
Prof. dr Vladimir Krstić (Canada)
Prof. dr Vladislav Kecojević (USA)
Prof. dr Vlastimir Trujić (Serbia)
Prof. dr Yong Du (China)
Prof. dr Zoran Marković (Serbia)
Prof. dr Žarko Radović (Montenegro)
Prof. dr Željko Kamberović (Serbia)
Prof. dr Živan Živković (Serbia)
Dr Walter Valery (Australia)
Dr Zvonko Gulišija (Serbia)

ORGANIZING COMMITTEE

Doc. dr Ivana Marković - president
Doc. dr Ljubiša Balanović - vice-president
Doc. dr Saša Stojadinović - vice-president
Prof. dr Svetlana Ivanov
Prof. dr Dragan Manasijević
Prof. dr Snežana Urošević
Dr Ana Kostov (IRM Bor)
Doc. dr Vesna Grekulović
Doc. dr Aleksandra Mitovski
Doc. dr Dejan Petrović
Doc. dr Milan Gorgievski
Doc. dr Ana Simonović
Doc.dr Tanja Kalinović
Doc.dr Marija Petrović Mihajlović
M.Sc. Uroš Stamenković
M.Sc. Oliver Marković
Slavica Stevanović, prof. engl.
Sandra Vasković, prof. engl.
Predrag Stolić, dipl. ing.
Dr Ana Radojević
M.Sc. Jelena Milosavljević

AIR MASS TRANSPORT OVER BALKANS REGION IDENTIFIED BY ATMOSPHERIC MODELING AND AEROSOL LIDAR TECHNIQUE

Zoran Mijić, Mirjana Perišić, Luka Ilić, Andreja Stojić, Maja Kuzmanoski

Institute of Physics Belgrade, University of Belgrade, Pregrevica 118, 11080 Belgrade, Serbia

Abstract

This study combines atmospheric modeling with lidar measurements in order to assess the origin of aerosols traveling over Balkan region, having an impact on regional radiative budget and air quality. Particulate matter potential source regions and transport pathways were investigated using hybrid receptor modeling and mass concentrations measured in Belgrade, Serbia. In addition, the case study evidencing transport of Saharan dust particles simulated by the DREAM model was presented. The capability of the lidar technique to derive range-resolved vertical profiles of aerosol optical parameters was used to analyze the aerosol layers altitude and temporal evolution.

***Keywords**: atmospheric modeling, transport, PM*

1. INTRODUCTION

Suspended particulate matter (PM) in the atmosphere, commonly known as aerosol, plays an important role in the climate system. Besides significant effect on climate change, air quality and human health, aerosols affect long-range transport and deposition of toxics and nutrients. The complexity of aerosol processes in the atmosphere leads to large uncertainties in understanding of their role in many of the major environmental issues [1]. The direct (scattering and absorbing incoming solar radiation) and indirect aerosol effects (as they act as a cloud condensation nuclei) make the two largest contributions to the total uncertainty of radiative forcing. Regarding the impact of aerosols on air quality, the same processes that govern the global distribution, control the aerosol properties on regional and local scales. While *in situ* measurements are most adequate for air quality monitoring at the ground level, the assessment of impact of remote sources and transformation processes requires aerosol vertical distribution observations. Key parameters to be observed for this purpose are the presence, altitude and extent of elevated aerosol layers, the height of the planetary boundary layer (PBL), aerosol type, and mass concentration. Since long-range transport occurs at elevated layers, surface-based measurements of aerosol properties, such as chemical composition and size distribution are not sufficient. For global coverage including all relevant parameters, an integrated approach including ground-level and airborne in-situ measurements, ground-based remote sensing, and space-borne observations in combination with advanced modeling is necessary. Large observational networks such as the European Aerosol Research Lidar Network (EARLINET) [2], provide the long-term measurement series needed to build an aerosol vertical profile climatology at the continental scale. The capability of the lidar system (Light Detection And Ranging) to derive range-resolved aerosol vertical profiles with high spatial and temporal resolution is used to identify layers altitude and temporal evolution of intrusions. Using altitudes as inputs in air mass back-trajectories tracing method identification of aerosol sources at large distances from the measurement point, if their contribution is important, can be conducted. In this study hybrid receptor models for identification of potential source regions of PM affecting air quality in Belgrade are presented together with a case study evidencing transport of Saharan dust particles.

2. METHODOLOGY

Lidar technique is an active remote sensing method based on laser emission of the short-duration light pulses to the atmosphere and the analysis of the return signal. The intensity of the light backscattered by atmospheric molecules and particles is measured versus time – through the telescope receiver, collimating optics, a bandpass filter for daylight suppression – by an appropriate detector. For vertical profiling and remote sensing of atmospheric aerosol layers, Raman lidar at the Institute of Physics Belgrade (44.860 N, 20.390 E) has been used. It is bi-axial system with combined elastic and Raman detection designed to perform continuous measurements of aerosols in the PBL layer and the lower free troposphere. It is based on the third harmonic frequency of a compact, pulsed Nd:YAG laser, emitting pulses of 65 mJ output energy at 355 nm with a 20 Hz repetition rate. The optical receiver is a Cassegrain reflecting telescope with a primary mirror of 250 mm diameter and a focal length of 1250 mm. Photomultiplier tubes are used to detect elastic backscatter lidar signal at 355 nm and Raman signal at 387 nm. The detectors are operated both in the analog and photon-counting mode with lidar profiles averaging time of the order of 1 min and the spatial raw resolution of the detected signals of 7.5 m. Lidar measurements can be used in synergy with numerical models in order to validate and compare information about aerosols. In this paper DREAM (Dust Regional Atmospheric Model) model, designed to simulate and/or forecast the atmospheric cycle of mineral dust aerosol [3], is used to analyze dust transport. To estimate potential PM remote emission sources and their impact at the receptor site, concentration weighted trajectory (CWT) hybrid receptor model [4] was applied to the data set comprised of hourly PM_{10} mass concentrations obtained from Belgrade suburban location "Ovča" during the period 2012-14, and 72-h air masses back-trajectories, calculated according to Perišić et al. [5]. Furthermore, to obtain the vertical profile of PM, concentration weighted boundary layer (CWBL) hybrid receptor model [6], which uses a two-dimensional grid and a planetary boundary layer height, or any altitude in general, as a frame of reference, was used. Although the model can be applied for analyzing the pollutant concentration vertical distribution along the transport pathway, in this paper we present its usage for the receptor site solely.

3. RESULTS AND DISCUSSION

According to the CWT analysis, the most prominent PM_{10} sources were located in neighboring countries and in the areas NW, E and S of Belgrade. Significant impact of Central and Eastern European sources was registered during the autumn season (Figure 1–left panel).

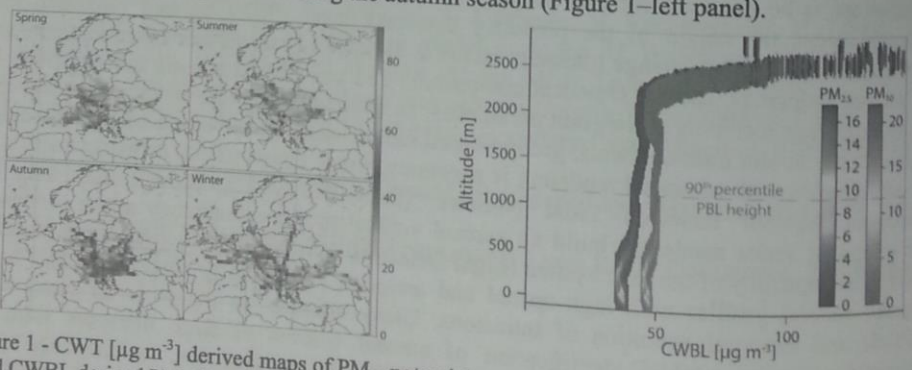

Figure 1 - CWT [μg m^{-3}] derived maps of PM_{10} potential sources in Europe – seasonal variations (left), and CWBL derived PM altitude distribution above the receptor site (right) – color scales indicate the number of events

Very similar, almost constant PM altitude distribution over the receptor site was observed for both coarse and fine particles (Figure 1–right panel), and the most common PBL heights (within 90th percentile). However, given the number of events (colored scale), it can be seen that concentrations exhibit decreasing trend to the height of about 400 m because the species emitted or generated near the ground level are mostly trapped and concentrated within the PBL, whereas free atmosphere concentrations remain low. Large CWBL values at higher altitudes correspond to rare PBL fluctuations which are not statistically significant, so the model results cannot be taken into consideration.

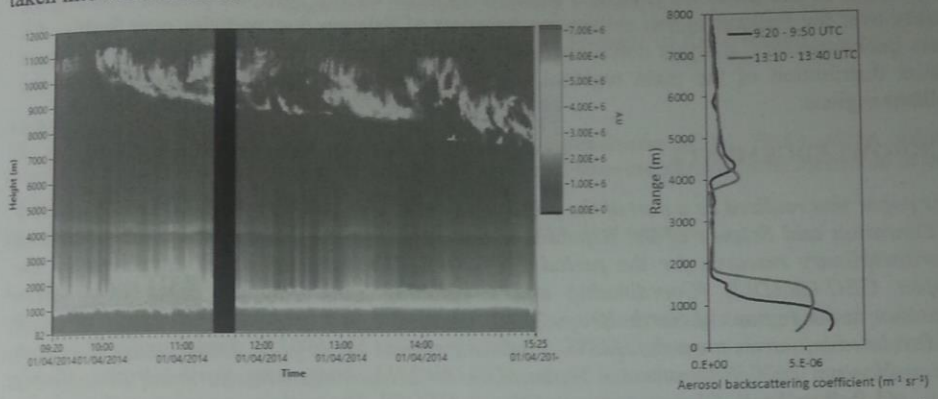

Figure 2 – Lidar range corrected signal (left) and backscatter coefficient at 355 nm (right) in Belgrade

Another aspect of aerosol climatology over Balkans region is related to the intrusions of Saharan dust which usually occurs during spring and summer periods. Such a case study evidencing transport of Saharan dust on 1st April 2014 is presented. From the RCS lidar time series (Figure 2), but also from the calculated backscatter coefficients profiles, the direct presence of an aerosol layer around 4-5 km altitude over Belgrade can been seen. This event was also successfully forecasted by DREAM model (Figure 3-left panel).

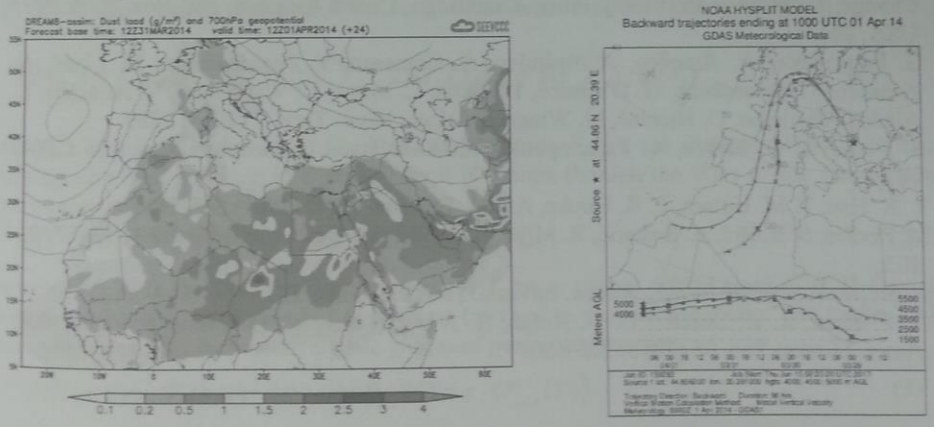

Figure 3 – Dust load over South Europe, estimated by the DREAM model (left) and air mass back-trajectories ending over Belgrade on 1st April, 2014 (righ)

Since the aerosols serve as a valuable tracer of air motion, using lidar observed altitudes of aerosol layer as inputs in the HYSPLIT [7] back-trajectory tracing method the source of aerosols was confirmed. As shown in Figure 3 (right panel) air masses reaching Belgrade traveled over

South Europe (Mediterranean Sea, Spain) and West Europe being influenced by continental pollution too.

4. CONCLUSION

The main advantage of lidar – real time observation of aerosol layering is that it can be used for air mass origin and path identification. Furthermore, in combination with statistical and numerical modeling, this technique can provide important information about aerosol type and distribution. In this paper we presented a case analysis of aerosol transport process affecting air quality over the Balkans region evidencing transport of Saharan dust particles over Serbia. Air mass back-trajectory analysis combined with hybrid receptor modeling were used to assess spatial distribution of the main regional sources for aerosols affecting air quality over the Balkans regions.

ACKNOWLEDGEMENTS

This paper was realized as a part of the projects III43007 and III41011 financed by the Ministry of Education and Science of the Republic of Serbia within the framework of integrated and interdisciplinary research for the period 2011-2017. The publication was supported by the project GEO-CRADLE (Coordinating and integRating state-of-the-art Earth Observation Activities in the regions of North Africa, Middle East, and Balkans and Developing Links with GEO related initiatives towards GEOSS), Grant Agreement No. 690133, funded under European Union Horizon 2020 Programme - Topic: SC5-18b-2015, Integrating North African, Middle East and Balkan Earth Observation capacities in GEOSS. The authors gratefully acknowledge the NOAA Air Resources Laboratory (ARL) for the provision of the HYSPLIT transport and dispersion model and/or READY website (http://www.ready.noaa.gov) used in this publication.

REFERENCES

[1] T. F. Stocker, D. Qin, G.-K. Plattner, M. Tignor, S. K. Allen, J. Boschung, A. Nauels, Y. Xia, V. Bex, P. M. Midgley, IPCC: The Physical Science Basis, Contribution of Working Group I to the Fifth Assessment Report of the Intergovernmental Panel on Climate Change, Cambridge University Press, Cambridge, United Kingdom and New York, NY, USA, 2013.

[2] G. Pappalardo, A. Amodeo, A. Apituley, A. Comeron, V. Freudenthaler, H. Linné, A. Ansmann, J. Bösenberg, G. D'Amico, I. Mattis, L. Mona, U. Wandinger, V. Amiridis, L. Alados Arboledas, D. Nicolae, M. Wiegner, Atmos. Meas. Tech. 7 (2014) 2389.

[3] S. Nickovic, G. Kallos, A. Papadopoulos, O. Kakaliagou, J. Geophys. Res. 106 (2001) 1813.

[4] Y. K. Hsu, T. M. Holsen, P. K. Hopke, Atmos. Environ. 37(4) (2003) 545-562.

[5] M. Perišić, S. Rajšić, A. Šoštarić, Z. Mijić, A. Stojić, Air Qual Atmos Health 10 (2017) 93-103.

[6] A. Stojić, S. Stanišić Stojić., Atmos. Environ. 164 (2017) 216-223.

[7] A. F. Stein, R. R. Draxler, G. D. Rolph, B. J. B. Stunder, M. D. Cohen, F. Ngan, Bull. Amer. Meteor. Soc. 96 (2015) 2059-2077.

EMEC21

21st European Meeting on Environmental Chemistry
November 30 – December 3, 2021, Novi Sad, Serbia

Association of Chemistry and the Environment

Serbian Chemical Society

Matica Srpska

www.emec21.rs

Scientific Committee
Jan Schwarzbauer, president

Organisational Committee
Branimir Jovančićević, president

Executive Committee
Vladimir Beškoski, president

BOOK OF ABSTRACTS

21st European Meeting
on Environmental Chemistry

EMEC 21

ASSOCIATION OF CHEMISTRY AND THE ENVIRONMENT

21st European Meeting on Environmental Chemistry

BOOK OF ABSTRACTS

EMEC 21

November 30 – December 3, 2021

Novi Sad, Serbia

Scientific Committee

Jan Schwarzbauer, Germany, president
Ivana Ivančev-Tumbas, Serbia, vice president

Marijana Ačanski, Serbia
Vladimir P. Beškoski, Serbia
Jelena Bošković, Serbia
Anne-Marie Delort, France
Stuart Gibb, UK
Branimir Jovančićević, Serbia
Đorđe Jovanović, Serbia
Albert T. Lebedev, Russia
Milan Matavulj, Serbia
Milica Balaban, Bosnia and Herzegovina
Polonca Trebše, Slovenia

Organisational Committee

Branimir Jovančićević, president
Maja Turk Sekulić, vice president

Mira Aničić-Urošević
Mališa Antić
Jelena Avdalović
Tanja Brdarić
Aleksandar Đorđević
Rada Đurović Pejčev
Gordana Gajica
Ljubiša Ignjatović
Marko Ilić
Konstantin Ilijević
Ivana Ivančev-Tumbas
Kristina Joksimović
Vladan Joldžić
Milica Kašanin-Grubin
Branka Lončarević
Nikoleta Lugonja
Marija Lješević
Snežana Maletić
Aleksandra J. Mihajlidi-Zelić
Maja Milanović
Srđan Miletić
Tijana Milićević
Dubravka Milovanović
Miloš Momčilović
Jovana Orlić
Kristijan Pastor
Ivana Perović
Petar Pfendt
Srđan Pokorni
Bojan Radak
Dubravka Relić
Goran Roglić
Sanja Sakan
Slađana Savić
Jelena Savović
Slavka Stanković
Vesna Stanković
Sanja Stojadinović
Aleksadra Šajnović
Tatjana Šolević Knudsen
Anđelka Tomašević
Aleksandra Tubić
Gorica Veselinović
Nenad Zarić
Vesna Zlatanović Tomašević
Aleksandra Žerađanin
Sanja Živković

Health Risk Assessment for Residents and Workers Based on Toxic and Carcinogenic Element Content from $PM_{2.5}$ in Belgrade Suburban Area

T. Milićević[1,], D. Mutavdžić[2], M. Aničić Urošević[1], M. Kuzmanoski[1], I. Kodranov[2], A. Popović[2], D. Relić[2]. (1) Environmental Physics Laboratory, Institute of Physics Belgrade, University of Belgrade, Pregrevica 118, Belgrade, Serbia; (2) University of Belgrade-Faculty of Chemistry, Studentski Trg 12-16, Belgrade, Serbia; *tijana.milicevic@ipb.ac.rs.*

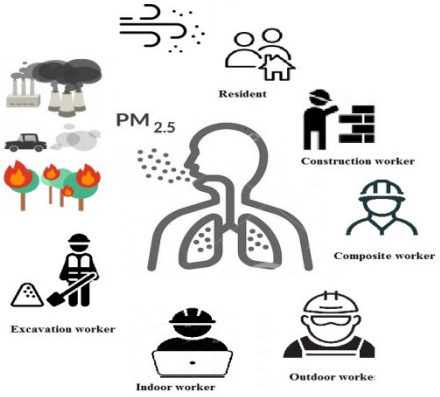

Particulate matter of diametar <2.5 μm ($PM_{2.5}$) pollution is recognized as one of primary pollution contaminant which directly affect human health. Toxic and carcinogenic elements originating from different pollution sources can be constituents of $PM_{2.5}$. Because of their small size, particles can penetrate deeper into the lungs and enter the bloodstream causing different disorders and threats to human health [1].

We performed elemental characterization of $PM_{2.5}$ samples collected during the spring/summer season 2019 in a suburban part of Belgrade (in the inner courtyard of Institute of Physics Belgrade). The spring/summer period was characterized by the industrial or different outdoor activities with several Saharan dust episodes. In addition, April and October were partly characterized by heating sources.

The quartz filters with $PM_{2.5}$ were digested by the microwave digestion system using 7 mL 65% HNO_3 and 1 mL 30% H_2O_2. The concentrations of Al, B, Ba, Bi, Ca, K, Fe, Mn, Ni, P, S and Sr were measured using inductively coupled plasma-optical emission spectrometry (ICP-OES), while concentrations of Ag, As, Be, Cd, Co, Cu, Cr, Hg, Pb, Se, Sb and Tl were measured using inductively coupled plasma mass spectrometry (ICP-MS).

The non-carcinogenic and carcinogenic risks for residents and for five different types of workers (outdoor, indoor, composite, construction and excavation workers) in this ambient were assessed by equations provided by The Risk Assessment Information System – RAIS [2].

Comparing the investigated scenarios, the highest non-carcinogenic and carcinogenic risks were observed for the residents. There were observed non-carcinogenic (HI>1) and carcinogenic ($R \geq 1 \times 10^{-5}$) risks for the residents from this area. The residents spent the most of their time in this ambient and they are most at the risk caused by the measured $PM_{2.5}$ pollution ($HI_{median:}$ 2.28; R_{median}: 1.25×10^{-4}). Observing the scenarios for workers, the risk mostly depends on the time that workers spent outside during working hours. Similar non-carcinogenic risks were observed for outdoor, indoor and composite workers, slightly higher risk was observed for construction workers, while the lowest risk was obtained for an excavation worker who is less exposed to the $PM_{2.5}$ atmospheric deposition than soil dust resuspension. The same was observed for the carcinogenic risk, while the similar risks were observed for all workers. Only for an excavation worker, the carcinogenic risk was significantly lower than for other workers. The most significant contributor to the non-carcinogenic risk in all scenarios was the concentration of Mn, and then the concentration of Be, while the most significant contributor to the carcinogenic risk was Cr^{6+}.

Observing the risks among the investigated period the highest non-carcinogenic and carcinogenic risks were observed in April and October based on the toxic and carcinogenic elements in $PM_{2.5}$. In these months beside the influence of the industrial activities, dust episodes or activity of heating sorces possibly caused the increase of the toxic and carcinogenic elements in $PM_{2.5}$.

Acknowledgements

The athors received funding by Institute of Physics Belgrade (No. 0801–116/1) and Faculty of Chemistry (No. 451-03 68/2020–14/200168) supported by Ministry of Education and Science of the Republic of Serbia.

References

[1] World Health Organization (WHO) 2021, www.who.int; 22.9.2021.

[2] Oak Ridge National Laboratory, Risk Assessment Information System (RAIS) http://rais.ornl.gov; 20.9.2021.

EGU21-7754, updated on 25 Feb 2022
https://doi.org/10.5194/egusphere-egu21-7754
EGU General Assembly 2021

Ice nucleating particle concentrations in Dust Regional Atmospheric Model (DREAM) – going one step further

Luka Ilić[1], Eleni Marinou[2,3], Aleksandar Jovanović[1], Maja Kuzmanoski[1], and Slobodan Ničković[4]

[1]Institute of Physics, Unviersity of Belgrade, Belgrade, Serbia (lukailicbgd@gmail.com)
[2]Institute for Astronomy, Astrophysics, Space Applications and Remote Sensing, National Observatory of Athens, Athens, Greece (elmarinou@noa.gr)
[3]Institute of Atmospheric Physics, German Aerospace Center, Oberpfaffenhofen, Germany (elmarinou@noa.gr)
[4]Republic Hydrometeorological Service of Serbia, Belgrade, Serbia (nickovic@gmail.com)

Mineral dust particles in the atmosphere have a large influence on the physical properties of clouds and their lifecycle. Findings from field experiments, modeling, and laboratory studies suggest that mineral dust particles are very efficient ice-nucleating particles (INPs) even in regions distant from the desert sources. The major sources of mineral dust present in the Mediterranean basin are located in the Sahara Desert. Understanding the significance of mineral dust in ice initiation led to the development of INPC parameterizations in presence of dust for immersion freezing and deposition nucleation processes. These parameterizations were mineralogically indifferent, estimating the dust ice nucleating particle concentrations (INPCs) based on dust concentration and thermodynamic parameters. In recent studies, feldspar and quartz minerals have shown to be significantly more efficient INPs than other minerals found in dust. These findings led to the development of mineralogy-sensitive immersion freezing parameterizations. In this study, we implement mineralogy-sensitive and mineralogically-indifferent INPC parameterizations into a regional coupled atmosphere-dust numerical model. We use the Dust Regional Atmospheric Model (DREAM) to perform one month of simulations of the atmospheric cycle of dust and its feldspar and quartz fractions during Saharan dust intrusion events in the Mediterranean. EARLINET (European Aerosol Lidar Network) and AERONET (AErosol RObotic NETwork) measurements are used with POLIPHON algorithm (Polarization Lidar Photometer Networking) to derive cloud-relevant dust concentration profiles. We compare DREAM results with lidar-based vertical profiles of dust mass concentration, surface area concentration, number concentration, and INPCs. This analysis is a step towards the systematic analysis of dust concentration and INPC parameterizations performance when compared to lidar derived vertical profiles.

WeBIOPATR 2021

The Eighth International WEBIOPATR
Workshop & Conference
Particulate Matter: Research and Management

Abstracts of Keynote Invited Lectures and Contributed Papers

Milena Jovašević-Stojanović,

Alena Bartoňová,

Miloš Davidović and Simon Smith, Eds

Vinča Institute of Nuclear Sciences

Vinča, Belgrade 2021

ABSTRACTS OF KEYNOTE INVITED LECTURES AND CONTRIBUTED PAPERS

The Eighth WeBIOPATR Workshop & Conference

Particulate Matter: Research and Management

WeBIOPATR 2021

29th November to 1st December 2021

Vinča, Belgrade, Serbia

Editors

Milena Jovašević-Stojanović

Alena Bartoňová

Miloš Davidović

Simon Smith

Publisher

Vinča Institute of Nuclear Sciences

Prof. Dr Snežana Pajović, Director

P.O.Box 522

11001 Belgrade, Serbia

Printed by

Vinča Institute of Nuclear Sciences

Number of copies

150

ISBN 978-86-7306-164-1

Vinča, Belgrade 2021.

www.vin.bg.ac.rs/

SCIENTIFIC COMMITTEE

Aleksandar Jovović, Serbia
Alena Bartoňová, Norway
Antonije Onjia, Serbia
David Broday, Israel
Dikaia Saraga, Greece
Griša Močnik, Slovenia
Ivan Gržetić, Serbia
María Cruz Minguillón, Spain
Milena Jovašević-Stojanović, Serbia
Miloš Davidović, Serbia
Saverio de Vito, Italy
Selahattin Incecik, Turkey
Slobodan Ničković, Serbia
Simone Barreira Morais, Portugal
Zoran Mijić, Serbia
Zoran Ristovski, Australia
Zorana Jovanović-Andersen, Denmark

ORGANIZING COMMITTEE

Aleksandra Stanković, Serbia
Alena Bartoňová, Norway
Andrej Šoštarić, Serbia
Anka Cvetković, Serbia
Biljana Filipović, Serbia
Branislava Matić, Serbia
Lidija Marić-Tanasković, Serbia
Uzahir Ramadani, Serbia
Ivan Lazović, Serbia
Sonja Dmitrašinović (Secretary), Serbia
Marija Živković (Secretary), Serbia
Milena Jovašević-Stojanović, Serbia
Miloš Davidović, Serbia
Mira Aničić Urošević, Serbia
Mirjana Perišić, Serbia
Nenad Živković, Serbia
Tihomir Popović, Serbia
Vesna Slepčević, Serbia
Viša Tasić, Serbia

CONFERENCE TOPICS

1. **Atmospheric Particulate Matter - Physical and Chemical Properties**
    i. Sources and formation of particulate matter
    ii. Particulate matter composition and levels outdoors and indoors
    iii. Environmental modeling
    iv. Nanoparticles in the environment
2. **Particulate Matter and Health**
    i. Exposure to particulate matter
    ii. Health aspects of atmospheric particulate matter
    iii. Full chain approach
    iv. COVID-19 and particulate matter
3. **Particulate Matter and Regulatory Issues**
    i. Issues related to monitoring of particulate matter
    ii. Legislative aspects
    iii. Abatement strategies

Organizers

Vinča Institute of Nuclear Sciences, University of Belgrade, National Institute of the Republic of Serbia, Serbia

Public Health Institute of Belgrade, Serbia

NILU Norwegian Institute for Air Research, Norway

The 8th WeBIOPATR Workshop and Conference,

Particulate Matter: Research and Management, WEBIOPATR2021

is supported by:

Virtual centre for
Distributed atmospheric
Sensing for reduction of pollution pressures

EC H2020 Framework Program for Research and Innovation,
area "Spreading excellence and widening participation",
VIDIS project (2020-2023) coordinated by Vinča Institute of Nuclear Sciences,
Grant agreement number 952433.

Ministry of Education, Science and Technological Development of the Republic of Serbia

TABLE OF CONTENTS

8.3 A STUDY ON TROPOSPHERIC AEROSOLS CHANGE DURING THE COVID-19 LOCK-DOWN PERIOD: EXPERIENCE FROM EARLINET MEASUREMENT CAMPAIGN

Z. Mijić, M. Kuzmanoski, L. Ilić
Institute of Physics Belgrade, University of Belgrade, Belgrade, Serbia
zoran.mijic@ipb.ac.rs

To slow down the rate of spread of corona virus, most of the countries in Europe have followed partial-to-complete lockdown measures in 2020. The lockdown period provided a unique opportunity to examine the effects of reduced anthropogenic activities on changes in the atmospheric environment. Aerosol lidars with their high temporal and vertical resolution, provide reliable information on the atmospheric structure, its dynamics, and its optical properties. The European Aerosol Research Lidar Network, EARLINET, was established in 2000 as a research project with the goal of creating a quantitative, comprehensive, and statistically significant database for the horizontal, vertical, and temporal distribution of aerosols on a continental scale (Pappalardo et al., 2014). EARLINET is part of ACTRIS (Aerosols, Clouds and Trace gases Research Infrastructure) a pan-European initiative consolidating actions among European partners producing high-quality observations of aerosols, clouds and trace gases.

As a part of the ACTRIS initiative for studying the changes in the atmosphere during the COVID-19 lockdown period in May 2020 a dedicated EARLINET measurement campaign was organized in order to: monitor the atmosphere's structure during the lockdown and early relaxation period in Europe, and to identify possible changes due to decreased emissions by comparison to the aerosol climatology in Europe. During the campaign the near-real-time (NRT) operation of the EARLINET was demonstrated following previous experience from the EUNADICS-AV exercise (Papagiannopoulos et al., 2020). The Belgrade lidar station (Ilić et al., 2018) participated in the campaign together with 21 EARLINET stations providing vertical aerosol profiles twice per day (minimum two hours measurements at noon, and minimum two hours after sunset). The measurements were submitted and processed by the Single Calculus Chain (SCC) in the near-real-time. The SCC is a tool for the automatic analysis of aerosol lidar measurements developed within EARLINET network (D'Amico et al., 2015, D'Amico et al., 2016). The main aim of SCC is to provide a data processing chain that allows all EARLINET stations to retrieve, in a fully automatic way, the aerosol backscatter and extinction profiles (measures of the aerosol load) together with other aerosol products. This first analysis was based on the data processed by the SCC and directly published on the THREDDS server in NRT. The preliminary analysis made on aerosol lidar data shows that by simply comparing the observed backscatter values with the climatological values from 2000-2015 is not sufficient to extract a clear conclusion on how much the COVID-19 lock-down has impacted the aerosols in the atmosphere, but a certain effect for low troposphere can be seen. Beyond the scientific goals of this campaign, the actions organized by EARLINET/ACTRIS (NRT delivery of the data and fast analysis of the data products) proved that aerosol lidars are useful for providing information not only for climatological purposes, but also in emergency situations. A more quantitative analysis based on re-analyzing additional data products will be made to consolidate the conclusions.

REFERENCES

Pappalardo, G., Amodeo, A., Apituley, A., Comeron, A., Freudenthaler, V., Linné, H., Ansmann, A., Bösenberg, J., D'Amico, G., Mattis, I., Mona, L., Wandinger, U., Amiridis, V., Alados-Arboledas, L., Nicolae, D., and Wiegner, M., 2014. EARLINET: towards an advanced sustainable European aerosol lidar network, Atmospheric Measurement Techniques 7, 2389–2409.

D'Amico, G., Amodeo, A., Baars, H., Binietoglou, I., Freudenthaler, V., Mattis, I., Wandinger, U., and Pappalardo, G., 2015. EARLINET Single Calculus Chain – overview on methodology and strategy, Atmospheric Measurement Techniques 8, 4891-4916.

D'Amico, G., Amodeo, A., Mattis, I., Freudenthaler, V., and Pappalardo, G., 2016. EARLINET Single Calculus Chaintechnical– Part 1: Pre-processing of raw lidar data, Atmospheric Measurement Techniques 9, 491-507.

Ilić, L., KuzmanoskiM., KolaržP., NinaA., SrećkovićV., MijićZ., BajčetićJ., AndrićM., 2018. Changes of atmospheric properties over Belgrade, observed using remote sensing and in situ methods during the partial solar eclipse of 20 March 2015,Journal of Atmospheric and Solar-Terrestrial Physics171,250-259.

Papagiannopoulos, N., D'Amico, G., Gialitaki, A., Ajtai, N., Alados-Arboledas, L., Amodeo, A., Amiridis, V., Baars, H. et al., 2020. An EARLINET early warning system for atmospheric aerosol aviation hazards, Atmospheric Chemistry and Physics 20, 10775–10789.

CIP - Каталогизација у публикацији
Народна библиотека Србије, Београд

502.3:502.175(082)(0.034.2)
613.15(082)(0.034.2)
66.071.9(082)(0.034.2)

INTERNATIONAL WeBIOPATR Workshop Particulate Matter: Research and Management (8 ; 2021 ; Vinča) Abstracts of keynote invited lectures and contributed papers [Elektronski izvor] / The Eighth International WEBIOPATR Workshop & Conference Particulate Matter: Research and Management, WeBIOPATR 2021, 29th November to 1st December 2021 Vinča, Belgrade, Serbia ; [organizers Vinča Institute of Nuclear Sciences, University of Belgrade, National Institute of the Republic of Serbia [and] Public Health Institute of Belgrade, Serbia [and] NILU Norwegian Institute for Air Research, Norway] ; Milena Jovašević-Stojanović ... [et al.], eds. - Belgrade : Vinča Institute of Nuclear Sciences, 2021 (Belgrade : Vinča Institute of Nuclear Sciences). - 1 elektronski optički disk (DVD) ; 12 cm

Sistemski zahtevi: Nisu navedeni. - Nasl. sa naslovne strane dokumenta. - "... Conference ... as a combination of online and face-to-face event." --> Preface. - Tiraž 150. - Preface / Milena Jovašević-Stojanović and Alena Bartoňová. - Bibliografija uz većinu apstrakata. - Registar.

ISBN 978-86-7306-164-1

1. International Conference Particulate Matter: Research and Management (8 ; 2021 ; Vinča)
а) Ваздух -- Контрола квалитета -- Зборници
б) Здравље -- Заштита -- Зборници
в) Отпадни гасови -- Штетно дејство -- Зборници

COBISS.SR-ID 53342985

WeBIOPATR

EGU2020-15857, updated on 01 Feb 2021
https://doi.org/10.5194/egusphere-egu2020-15857
EGU General Assembly 2020

Mineralogy sensitive ice nucleation parameterizations in Dust Regional Atmospheric Model (DREAM)

Luka Ilić[1], Aleksandar Jovanović[1], Maja Kuzmanoski[1], Fabio Madonna[2], Marco Rosoldi[2], Eleni Marinou[3,4], and Slobodan Ničković[5]

[1]Institute of Physics, Unviersity of Belgrade, Environmental Physics Laboratory, Belgrade, Serbia (lukailicbgd@gmail.com)
[2]Consiglio Nazionale delle Ricerche - Istituto di Metodologie per l'Analisi Ambientale (CNR-IMAA), Italy
[3]Institute for Astronomy, Astrophysics, Space Applications and Remote Sensing, National Observatory of Athens
[4]Institute of Atmospheric Physics, German Aerospace Center
[5]Republic Hydrometeorological Service of Serbia

The Sahara Desert is the major source of mineral dust, which is a significant portion of atmospheric aerosol. Mineral dust particles play a role in radiative balance, with a direct effect and by influencing cloud formation and lifetime. They have been recognized as highly efficient ice nuclei, fostering the development of parameterizations for immersion and deposition freezing involving dust particles. Feldspar minerals have shown to be a significantly more efficient ice nucleating agents than other dust minerals which led to the development of a 'mineralogy sensitive' immersion freezing parameterization. The investigation of the relative efficiency of quartz compared to feldspars for the immersion ice nucleation, based upon literature data and new experiments, led to the development of a new parameterization to be applied to mineral dust concentrations. Within numerical models, explicit simulation of mineral dust fractions enables the use of 'mineralogy sensitive' immersion parameterizations.

The operational DREAM model calculates the number of ice nuclei,but does not take into consideration the mineral composition of dust. In this study, instead, we use DREAM model to simulate the atmospheric cycle of feldspar and quartz fractions of dust. Dust mineral composition is used to calculate ice nucleating particle concentrations based on mineral-specific immersion freezing parameterizations. A case study related to the observations of geometrical and microphysical characteristics of the clouds formed in the Mediterranean, in April 2016 is considered. We compare the model results with ice nucleating particle concentrations retrieved using lidar and radar ground-based remote sensing observations at Cyprus and Potenza. The analysis explores how the mineral composition of dust and the parameterization of its effects on ice initiation could further improve ice nucleation representation in numerical models.

WeBIOPATR 2019

The Seventh International WEBIOPATR
Workshop & Conference
Particulate Matter: Research and Management

Abstracts of Keynote Invited Lectures and Contributed Papers

Milena Jovašević-Stojanović and Alena Bartoňová, Eds

Public Health Institute of Belgrade

Belgrade 2019

ABSTRACTS OF KEYNOTE INVITED LECTURES AND CONTRIBUTED PAPERS

The Seventh International WeBIOPATR Workshop & Conference

Particulate Matter: Research and Management

WeBIOPATR 2019

1st to 3rd October, 2019

Belgrade, Serbia

Editors

Milena Jovašević-Stojanović

Alena Bartoňová

Publisher

Public Health Institute of Belgrade

Prof. Dr Dušanka Matijević, Director

Boulevar Despota Stefana 54a

Serbia, 11000 Belgrade

Printed by

Printing office of the Public Health Institute of Belgrade

Number of copies

150

ISBN 978-86-83069-56-9

www.zdravlje.org.rs

SCIENTIFIC COMMITTEE

Aleksandar Jovović, Serbia
Alena Bartoňová, Norway
Antonije Onjia, Serbia
David Broday, Israel
Dikaia Saraga, Greece
Griša Močnik, Slovenia
Ivan Gržetić, Serbia
María Cruz Minguillón, Spain
Milena Jovašević-Stojanović, Serbia
Radim J. Šrám, Czech Republic
Renata Kovačević, Serbia
Selahattin Incecik, Turkey
Slobodan Ničković, Serbia
Simone Barreira Morais, Portugal
Zoran Mijić, Serbia
Zoran Ristovski, Australia
Zorana Jovanović-Andersen, Denmark

ORGANIZING COMMITTEE

Aleksandra Stanković, Serbia
Alena Bartoňová, Norway
Andrej Šoštarić, Serbia
Anka Cvetković, Serbia
Biljana Filipović, Serbia
Branislava Matić, Serbia
Dejan Lekić, Serbia
Dragan Alavantić, Serbia
Ivan Lazović, Serbia
Jasmina Jović-Stošić, Serbia
Maja Jovanović (Secretary), Serbia
Marija Živković (Secretary), Serbia
Milena Jovašević-Stojanović, Serbia
Miloš Davidović, Serbia
Mira Aničić Urošević, Serbia
Mirjana Perišić, Serbia
Nenad Živković, Serbia
Tihomir Popović, Serbia
Vesna Slepčević, Serbia
Viša Tasić, Serbia

CONFERENCE TOPICS

1. **Atmospheric Particulate Matter - Physical and Chemical Properties**
    i. Sources and formation of particulate matter
    ii. Particulate matter composition and levels outdoors and indoors
    iii. Environmental modeling
    iv. Nanoparticles in the environment
2. **Particulate Matter and Health**
    i. Exposure to particulate matter
    ii. Health aspects of atmospheric particulate matter
    iii. Full chain approach
3. **Particulate Matter and Regulatory Issues**
    i. Issues related to monitoring of particulate matter
    ii. Legislative aspects
    iii. Abatement strategies

Organizers

Vinča Institute of Nuclear Sciences, Serbia

Public Health Institute of Belgrade, Serbia

NILU Norwegian Institute for Air Research, Norway

The Seventh WeBIOPATR Workshop and Conference,

Particulate Matter: Research and Management, WEBIOPATR 2019

is supported by:

Ministry of Education, Science and Technological Development of Republic of Serbia

TABLE OF CONTENTS

9.3. MODELING OF IMMERSION FREEZING INITIATION ON MINERAL DUST IN DUST REGIONAL ATMOSPHERIC MODEL (DREAM)

L. Ilić (1), A. Jovanović (1), M. Kuzmanoski (1), S. Ničković (2)
(1) Institute of Physics, University of Belgrade, Belgrade, Serbia, (2) Republic Hydrometeorological Service of Serbia – South East European Viertual Climate Change Center, Belgrade, Serbia
luka.ilic@ipb.ac.rs

Mineral dust particles are atmospheric aerosol suspended from arid areas. The Sahara Desert is the major source of mineral dust, producing a significant part atmospheric aerosol. There is a large uncertainty in estimating role of dust in the Earth's climate system. Mineral dust particles influence the radiative balance of the planet in two different ways, by directly interacting with radiation and indirectly by playing a role in cloud formation. Research showed that mineral dust particles are very efficient ice nuclei, which glaciate supercooled cloud water through a process of heterogeneous ice nucleation even in regions distant from the desert sources (Cziczo et al, 2013). Due to recognition of the dominant role of dust as ice nuclei, parameterizations for immersion and deposition freezing specifically due to dust have been developed (Niemand et al, 2012; DeMott et al, 2015; Ullrich et al, 2017). A study by Atkinson et al, 2013, showed that feldspars are at least by an order of magnitude more efficient ice nucleating agents than other dust minerals. This breakthrough contrasts with the prevailing view that clay minerals are the most important component of atmospheric mineral dust for ice nucleation.

The calculation of the number of ice nuclei in the operational DREAM model is based on atmospheric parameters and on dust concentration (Nickovic et al, 2016). The immersion and deposition ice nucleation parameterizations due to dust have been implemented in the model, not taking into consideration the mineral composition of dust. In this study, we use DREAM model to simulate atmospheric cycle of different mineral fractions of dust. Dust concetration, thermodynamic quantities and dust mineral composition are used to calculate ice nucleating particle concentration based on mineral specific immersion freezing parameterizations. We compare the model results with relevant observations from remote sensing instruments and ice nucleation chambers. We analyze the results to explore how the mineral composition of dust and appropriate parameterization of its effects on ice initiation could further improve ice nucleation representation in the model.

REFERENCES

Atkinson, J. D., Murray, B. J., Woodhouse, M. T., Whale, T. F., Baustian, K. J., Carslaw, K. S., Dobbie, S., O'Sullivan, D., andMalkin, T. L. 2013. The importance of feldspar for ice nucleation by mineral dust in mixed-phase clouds, Nature, 498, 355–358.

Cziczo, D., Froyd, K. D., Hoose, C., Jensen, E. J., Diao, M., Zondlo, M. A., Smith, J. B., Twohy, C. H., Murphy, D. M. 2013. Clarifying the Dominant Sources and Mechanisms of Cirrus Cloud Formation, Science http://dx.doi.org/10.1126/science.1234145.

DeMott, P. J., Prenni, A. J., McMeeking, G. R., Sullivan, R. C., Petters, M. D., Tobo, Y., Niemand, M., Möhler, O., Snider, J. R., Wang, Z., and Kreidenweis, S. M. 2015. Integrating laboratory and field data to quantify the immersion freezing ice nucleation activity of mineral dust particles, Atmos. Chem. Phys., 15, 393-409, doi:10.5194/acp-15-393-2015.

Nickovic, S., Cvetkovic, B., Madonna, F., Rosoldi, M., Pejanovic, G., Petkovic, S., and Nikolic, J. 2016. Cloud ice caused by atmospheric mineral dust – Part 1: Parameterization of ice nuclei concentration in the NMME-DREAM model, Atmos. Chem. Phys., 16, 11367-11378, https://doi.org/10.5194/acp-16-11367-2016.

Niemand, M., Moehler, O., Vogel, B., Vogel, H., Hoose, C., Connolly, P., Klein, H., Bingemer, H., DeMott, P., Skrotzki, J., and Leisner, T. 2012. A Particle-Surface Area absed Parametrization of Immersion Freezing on Desert Dust Particles, J. Atmos. Sci., 69, 3077–3092.

Ullrich, R., C. Hoose, O. Möhler, M. Niemand, R. Wagner, K. Höhler, N. Hiranuma, H. Saathoff, and T. Leisner, 2017: A New Ice Nucleation Active Site Parameterization for Desert Dust and Soot. J. Atmos. Sci., 74, 699–717, https://doi.org/10.1175/JAS-D-16-0074.1

10.2. A CLIMATOLOGY OF SATELLITE DERIVED AEROSOL OPTICAL DEPTH OVER BELGRADE REGION, SERBIA

Z. Mijić, A. Jovanović, M. Kuzmanoski, L. Ilić
(1) Institute of Physics Belgrade, University of Belgrade, Belgrade, Serbia,
zoran.mijic@ipb.ac.rs

Suspended particulate matter (PM) in the atmosphere, commonly known as atmospheric aerosol plays one of the most important roles in climate change, air quality, and human health. Atmospheric aerosol affects climate through the direct (scattering and absorption both solar and terrestrial radiation) and indirect effects (modification of cloud through aerosol-cloud interaction) introducing one of the major uncertainty in our quantitative understanding of the radiative forcing (IPCC, 2007). Numerous studies have shown a significant association between particle matter concentrations and health risk especially airborne particle matter with diameter less than 10 μm (PM_{10}) and 2.5 μm ($PM_{2.5}$) (Yang et al. 2018). As the evidence base for the association between PM and short-term, as well as long-term, health effects has become much larger and broader, it is important to regularly update the guidelines for PM and PM-bound components limit values. Usually ground-based monitoring networks are used for PM assessment but still with no adequate spatial and time coverage. For the last decade various studies have been conducted to overcome this problem and to get PM estimates from satellite measurements (Kumar et al. 2007, Li et al. 2015). One of the most important aerosol products retrieved from satellite measurement is aerosol optical depth (AOD) which is the integration of the aerosol extinction coefficient from the Earth's surface to the top of the atmosphere, and it represents the attenuation of solar radiation caused by aerosols. The relationship between AOD and surface PM concentrations depends on various factors, including aerosol vertical distribution, aerosol type and its chemical composition, as well as its spatial and temporal variability, which are governed by spatio-temporal distribution of emissions and meteorological conditions (Kong et al., 2016). Due to their short lifetime and the large variability in space and time it is necessary to establish a climatology of the aerosol distribution both on regional and global scale thus satellite-retrieved AOD has become an important indicator of ground-level PM and aerosol burden in the atmosphere. The Moderate Resolution Imaging Spectroradiometer (MODIS) is aboard two polar orbiting satellites Terra and Aqua and measures the upwelling radiance from the Earth–atmosphere system at 36 wavelength bands, ranging from 0.4 to 14 μm. MODIS provides a daily near-global distribution of AOD over both ocean and land (Sayer et al., 2013). In this study long-term temporal variation and trend of AOD over Belgrade region are presented. Monthly mean values of MODIS aerosol optical depth at 550 nm were examined for the 10 year period 2005–2015. The MOD08 Combined Dark Target and Deep Blue AOD data products from MODIS Terra platform (Collection 6.1, Level 3 AOD data downloaded through NASA GIOVANNI web portal https://giovanni.gsfc.nasa.gov/giovanni/) at 1 degree spatial resolution were utilized. Frequency distributions of the AOD values were examined together with monthly and seasonal variations. The annual AOD mean was 0.17 with standard deviation of 0.07 over ten year period. AOD values exhibited seasonal annual mean variation and slightly negative trend. Significant monthly AOD variability is observed with maximum in August (~0.28) and a minimum in winter months (~0.06). Analysis of long term time series of AOD data could reveal how AOD regarding ground-based PM measurement in Belgrade changes over time. The aerosol climatology can be useful in the climate change assessment, weather and environmental monitoring over Belgrade region with the potential for further application in particle matter estimates from satellite measurement.

REFERENCES

IPCC. 2007c. Climate Change 2007: Impacts, Adaptation and Vulnerability. Contribution of Working Group II to the Fourth Assessment Report of the IPCC. In M.L. Parry, M., Canziani, O., Palutikof, J., van der Linden, and Hanson, C.E. University Press, Cambridge, UK, pp 976.

Kong, L., Xin, J., Zhang, W., Wang, Y. 2016. The empirical correlations between PM2.5, PM10 and AOD in the Beijing metropolitan region and the PM2.5, PM10 distributions retrieved by MODIS, Environmental Pollution 216, 350-360.

Kumar, N., Chu, S.A., Foster A. 2007. An empirical relationship between PM2.5 and aerosol optical depth in Delhi Metropolitan, Atmospheric Environment 41, 4492-4503.

Li., J., Carlson, E. B., Lacis, A. A., 2015. How well do satellite AOD observations represent the spatial and temporal variability of PM2.5 concentration for the United States?,Atmospheric Environment 102, 260-273.

Sayer, A. M., N. C. Hsu, C. Bettenhausen, and M.-J. Jeong, 2013. Validation and uncertainty estimates for MODIS Collection 6 "Deep Blue" aerosol data, Journal of Geophysics Researh Atmosphere 118, 7864–7872.

Yang, Y., Vivian, C. Pun., Shengzhi, S., Hualiang L., Tonya, G., M., Hong, Q., 2018. Particulate matter components and health: a literature review on exposure assessment, Journal of Public Health and Emergency 2, 14.

10.8. CASE STUDY OF THE VERTICAL DISTRIBUTION OF SAHARAN DUST OVER BELGRADE

A. Jovanović, L. Ilić, M. Kuzmanoski, Z. Mijić
Institute of Physics Belgrade, University of Belgrade, Belgrade, Serbia
aleksandar.jovanovic@ipb.ac.rs

Mineral dust aerosol is ubiquitous in the troposphere around the globe, and dominant in terms of mass concentration (Grini et al., 2005). Sahara is the largest source of dust emission and atmospheric dust loading in the world (Choobari et al., 2014). Strong low-level winds and convection can uplift mineral dust particles into the free troposphere, where they are transported over large distances even at intercontinental scales (Goudie and Middleton, 2001). Dust aerosols have a direct impact on the global radiative budget of the atmosphere by scattering and absorbing shortwave and longwave radiation. Also, dust aerosols can change the microphysical characteristics of clouds and precipitation due to their role in the nucleation of cloud ice and droplets (Rosenfeld et al., 2001). Furthermore, dust impacts air quality even at locations distant from its source region (Prospero, 1999). To improve understanding of these effects, it is important to characterize dust horizontal and vertical distribution, as well as meteorological conditions that lead to dust outbreaks in region of interest.

In this study, four episodes of long-range transport of Saharan dust to Balkans will be investigated based on results of numerical model and available ground-based measurements. Synoptic circulation patterns and airmass backtrajectories during these events will also be analyzed. For dust forecast, we used the Dust Regional Atmospheric Model – DREAM. The model was developed to predict the concentration of dust aerosol in the troposphere, and includes processes of dust emission, dust horizontal and vertical turbulent mixing, long-range transport and dust deposition (Ničković et al., 2001). Modeled dust concentration vertical profiles and concentrations at surface level during the selected events will be discussed. A qualitative comparison of modeled dust vertical profiles and results of LIDAR (Light Detection and Ranging) measurements in Belgrade will be presented. Furthermore, comparison of modeled dust surface concentrations with the measurements of PM_{10} particle mass concentration in two urban background stations in Belgrade will be shown, to give insight into the effect of dust on air quality during these dust episodes.

REFERENCES

Choobari, O. A., Zawar-Reza, P., and Sturman, A., 2014. The global distribution of mineral dust and its impacts on the climate system: A review, Atmospheric Research, 138, 152–165.

Goudie, A. S. and Middleton, N. J., 2001. Saharan dust storms: nature and consequences, Earth-Science Reviews, 56, 179–204.

Grini, A., Myhre, G., Zender, C. S., and Isaksen, I. S. A., 2005. Model simulations of dust sources and transport in the global atmosphere: Effects of soil erodibility and wind speed variability, Journal of Geophysical Research, 110, D02205.

Ničković, S., Kallos, G., Papadopoulos, A., Kakaliagou, O., 2001. A model for prediction of desert dust cycle in the atmosphere, Journal of Geophysical Research 106, 18113-18130.

Prospero, J. M., 1999. Long-term measurements of the transport of African mineral dust to the southeastern United States: Implications for regional air quality, Journal of Geophysical Research 104, 15917–15927.

Rosenfeld, D., Y. Rudich, and R. Lahav 2001. Desert dust suppressing precipitation: A possible desertification feedback loop, Proceedings of the National Academy of Sciences of the United States of America, 98, 5975–5980.

CIP - Каталогизација у публикацији
Народна библиотека Србије, Београд

502.3:502.175(048)
613.15(048)
66.071.9(048)

INTERNATIONAL WeBIOPATR Workshop & Conference,
Particulate Matter: Research and Management (7 ; 2019 ; Beograd)

Abstracts of keynote invited lectures and contributed papers /
The Seventh International WeBIOPATR Workshop & Conference
Particulate Matter: Research and Management, WeBIOPATR 2019,
1st to 3rd October, 2019 Belgrade, Serbia ;
[organizers Vinča Institute of Nuclear Sciences, Serbia,
[and] Public Health Institute of Belgrade, Serbia
[and] NILU Norwegian Institute for Air Research, Norway] ;
editors Milena Jovašević-Stojanović, Alena Bartoňová.
- Belgrade : Public Health Institute, 2019
(Belgrade : Printing Office of the Public Health Institute). - 104 str. : ilustr. ; 30 cm

Tiraž 150.
- Str. 7: Preface / Milena Jovašević-Stojanović and Alena Bartoňová.
- Bibliografija uz većinu apstrakata. – Registar

ISBN 978-86-83069-56-9

1. Conference Particulate Matter: Research and Management (7 ; 2019 ; Beograd)
а) Ваздух -- Контрола квалитета -- Апстракти
б) Здравље -- Заштита -- Апстракти
в) Отпадни гасови -- Штетно дејство -- Апстракти

COBISS.SR-ID 279772172

ISBN 978-86-83069-56-9

Geophysical Research Abstracts
Vol. 20, EGU2018-16921, 2018
EGU General Assembly 2018

Modeling of mineral composition effects on ice nucleation due to dust in Dust Regional Atmospheric Model (DREAM)

Luka Ilić (1), Bojan Cvetković (2), Goran Pejanović (2), Slavko Petković (2), Maja Kuzmanoski (1), Slobodan Ničković (2,1)

(1) Institute of Physics, University of Belgrade, Belgrade, Serbia, (2) Republic Hydrometeorological Service of Serbia - South East European Virtual Climate Change Center, Belgrade, Serbia

Mineral dust comprises a significant part of global aerosol burden. There is a large uncertainty in estimating role of dust in the Earth's climate system, partly due to its effects on radiation and cloud formation. Research showed that mineral dust was found in the samples of residual particles from cloud ice crystals collected by aircraft measurements. These results indicated that dust particles dominate over other known ice nuclei such as soot and biological particles even in regions distant from desert sources. Most recently, due to recognition of the dominant role of dust as ice nuclei, parameterizations for immersion and deposition icing specifically due to dust have been developed. The icing process is strongly influenced by dust mineral composition. A breakthrough in understanding the role of different minerals was made by Atkinson et al. [Nature, 498, 355–358 (2013)], showing that feldspars are at least by an order of magnitude more efficient nucleating catalysts than other dust minerals. This contrasts with the prevailing view that clay minerals are the most important component of atmospheric mineral dust for ice nucleation. The calculation of the number of ice nuclei in the operational DREAM model is based on atmospheric parameters and on dust concentration. The immersion and deposition ice nucleation parameterizations due to dust have been implemented in the model not taking into consideration the mineral composition of dust.
In this study, we use DREAM model with incorporated particle mineral composition to calculate ice nuclei number concentrations. Our study is focused to explore if the Atkinson's parameterization could further improve ice nucleation representation in the model. We compare the model results with relevant observations from remote sensing instruments. Synergistic sun-photometer and lidar measurements and cloud radar observations are used to explore the model capability to represent vertical features of the cloud and aerosol vertical profiles. In addition, MSG/SEVIRI ice water path satellite observations (Meteosat Second Generation the Spinning Enhanced Visible and InfraRed Imager) will be used to evaluate horizontal distribution of modeled IN.
Acknowledgements
The publication was supported by the project GEO-CRALDE (Coordinating and integRating state-of-the-art Earth Observation Activities in the region of North Africa, Middle East, and Balkans and Developing Links with GEO related initiatives towards GEOSS), Grant Agreement No. 690133, funded under European Union Horizon 2020 Programme - Topic: SC5-18b-2015, Integrating North African, Middle East and Balkan Earth Observation capacities in GEOSS. We Acknowledge EUMETSAT for use of its Satellite Application Facility on Climate Monitoring (CM SAF) data.

Book of abstracts

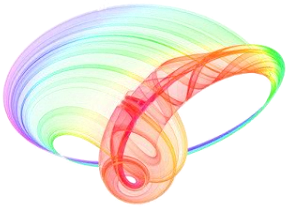

PHOTONICA2017

The Sixth International School and Conference on Photonics

& COST actions: MP1406 and MP1402

MultiscaleSolar

HERALD

&H2020-MSCA-RISE-2015 CARDIALLY workshop

CARDIALLY

28 August – 1 September 2017

Belgrade, Serbia

Editors

Marina Lekić and Aleksandar Krmpot

Institute of Physics Belgrade, Serbia

Belgrade, 2017

ABSTRACTS OF TUTORIAL, KEYNOTE, INVITED LECTURES, PROGRESS REPORTS AND CONTRIBUTED PAPERS

of

The Sixth International School and Conference on Photonics PHOTONICA2017

28 August – 1 September 2017
Belgrade Serbia

Editors
Marina Lekić and Aleksandar Krmpot

Technical assistance
Marko Nikolić and Danica Pavlović

Publisher
Institute of Physics Belgrade
Pregrevica 118
11080 Belgrade, Serbia

Printed by
Serbian Academy of Sciences and Arts

Number of copies
300

ISBN 978-86-82441-46-5

Committees

Scientific Committee

Aleksandar Krmpot, Serbia
Antun Balaž, Serbia
Arlene D. Wilson-Gordon, Israel
Bojan Resan, Switzerland
Boris Malomed, Israel
Branislav Jelenković, Serbia
Dejan Gvozdić, Serbia
Detlef Kip, Germany
Dragan Indjin, United Kingdom
Edik Rafailov, United Kingdom
Feng Chen, China
Francesco Cataliotti, Italy
Giannis Zacharakis, Greece
Goran Isić, Serbia
Goran Mašanović, United Kingdom
Isabelle Philippa Staude, Germany
Jelena Radovanović, Serbia
Jerker Widengren, Sweden
Jovana Petrović, Serbia
Laurent Sanchez, France
LjupčoHadžievski, Serbia
Marco Santagiustina, Italy
Milan Mashanović, United States of America
Milan Trtica, Serbia
Miloš Živanov, Serbia
Milutin Stepić, Serbia
Milivoj Belić, Qatar
Nikola Stojanović, Germany
Pavle Anđus, Serbia
Peđa Mihailović, Serbia
Radoš Gajić, Serbia
Schaaf Peter, Germany
Sergei Turitsyn, United Kingdom
Suzana Petrović, Serbia
Ticijana Ban, Croatia
Vladana Vukojević, Sweden
Zoran Jakšić, Serbia
Željko Šljivančanin, Serbia

Organizing Committee

Aleksandar Krmpot, (Chair)
Marina Lekić (Secretary)
Stanko Nikolić (webmaster)
Marko Nikolić,
Vladimir Veljić
Danica Pavlović

Technical Organizer

Conference Topics

1. Quantum optics and ultracold systems
2. Nonlinear optics
3. Optical materials
4. Biophotonics
5. Devices and components
6. Optical communications
7. Laser spectroscopy and metrology
8. Ultrafast optical phenomena
9. Laser - material interaction
10. Optical metamaterials and plasmonics
11. Other topics in photonics

Table of Contents

Tutorial lectures

Keynote lectures

Invited lectures

11. Other topics in photonics

Vertical Raman LIDAR profiling of atmosphericaerosol optical properties over Belgrade

Z. Mijić, L. Ilić and M. Kuzmanoski
Institute of Physics,Belgrade, Serbia
e-mail:luka.ilic@ipb.ac.rs

The direct radiative effect due to aerosol–radiation interactions is the change in radiative flux caused by the combined scattering and absorption of radiation by anthropogenic and natural aerosols. Due to their short lifetime and the large variability in space and time atmospheric aerosols are considered one of the major uncertainties in climate forcing and atmospheric processes [1]. For radiative studies it is necessary to measure aerosol optical properties, size, morphology and composition as a function of time and space, with a high resolution in both domains to account for the large variability. Lidar (Light Detection And Ranging), an active remote sensing technique, represents the optimal tool to provide range-resolved aerosol optical parameters. Large observational networks such as the European Aerosol Research Lidar Network (EARLINET) [2], the Aerosol Robotic Network (AERONET), provide the long-term measurement series needed to build a climatology of aerosol optical properties at the continental and global scales.

In order to assess the origin and type of aerosols which travel over Balkan region, having an impact on modification of the regional radiative budget, case studies combining measurements at the EARLINET joining lidar station in Belgrade with atmospheric modeling have been analyzed. For vertical profiling and remote sensing of atmospheric aerosol layers the Raman lidar system at the Institute of Physics Belgrade (44.860 N, 20.390 E) has been used. It is bi-axial system with combined elastic and Raman detection designed to perform continuous measurements of aerosols in the planetary boundary layer and the lower free troposphere. It is based on the third harmonic frequency of a compact, pulsed Nd:YAG laser, emitting pulses of 65 mJ output energy at 355 nm with a 20 Hz repetition rate. The optical receiver is a Cassegrain reflecting telescope with a primary mirror of 250 mm diameter and a focal length of 1250 mm. Photomultiplier tubes are used to detect elastic backscatter lidar signal at 355 nm and Raman signal at 387 nm. The detectors are operated both in the analog and photon-counting mode and the spatial raw resolution of the detected signals is 7.5 m. Averaging time of the lidar profiles is of the order of 1 min corresponding to 1200 laser shots. Lidar measurements can be used in synergy with numerical models in order to validate and compare information about aerosols. In this paper DREAM (Dust Regional Atmospheric Model) model, designed to simulate and/or predict the atmospheric cycle of mineral dust aerosol [3], will be used to analyze dust transport. The capability of the lidar technique to derive range-resolved vertical profiles of aerosol optical parameters (backscatter and extinction coefficient) with very high spatial and temporal resolution will be used to identify the altitude of layers and the temporal evolution of intrusions. Using these altitudes as inputs in air mass trajectory model, the source of aerosols can be identified. The additional techniques (satellite remote sensing) will be also discussed for selected case-studies.

REFERENCES

[1] IPCC: The Physical Science Basis, Contribution of Working Group I to the Fifth Assessment Report of the Intergovernmental Panel on Climate Change, edited by: Stocker, T. F., Qin, D., Plattner, G.-K., Tignor, M., Allen, S. K., Boschung, J., Nauels, A., Xia, Y., Bex, V., and Midgley, P. M., Cambridge University Press, Cambridge, United Kingdom and New York, NY, USA, (2013).

[2] G. Pappalardo, A. Amodeo, A. Apituley, A. Comeron, V. Freudenthaler, H. Linné, A.Ansmann, J. Bösenberg, G. D'Amico, I.Mattis, L. Mona, U. Wandinger, V Amiridis, L. Alados Arboledas, D. Nicolae, and M. Wiegner,: EARLINET: towards an advanced sustainable European aerosol lidar network, Atmos. Meas. Tech. 7, 2389 (2014).

[3] S. Nickovic, G. Kallos, A. Papadopoulos, O. Kakaliagou, J. Geophys. Res. 106, 1813 (2001).